THE PLASTIC ZONES FORMED IN AN AXIALLY SYMMETRICAL BODY BY STEADY AND TRANSIENT TEMPERATURE DISTRIBUTIONS

BY

B.H. BAINES B.Sc., A.C.G.I., G.I.Mech.E.

A thesis submitted for the degree of Doctor of Philosophy, in the Faculty of Engineering, University of London

also for

the Diploma of the Imperial College of Science and Technology.

1960

City and Guilds College

Imperial College

ABSTRACT

The thermal stresses in axially symmetrical elastic bodies with irregular boundaries can only be obtained used relaxation techniques. Hoyle demonstrated that a solution can be computed by using the two-diagram technique but the two stress functions used have proved to be difficult to handle. These difficulties are analysed and two other stress functions are suggested which have several advantages, one of which is that these functions converge satisfactorily when completely relaxed alternately. The boundary conditions which these functions must satisfy have been rationalised and a new approach to boundaries developed which removes the worst of the difficulties formerly associated with curved boundaries.

A rigorous solution of an overstrained axially symmetrical body is extremely unlikely with current plasticity theory. To ascertain the likely behaviour of surface strains in such a body specimens were overstrained by temperature gradients only, surface temperatures being recorded and strains measured on the cooler parts of the specimens using strain gauges. No spectacular evidence of plastic straining was obtained even at more than three times the temperature gradient which should have caused yield under the gauges. On one specimen several strain gauges showed a small increase in the gradient $\frac{e_\theta}{T_o - T_i}$ as higher temperature gradients were used.

Solutions for an overstrained long cylinder and an overstrained disc are developed, that for the disc giving a quick and simple method of solution but the cylinder requires a considerable amount of computing which may take weeks. These solutions are in indicative agreement with the experimental results.

Computed solutions for elastic specimens are compared with the experimental results during elastic straining. Hoop strains are found to be in good agreement but there is evidence that the computed solution for one specimen tended to over-estimate axial strains in the bore and over-emphasize the possible presence of a small stress concentration.

ACKNOWLEDGEMENTS

The work described in this thesis was undertaken on behalf of the British Admiralty, who financed the project, and to whom thanks are due.

Thanks are also due to Firth Brown Ltd. of Sheffield for the kind loan of two specimens.

I am particularly grateful to Mrs. M. Parfitt, B.A., who performed most of the elastic computations and contributed much useful criticism.

I am also very grateful to Dr. R.D. Hoyle, B.A., Ph.D., A.M.I.Mech.E. under whose supervision this research was performed, for his help and continued interest.

LIST OF CONTENTS

Page

Abstract

Acknowledgements

List of Contents

Symbols

1. A Survey of the Problem of Estimating the Thermal Stresses in an Axially Symmetrical Body 1

2. The Thermal Stresses in an Axially Symmetrical Elastic Body 8

2:1 The Single Stress Function Solution 9

2:2 The Double Stress Function Solution 13

2:3 The Form of the Stress Functions and the Introduction of X and γ 17

2:4 Finite Difference Equations for Boundary Conditions containing First Order Derivatives 28

Appendices

2:1 Directional Derivatives of a Scalar Field 44

2:2 To Express r and z Derivatives of γ in terms of p and s Derivatives of γ 46

2:3 To Express r and z Derivatives of $\left\{\frac{X}{r}\right\}$ in terms of p and s derivatives of $\left\{\frac{X}{r}\right\}$ 47

2:4 Alternative Stress Function η 48

2:5 Centrifugal Stresses 50

2:6 Pressure Stresses 52

2:7 Elastic Computations

1. Specimens A and B 53 - 54

2. Specimen C 55 - 56

3. Simulation of Impulse Wheel of H.P. Rotor 57 - 58

3. The Thermal Stresses in an Overstrained Axially Symmetrical Body 59

3:1 Development of Disc and Long Cylinder Theories 61

3:2 The Thermal Stresses in an Overstrained Long Cylinder

3:3 The Thermal Stresses in an Overstrained Disc (i.e. Plane Stress) 77

3:4 Computations 88

3:5 A Discussion of Computational Results 88

Appendices Computations for

an overstrained disc 92 - 94

an overstrained long cylinder 95 - 104

4. The Experimental Determination of Thermal Strains in Axially Symmetrical Specimens 105

4:1 Preamble 105

4:2 Detailed Description of Experimental Apparatus 110

4:3 Subsidiary Checks and Tests 124

4:4 Straining Tests 131

4:5 Assessment of Test Results 134

4:6 A Discussion of the Results of the Initial Straining Sequences 137

4:7 Comparison Between Test Results and Computed Solutions for the Elastic Specimens 152

5. Conclusions 158

References

Experimental Results in Graphical Form

Diagrams

Specimens A, B and C, Indicating Dimensions, and Axial and Circumferential Station Positions 122

Mounting Temperature Compensating Gauges and Thermocouples 123

SYMBOLS

∂ Partial Derivative

$$V^2 = \frac{\partial^2}{\partial r^2} + \frac{1}{r}\frac{\partial}{\partial r} + \frac{\partial^2}{\partial z^2} \qquad I^2 = \frac{\partial^2}{\partial r^2} - \frac{1}{r}\frac{\partial}{\partial r} + \frac{\partial^2}{\partial z^2}$$

$V^4 = V^2(V^2)$ ln, natural logarithm

α coefficient of linear expansion

σ Poisson's Ratio

E Young's Modulus of Elasticity

T Temperature

T_o Temperature on outer surface

T_i Temperature on inner surface

$T_o - T_i$ Mean temperature gradient

p Direction of normal to boundary, outward being positive

r Radius, radial direction

r_o Radius of outer surface

r_i Radius of inner surface

s Direction around boundary, clockwise being positive

u Radial displacement

w Axial displacement

z Axial direction

rr, ~~$\theta\theta$~~, zz, rz, pp, ss Stresses

e_{rr}, ~~$e_{\theta\theta}$~~, e_{zz}, e_{rz}, e_{pp}, e_{ss} Strains (these are abbreviated to e_r, e_θ etc. where possible)

Other symbols arising in the theoretical sections of this thesis are defined as they occur.

Strain Gauge Stations

In order to give easy reference to strain gauges the following system is used:- specimens are designated by a capital letter, the axial position of the gauge is designated by the distance from the upper surface of the specimen, six circumferential positions were used and these are designated i, ii, iii, iv etc. the odd designations are active gauges and the even are compensating gauges, ii compensating i, etc., finally the direction of

of the strain, i.e. θ, r, z or s is appended e.g. C, 10·8, i, θ - hoop strain 10·8 in. from top of specimen C on plane i.

On radial surfaces the radius is placed after the axial station, e.g. B, 0, 2·4, r or B, 6·0, 3·9, θ.

I. A SURVEY OF THE PROBLEM OF ESTIMATING THE THERMAL STRESSES IN AN AXIALLY SYMMETRICAL BODY.

A study has been made of the thermal stresses in an axially-symmetrical body, the main interest being directed towards a better understanding of conditions in a steam turbine rotor during an accelerated warming-up period. The ultimate objective is to supply the turbine designer with a reliable assessment of the stresses in a rotor resulting from a given temperature distribution. By studying the temperature and stress history it is hoped to modify (if necessary) starting procedures and/or rotor design in order to shorten the time required to put the turbine under load. This will require a large amount of computing and it is emphasised that this report is primarily concerned with the methods used in such a computation and not with the final answers.

The determination of the temperature distribution is being studied separately, both by temperature measurement on a rotor in situ and by the experimental determination of heat transfer coefficients between a steam atmosphere and rotating discs and cylinders. An electric resistance analogue computer is available for calculating the temperature distribution within the rotor from the surface information obtained experimentally. This report starts, then, from the assumed position of a known temperature distribution.

At the outset of the period covered by this report, Hoyle (ref. 3) had shown that the thermal stresses in a wholly elastic body could be computed using relaxation techniques. This requires the relaxation of two stress functions, called here $\overline{X}$ and φ. With the interchange of certain information between the functions a solution progresses until the functions converge i.e. no change is required when the appropriate information is exchanged.

The next stage appeared to be an assessment of the possible seriousness of overstraining the rotor, if possible bringing plastic straining within the framework of the relaxation method

suggested by Hoyle.

The first difficulty encountered was the extremely slow rate of convergence of the functions, $\overline{X}$ and φ. The A.E.I. Research Laboratories were asked to investigate the possibility of constructing a computer for $\overline{X}$ and φ; meanwhile an attempt was made to find a method of solution to a rotor with a plastic zone, the elastic zone to be solved using $\overline{X}$ and φ. The same difficulties which make hand relaxation of $\overline{X}$ and φ so difficult also prevented the construction of a suitable computer. It thus became necessary to reconsider the solution of the elastic body.

The Elastic Body

An elementary consideration of the two diagram technique used by Hoyle immediately suggests the simplification of completely relaxing the two functions alternately. This had already been found to destroy the convergence of the $\overline{X}$, φ functions and some degree of simultaneous relaxation has to be adopted. The computer thus carries the responsibility of deciding how far to take each relaxation before interchanging more information, with the ever present threat that too much relaxation and the solution may be receeding. This also proved to be a very serious problem in the construction of an analogue computer.

The two diagram technique was first proposed by Southwell (ref. 1) in 1942 and, despite considerable attention since then, it was not known whether completely relaxing two functions alternately was capable of producing a solution, indeed the reason for the divergence of $\overline{X}$ and φ when treated in this way was not understood.

Following an extensive analysis of the boundary problem associated with the $\overline{X}$ and φ functions and other experimental functions and consideration of the difficulties encountered in analogising functions to electrical circuits, two new functions X and γ were introduced to replace $\overline{X}$ and φ.

The finite difference equations in X and γ representing boundary mesh points have been rationalised and one algebraic

equation for each function represents all boundary mesh points. This is a consequence of a wholly new approach which has resulted in vastly improved relaxation characteristics and the virtual elimination of boundaries as a problem in hand relaxation.

Several solutions for different shapes have been obtained in which the functions have been completely relaxed alternately and convergence was quite satisfactory. Experience suggests that six cycles of relaxation give a good guide to conditions in the rotor and may prove sufficient for design purposes. Complete convergence, to a final relaxation residual of about $\pm$ 0·3, so far has taken about ten cycles. Comparing the two pairs of functions, $\bar{X}$ and φ with X and γ it appears very likely that the boundary difficulties associated with $\bar{X}$ and φ are at the root of the convergence difficulties.

No new relaxation principle is involved in using X and γ although several new ideas are introduced. The usual grid is drawn on the cross-section of the rotor, and mesh points established where mesh lines cross each other and also where mesh lines come into contact with the boundary. In order to take most advantage of the new boundary approach the position and size of the mesh is adjusted, by eye, to arrange so that each boundary mesh point can be associated with a body mesh point which is nearby and on, or nearly on, the normal to the boundary at the mesh point (see sections 2:4:1 and 2:4:3). This is not a very difficult condition since with axial and radial mesh lines it is already satisfied on axial and radial boundaries leaving the computer free to concentrate on oblique or curved boundaries.

The governing equations for X and γ are next calculated in finite difference form and the relaxation patterns evolved. Hitherto it has been usual with the two-diagram technique to perform both relaxations on one network. This is a source of possible confusion and is not necessary for X and γ. Two separate networks (on two sheets of paper) are much more convenient. The two functions are now alternately completely relaxed and the

interchange of information between the two nets $\left\{\frac{\partial\gamma}{\partial s}, \frac{\partial^2\gamma}{\partial r \partial z}, \frac{\partial X}{\partial s} \text{ etc.}\right\}$ is only performed when changing from one function to the other. When the interchange of information calls for no further correction at any mesh point the functions have converged upon the correct solution.

To start a solution, the possible values of stresses can be estimated using disc or long cylinder elastic solutions (given at the end of section 3:1) across one or two radii and translated into values of X and/or γ (see section 2:3:2). Some advantage might be expected from relaxing γ first since γ is very easy and the first relaxation of X, usually the worst of all, is given coherent information.

The introduction of X and γ has removed the mathematical obscurity formerly surrounding the two-diagram technique referred to by Southwell (ref. 4, p. 363). The relaxation of X and γ is tantamount to relaxing the stress equilibrium equations in the radial and axial directions respectively, and the alternate relaxation of X and γ can be demonstrated to be the alternate establishment of stress equilibrium in these two directions, a residual representing a spurious body force acting in the radial (X) or axial (γ) direction.

The second chapter of this report is primarily concerned with the presentation of X and γ and the rationalisation of the boundary conditions. Eventually, centrifugal and pressure effects will have to be brought within the stress functions and a method of doing so, causing only minor changes in equation constants, is suggested.

Plastic Straining in an otherwise elastic body

With the introduction of the stress functions X and γ and the technique of alternate complete relaxation it is possible that plastic components could be incorporated in the relaxation equations, the appropriate corrections being made also in the plastic zone during the change over from one function to the other.

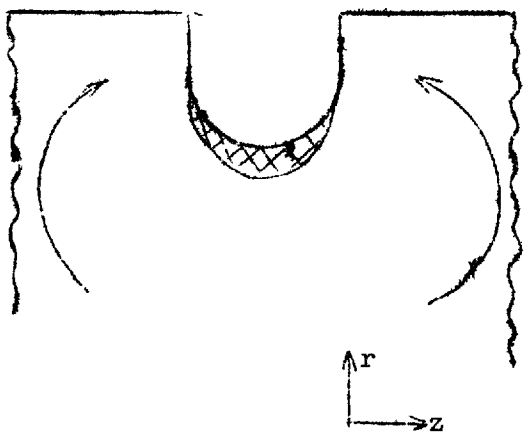
Even when using the simplest acceptable form of current plasticity theory the resultant equations are complicated and a solution would require such a large amount of computation that this approach is impractical. Nor is it really practical to make assumptions concerning the possible behaviour of strains in a plastic zone, in order to simplify the problem, and then spend a large amount of computing time on the relaxation of the surrounding elastic material. Once simplifying assumptions were accepted for the plastic zone it was expedient to extend such assumptions to the elastic zone also. Even then, only the simplest worthwhile problem, namely the disc, allows a quick, simple method of solution. The next obvious assumption, that plane sections remain plane (as in the long cylinder) leads to a method of solution which requires a considerable amount of computing. Methods of solutions based on each of these assumptions are given in chapter 3 and, for the present, the behaviour of an overstrained rotor must be estimated with the assistance of these solutions.

There are two main types of plastic zone to be considered a) a possibly large plastic zone due to the temperature distribution and not in the vicinity of a thermal stress raiser, and b) a small highly stressed area near a stress raiser producing a very small plastic zone.

In the case of the larger plastic zone, not centred upon a stress raiser, the disc and long cylinder solutions will give very useful information. Following a relaxation of the X and γ functions the elastic solution will indicate the likely position(s) of the first plastic zone(s). An elastic solution of the long cylinder equations (section 3:1) can now be performed using the appropriate temperature distribution (only the steady state temperature distribution is considered in most text-books). The $\theta\theta$ and rr stresses in the elastic disc solution are $(1-\sigma)$ times those from the long cylinder solution for the same temperature distribution. Now comparing the elastic solutions for a long cylinder and a disc with the elastic solution from the X, γ relaxation will indicate the extent to which faith can be entrusted

in a long cylinder and/or a disc solution with plastic straining and representing the axial plane concerned. Following the experimental determination of strains resulting from overstraining specimens by temperature gradients alone, this type of comparison was made between the test results and the simplified solutions. At all stations strain orientations obtained experimentally differed from the estimates of the simplified solutions since neither of the simplifying assumptions ($rz = 0$ with $\frac{\partial w}{\partial r} = 0$ or $zz = 0$) were truly satisfied in the specimens. Nevertheless predictions of the severity of plastic straining (as indicated by the maximum shear strain) based on the comparison method outlined would, using a long cylinder solution, have been in error by only about ten per cent. for temperature gradients over three times more severe than those at the start of plastic straining. The disc solution was less applicable to the specimens used and predictions from this may have been in error by thirty per cent. to fifty per cent. (a disc solution will always indicate less severe straining than a long cylinder solution). In any event, the test results support the idea of using the simplified solutions in the manner described as a guide to the likely severity of a plastic zone in an otherwise insoluble shape.

In the case of the small zone the area of plastic straining is dominated by the surrounding elastic material in which forces and bending moments are set up by the differential expansions and it is these forces and moments which produce the thermal stress concentration. A typical concentration of this type is shown in diagram If there is a temperature gradient in the r direction the bending moments within the material will tend to open $\left\{\frac{\partial T}{\partial r} - ve\right\}$ or close $\left\{\frac{\partial T}{\partial r} + ve\right\}$ this gap,



thereby creating a highly stressed area in the root. This type of concentration was present in the solution given by Hoyle (ref. 3 also Report to Admiralty 1951). The influence of these moments upon the radial, hoop and (perhaps) shear stresses is expected to be small but the resistance to these moments will be reflected in a serious increase in the axial stress (Hoyle quotes $\theta\theta = -18.8$ and $zz = -27.0$). Such a plastic zone is so small and so dominated by surrounding elastic material that plastic straining here will offer little or no stress relief to the rest of the body and the stresses within the zone acting through such a small area probably provide negligible resistance to the bending moments resulting from the lower stressed but considerably larger elastic areas. What may happen here, then, is the axial strain within the zone will continue almost proportional to increasing temperature distribution. If the radial temperature gradients in the anticipated plastic zone are large then the disc and/or long cylinder solutions can be used to indicate the likely behaviour of the hoop and radial strains as suggested above. Otherwise, strains from an elastic solution can be used to estimate the position on the stress-strain curve and an ignorance factor may be applied by multiplying the plastic component of strain by, say, two. There appears to be no question of "run-away" plastic straining and for single loading the question of safety is hardly involved for temperature distributions several times more severe than that at which the elastic solution anticipates the onset of plastic straining.

It is expected that the presence of either type of plastic zone is not as serious as has hitherto been feared. Severe strains can be expected but single loading (and the accompanying residual strains) is not likely to cause failure of a rotor. The methods of estimating the plastic strains will at least indicate whether fatigue due to cyclic thermal strains is a possible danger.

Chapter 3 of this report is primarily concerned with the solutions of the disc and of the long cylinder, each containing one or two plastic zones, and with consideration of the simplifying assumptions necessary in order to obtain solutions.

2. THE THERMAL STRESSES IN AN AXIALLY SYMMETRICAL ELASTIC BODY

The problem of thermal stresses in simple shapes, such as discs and long plain cylinders, presents no serious difficulties and closed-form solutions can be found in many standard textbooks (see also Section 3:1). This type of solution, using numerical integrations for transient temperatures, will also provide useful information about stress conditions on planes some distance from boundary irregularities and cylinder ends. In these cases, the shear stress and strain become far too large to be considered negligible, as is done in the disc and long cylinder theories, and a more rigorous approach is needed.

No closed-form solution of the general case appears possible; even stating the problem in stress function form offers little assistance. One such method, using Bessell's Functions, for a plain cylinder with steady state axial and radial temperature gradients was proposed by Parkus (ref. 8) but extension of this method to irregular boundaries would appear to be very cumbersome even if not impracticable. The difficulty here, and with all closed-form solutions, is feeding the shape of the boundary and also the temperature distribution into the solution. This difficulty is immense, and except for a few special cases a numerical method would appear to be quicker and easier.

The finite difference method is the method most likely to lead to a satisfactory solution of a difficult shape, e.g. a steam turbine rotor. The finite difference equations, resulting from the usual consideration of a mesh or grid drawn on the shape, can be solved by two methods a) treating the equations as algebraic simultaneous equations and b) using relaxation techniques. With the advent of the digital computer the former method may find favour, perhaps inverting a matrix on the computer. The relaxation approach is more useful for hand computation or in the construction of a suitable resistance network analogue computer. All the experimental relaxation given was done by hand computation.

2:1 The Single Stress Function Solution

The stress function chosen for relaxation can take many forms, subject to satisfying the equilibrium of stress, and compatability of strain equations. As in many other stress systems a stress function can be chosen which leads to a biharmonic equation. In this case the governing equation can be written in the form $(1-\sigma)\ V^4\mu + V^2\ (E\alpha T) = 0$ (which is developed later) and a correct solution requires this equation to be satisfied throughout the body in conjunction with the two appropriate stress conditions on the boundaries. It is recognised that a successful method of solving the biharmonic equation, using only one stress function, should be the most satisfactory approach to the problem but the resultant relaxation equations are cumbersome, especially near boundaries, and convergence was found to be too slow for practical purposes.

A discussion on the difficulties of relaxing the biharmonic equation is given by Fox (ref. 7) which agrees with the experience gained whilst attempting to apply the biharmonic to temperature stresses.

Southwell (ref. 4 p. 279) also mentions the slow convergence and appends a note "this fact has led to much discussion of the question, whether biharmonic problems can be 'broken down' into two or more plane-harmonic problems".

The biharmonic approach was eventually abandoned and the biharmonic was broken down into two equations. The development of the biharmonic equation is given in the following section.

Development of Biharmonic Equation

The stress function ϕ is defined by the equation

$$rz = -\frac{\partial^2 \phi}{\partial r \, \partial z} \tag{1}$$

and using the stress equilibrium equation

$$\frac{\partial zz}{\partial z} + \frac{\partial rz}{\partial r} + \frac{rz}{r} = 0 \tag{2}$$

it can be shown that

$$zz = \frac{\partial^2 \phi}{\partial r^2} + \frac{1}{r}\frac{\partial \phi}{\partial r} \tag{3}$$

Another stress function, μ, is defined by the equation

$$rr = \frac{\partial^2 \phi}{\partial z^2} + \frac{1}{r}\frac{\partial \mu}{\partial r} \tag{4}$$

and using the stress equilibrium equation

$$\frac{\partial rr}{\partial r} + \frac{\partial rz}{\partial z} + \frac{rr - \theta\theta}{r} = 0 \tag{5}$$

it can be shown that

$$\theta\theta = \frac{\partial^2 \phi}{\partial z^2} + \frac{\partial^2 \mu}{\partial r^2} \tag{6}$$

The relationship

$$\frac{\partial}{\partial r}\left\{\frac{u}{r}\right\} = \frac{1}{r}\frac{\partial u}{\partial r} - \frac{u}{r^2} \tag{7}$$

must hold if the radial $\left\{\frac{\partial u}{\partial r}\right\}$ and circumferential $\left\{\frac{u}{r}\right\}$ displacements are to be compatable. Substituting $E\frac{u}{r} = \theta\theta - \sigma\,(rr + zz) + E\alpha T$ and $E\frac{\partial u}{\partial r} = rr - \sigma\,(\theta\theta + zz) + E\alpha T$ in (7) and considering $\frac{\partial E}{\partial r}$ and $\frac{\partial \sigma}{\partial r}$ to be negligible, gives

$$\frac{\partial}{\partial r}\left\{\overline{\theta\theta - \sigma\,(rr + zz)}\right\} + (1 + \sigma)\left\{\frac{\theta\theta - rr}{r}\right\} + E\alpha\frac{\partial T}{\partial r} = 0 \tag{8}$$

and substituting for $\theta\theta - rr$ from equilibrium equation (5) and

rearranging

$$\frac{\partial}{\partial r}\left\{\overline{rr + \theta\theta + zz + E\alpha T}\right\} + (1 + \sigma)\left\{\overline{\frac{\partial rz}{\partial z} - \frac{\partial zz}{\partial r}}\right\} = 0 \qquad (9)$$

Writing the stresses in stress function form and integrating with respect to radius gives

$$V^2\mu - \sigma V^2\phi + \frac{\partial^2\phi}{\partial z^2} - \frac{\partial^2\mu}{\partial z^2} + E\alpha T = 0 \qquad (10)$$

From $u = re_{\theta\theta} + r\alpha T$ it can be shown, using (10), that

$$u = -\frac{1 + \sigma}{E}\frac{\partial\mu}{\partial r} \qquad (11)$$

The other compatability requirement is that

$$\frac{\partial}{\partial r}\left\{\frac{\partial w}{\partial z}\right\} = \frac{\partial}{\partial z}\left\{\frac{\partial w}{\partial r}\right\}$$

Now

$$e_{rz} = \frac{\partial u}{\partial z} + \frac{\partial w}{\partial r} = \frac{2(1 + \sigma)}{E}rz = -\frac{2(1 + \sigma)}{E}\frac{\partial^2\phi}{\partial r\,\partial z} \qquad (12)$$

and using (11)

$$\frac{\partial w}{\partial r} = \frac{1 + \sigma}{E}\left\{\overline{\frac{\partial^2\mu}{\partial r\,\partial z} - \frac{2\,\partial^2\phi}{\partial r\,\partial z}}\right\} \qquad (13)$$

Integrating with respect to radius and differentiating with respect to z gives $\frac{\partial w}{\partial z}$, equating to $\frac{\partial w}{\partial z} = e_{zz} + \alpha T$ and using (10) gives

$$V^2\mu = V^2\phi \qquad (14)$$

whence

$$(1 - \sigma)V^2\mu + \frac{\partial^2\phi}{\partial z^2} - \frac{\partial^2\mu}{\partial z^2} + E\alpha T = 0 \qquad (15)$$

and using the operator V^2 throughout this equation

$$(1 - \sigma)V^4\mu + V^2\left\{\overline{E\alpha T}\right\} = 0 \qquad (16)$$

since $\frac{\partial^2}{\partial z^2}(V^2\phi) = \frac{\partial^2}{\partial z^2}(V^2\mu)$

Using (15) to express $\frac{\partial^2\phi}{\partial z^2}$ the stresses are

$$
\begin{aligned}
\theta\theta &= \sigma V^2\mu - \frac{1}{r}\frac{\partial \mu}{\partial r} - E\alpha T \\
rr &= \sigma V^2\mu - \frac{\partial^2 \mu}{\partial r^2} - E\alpha T \\
zz &= (1-\sigma)V^2\mu + \frac{1}{r}\frac{\partial \mu}{\partial r} + \frac{\partial^2 \mu}{\partial r^2} + E\alpha T \\
\frac{\partial rz}{\partial z} &= (1-\sigma)\frac{\partial}{\partial r}(V^2\mu) - \frac{\partial^3 \mu}{\partial r\,\partial z^2} + E\alpha\frac{\partial T}{\partial r}
\end{aligned}
\qquad (17)
$$

The shear stress, rz, cannot be expressed directly with the stress function in the form defined but if specifically required then μ can be replaced by $\frac{\partial \mu}{\partial z}$ in all equations; whence $\frac{\partial rz}{\partial z}$ above can be integrated. For computing this is not convenient since the stresses will be expressed by 3rd derivatives.

2:2 The Double Stress Function Solution

The axially-symmetrical stress problem can also be stated in the form of two governing equations in two inter-dependent stress functions. As with the biharmonic approach, there are two boundary conditions, and one boundary condition and one governing equation are associated with each stress function. The stress functions are relaxed and information is interchanged as the solution progresses until the two functions converge i.e. no change is needed when the appropriate information is exchanged.

This method was proposed by Southwell (ref.1) who suggested two stress functions, $\overline{X}$ and φ, for the axially-symmetrical body. Subsequently these functions were used by Allen, Fox and Southwell (refs. 2 and 4) to solve pressure stresses (e.g. gun barrels) and, with the inclusion of a temperature term and written negative, were also used by Hoyle (ref. 3) to solve the thermal stress problem, thereby showing that body forces are within the scope of this method.

deVries and Oerth (ref. 6) introduced a slight modification to the Southwell functions by writing $\overline{X} = \frac{X}{r}$ and $\varphi = \frac{\varphi}{r}$ which, they claim, "give results that are a little more convenient to handle numerically". This apart, the behaviour of these functions is very similar to that reported by the above mentioned contributors.

The double stress function approach is a breaking down of the biharmonic equation, although not necessarily into plane-harmonic equations.

2:2:1 The Hoyle Stress Functions $\bar{X}$ and φ

As stated by Hoyle, the thermal stress problem reduces to a solution of two governing equations

$$I^2\bar{X} = 0 \quad \text{where } I^2 = \frac{\partial^2}{\partial r^2} - \frac{1}{r}\frac{\partial}{\partial r} + \frac{\partial^2}{\partial z^2} \tag{a}$$

and $$I^2\varphi + \frac{E\alpha}{1-\sigma} r \frac{\partial T}{\partial r} = \frac{\partial^2 \bar{X}}{\partial z^2} \tag{b}$$

which can be shown to be a breaking down of the biharmonic equation as follows:

Equation (16) can be written in the form

$$V^2 \left\{ \bar{(1-\sigma)V^2\mu + E\alpha T} \right\} = 0$$

Put $(1-\sigma)V^2\mu + E\alpha T = -(1-\sigma)\frac{1}{r}\frac{\partial \bar{X}}{\partial r}$

Then substitute in (16) gives $V^2\left\{\frac{1}{r}\frac{\partial \bar{X}}{\partial r}\right\} = 0$

and using the identity $V^2\left\{\frac{1}{r}\frac{\partial}{\partial r}\right\} = \frac{1}{r}\frac{\partial}{\partial r}(I^2)$

and integrating $I^2\bar{X} = 0$ (a)

Now put $\frac{\partial \mu}{\partial r} = \frac{\varphi}{r} + (1-\sigma)\frac{\bar{X}}{r}$

and $(1-\sigma)\frac{\partial}{\partial r}(V^2\mu) + E\alpha\frac{\partial T}{\partial r} = -(1-\sigma)\frac{\partial}{\partial r}\left\{\frac{1}{r}\frac{\partial \bar{X}}{\partial r}\right\}$

and using $\frac{\partial}{\partial r}(V^2\mu) = \frac{1}{r}I^2\left\{r\frac{\partial \mu}{\partial r}\right\}$ and $I^2(\bar{X}) = 0$

$$(1-\sigma)I^2\left\{r\frac{\partial \mu}{\partial r}\right\} + E\alpha r\frac{\partial T}{\partial r} = -(1-\sigma)r\frac{\partial}{\partial r}\left\{\frac{1}{r}\frac{\partial \bar{X}}{\partial r}\right\}$$

$$(1-\sigma)I^2(\varphi) + E\alpha r\frac{\partial T}{\partial r} = (1-\sigma)\frac{\partial^2 \bar{X}}{\partial z^2}$$

i.e. $$I^2\varphi + \frac{E\alpha}{1-\sigma} r\frac{\partial T}{\partial r} = \frac{\partial^2 \bar{X}}{\partial z^2} \tag{b}$$

and substituting above in expressions for stresses, (17), the stresses become

$$\left.\begin{aligned} \theta\theta &= -\frac{\varphi+(1-\sigma)\bar{X}}{r^2} - \frac{\sigma}{r}\frac{\partial \bar{X}}{\partial r} - \frac{E\alpha T}{1-\sigma} & zz &= \frac{1}{r}\frac{\partial \varphi}{\partial r} \\ rr &= \frac{\varphi+(1-\sigma)\bar{X}}{r^2} - \frac{1}{r}\frac{\partial}{\partial r}(\varphi+\bar{X}) - \frac{E\alpha T}{1-\sigma} & rz &= -\frac{1}{r}\frac{\partial \varphi}{\partial z} \end{aligned}\right\} \tag{c}$$

with the boundary conditions

$$zz \sin\theta + rz \cos\theta = 0$$

$$rr \cos\theta + rz \sin\theta = 0$$

leading to $\varphi = 0$ on all boundaries (d)

and $$\left\{\frac{\bar{\varphi}+(1-\sigma)\bar{X}}{r^2} - \frac{1}{r}\frac{\partial}{\partial r}(\varphi+\bar{X}) - \frac{E\alpha\bar{T}}{1-\sigma}\right\}\cos\theta - \frac{1}{r}\frac{\partial\varphi}{\partial z}\sin\theta = 0 \qquad (e)$$

Thus, in finite difference form, equation (b) is relaxed with $\varphi = 0$ on the boundaries and taking $\frac{\partial^2 X}{\partial z^2}$ from the $\bar{X}$ network; and equation (a) is relaxed using (e) as the boundary condition for $\bar{X}$, taking $\frac{\partial\varphi}{\partial r}$ and $\frac{\partial\varphi}{\partial z}$ from the φ network. The boundary condition (e) used with equation (a) gives equations very suitable for relaxation on or near axial boundaries but the equations become increasingly more difficult as the boundary approaches the radial direction. When the boundary is radial (e) becomes inoperative and equation (b) (which is not otherwise used on radial boundaries) is used in conjunction with equation (a) viz.

$$\frac{\partial^2\bar{X}}{\partial r^2} - \frac{1}{r}\frac{\partial\bar{X}}{\partial r} = -\frac{\partial^2\varphi}{\partial z^2} - \frac{E\alpha}{1-\sigma}r\frac{\partial T}{\partial r} \qquad (f)$$

2:2:2 Convergence of the Hoyle Functions

The relaxation characteristics of $\bar{X}$ and φ are not entirely satisfactory. The individual relaxation of φ is very simple but $\bar{X}$ is rather difficult.

All workers who have used these functions (refs. 3,5 and 6) report that the functions do not converge to a final solution when fully relaxed alternately. When relaxing $\bar{X}$ near radial boundaries large increments are necessary to eliminate quite small residuals of $\bar{X}$ with the result that a large residual is produced in φ. The solution appears to be convergent only if $\bar{X}$ residuals are reduced by a combination of relaxation of $\bar{X}$ and φ. Allen (ref. 5) suggests completely relaxing φ but only tentatively relaxing $\bar{X}$ and convergent solutions have been

obtained using this method. Nevertheless, this is unsatisfactory as it introduces some element of guesswork and requires a degree of skill above that to be expected of most computors.

The major difficulty with these functions is due to the introduction of an inconsistency, namely using the governing equation (b) as a boundary condition with governing equation (a) for radial boundaries only. The resulting equation (f) does not impose upon $\overline{X}$ any indication of the required gradient in the axial direction. In finite difference form the equation contains only boundary points and the radial boundary thus becomes disconnected from the rest of the body.

The author's opinion is that the poor mapping of the $\overline{X}$ function field on or near radial or almost radial boundaries is a possible cause of the necessity for some degree of simultaneous relaxation of $\overline{X}$ and φ.

2:2:3 Electrical Analogue for $\overline{X}$ and φ

In view of the difficulty of relaxing $\overline{X}$ by hand computation, the A.E.I. Research Laboratory was requested by the Admiralty to investigate the possibility of solving the $\overline{X}$ and φ functions by electrical analogue methods. The two main difficulties encountered in the hand computation, i.e. the disconnection of $\overline{X}$ radial boundaries from the body and the necessity for some degree of simultaneous relaxation of $\overline{X}$ and φ, also create problems in the analogue approach. As Liebmann (of the A.E.I.) points out (Communication following ref. 3) a "resistance network analogue always relaxed the solution completely for the imposed boundary conditions" and "the situation arose which the author had found to destroy the convergence when carrying out the relaxation by hand compution". No satisfactory method of overcoming these difficulties was discovered and the project was abandoned.

2:3 The form of the Stress Functions

The form of each stress function is largely a matter of choice, but, of course, the connection between the two is fixed by consideration of equilibrium of stresses and compatability of strains. If the problem is to be solved using relaxation methods a further consideration applies; the resultant finite difference equations must be suitable for the relaxation approach, especially equations representing boundaries, since it is at the boundaries that most information is interchanged. Ideally both stress functions should be relaxable by operators without special knowledge and one way of assisting this aim is to choose functions which will converge to a final answer when each is fully relaxed alternately.

Taking as a starting point the accumulated experience of all workers who have relaxed the Hoyle functions it is apparent that the equations for $\bar{X}$ representing radial boundaries are undesirable. The "disconnection" of radial boundaries from the remainder of the body is probably the cause of the boundaries being "ill-conditioned". Axial boundaries in $\bar{X}$ are not so "ill-conditioned" and these equations are quite reasonable to relax. On axial boundaries fictitious points are eliminated using $rr = 0$, which incorporates a first derivative of $\bar{X}$ normal to the boundary; on radial boundaries a second derivative of $\bar{X}$ normal to the boundary is used to eliminate fictitious points and it is this which also eliminates body points from the boundary equations. Thus, the first desirable feature of the stress-functions is that all stresses shall be stated in terms below second derivatives.

Another consideration applicable to boundary conditions is the effective mapping of the function field by the finite difference equations. The most effective mapping is obtained by stating derivatives in two mutually perpendicular directions by increments on both sides of the point considered. This is the usual practice in the body but this degree of accuracy has not previously been realised for points near or on boundaries, where

one or even two increments become fictitious. To avoid more than one fictitious increment being associated with each boundary point (thus reducing the complexity of boundary equations) mesh points can be established on the boundary and the two mutually perpendicular directions can be chosen to be in the direction of the boundary and normal to the boundary. If the boundary condition can be written to incorporate the first derivative normal to the boundary then with one increment in this direction into the body and two increments along the boundary no loss of accuracy will be suffered in the region of boundaries.

Ideally, therefore, the boundary conditions associated with the stress function will state the first derivative of that function perpendicular to the boundary, in terms of the other stress function. This will give each stress function a very large degree of control over the behaviour of the related function. Also, by imposing such gradients upon a function the ill-conditioning of the Hoyle functions should be reduced.

This ideal condition is very severe but has been successfully achieved. Many forms of stress function were tried and to avoid excess labour, the approach adopted was to break down the biharmonic equation into two, initially, plane-harmonic equations. The chosen function form was substituted and the resulting boundary conditions obtained. The process was repeated until eventually the two stress functions X and γ were developed[i].

Another successful stress function, η, was also paired with this X during an investigation into factors influencing rate of convergence and this is given and discussed in Appendix 2.4.

Footnote i : the inclusion of centrifugal forces and surface tractions in the equations for X and γ is discussed in Appendices 2.5 and 2.6.

2:3:1 Introduction of Stress Functions, X and γ

Rewrite equation (16) in the following form

$$\nabla^2\left\{(1-\sigma)\,\nabla^2\mu + E\alpha T\right\} = 0 \tag{18}$$

Putting $(1-\sigma)\nabla^2\mu + E\alpha T = \frac{\partial\gamma}{\partial z}$ (19)

this becomes

$$\frac{\partial}{\partial z}\,(\nabla^2\gamma) = 0 \tag{20}$$

Integrating $$\nabla^2\gamma = 0 = \frac{\partial^2\gamma}{\partial r^2} + \frac{1}{r}\frac{\partial\gamma}{\partial r} + \frac{\partial^2\gamma}{\partial z^2} \tag{21}$$

Now put $\frac{\partial\mu}{\partial r} = \frac{X}{r}$ (22)

From (19) $$(1-\sigma)\,\frac{\partial}{\partial r}\,(\nabla^2\mu) = \left\{\frac{\partial^2\gamma}{\partial r\,\partial z} - E\alpha\,\frac{\partial T}{\partial r}\right\} \tag{23}$$

and substituting from (22)

$$I^2X = \frac{r}{1-\sigma}\left\{\frac{\partial^2\gamma}{\partial r\,\partial z} - E\alpha\,\frac{\partial T}{\partial r}\right\} \tag{24}$$

where $I^2X = \frac{\partial^2X}{\partial r^2} - \frac{1}{r}\frac{\partial X}{\partial r} + \frac{\partial^2X}{\partial z^2}$

and the stresses become, using (19) and (22) in (17)

$$\left.\begin{aligned} \theta\theta &= \frac{\sigma}{1-\sigma}\frac{\partial\gamma}{\partial z} - \frac{X}{r^2} - \frac{E\alpha T}{1-\sigma} \\ rr &= \frac{\sigma}{1-\sigma}\frac{\partial\gamma}{\partial z} - \frac{\partial}{\partial r}\frac{(X)}{(r)} - \frac{E\alpha T}{1-\sigma} \\ zz &= \frac{\partial\gamma}{\partial z} + \frac{1}{r}\frac{\partial X}{\partial r} \qquad\qquad rz = \frac{\partial\gamma}{\partial r} - \frac{1}{r}\frac{\partial X}{\partial z} \end{aligned}\right\} \tag{25}$$

2:3:2 Physical Significance of X and γ

From (11) $u = -\frac{1+\sigma}{E}\frac{\partial \mu}{\partial r}$

and using (22)

$$\frac{u\,E}{1+\sigma} = -\frac{X}{r}$$

$$\text{or} \quad X = -\frac{E}{1+\sigma}(u\,r) \tag{26}$$

The displacement, u, has a definite value for any fixed set of conditions. X must therefore also have a definite value.

Adding the stresses rr, $\theta\theta$ and zz from (25) and rearranging

$$\frac{\partial \gamma}{\partial z} = \left\{ (1-\sigma)\,(rr + \theta\theta + zz) + 2\,E\alpha T \right\} \frac{1}{1+\sigma} \tag{27}$$

also $\frac{\partial \gamma}{\partial r} = rz + \frac{1}{r}\frac{\partial X}{\partial z}$ from (25)

and again, for a fixed set of conditions, the stress distribution will have a definite value, therefore $\frac{\partial \gamma}{\partial r}$ and $\frac{\partial \gamma}{\partial z}$ must also have a definite value. Thus γ has a definite variation but can take a constant.

2:3:3 Boundary Conditions in terms of X and γ

The stress boundary conditions are

$$rr \cos\theta + rz \sin\theta = 0 \tag{28}$$

$$zz \sin\theta + rz \cos\theta = 0 \tag{29}$$

where θ is the angle between the outward radial direction and the outward normal to the boundary, clockwise being positive.

Expressing (28) in terms of X and γ

$$\left\{-\frac{\sigma}{1-\sigma}\frac{\partial\gamma}{\partial z} - \frac{\partial}{\partial r}\left(\frac{X}{r}\right) - \frac{E\alpha T}{1-\sigma)}\right\}\cos\theta + \left\{\frac{\partial\gamma}{\partial r} - \frac{1}{r}\frac{\partial X}{\partial z}\right\}\sin\theta = 0$$

$$\text{or } -\frac{\partial\gamma}{\partial z}\cos\theta + \frac{\partial\gamma}{\partial r}\sin\theta - \frac{\partial}{\partial r}\left(\frac{X}{r}\right)\cos\theta - \frac{\partial}{\partial z}\left(\frac{X}{r}\right)\sin\theta + \left\{\frac{\partial\gamma}{\partial z} - E\alpha T\right\}\frac{\cos\theta}{1-\sigma} = 0$$

and using $\frac{i}{\partial s} = -\sin\theta\frac{\partial}{\partial r} + \cos\theta\frac{\partial}{\partial z}$

and $\frac{\partial}{\partial p} = \cos\theta\frac{\partial}{\partial r} + \sin\theta\frac{\partial}{\partial z}$ from appendix 2.1

$$\frac{\partial}{\partial p}\left(\frac{X}{r}\right) = -\frac{\partial\gamma}{\partial s} + \left\{\frac{\partial\gamma}{\partial z} - E\alpha T\right\}\frac{\cos\theta}{1-\sigma} \tag{30}$$

$$\text{or } \frac{\partial}{\partial p}\left(\frac{X}{r}\right) = K \tag{31}$$

$$\text{where } K = -\frac{\partial\gamma}{\partial s} + \left\{\frac{\partial\gamma}{\partial z} - E\alpha T\right\}\frac{\cos\theta}{1-\sigma} \tag{32}$$

and expressing (29) in terms of X and γ

$$\left\{\frac{\partial\gamma}{\partial z} + \frac{1}{r}\frac{\partial X}{\partial r}\right\}\sin\theta + \left\{\frac{\partial\gamma}{\partial r} - \frac{1}{r}\frac{\partial X}{\partial z}\right\}\cos\theta = 0$$

$$\text{or } \frac{\partial\gamma}{\partial p} = \frac{1}{r}\frac{\partial X}{\partial s} \tag{33}$$

$$\text{or } \frac{\partial\gamma}{\partial p} = G \tag{34}$$

$$\text{where } G = \frac{1}{r}\frac{\partial X}{\partial s} \tag{35}$$

Footnote i : p is the outward normal to boundary and s is clockwise direction around boundary.

2:3:4 Collection of Relevant Formulae in Solution for X and γ

The problem has, therefore, taken the form of two stress functions, X and γ, which are relaxed alternately.

For γ

$$V^2\gamma = 0 \tag{21}$$

with the boundary condition

$$\frac{\partial\gamma}{\partial p} = G \tag{34}$$

and for X

$$I^2X = \frac{r}{1-\sigma}\left\{\frac{\partial^2\gamma}{\partial r\,\partial z} - E\alpha\frac{\partial T}{\partial r}\right\} \tag{24}$$

with the boundary condition

$$\frac{\partial}{\partial p}\begin{Bmatrix}X\\ r\end{Bmatrix} = K \tag{31}$$

the value of G or K being calculated according to equations (32) or (35) from the previous relaxation of the other stress function.

i.e.

$$K = -\frac{\partial\gamma}{\partial s} + \left\{\frac{\partial\gamma}{\partial z} - E\alpha T\right\}\frac{\cos\theta}{1-\sigma} \tag{32}$$

$$\text{and } G = \frac{1}{r}\frac{\partial X}{\partial s} \tag{35}$$

2:3:5

The Convergence of X and γ

In the solutions so far performed, each relaxation was taken to small residuals (in the range $\pm$ 0·3) in an attempt to follow, manually, the behaviour of X and γ as if the solution was being performed on two analogous electric networks. Information was exchanged only when changing from one function to the other as the functions were alternately relaxed. Convergence was satisfactory and final residuals in the range $\pm$ ·3 were obtained after about 10 cycles, and this (so far) appears to be independent of shape and/or temperature distribution.

Taking the convergence of X and γ at individual mesh points two convergence patterns have so far emerged, 1) a continuous convergence to which the final solution is an asymptote and 2) an oscillating convergence, though not necessarily about the final solution. With both types convergence is rapid in the first few cycles, decaying as the final solution is approached. The type of convergence appears to be dictated by the position of the first estimate of the functions compared with the final solution. This was demonstrated by over-relaxing one function whose convergence pattern then changed from oscillating to continuous. As there appears, so far, to be little advantage for either convergence pattern, this point was not pursued.

Superimposed upon this individual convergence another pattern is beginning to be detected. If a body has a large, strong mass of metal this part of the body rapidly converges on or near the final solution (three or four cycles) but weaker or more remote parts of the body (section changes, stress raisers, etc.) appear to await the initial convergence of the stronger part before a definite convergence is detectable.

With more experience of the convergence behaviour of X and γ some system may be developed so that, after a few cycles, the computer can jump ahead (missing out the middle cycles) on to, or nearly on to, the final solution. This possibility is worth considering, especially when investigating a number of temperature distributions for any one body shape.

2:3:6 The Practical Significance of the Two-Diagram Technique applied to X and γ

It is interesting to consider the implications behind relaxing one stress function whilst temporarily holding the other fixed. Obviously, for each pair of functions some physical or mathematical assumption is implied, (even if of complicated form) but no suggestions have so far been advanced by workers in this field. One interpretation for X and γ can be obtained as follows:-

If the expressions giving rz and zz in terms of X and γ (25) be substituted into the stress equilibrium equation for the axial direction (2) the governing equation for γ (21) is obtained. The stress boundary condition used with γ (29) is also associated with stress equilibrium in the axial direction.

Similarly, the governing equation for X (24) can be obtained by substituting for rr, $\theta\theta$, and rz in terms of X and γ (25) in the stress equilibrium equation for the radial direction (5). Again the stress boundary condition used with X (28) is associated with stress equilibrium in the radial direction.

Thus it is apparent that a γ residual represents a lack of stress equilibrium in the axial direction at that particular mesh point, whether the mesh point be in the body or on the boundary. The same is true for X, a X residual representing a lack of stress equilibrium in the radial direction at that particular mesh point, and again this is true for body and boundary mesh points.

The liquidation of γ and X residuals, alternately, is thus seen to be the alternate establishment of stress equilibrium in the axial and radial directions respectively. A residual produced by a "change over" is thus seen to be a correction produced by previously correcting the stress equilibrium in the other direction. Most computers arrange the governing equations in the most convenient numerical form (usually as near to the 1, 1, 1, 1 and 4 configuration as possible) by multiplying the equation through

by some arbitary constant. Nevertheless, the actual out-of-balance stress can be obtained from the residual using this arbitrary constant and will give a better assessment of the current accuracy of the solution than considering the residual as a percentage of the function at the mesh point.

The picture created above is consistent and simple but may not be the only interpretation. For example $(1+\sigma)X = -E.u.r$ (26) and so holding X fixed also holds the radial displacement fixed. Complementary to this it is apparent that holding γ fixed denies change to the volumetric strain (from (27)) and also to the average rotation of the principal axes, r and z i.e. $\frac{1}{2}\left\{\frac{\partial \bar{w}}{\partial r} - \frac{\partial \bar{u}}{\partial z}\right\}$ (from (12), (25) and (26)).

No similar consistent and simple pattern has been identified in the Southwell/Hoyle functions. The governing equation for φ can be obtained directly by substituting the stress expressions in the stress equilibrium equation for the radial direction but the boundary condition used with φ, $\varphi = 0$, comes from the stress boundary condition associated with stress equilibrium in the axial direction. The governing equation for $\bar{X}$ cannot be obtained directly from either stress equilibrium equation.

2:3:7 Advantages of Stress Functions X and γ

The advantages claimed for the new stress functions X and γ are as follows:

a) both functions relax easily, γ is particularly easy

b) the two functions converge when fully relaxed alternately, even when a large area of the specimen is dominated by a curved boundary

c) the two-diagram technique using X and γ can be shown to have physical meaning

d) stating the stress boundary conditions in terms of X and γ gives two equations, one of which states $\frac{\partial X}{\partial p}$ in terms of $\frac{\partial \gamma}{\partial s}$ and the other $\frac{\partial \gamma}{\partial p}$ in terms of $\frac{\partial X}{\partial s}$

e) using the boundary condition $\frac{\partial \gamma}{\partial p} = f\{\frac{\partial X}{\partial s}\}$ with the governing equation for γ, $V^2\gamma = 0$, most effectively imposes upon the γ network, the information taken from the X network. Similarly for X. This will result in a much improved accuracy of solution

f) this type of boundary condition, i.e. $\frac{\partial \gamma}{\partial p} = f\{\frac{\partial X}{\partial s}\}$, and $\frac{\partial X}{\partial p} = f\{\frac{\partial \gamma}{\partial s}\}$ has enabled a completely new and more powerful approach to curved boundaries to be developed.* It is now possible, at a glance, to assess the possible computational difficulties created by a particular grid on a particular specimen; and, furthermore, to adjust the grid until curved boundaries are no more difficult than the axial boundaries of the Hoyle functions

g) the new approach to boundaries enables a universal boundary equation (in algebraic form) to be stated which satisfies both the boundary condition and governing equation. As this requires only the substitution of numerical values of mesh lengths and angles, computing time is much reduced over previous methods which usually required the setting up of boundary equations for each mesh point on or near the boundary, starting each time from the basic equations.

* given in the next section.

h) the serious "ill-conditioning" of the Hoyle function $\overline{X}$ on radial boundaries is eliminated. Some degree of general "ill-conditioning" remains but it seems likely that the stress equilibrium and strain compatability equations contribute to this in the case of an axially symmetrical body. This point can be illustrated by writing the relevant equations as follows

$$\frac{\partial}{\partial r}(r\,rr) + \frac{r\partial rz}{\partial z} - \theta\theta = 0 \qquad \text{from (5)}$$

and

$$\frac{\partial}{\partial r}(re_\theta) - e_r + r\frac{\partial}{\partial r}(\alpha T) = 0 \qquad \text{from (7)}$$

thus small changes in rr or $\frac{\partial rz}{\partial z}$ can have a large influence upon $\theta\theta$ and similarly, small changes in e_θ can have a large influence upon e_r.

i) the two major difficulties encountered in the attempt to analogise $\overline{X}$ and φ to an electric resistance network, viz: the disconnection of $\overline{X}$ radial boundaries from the body and the necessity for some degree of simultaneous relaxation of $\overline{X}$ and φ, have been completely eliminated. The construction of two electric resistance networks to represent X and γ appears to be possible and the way is now open for another attempt to construct an analogue computer, should this be desired.

However, it should be noted that whilst the relaxation is considerably easier for the X, γ functions than for the $\overline{X}$, φ functions, the labour involved in each change over (i.e. re-calculation of equation constants) remains almost unaffected. The improvement in the relaxation characteristics is considerable and the time taken by the changeover is now almost half the total computing time required for a solution. No analogue machine which requires this change-over to be performed wholly by hand computing will have much advantage over complete hand relaxation except, perhaps, allowing a less skilled computer to be employed.

2:4 Finite Difference Equations for Boundary Conditions containing first order derivatives

a) Rectangular Boundaries

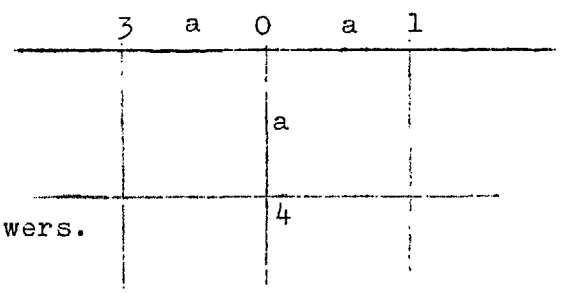
In general, rectangular boundaries present no problem when the gradient normal to the boundary can be stated. With one internal point on the normal plus the normal gradient the field in this direction can be expressed satisfactorily as far as the second derivative term. viz. for an arbitrary function, j

$$\left\{\frac{\partial j}{\partial r_o}\right\} = J_o$$

$$j_4 = j_o - a\frac{\partial j}{\partial r} + \frac{a^2}{2}\frac{\partial^2 j}{\partial r^2}$$

neglecting higher powers.

whence $$\frac{\partial^2 j}{\partial r^2} = \frac{2(j_4 - j_o)}{a^2} + \frac{2}{a} J_o$$



Diag. 2.1

This approach is well established and a number of solutions employing this technique are known (see, for example, ref. 2, 3, 4, 5 and 6). Fox (ref. 7) discusses the possibility of increasing accuracy by taking more than one internal mesh point on the normal.

The equations obtained using this approach give reasonable dominance to the coefficient for j_o, e.g. for $V^2 j$ + constant = 0.

$$j_1 + j_3 + 2j_4 - 4j_o + \text{constant} = f(j)$$

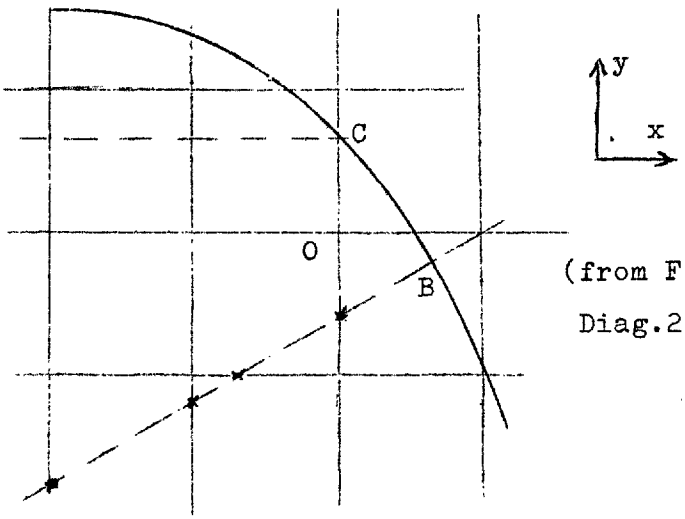
and so relax fairly easily. This approach is therefore retained for both axial and radial boundaries, and the general equations, (44) and (54), developed later, reduce to this approach for these boundaries.

b) Oblique or Curved Boundaries

No convincing and satisfactory approach for oblique or curved boundaries has been suggested hitherto. The Southwell/Hoyle

function, $\bar{X}$, has a boundary condition stating $\frac{d\bar{X}}{dr}$ which becomes progressively more unsatisfactory as boundaries approach the radial direction. Despite this Hoyle (ref. 3) did successfully relax a body containing curved boundaries. deVries and Oerth (ref. 6) suggested approximating the curve by a series of axial and radial boundaries. This involves a number of right-angle corners and they suggest that such corners can best be "handled, not by performing any relaxation but assuming some reasonable value for $\bar{X}$ from extrapolation from the neighbouring points". This cannot be described as a satisfactory system.

Fox (ref. 7) considers the case of curved boundaries when the normal derivative is known (a general case, the axially-symmetrical system was not derived in this form). Two possible methods are suggested, "neither of which is completely satisfactory". One method involves a statement of the boundary condition at a point such as B plus one or more of the internal crossed points on the normal, the crossed points to be obtained by interpolation along local mesh lines. The alternative method is to state the derivatives at C in terms of internal mesh points in the x and y directions, again using interpolation along local mesh lines where necessary. This method was also suggested by Hoyle (ref. 3). Both systems were rejected for the same reasons



(from Fox)
Diag.2·2

a) too many internal points are needed, without substantially improving accuracy

b) the finite difference equation must be evolved for many different boundary configurations

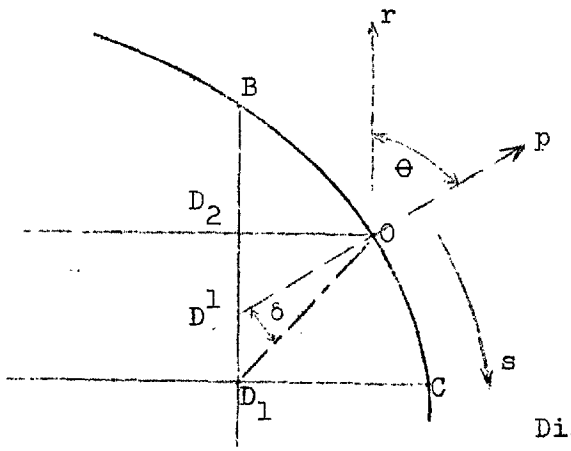
c) the equation is seldom easy to relax.

Allen has written of this problem (ref. 5, p.74) "One of the

most difficult types of problem to tackle by the relaxation method is the determination of a solution of a Poisson's equation when a specified normal gradient of the wanted quantity is given as a boundary condition". The two-diagram technique requires a dozen or more such solutions and the usefulness of the technique turns upon the development of a satisfactory approach to boundary problems. In the next section a wholly new approach is presented which is much superior to any previous suggestions and adequately meets the above three criticisms of all previous systems.

2:4:1 Finite Difference form of Boundary Conditions for X and γ

As discussed in section 2:3 , boundary derivatives are best stated in mutually perpendicular directions. The establishment of mesh points where mesh lines cross the boundary make a statement of derivatives around the boundary (the s direction is measured clockwise) a simple matter. The first derivative normal to this (p is the outward normal direction) is fixed by the boundary condition. The second normal derivative $\left\{\frac{\partial^2}{\partial p^2}\right\}$ can be written in finite difference form by choosing an increment to a point inside the body in the p direction (see diag.2.3) However, seldom can D^1 be a mesh point at a reasonable increment from the boundary point O, if the condition that the increment be normal to the boundary is to be strictly observed. By allowing some latitude in this condition and taking the increment in a direction at an angle δ to the normal direction any suitable internal mesh point D can be employed. (e.g. D_1 or D_2 in diag.2.3). This possibly results in a small loss of accuracy but is preferable to increasing the number of points involved when stating D^1 in terms of surrounding points, which is the only feasible alternative.



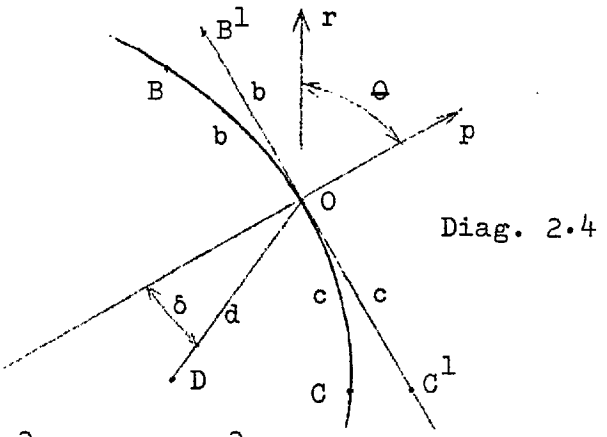
Diag. 2.3

When D is on the normal to the boundary, the boundary condition $\frac{\partial}{\partial p}$ and the points B, C and D are sufficient to state $\frac{\partial^2}{\partial p^2}$, $\frac{\partial}{\partial s}$ and $\frac{\partial^2}{\partial s^2}$ and hence $\frac{\partial}{\partial r}$, $\frac{\partial}{\partial z}$, $\frac{\partial^2}{\partial r^2}$ and $\frac{\partial^2}{\partial z^2}$ but not $\frac{\partial^2}{\partial r\,\partial z}$

To obtain $\frac{\partial^2}{\partial r\,\partial z}$ another boundary condition can be invoked

viz. $\frac{\partial^2}{\partial s\,\partial p}$ since $\frac{\partial}{\partial p}$ can be calculated at all points. If D is not on the normal to the boundary this second boundary condition is required to state all r and z derivatives required.

Curved boundaries present a problem due to the curved nature of the path of the s direction. The finite difference equations for $\frac{\partial}{\partial s}$ and $\frac{\partial^2}{\partial s^2}$ at O state the derivatives in the direction of the tangent to the curve at point O. Thus, the transfer from s and p to r and z directions,



Diag. 2.4

$$\frac{\partial}{\partial s} = -\sin\theta\,\frac{\partial}{\partial r} + \cos\theta\,\frac{\partial}{\partial z}$$

$$\frac{\partial^2}{\partial s^2} = \sin^2\theta\,\frac{\partial^2}{\partial r^2} - 2\sin\theta\cos\theta\,\frac{\partial^2}{\partial r\partial z} + \cos^2\theta\,\frac{\partial^2}{\partial z^2}$$

as given in standard text books is somewhat in error since the right hand side of these expressions, when used with finite differences, specify points B^1 or C^1 on the tangent to point O and distance b or c respectively from O. For shallow curves the worst error is probably that due to the rotation of the s direction in the function field and the expression for $\frac{\partial}{\partial s}$ is expected to be within the accuracy of finite differences. Accepting this then $\frac{\partial}{\partial s}\left(\frac{\partial}{\partial s}\right)$ gives, for $\frac{\partial^2}{\partial s^2}$ (see appendix 2.1) in which θ is a variable with s,

$$\frac{\partial^2}{\partial s^2} = \sin^2\theta\frac{\partial}{\partial r^2} - 2\sin\theta\cos\theta\frac{\partial^2}{\partial r\partial z} + \cos^2\theta\,\frac{\partial^2}{\partial z^2} - \frac{\partial}{\partial p}\cdot\frac{\partial\theta}{\partial s}$$

and it can be shown that $\frac{\partial}{\partial p}\cdot\frac{\partial\theta}{\partial s}$ is tantamount to a correction, in the p direction, for the distance BB^1 or CC^1 within the accuracy of such small angle formulae as $\sin\phi = \phi$ and $1 - \cos\phi = \frac{\phi^2}{2}$

Similarly,

$$\frac{\partial}{\partial s}\left\{\frac{\partial}{\partial p}\right\} = \frac{\partial^2}{\partial s \partial p} = \sin\theta\cos\theta \left\{\frac{\partial^2}{\partial z^2} - \frac{\partial^2}{\partial r^2}\right\} + \left\{\cos^2\theta - \sin^2\theta\right\}\frac{\partial^2}{\partial r \partial z} + \frac{\partial}{\partial s}\cdot\frac{\partial\theta}{\partial s}$$

and $\frac{\partial}{\partial s}\cdot\frac{\partial\theta}{\partial s}$ can be shown to be a correction for the rotation of direction p.

N.B. If the curve can be considered circular then $\frac{\partial\theta}{\partial s} = \frac{1}{R}$ where R is the radius of curvature of the boundary between points B and C.

The assumptions used in the above analysis are reasonable for moderate, continuous curves and can also be used for deeper curves (i.e. of small radius) if the local mesh lengths are small. In the unlikely event of higher accuracy being required further corrections can be applied in the above analysis or the approach outlined for discontinuous boundaries (section 2:4:6) adapted.

2:4:2

The Governing Equation for γ for Boundary Mesh Points

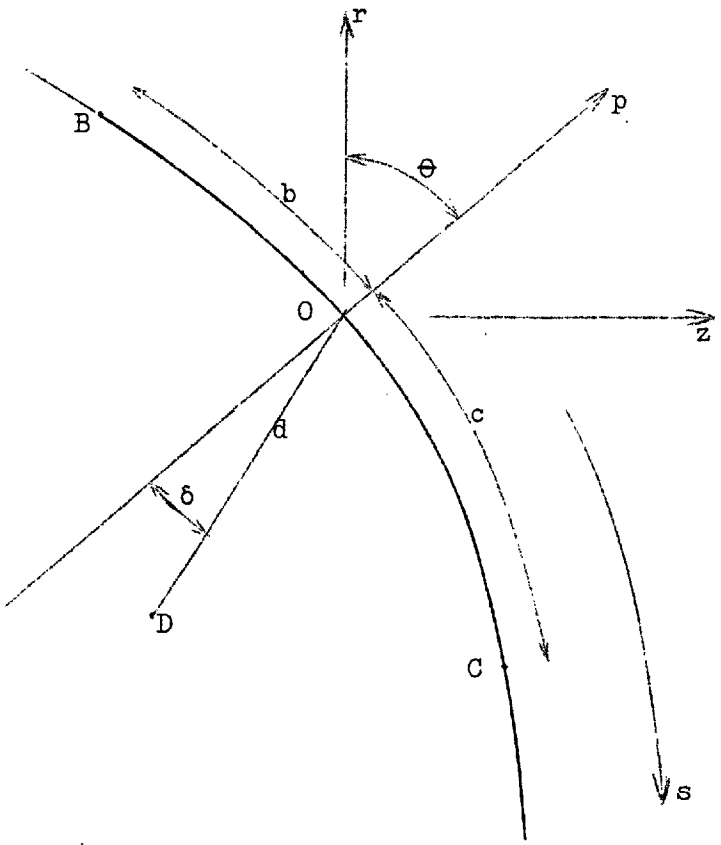
It has been shown that $\frac{\partial \gamma}{\partial p}$ is known in terms of the other stress function i.e.

$$\frac{\partial \gamma}{\partial p} = G \tag{34}$$

and as G is known at all points on the boundary, $\frac{\partial G}{\partial s}$ can be calculated

$$\text{i.e. } \frac{\partial^2 \gamma}{\partial s \, \partial p} = \frac{\partial G}{\partial s} \tag{36}$$

Now consider boundary point O at which the outward normal is at angle θ to outward radial direction. Proceeding clockwise around the boundary, point B is at distance -b from O, point C is at distance +c from O and D is a point inside the boundary (a suitable mesh point in the body) at distance d from O with direction OD at angle δ (measured anti-clockwise) to the normal.



Diag. 2.5

The following equations can be written

$$\gamma_B = \gamma_O - b\frac{\partial\gamma}{\partial s} + \frac{b^2}{2}\frac{\partial^2\gamma}{\partial s^2} \tag{37}$$

$$\gamma_C = \gamma_O + c\frac{\partial\gamma}{\partial s} + \frac{c^2}{2}\frac{\partial^2\gamma}{\partial s^2} \tag{38}$$

whence

$$\frac{\partial\gamma}{\partial s} = \left\{\frac{b}{c(b+c)}\right\}\gamma_C - \left\{\frac{c}{b(b+c)}\right\}\gamma_B - \left\{\frac{b-c}{bc}\right\}\gamma_O \tag{39}$$

$$\frac{\partial^2\gamma}{\partial s^2} = \left\{\frac{2}{c(b+c)}\right\}\gamma_C + \left\{\frac{2}{b(b+c)}\right\}\gamma_B - \left\{\frac{2}{bc}\right\}\gamma_O \tag{40}$$

and

$$\gamma_D = \gamma_O - d\cos\delta\frac{\partial\gamma}{\partial p} + d\sin\delta\frac{\partial\gamma}{\partial s} + \frac{d^2\cos^2\delta}{2}\frac{\partial^2\gamma}{\partial p^2} - d^2\sin\delta\cos\delta\frac{\partial^2\gamma}{\partial s\partial p} + \frac{d^2\sin^2\delta}{2}\frac{\partial^2\gamma}{\partial s^2} \tag{41}$$

whence

$$\frac{\partial^2\gamma}{\partial p^2} = \frac{2}{d^2\cos^2\delta}\left\{\gamma_D - \gamma_O\right\} + \frac{2}{d\cos\delta}\frac{\partial\gamma}{\partial p} - \frac{2\sin\delta}{d\cos^2\delta}\frac{\partial\gamma}{\partial s} + 2\tan\delta\frac{\partial^2\gamma}{\partial s\partial p} - \tan^2\delta\frac{\partial^2\gamma}{\partial s^2} \tag{42}$$

Substituting in equation (10) (appendix 2.2)

$$\nabla^2\gamma = \left\{\frac{2}{d^2\cos^2\delta}\right\}\left\{\gamma_D - \gamma_O\right\} + \left\{\frac{\cos\theta}{r} + \frac{2}{d\cos\delta} + \frac{\partial\theta}{\partial s}\right\}\frac{\partial\gamma}{\partial p} - \left\{\frac{\sin\theta}{r} + \frac{2\tan\delta}{d\cos\delta}\right\}\frac{\partial\gamma}{\partial s} + 2\tan\delta\frac{\partial^2\gamma}{\partial s\partial p} + \left\{1 - \tan^2\delta\right\}\frac{\partial^2\gamma}{\partial s^2} \tag{43}$$

In this expression $\frac{\partial\gamma}{\partial p}$, $\frac{\partial^2\gamma}{\partial s\partial p}$ are known boundary conditions and $\frac{\partial\gamma}{\partial s}$ and $\frac{\partial^2\gamma}{\partial s^2}$ are expressed in terms of B, C and O using equations (39) and (40), whence equation (43) becomes

$$
\left.
\begin{aligned}
V^2\gamma = {} & \left\{\frac{\cos\theta}{r} + \frac{2}{d\cos\delta} + \frac{\partial\theta}{\partial s}\right\}G + 2.\tan\delta.\frac{\partial G}{\partial s} + \left\{\frac{2}{d^2\cos^2\delta}\right\}\left\{\gamma_D - \gamma_O\right\} \\
& + \left\{2(1 - \tan^2\delta) - b\left\{\frac{\sin\theta}{r} + \frac{2}{d}\,\frac{\tan\delta}{\cos\delta}\right\}\right\}\frac{\gamma_C}{c(b+c)} \\
& + \left\{2(1 - \tan^2\delta) + c\left\{\frac{\sin\theta}{r} + \frac{2}{d}\,\frac{\tan\delta}{\cos\delta}\right\}\right\}\frac{\gamma_B}{b(b+c)} \\
& - \left\{2(1 - \tan^2\delta) - (b-c)\left\{\frac{\sin\theta}{r} + \frac{2\tan\delta}{d\cos\delta}\right\}\right\}\frac{\gamma_O}{b.c}
\end{aligned}
\right\} \qquad (44)
$$

N.B. In this equation b, c and d are positive numerically, the essentially negative character of b and d being incorporated in the analysis.

2:4:3
Special Values of δ

If δ is zero equation (44) reduces to

$$
\left.
\begin{aligned}
V^2\gamma = {} & \left\{\frac{\cos\theta}{r} + \frac{2}{d} + \frac{\partial\theta}{\partial s}\right\}G + \frac{2}{d^2}\left\{\gamma_D - \gamma_O\right\} \\
& + \left\{2 - \frac{b}{r}\sin\theta\right\}\frac{\gamma_C}{c(b+c)} + \left\{2 + \frac{c}{r}\sin\theta\right\}\frac{\gamma_B}{b(b+c)} \\
& - \left\{2 - (b-c)\frac{\sin\theta}{r}\right\}\frac{\gamma_O}{b.c}
\end{aligned}
\right\} \qquad (45)
$$

and $\frac{b}{r}\sin\theta$ and $\frac{c}{r}\sin\theta$ will usually be much smaller than 2, i.e. coefficients for γ_C, γ_B, and γ_D will be positive and coefficient for γ_O will, of course, be negative. The easiest equations to relax are those in which the coefficient for γ_O is appreciably larger than the individual coefficient of any other point in the equation, e.g. $\gamma_B + \gamma_C + 2\gamma_D - 4\gamma_O$ + constant = $F(\gamma)$ would relax quite easily. Equation (45) produces equations very similar to this.

As δ increases in value from zero the coefficient of γ_C decreases passing through zero at about $+25^\circ$ to $+35^\circ$ depending upon $\frac{b}{d}$ and $\frac{b\sin\theta}{r}$. Similarly, the coefficient of γ_B passes

through zero at about -25° to -35° depending upon $\frac{c}{d}$ and $\frac{c\sin\theta}{r}$ e.g. for δ of about -30°, $\gamma_C+3\gamma_D-4\gamma_O$ + constant = $F(\gamma)$. By about $+45^\circ$ the equation is approximately $2\gamma_B-2\gamma_C+4\gamma_D-4\gamma_O+\text{const.}=F(\gamma)$ and at -45°, $-2\gamma_B+2\gamma_C+4\gamma_D-4\gamma_O$ + constant = $F(\gamma)$.

All these equations can be relaxed, but the equation for $\delta = 0$ is much quicker and simpler, the equation becoming progressively more difficult as δ increases or decreases from $\delta = 0$. In addition to computational convenience accuracy is enhanced by $\delta = 0$ since derivatives in the field are most accurately stated by two pairs of Taylor's Series, each pair being mutually at right angles, i.e. $\frac{\partial}{\partial p}$ and γ_D in p direction γ_B and γ_C in s direction.

2:4:4
Value of $\frac{\partial^2\gamma}{\partial r\partial z}$

From (11) (appendix2·2)

$$\frac{\partial^2\gamma}{\partial r\partial z} = \left\{\frac{\partial^2\gamma}{\partial s\partial p} - \frac{\partial\gamma}{\partial s}\frac{\partial\theta}{\partial s}\right\}\cos2\theta - \left\{\frac{\partial^2\gamma}{\partial s^2} - \frac{\partial^2\gamma}{\partial p^2} + \frac{\partial\gamma}{\partial p}\frac{\partial\theta}{\partial s}\right\}\frac{\sin2\theta}{2}$$

Substitute for $\frac{\partial^2\gamma}{\partial p^2}$ from (42)

$$\frac{\partial^2\gamma}{\partial r\partial z} = \left\{\cos2\theta + \tan\delta.\sin2\theta\right\}\frac{\partial^2\gamma}{\partial s\partial p} - \left\{\frac{\sin\delta}{d\cos^2\delta}\sin2\theta+\frac{\partial\theta}{\partial s}\cos2\theta\right\}\frac{\partial\gamma}{\partial s}$$
$$- \left\{(1+\tan^2\delta)\frac{\sin2\theta}{2}\right\}\frac{\partial^2\gamma}{\partial s^2}+\left\{\frac{\sin2\theta}{d\cos\delta} - \frac{\partial\theta}{\partial s}.\frac{\sin2\theta}{2}\right\}\frac{\partial\gamma}{\partial p} + \frac{\sin2\theta}{d^2\cos^2\delta}\left\{\gamma_D-\gamma_O\right\} \qquad (46)$$

and using (34), (36), (39) and (40)

$$\frac{\partial^2\gamma}{\partial r\partial z}=\left\{\cos2\theta+\tan\delta.\sin2\theta\right\}\frac{\partial G}{\partial s}+\left\{\frac{\sin2\theta}{d\cos\delta}\frac{\partial\theta}{\partial s}-\frac{\sin2\theta}{2}\right\}G+\frac{\sin2\theta}{d^2.\cos^2\delta}.\left\{\gamma_D-\gamma_O\right\}$$
$$- \left\{b\left\{\frac{\sin\delta}{d\cos^2\delta}\sin2\theta+\frac{\partial\theta}{\partial s}\cos2\theta\right\}+(1+\tan^2\delta)\sin2\theta\right\}\frac{\gamma_C}{c(b+c)}$$
$$+ \left\{c\left\{\frac{\sin\delta}{d\cos^2\delta}\sin2\theta+\frac{\partial\theta}{\partial s}\cos2\theta\right\}-(1+\tan^2\delta)\sin2\theta\right\}\frac{\gamma_B}{b(b+c)} \qquad (47)$$
$$+ \left\{(b-c)\left\{\frac{\sin\delta}{d\cos^2\delta}\sin2\theta+\frac{\partial\theta}{\partial s}\cos2\theta\right\}+(1+\tan^2\delta)\sin2\theta\right\}\frac{\gamma_O}{bc}$$

Taking $\frac{\sin 2\theta}{2} \cdot V^2\gamma = 0$ (Using equation (44)) from (47)

$$\frac{\partial^2\gamma}{\partial r \partial z} = \cos 2\theta \frac{\partial G}{\partial s} - \left\{\left\{\frac{\cos\theta}{2r} + \frac{\partial\theta}{\partial s}\right\}\sin 2\theta\right\}.G \qquad (48)$$

$$- \left\{2\sin 2\theta + b\left\{\frac{\partial\theta}{\partial s}\cos 2\theta - \frac{\sin\theta\sin 2\theta}{2r}\right\}\right\}\frac{\gamma_C}{c(b+c)}$$

$$- \left\{2\sin 2\theta - c\left\{\frac{\partial\theta}{\partial s}\cos 2\theta - \frac{\sin\theta\sin 2\theta}{2r}\right\}\right\}\frac{\gamma_B}{b(b+c)}$$

$$+ \left\{2\sin 2\theta + (b-c)\left\{\frac{\partial\theta}{\partial s}\cos 2\theta - \frac{\sin\theta\sin 2\theta}{2r}\right\}\right\}\frac{\gamma_O}{bc}$$

i.e. δ is eliminated.

2:4:5

The Governing Equations for X for Boundary Mesh Points

In section 2:3:3 it was shown that the derivative $\frac{\partial}{\partial p}\begin{Bmatrix}X\\r\end{Bmatrix}$ is known in terms of the other stress function i.e.

$$\frac{\partial}{\partial p}\begin{Bmatrix}X\\r\end{Bmatrix} = K \tag{31}$$

and hence

$$\frac{\partial^2}{\partial s \partial p}\begin{Bmatrix}X\\r\end{Bmatrix} = \frac{\partial K}{\partial s} \tag{49}$$

Diagram 2:5 and the explanation between equations 36 and 37 equally apply here.

Writing $\frac{X}{r}$ for γ in (39) and (40).

$$\frac{\partial}{\partial s}\begin{Bmatrix}X\\r\end{Bmatrix} = \begin{Bmatrix}\frac{b}{c(b+c)}\end{Bmatrix}\begin{Bmatrix}X\\r\end{Bmatrix}_C - \begin{Bmatrix}\frac{c}{b(b+c)}\end{Bmatrix}\begin{Bmatrix}X\\r\end{Bmatrix}_B - \begin{Bmatrix}\frac{b-c}{bc}\end{Bmatrix}\begin{Bmatrix}X\\r\end{Bmatrix}_O \tag{50}$$

$$\frac{\partial^2}{\partial s^2}\begin{Bmatrix}X\\r\end{Bmatrix} = \begin{Bmatrix}\frac{2}{c(b+c)}\end{Bmatrix}\begin{Bmatrix}X\\r\end{Bmatrix}_C + \begin{Bmatrix}\frac{2}{b(b+c)}\end{Bmatrix}\begin{Bmatrix}X\\r\end{Bmatrix}_B - \begin{Bmatrix}\frac{2}{bc}\end{Bmatrix}\begin{Bmatrix}X\\r\end{Bmatrix}_O \tag{51}$$

and the same substitution in (42) gives

$$\frac{\partial^2}{\partial p^2}\begin{Bmatrix}X\\r\end{Bmatrix} = \frac{2}{d^2\cos^2\delta}\left\{\begin{Bmatrix}X\\r\end{Bmatrix}_D - \begin{Bmatrix}X\\r\end{Bmatrix}_O\right\} + \frac{2}{d\cos\delta}\frac{\partial}{\partial p}\begin{Bmatrix}X\\r\end{Bmatrix} - \frac{2\sin\delta}{d\cos^2\delta}\frac{\partial}{\partial s}\begin{Bmatrix}X\\r\end{Bmatrix} + 2\tan\delta\frac{\partial^2}{\partial s \partial p}\begin{Bmatrix}X\\r\end{Bmatrix} - \tan^2\delta\frac{\partial^2}{\partial s^2}\begin{Bmatrix}X\\r\end{Bmatrix} \tag{52}$$

and substitute in (13) (Appendix 2·3)

$$\frac{1}{r}I^2X = \begin{Bmatrix}\frac{2}{d^2\cos^2\delta}\end{Bmatrix}\left\{\begin{Bmatrix}X\\r\end{Bmatrix}_D - \begin{Bmatrix}X\\r\end{Bmatrix}_O\right\} + \begin{Bmatrix}\frac{\cos\theta}{r} + \frac{2}{d\cos\delta} + \frac{\partial\theta}{\partial s}\end{Bmatrix}\frac{\partial}{\partial p}\begin{Bmatrix}X\\r\end{Bmatrix} - \begin{Bmatrix}\frac{\sin\theta}{r} + \frac{2\tan\delta}{d\cos\delta}\end{Bmatrix}\frac{\partial}{\partial s}\begin{Bmatrix}X\\r\end{Bmatrix} + 2\tan\delta\frac{\partial^2}{\partial s \partial p}\begin{Bmatrix}X\\r\end{Bmatrix} + (1-\tan^2\delta)\frac{\partial^2}{\partial s^2}\begin{Bmatrix}X\\r\end{Bmatrix} - \frac{X_O}{r_O^3} \tag{53}$$

and substitute from (31), (49), (50) and (51) and rearranging

$$\frac{1}{r}I^2X = \left\{\frac{\cos\theta}{r} + \frac{2}{d\cos\delta} + \frac{\partial\theta}{\partial s}\right\}K + 2\tan\delta\frac{\partial K}{\partial s} + \left\{\frac{2}{d^2\cos^2\delta}\right\}\left\{\left\{\frac{X}{r}\right\}_D - \left\{\frac{X}{r}\right\}_O\right\}$$

$$+\left\{2(1-\tan^2\delta) - b\left\{\frac{\sin\theta}{r} + \frac{2}{d}\frac{\tan\delta}{\cos\delta}\right\}\right\}\frac{X_C}{r_C.c.(b+c)}$$

$$+\left\{2(1-\tan^2\delta) + c\left\{\frac{\sin\theta}{r} + \frac{2}{d}\frac{\tan\delta}{\cos\delta}\right\}\right\}\frac{X_B}{r_B.b.(b+c)}$$

$$-\left\{2(1-\tan^2\delta) - (b-c)\left\{\frac{\sin\theta}{r} + \frac{2\tan\delta}{d\cos\delta}\right\}\right\}\frac{X_O}{r_O.b.c} - \frac{X_O}{r_O^3} \qquad (54)$$

and from (24)

$$\frac{1}{r}I^2X = \frac{1}{1-\sigma}\left\{\frac{\partial^2\gamma}{\partial r\partial z} - E\alpha\frac{\partial T}{\partial r}\right\} \qquad (55)$$

A comparison of the equation for $\frac{1}{r}I^2X$ (54) and the equation for $V^2\gamma$ (44) shows a very close similarity in coefficients. The comments upon the value of δ (Section 2:4:3) are therefore also applicable to equation (54).

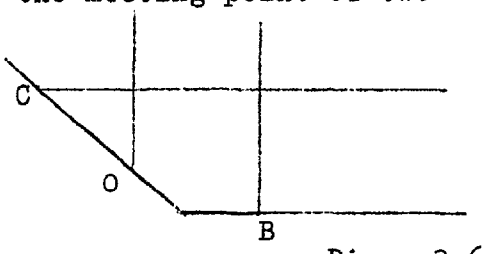
It should be noted by the computer that an intelligent examination of the coefficients in equations (44) and (54) will much reduce the labour required in the establishment of the governing equations for γ and X at each boundary point.

2:4:6

DISCONTINUOUS BOUNDARIES

(i) General Case

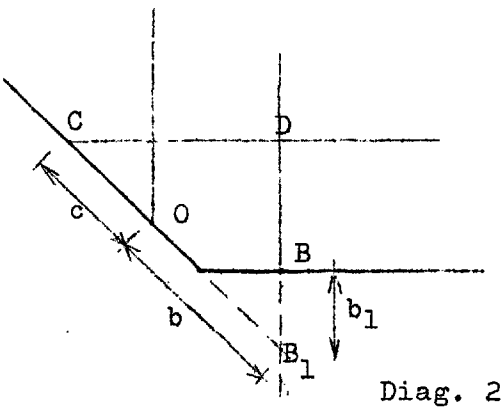
If the increment b or c contains the meeting point of two boundary directions (as in diagram) then the universal boundary equations need some modifications in use, since at the meeting point of these two directions $\frac{\partial\theta}{\partial s}$ is very large or infinity.



Diag. 2.6

One possible approach would be to replace the abrupt corner by a smooth curve for computational purposes and for many problems this may be a reasonable approximation. On the other hand, if the area adjoining the corner is of particular interest a more accurate approach may be necessary. The approach adopted in the computed solution enclosed was as follows.

The boundary direction at O was extended to cut the normal from B at B_1 The universal boundary equations were then calculated in terms of C, B_1, O and D. B_1 is, of course, a fictitious point and can be expressed in terms of derivatives at point B. If b_1 is small then $\gamma_{B_1} = \gamma_B + G_B b_1$ can be substituted in the universal boundary equation giving an equation in terms of γ_C, γ_B, γ_O and γ_D. In the change over $\left\{\frac{\partial\gamma}{\partial s}\right\}_o$ was required and to obtain this γ_{B_1} was calculated and $\left\{\frac{\partial\gamma}{\partial s}\right\}_o$ then obtained from γ_C, γ_O and γ_{B_1}. The value of $\left\{\frac{\partial G}{\partial s}\right\}_o$ was obtained using $G_C = G_O + c\frac{\partial G}{\partial s}$ and $\frac{\partial^2\gamma}{\partial r\partial z}$ from equation (48) using C, O and B_1. If more

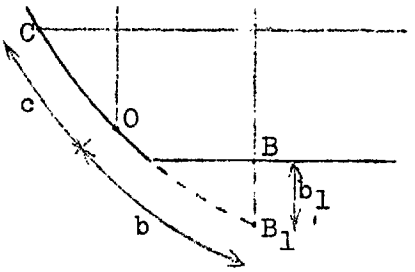


Diag. 2.7

accuracy in $\frac{\partial G}{\partial s}$ is required then more terms in the c direction could be taken.

The equation for X was obtained in the same manner.

Each boundary discontinuity will have to be considered individually and if a smooth curve approximation is inadequate it is suggested that the method of approach outlined above should form the basis of a more accurate method. If the boundary directions are curved then the $\frac{\partial \theta}{\partial s}$ terms in the universal boundary equations should be retained and the continuation of the boundary direction given a suitable curve as in diagram 2.8.



Diag. 2.8

(ii) Axial/Radial Right Angle Corners

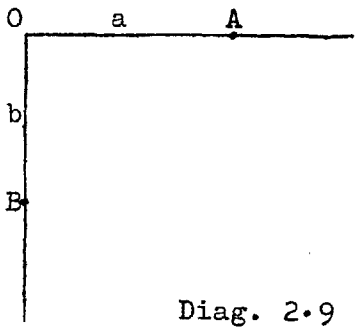
At a boundary discontinuity formed by the meeting of an axial and a radial boundary direction, the following stress conditions are known and from these, four boundary conditions must be deduced.

$$rr = zz = rz = \frac{\partial rz}{\partial z} = \frac{\partial zz}{\partial r} = \frac{\partial rr}{\partial z} = \frac{\partial rz}{\partial r} = 0$$

Using $\frac{\partial zz}{\partial r} = \frac{\partial rz}{\partial z} = 0$ gives $I^2X = 0$ i.e. $\frac{\partial^2 \gamma}{\partial r \partial z} = E\alpha \frac{\partial T}{\partial r}$

also $\frac{\partial^2 zz}{\partial r \partial z} = \frac{\partial^2 rz}{\partial z^2} = 0$ leads to $\frac{\partial^3 \gamma}{\partial r \partial^2 z} = E\alpha \left\{\frac{\partial^2 T}{\partial r \partial z}\right\}$

If point A is distance a from point O, the corner point,



Diag. 2.9

$$\left\{\frac{\partial \gamma}{\partial r}\right\}_A = \left\{\frac{\partial \gamma}{\partial r}\right\}_O + a\left\{\frac{\partial^2 \gamma}{\partial r \partial z}\right\}_O + \frac{a^2}{2}\left\{\frac{\partial^3 \gamma}{\partial r \partial z^2}\right\}_O$$

i.e. $$\left\{\frac{\partial \gamma}{\partial r}\right\}_A = \left\{\frac{\partial \gamma}{\partial r}\right\}_O + aE\alpha\left\{\frac{\partial T}{\partial r}\right\}_O + \frac{a^2}{2} E\alpha \left\{\frac{\partial^2 T}{\partial r \partial z}\right\}_O$$

and $$\left\{\frac{\partial T}{\partial r}\right\}_A = \left\{\frac{\partial T}{\partial r}\right\}_O + a\left\{\frac{\partial^2 T}{\partial r \partial z}\right\}_O$$

whence $\left\{\frac{\partial\gamma}{\partial r}\right\}_O = \left\{\frac{\partial\gamma}{\partial r}\right\}_A + \frac{a}{2}E\alpha \left\{\left\{\frac{\partial T}{\partial r}\right\}_O + \left\{\frac{\partial T}{\partial r}\right\}_A\right\}$ (i)

and from zz = 0 $\frac{\partial\gamma}{\partial z} = -\frac{1}{r}\frac{\partial X}{\partial r}$ also $\gamma_B = \gamma_O + b\frac{\partial\gamma}{\partial r} + \frac{b^2}{2}\frac{\partial^2\gamma}{\partial r^2}$

$$V^2\gamma = 0 = \frac{2}{a^2}\{\gamma_A - \gamma_O\} + \frac{2}{b^2}\{\gamma_B - \gamma_O\} - \frac{2}{a}\frac{\partial\gamma}{\partial z} - \left\{\frac{2}{b} - \frac{1}{r}\right\}\frac{\partial\gamma}{\partial r} \quad \text{(ii)}$$

and from rr = 0 $\frac{\partial}{\partial r}\left\{\frac{X}{r}\right\} = \frac{\sigma}{1-\sigma}\frac{\partial\gamma}{\partial z} - \frac{E\alpha T}{1-\sigma} = \frac{1}{r}\frac{\partial X}{\partial r} - \frac{X}{r^2}$ (iii)

and from rz = 0 $\frac{\partial X}{\partial z} = r\frac{\partial\gamma}{\partial r}$ (iv)

whence

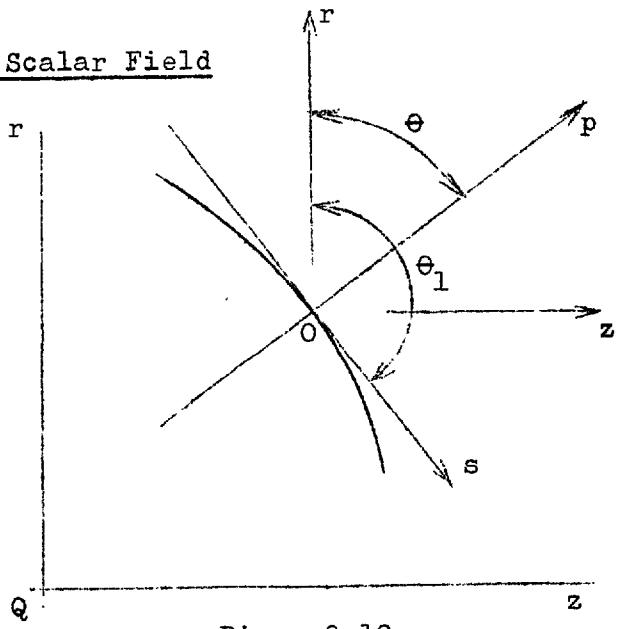
$$I^2X = 0 = \frac{2}{a^2}\{X_A - X_O\} + \frac{2}{b^2}\{X_B - X_O\} - \left\{\frac{2}{b} + \frac{1}{r}\right\}X_O - \frac{2}{a}\frac{\partial X}{\partial z} - \left\{\frac{2}{b} + \frac{1}{r}\right\}\left\{r\frac{\partial}{\partial r}\left\{\frac{X}{r}\right\}\right\} \quad \text{(v)}$$

In using these equations it is important to note that point A refers to the point adjacent to the corner and on the <u>axial</u> boundary direction. The governing equation for γ is equation (ii) in which $\left\{\frac{\partial\gamma}{\partial r}\right\}_O$ is given by equation (i) and $\frac{\partial\gamma}{\partial z} = -\frac{1}{r}\frac{\partial X}{\partial r}$ The governing equation for X is equation (v) and $\frac{\partial}{\partial r}\left\{\frac{X}{r}\right\}$ is given by equation (iii) and $\frac{\partial X}{\partial z}$ by equation (iv). $\left\{\frac{\partial\gamma}{\partial r}\right\}_A$ in equation (i) is calculated at point A in the normal manner when setting up the equations at point A.

Appendix 2.1

Directional Derivatives of a Scalar Field

If γ is a function varying according to position in the rQz plane, where r and z are two directions mutually at right angles then the derivatives of γ in any two other directions, p and s, also mutually at right angles, can be expressed as follows.



Diag. 2.10

$$\frac{\partial\gamma}{\partial p} = \cos\theta\frac{\partial\gamma}{\partial r} + \sin\theta\frac{\partial\gamma}{\partial z} \qquad (1)$$

where θ is the angle between the r direction and the p direction, measured clockwise

$$\text{and } \frac{\partial\gamma}{\partial s} = \cos\theta_1\frac{\partial\gamma}{\partial r} + \sin\theta_1\frac{\partial\gamma}{\partial z} \qquad (2)$$

where θ_1 is the angle between the r direction and the s direction, measured clockwise.

By definition, the angle between the p direction and the s direction is $\frac{\pi}{2}$

Therefore $\theta_1 = \theta + \frac{\pi}{2}$

$$\sin\theta_1 = \sin\left\{\theta + \frac{\pi}{2}\right\} = \cos\theta$$

$$\cos\theta_1 = \cos\left\{\theta + \frac{\pi}{2}\right\} = -\sin\theta$$

whence (2) becomes, in terms of θ, $\frac{\partial\gamma}{\partial s} = -\sin\theta\frac{\partial\gamma}{\partial r} + \cos\theta\frac{\partial\gamma}{\partial z}$

From (1) it is apparent that

$$\frac{\partial}{\partial p} = \cos\theta\frac{\partial}{\partial r} + \sin\theta\frac{\partial}{\partial z} \qquad (3)$$

Therefore

$$\frac{\partial}{\partial p}\left\{\frac{\partial \gamma}{\partial p}\right\} = \left\{\cos\theta \frac{\partial}{\partial r} + \sin\theta \frac{\partial}{\partial z}\right\}\left\{\cos\theta \frac{\partial \gamma}{\partial r} + \sin\theta \frac{\partial \gamma}{\partial z}\right\}$$

$$\text{i.e. } \frac{\partial^2 \gamma}{\partial p^2} = \cos^2\theta \frac{\partial^2 \gamma}{\partial r^2} + 2\cos\theta \sin\theta \frac{\partial^2 \gamma}{\partial r \partial z} + \sin^2\theta \frac{\partial^2 \gamma}{\partial z^2} \qquad (4)$$

During the derivation of (4) the angle is considered constant in the p direction. It is desirable to consider the possibility of the s direction being curved, i.e. $\frac{\partial \theta}{\partial s} \neq 0$.

From (3)

$$\frac{\partial}{\partial s} = -\sin\theta \frac{\partial}{\partial r} + \cos\theta \frac{\partial}{\partial z}$$

$$\frac{\partial}{\partial s}\left\{\frac{\partial \gamma}{\partial s}\right\} = \frac{\partial}{\partial s}\left\{-\sin\theta \frac{\partial \gamma}{\partial r} + \cos\theta \frac{\partial \bar{\gamma}}{\partial \underline{z}}\right\}$$

$$= -\sin\theta \frac{\partial}{\partial s}\left\{\frac{\partial \gamma}{\partial r}\right\} + \cos\theta \frac{\partial}{\partial s}\left\{\frac{\partial \gamma}{\partial z}\right\} - \frac{\partial \gamma}{\partial r}\frac{\partial}{\partial s}(\sin\theta) + \frac{\partial \gamma}{\partial z}\frac{\partial}{\partial s}(\cos\theta)$$

$$= -\sin\theta \left\{-\sin\theta \frac{\partial}{\partial r} + \cos\theta \frac{\partial}{\partial \underline{z}}\right\}\frac{\partial \gamma}{\partial r} + \cos\theta\left\{-\sin\theta \frac{\partial}{\partial r} + \cos\theta \frac{\partial}{\partial \underline{z}}\right\}\frac{\partial \gamma}{\partial z}$$

$$- \frac{\partial \gamma}{\partial r}.\cos\theta.\frac{\partial \theta}{\partial s} - \frac{\partial \gamma}{\partial z}\sin\theta.\frac{\partial \theta}{\partial s}$$

and using (1) this becomes

$$\frac{\partial^2 \gamma}{\partial s^2} = \sin^2\theta \frac{\partial^2 \gamma}{\partial r^2} - 2\sin\theta\cos\theta \frac{\partial^2 \gamma}{\partial r \partial z} + \cos^2\theta \frac{\partial^2 \gamma}{\partial z^2} - \frac{\partial \gamma}{\partial p}.\frac{\partial \theta}{\partial s} \qquad (5)$$

similarly

$$\frac{\partial}{\partial s}\left\{\frac{\partial \gamma}{\partial p}\right\} = \frac{\partial}{\partial s}\left\{\cos\theta \frac{\partial \gamma}{\partial r} + \sin\theta \frac{\partial \bar{\gamma}}{\partial \underline{z}}\right\}$$

$$= \cos\theta \frac{\partial}{\partial s}\left\{\frac{\partial \gamma}{\partial r}\right\} + \sin\theta \frac{\partial}{\partial s}\left\{\frac{\partial \gamma}{\partial z}\right\} + \frac{\partial \gamma}{\partial r}\frac{\partial}{\partial s}(\cos\theta) + \frac{\partial \gamma}{\partial z}\frac{\partial}{\partial s}(\sin\theta)$$

$$\frac{\partial^2 \gamma}{\partial s \partial p} = -\sin\theta\cos\theta \frac{\partial^2 \gamma}{\partial r^2} + (\cos^2\theta - \sin^2\theta)\frac{\partial^2 \gamma}{\partial r \partial z} + \sin\theta\cos\theta \frac{\partial^2 \gamma}{\partial z^2} + \frac{\partial \gamma}{\partial s}\frac{\partial \theta}{\partial s} \qquad (6)$$

N.B. if $\frac{\partial \theta}{\partial s} \neq 0$ $\quad \frac{\partial^2 \gamma}{\partial s \partial p} \neq \frac{\partial^2 \gamma}{\partial p \partial s}$ in this system.

Appendix 2.2

To express r and z derivatives of γ in terms of p and s derivatives of γ

The equations (1), (3), (4), (5) and (6) can be rewritten to express r and z derivatives as follows

From (1) and (3)

$$\frac{\partial\gamma}{\partial z} = \cos\theta \frac{\partial\gamma}{\partial s} + \sin\theta \frac{\partial\gamma}{\partial p} \tag{7}$$

$$\frac{\partial\gamma}{\partial r} = \cos\theta \frac{\partial\gamma}{\partial p} - \sin\theta \frac{\partial\gamma}{\partial s} \tag{8}$$

and adding (4) and (5)

$$\frac{\partial^2\gamma}{\partial r^2} + \frac{\partial^2\gamma}{\partial z^2} = \frac{\partial^2\gamma}{\partial p^2} + \frac{\partial^2\gamma}{\partial s^2} + \frac{\partial\gamma}{\partial p}.\frac{\partial\theta}{\partial s} \tag{9}$$

hence from (8) and (9)

$$V^2\gamma = \frac{\partial^2\gamma}{\partial p^2} + \frac{\partial^2\gamma}{\partial s^2} + \frac{\cos\theta}{r}\frac{\partial\gamma}{\partial p} - \frac{\sin\theta}{r}\frac{\partial\gamma}{\partial s} + \frac{\partial\gamma}{\partial p}.\frac{\partial\theta}{\partial s} \tag{10}$$

and using (5) - (4) in conjunction with (6)

$$\frac{\partial^2\gamma}{\partial r\partial z} = \left\{\frac{\partial^2\gamma}{\partial s\partial p} - \frac{\partial\gamma}{\partial s}.\frac{\partial\theta}{\partial s}\right\}\cos 2\theta - \left\{\frac{\partial^2\gamma}{\partial s^2} - \frac{\partial^2\gamma}{\partial p^2} + \frac{\partial\gamma}{\partial p}.\frac{\partial\theta}{\partial s}\right\}\frac{\sin 2\theta}{2} \tag{11}$$

Appendix 2.3

To express r and z derivatives of $\begin{Bmatrix} X \\ \overline{r} \end{Bmatrix}$ in terms of p and s derivatives of $\begin{Bmatrix} X \\ \overline{r} \end{Bmatrix}$

The value of $I^2(X)$ in terms of $\begin{Bmatrix} X \\ \overline{r} \end{Bmatrix}$ can be ascertained as follows:

$$\frac{\partial}{\partial r}\begin{Bmatrix} X \\ \overline{r} \end{Bmatrix} = \frac{1}{r}\frac{\partial X}{\partial r} - \frac{X}{r^2}$$

$$\frac{\partial^2}{\partial r^2}\begin{Bmatrix} X \\ \overline{r} \end{Bmatrix} = \frac{1}{r}\frac{\partial^2 X}{\partial r^2} - \frac{1}{r^2}\frac{\partial X}{\partial r} - \frac{1}{r^2}\frac{\partial X}{\partial r} + \frac{2X}{r^3} = \frac{1}{r}\frac{\partial^2 X}{\partial r^2} - \frac{2}{r^2}\frac{\partial X}{\partial r} + \frac{2X}{r^3}$$

i.e. $$\frac{1}{r}\frac{\partial X}{\partial r} = \frac{\partial}{\partial r}\begin{Bmatrix} X \\ \overline{r} \end{Bmatrix} + \frac{X}{r^2}$$

$$\frac{\partial^2 X}{\partial r^2} = r\frac{\partial^2}{\partial r^2}\begin{Bmatrix} X \\ \overline{r} \end{Bmatrix} + \frac{2}{r}\frac{\partial X}{\partial r} - \frac{2X}{r^2} = r\frac{\partial^2}{\partial r^2}\begin{Bmatrix} X \\ \overline{r} \end{Bmatrix} + 2\frac{\partial}{\partial r}\begin{Bmatrix} X \\ \overline{r} \end{Bmatrix}$$

$$\frac{\partial^2 X}{\partial r^2} - \frac{1}{r}\frac{\partial X}{\partial r} = r\frac{\partial^2}{\partial r^2}\begin{Bmatrix} X \\ \overline{r} \end{Bmatrix} + \frac{\partial}{\partial r}\begin{Bmatrix} X \\ \overline{r} \end{Bmatrix} - \frac{X}{r^2}$$

Therefore $$I^2X = \frac{\partial^2 X}{\partial r^2} - \frac{1}{r}\frac{\partial X}{\partial r} + \frac{\partial^2 X}{\partial z^2}$$

$$= r\frac{\partial^2}{\partial r^2}\begin{Bmatrix} X \\ \overline{r} \end{Bmatrix} + \frac{\partial}{\partial r}\begin{Bmatrix} X \\ \overline{r} \end{Bmatrix} + r\frac{\partial^2}{\partial z^2}\begin{Bmatrix} X \\ \overline{r} \end{Bmatrix} - \frac{X}{r^2}$$

$$I^2X = rV^2\begin{Bmatrix} X \\ \overline{r} \end{Bmatrix} - \frac{X}{r^2} \qquad (12)$$

Substitute $\frac{X}{r}$ for γ in equation (10) appendix 2.2

$$\frac{1}{r}\cdot I^2X = \frac{\partial^2}{\partial p^2}\begin{Bmatrix} X \\ \overline{r} \end{Bmatrix} + \frac{\partial^2}{\partial s^2}\begin{Bmatrix} X \\ \overline{r} \end{Bmatrix} + \frac{\cos\theta}{r}\frac{\partial}{\partial p}\begin{Bmatrix} X \\ \overline{r} \end{Bmatrix} - \frac{\sin\theta}{r}\frac{\partial}{\partial s}\begin{Bmatrix} X \\ \overline{r} \end{Bmatrix} + \frac{\partial}{\partial p}\begin{Bmatrix} X \\ \overline{r} \end{Bmatrix}\cdot\frac{\partial\theta}{\partial s} - \frac{X}{r^3} \qquad (13)$$

Appendix 2.4

Alternative Stress Function η

The early experimental computing used stress function η instead of γ. η was derived in a similar manner to γ; from (16)

$$\nabla^2\{\bar{(1-\sigma)}\ \nabla^2\bar{\mu}\} + \nabla^2\ (E\alpha T) = 0 \tag{18i}$$

Putting $\frac{\partial\eta}{\partial z} = \nabla^2\mu$ (19i)

$$(1-\sigma)\frac{\partial}{\partial z}(\nabla^2\eta) + \nabla^2 E\alpha T = 0 \tag{20i}$$

$$\text{i.e. } (1-\sigma)\nabla^2\eta + \int \nabla^2 E\alpha T dz = 0 \tag{21i}$$

and for steady state temperature distribution this can be written

$$\nabla^2\eta = 0. \quad = \frac{\partial^2\eta}{\partial r^2} + \frac{1}{r}\frac{\partial\eta}{\partial r} + \frac{\partial^2\eta}{\partial z^2}$$

and using X as before, i.e. $\frac{\partial\mu}{\partial r} = \frac{X}{r}$, and $\frac{\partial^2\eta}{\partial r\partial z} = \frac{\partial}{\partial r}(\nabla^2\mu)$ this becomes

$$I^2X = r\frac{\partial^2\eta}{\partial r\partial z} = \frac{\partial^2 X}{\partial r^2} - \frac{1}{r}\frac{\partial X}{\partial r} + \frac{\partial^2 X}{\partial z^2} \tag{24i}$$

and the stresses become

$$\left.\begin{aligned}
\theta\theta &= \sigma\frac{\partial\eta}{\partial z} - \frac{X}{r^2} - E\alpha T \\
rr &= \sigma\frac{\partial\eta}{\partial z} - \frac{\partial}{\partial r}\left\{\frac{X}{r}\right\} - E\alpha T \\
zz &= (1-\sigma)\frac{\partial\eta}{\partial z} + \frac{1}{r}\frac{\partial X}{\partial r} + E\alpha T \\
rz &= (1-\sigma)\frac{\partial\eta}{\partial r} - \frac{1}{r}\frac{\partial X}{\partial z} + \int E\alpha\frac{\partial T}{\partial r}dz \\
&\qquad\qquad \text{after integrating.}
\end{aligned}\right\} \tag{25i}$$

The two temperature integrals can be computed by numerical integration methods. Using the same approach as that outlined for γ, the relaxation equations for η differ from those for γ only in the values of the equation constants. The relaxation characteristics for η and γ are, therefore, similar.

η was originally favoured because the presence of the two temperature integrals suggested that a more complete picture of the body was incorporated in the equations for each point and there was a possibility that this would improve convergence. It now seems less likely that this view is correct and the evaluation of the two temperature integrals by numerical methods can introduce large errors, and be very wasteful of time, especially for transient conditions.

The first computed solution given is steady state and the η function was used. This solution gave no indication that the temperature integrals influenced convergence and so the later solutions employed the γ function. This showed that γ is in no way inferior to η and, not requiring the integration terms, is probably quicker and more accurate.

The method of developing boundary equations, etc., for η is exactly the same as that given for γ and will not, therefore, be given.

Appendix 2·5

Centrifugal Stresses

The difficulties which were encountered in the thermal stress problem were all factors of the relaxation method, the prime difficulty being the choice of stress functions and the transformation of the resulting boundary equations into easily relaxable finite difference form. This being so, there is no foreseeable barrier to the inclusion of centrifugal components in the equations given earlier.

To include centrifugal components the stress equilibrium equation (5) becomes: $\frac{\partial rr}{\partial r} + \frac{\partial rz}{\partial z} + \frac{rr - \theta\theta}{r} + mr = 0$ (5ii)

After taking this through the analysis the biharmonic equation, (16) becomes $$V^2\left\{\overline{(1-\sigma)V^2\mu + E\alpha T + \left\{\frac{3-2\sigma}{2}\right\}mr^2}\right\} = 0 \quad (16ii)$$

where $m = \frac{\text{density x (angular velocity)}^2}{g}$ and the stress, (17) are

$$\left.\begin{aligned} \theta\theta &= \sigma V^2\mu - \frac{1}{r}\frac{\partial \mu}{\partial r} - E\alpha T - \left\{\frac{1-2\sigma}{2}\right\}mr^2 \\ rr &= \sigma V^2\mu - \frac{\partial^2 \mu}{\partial r^2} - E\alpha T - \left\{\frac{3-2\sigma}{2}\right\}mr^2 \\ zz &= (2-\sigma)V^2\mu - \frac{\partial^2 \mu}{\partial z^2} + E\alpha T + (3-\sigma)mr^2 \\ \frac{\partial rz}{\partial z} &= (1-\sigma)\frac{\partial}{\partial r}(V^2\mu) - \frac{\partial^3 \mu}{\partial r \partial z^2} + E\alpha\frac{\partial T}{\partial r} + (3-2\sigma)mr \end{aligned}\right\} \quad (17ii)$$

To express these equations in terms of X and γ it is suggested that the following substitution be made,

$$\frac{\partial \gamma}{\partial z} = (1-\sigma)V^2\mu + E\alpha T + \left\{\frac{3-2\sigma}{2}\right\}mr^2 \quad (19ii)$$

and $X = r\frac{\partial \mu}{\partial r} + \frac{3}{8}\cdot m.r^4$ (22ii)

giving $V^2\gamma = 0$ (21ii)

$$I^2X = \frac{r}{1-\sigma}\left\{\overline{\frac{\partial^2 \gamma}{\partial r \partial z} - E\alpha\frac{\partial T}{\partial r} - \sigma.mr}\right\} \quad (24ii)$$

$$\left.\begin{aligned} \theta\theta &= \frac{\sigma}{1-\sigma}\frac{\partial\gamma}{\partial z} - \frac{X}{r^2} - \frac{E\alpha T}{1-\sigma} - \left\{\frac{1+3\sigma}{8(1-\sigma)}\right\}mr^2 \\ rr &= \frac{\sigma}{1-\sigma}\frac{\partial\gamma}{\partial z} - \frac{\partial}{\partial r}\left\{\frac{X}{r}\right\} - \frac{E\alpha T}{1-\sigma} - \left\{\frac{3+\sigma}{8(1-\sigma)}\right\}mr^2 \\ zz &= \frac{\partial\gamma}{\partial z} + \frac{1}{r}\frac{\partial X}{\partial r} \qquad rz = \frac{\partial\gamma}{\partial z} - \frac{1}{r}\frac{\partial X}{\partial z} \end{aligned}\right\} \quad (25ii)$$

Comparing these equations with the equations without the centrifugal components, i.e. (19), (21), (22), (24) and (25) it is apparent that the boundary equation in finite difference form for γ and X can be used with the minimum of modification. Thus the governing equation for γ, and the two stresses used in the boundary condition are unaltered therefore the universal boundary equation for γ, (44) the equation for $\frac{\partial^2\gamma}{\partial r\partial z}$, (48) and the value of G, (35) require no modification.

Some modification will be required in the boundary equation $\frac{\partial}{\partial p}\left\{\frac{X}{r}\right\} = K$ since rr contains a centrifugal component.

Putting rr and rz from (25ii) into the stress boundary conditions $rr\cos\theta + rz\sin\theta = 0$ gives

$$K = -\frac{\partial\gamma}{\partial s} + \left\{\frac{\partial\gamma}{\partial z} - E\alpha T - \frac{(3+\sigma)mr^2}{8}\right\}\frac{\cos\theta}{1-\sigma} \quad (32ii)$$

Hence the only modification required in the use of the universal boundary equations is the calculation of K from (32ii) instead of (32). Also, of course, at all mesh points the value of I^2X is as given in equation (24ii) instead of (24).

No relaxation involving these centrifugal components has been performed but it is inconceivable that any serious problem will arise in their application.

It should be noted that these equations are quite suitable for the centrifugal stress problem without the inclusion of the thermal components. If T is constant throughout the body, $E\alpha T$ is a constant and can be considered to be included in a stress function, hence in all equations, $E\alpha T$ can be ignored. Southwell considers this problem (ref.4) deriving the governing equations and stresses using stress functions akin to those given in Section 2:2:1 but gives no indication that the problem was taken beyond this stage.

Appendix 2.6

Pressure Stresses

The stresses due to pressures acting on the boundary can also be included along with centrifugal and thermal components by a modification of the boundary stress conditions. As fluid pressures act normally to the surface the stress boundary equations become

$$rr \cos\theta + rz \sin\theta + P \cos\theta = 0$$

and

$$zz \sin\theta + rz \cos\theta + P \sin\theta = 0$$

where P is the pressure.

This requires some modification to G (equation 35) and K (equation 32ii) as follows

$$G = \frac{1}{r}\frac{\partial X}{\partial s} - P \sin\theta \qquad (35iii)$$

$$K = -\frac{\partial Y}{\partial s} + \left\{\frac{\partial Y}{\partial z} - E\alpha T - \frac{(3+\sigma)mr^2}{8} + (1-\sigma)P\right\}\frac{\cos\theta}{(1-\sigma)} \qquad (32iii)$$

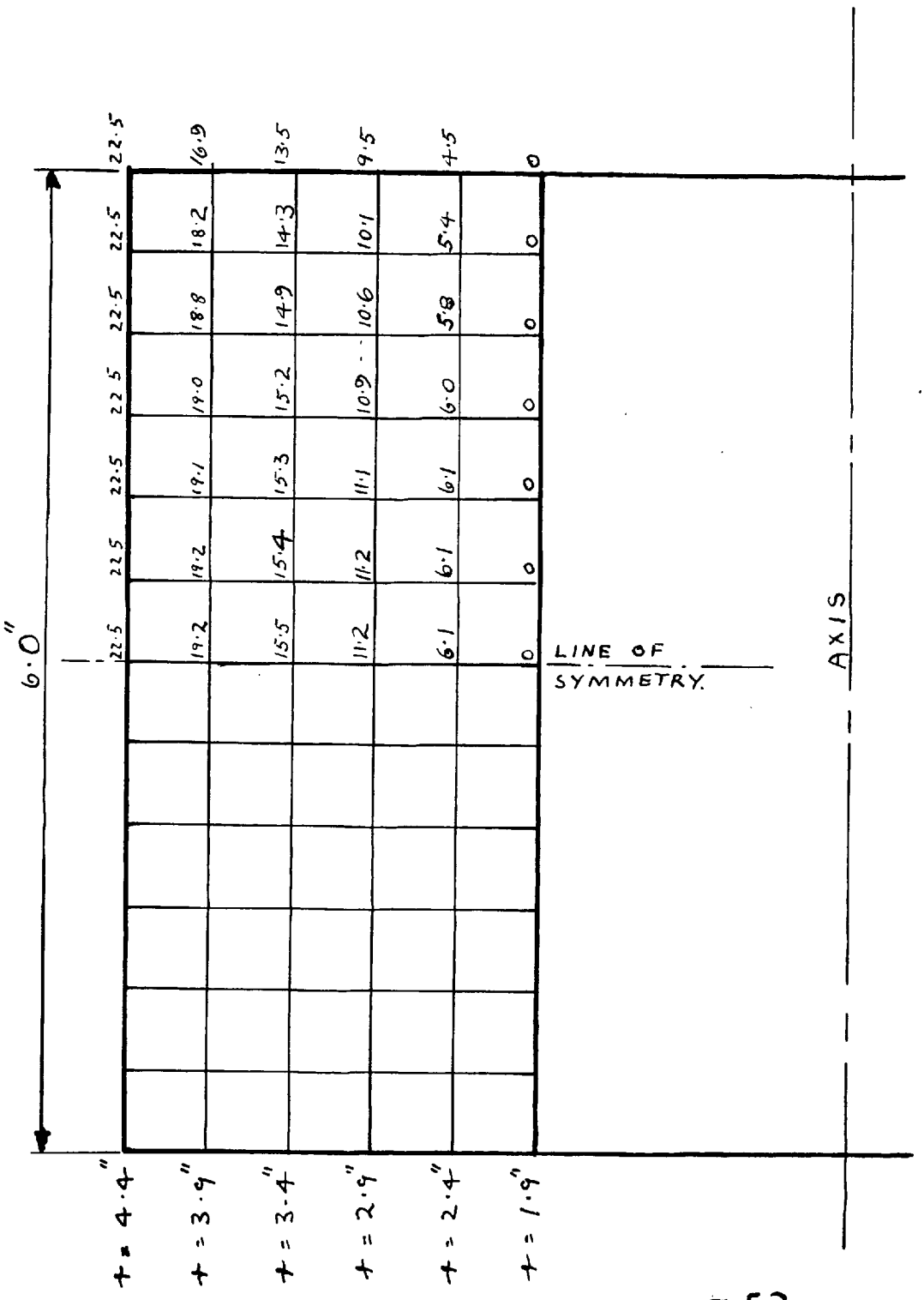
Thus the inclusion of both pressure and centrifugal components need not require a change of stress function form. It has been shown that the only changes required are the inclusion of known constants in the finite difference equations, a change which is of little significance to the relaxation process.

The pressure problem alone has been fairly extensively considered by Southwell, Allen, Fox et al (see ref. 4) and a number of solutions, by relaxation, have been obtained to such exercises as gun barrels and shells. In general the boundaries in these solutions are straight and used the Southwell stress functions. It is in this type of problem that much of the experience of the behaviour of these functions has been obtained. No satisfactory approach to curved boundaries was evolved and it is considered that the equations and techniques given here will have definite advantages over those given by Southwell.

COMPUTATION NO. 1

SPECIMENS A & B

DIMENSIONS & VALUES OF E&T (TN/IN²)



COMPUTATION NO. 1
SPECIMENS A & B
STRESSES (TN/IN^2)

RADIAL	HOOP
SHEAR	AXIAL

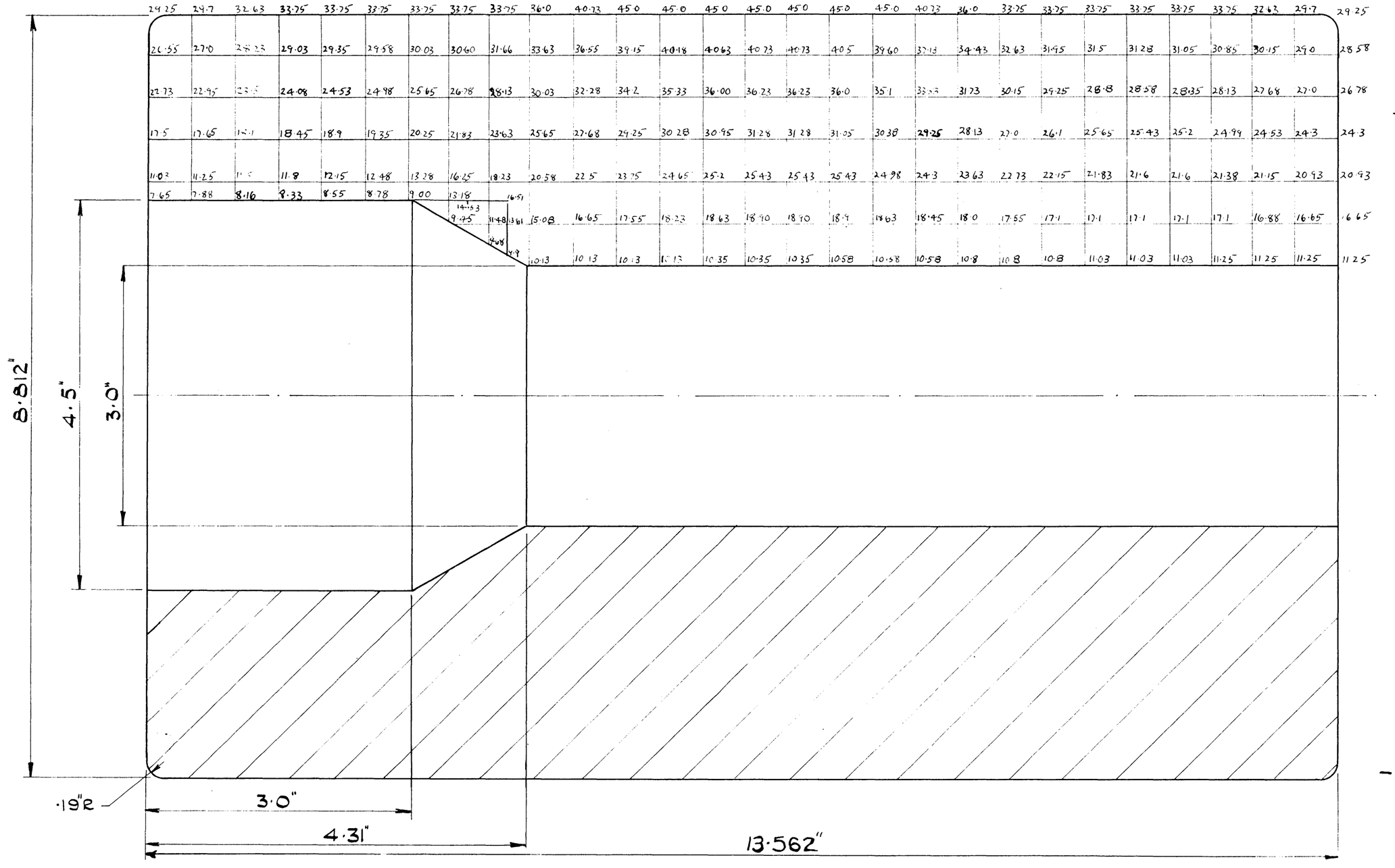
r = 4.4"	0	-8.17	+.16	-8.21	+.29	-8.37	+.19	-8.71	+.21	-9.42	+.14	-11.02	+.05	-12.27
	0	-4.58	0	-4.44	0	-3.76	0	-2.54	0	-1.39	0	-.51	0	0
	+1.19	-5.15	+1.19	-5.24	+1.25	-5.45	+1.33	-5.97	+1.13	-6.83	+1.36	-8.0	+2.88	-8.68
	0	-3.02	+.42	-2.88	+.77	-2.35	+.97	-2.11	+.85	-1.19	+.45	-.65	0	+.01
	+2.39	-1.43	+2.32	-1.52	+2.23	-1.93	+2.04	-2.66	+1.94	-3.78	+1.95	-5.29	+2.45	-7.32
	0	-1.33	+.62	-1.25	+1.13	-1.14	+1.44	-.98	+1.34	-.78	+.9	-.33	-.18	0
	+3.26	+3.42	+3.27	+3.23	+3.02	+2.66	+2.85	+1.65	+2.49	+.09	+2.2	-2.07	+2.29	-5.08
	0	+.86	+.69	+.78	+1.27	+.66	+1.64	+.26	+1.66	+.06	+1.27	0	+.07	+.01
	+3.2	+10.29	+3.11	+10.05	+2.91	+9.22	+2.55	+2.72	+2.22	+5.47	+1.92	+2.37	+1.86	-1.5
	0	+4.28	+.49	+4.12	+.95	+3.51	+1.24	+2.67	+1.42	+1.62	+1.15	+.63	+.11	0
r = 1.9"	+.23	+21.44	-.03	+20.94	+.08	+19.71	+.18	+17.39	+.06	+13.91	0	+9.01	+.05	+2.43
	0	+10.05	0	+9.73	-.01	+8.43	+.01	+6.39	0	+4.23	-.01	+1.99	-.01	0

COMPUTATION NO. 2

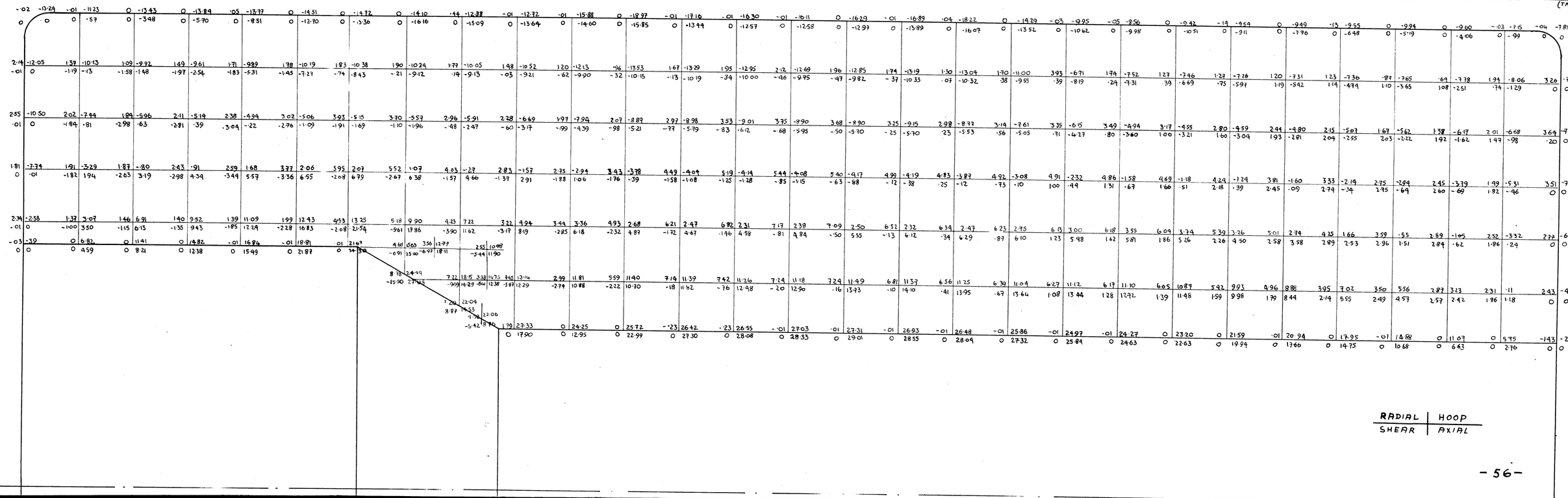
SPECIMEN C

DIMENSIONS & VALUES OF E∝T

(TN/IN²)



29.25	29.7	32.63	33.75	33.75	33.75	33.75	33.75	33.75	36.0	40.73	45.0	45.0	45.0	45.0	45.0	45.0	45.0	40.73	36.0	33.75	33.75	33.75	33.75	33.75	33.75	32.63	29.7	29.25
26.55	27.0	28.23	29.03	29.35	29.58	30.03	30.60	31.66	33.63	36.55	39.15	40.18	40.63	40.73	40.73	40.5	39.60	37.13	34.43	32.63	31.95	31.5	31.28	31.05	30.85	30.15	29.0	28.58
22.73	22.95	23.5	24.08	24.53	24.98	25.65	26.78	28.13	30.03	32.28	34.2	35.33	36.00	36.23	36.23	36.0	35.1	33.23	31.73	30.15	29.25	28.8	28.58	28.35	28.13	27.68	27.0	26.78
17.5	17.65	18.1	18.45	18.9	19.35	20.25	21.83	23.63	25.65	27.68	29.25	30.28	30.95	31.28	31.28	31.05	30.38	29.25	28.13	27.0	26.1	25.65	25.43	25.2	24.99	24.53	24.3	24.3
11.02	11.25	11.5	11.8	12.15	12.48	13.28	16.25	18.23	20.58	22.5	23.75	24.65	25.2	25.43	25.43	25.43	24.98	24.3	23.63	22.73	22.15	21.83	21.6	21.6	21.38	21.15	20.93	20.93
7.65	7.88	8.16	8.33	8.55	8.78	9.00	13.18	14.53	15.08	16.65	17.55	18.23	18.63	18.90	18.90	18.9	18.63	18.45	18.0	17.55	17.1	17.1	17.1	17.1	17.1	16.88	16.65	16.65
							9.45	11.48	13.61	10.13	10.13	10.13	10.13	10.35	10.35	10.35	10.58	10.58	10.58	10.8	10.8	10.8	11.03	11.03	11.03	11.25	11.25	11.25



RADIAL	HOOP
SHEAR	AXIAL

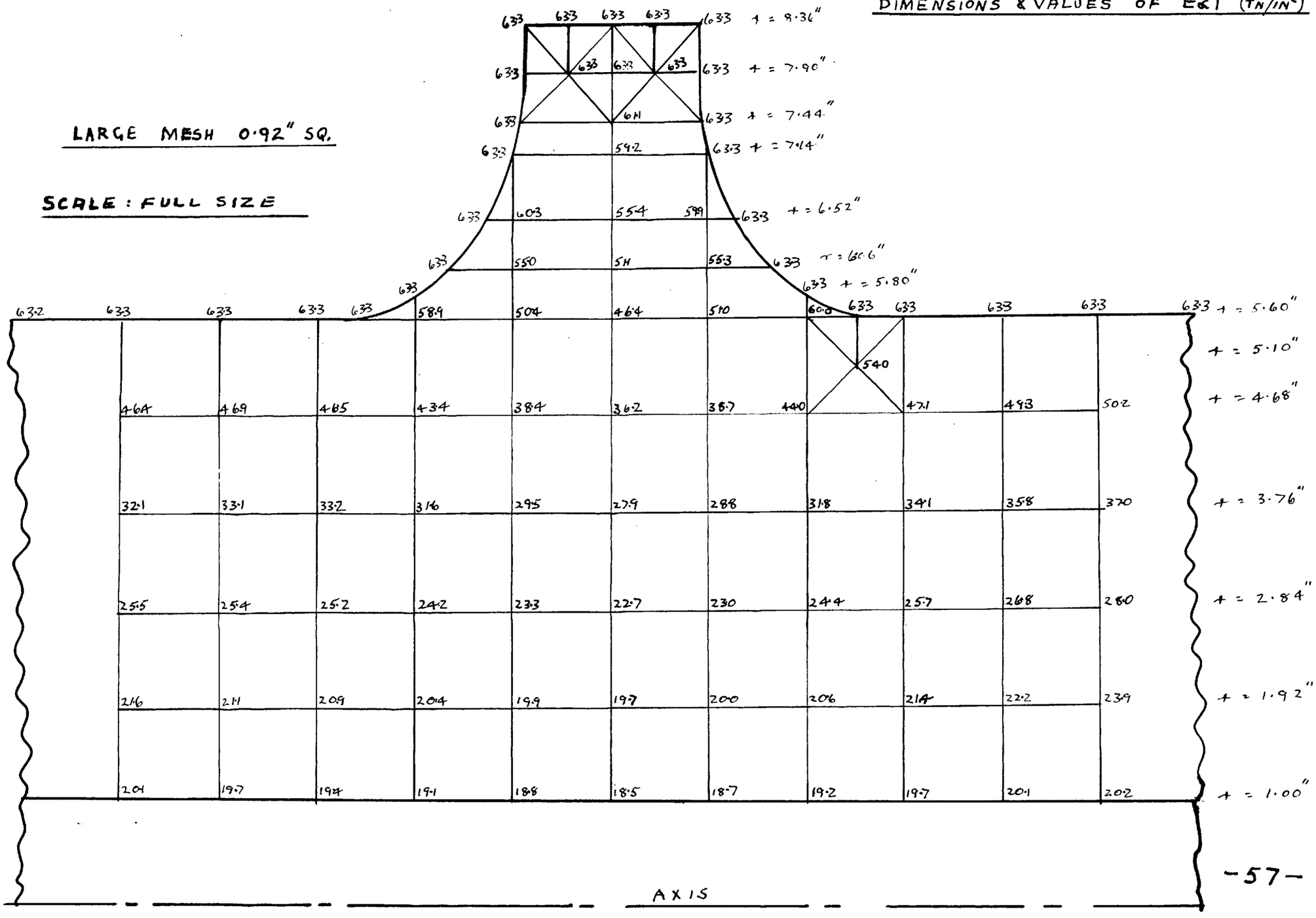
COMPUTATION NO 3

SIMULATION OF IMPULSE WHEEL OF H.P. ROTOR

DIMENSIONS & VALUES OF E∝T (TN/IN²)

LARGE MESH 0·92" SQ.

SCALE : FULL SIZE



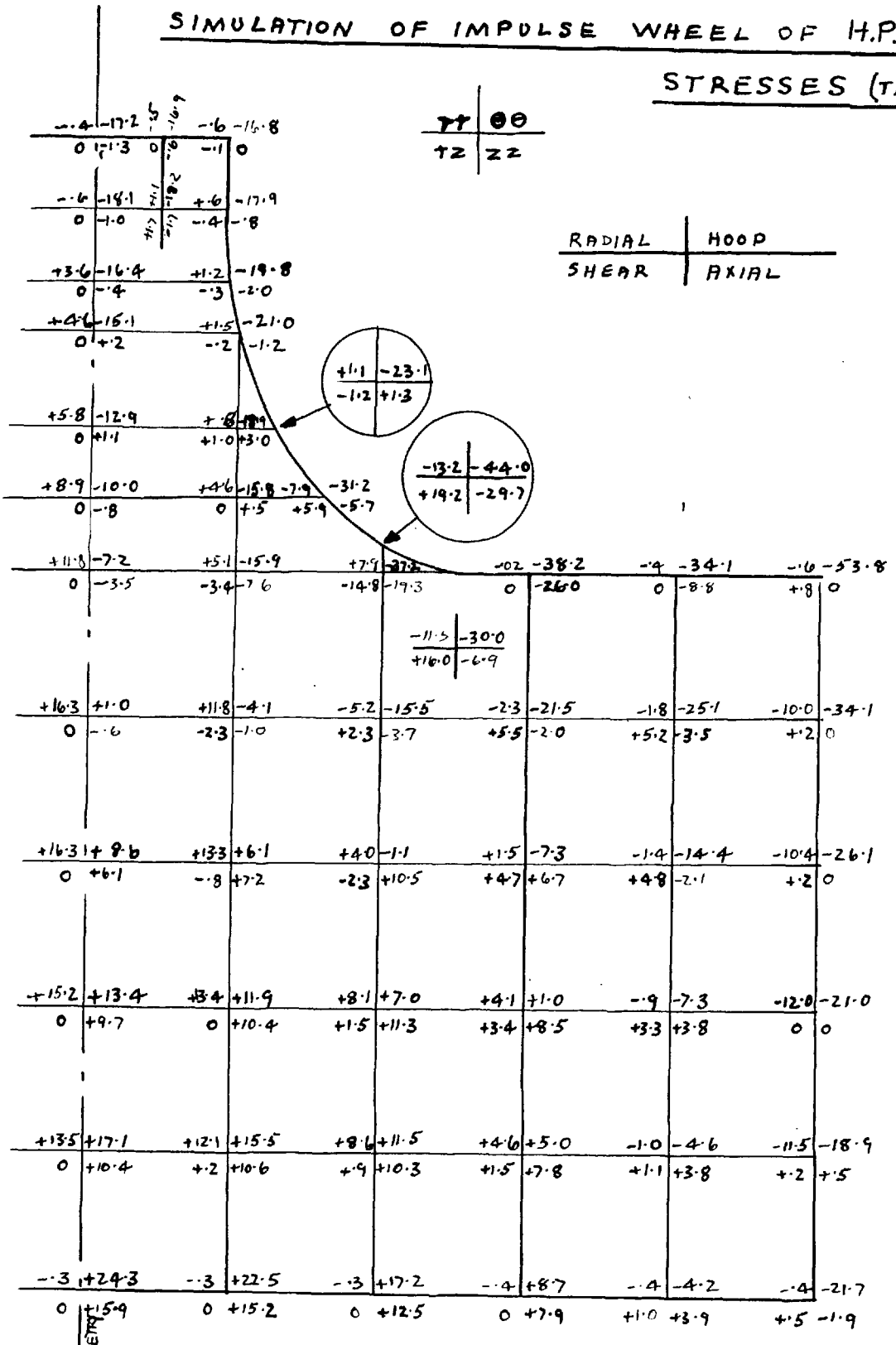
COMPUTATION NO. 3

SIMULATION OF IMPULSE WHEEL OF H.P. ROTOR

STRESSES (TN/IN²)

RR	θθ
RZ	ZZ

RADIAL	HOOP
SHEAR	AXIAL



3. THE THERMAL STRESSES IN AN OVERSTRAINED AXIALLY SYMMETRICAL BODY

The problem of plastic strains associated with thermal stresses in axially symmetrical bodies has not yet received a rigorous treatment. The general case, with the shear stress rz present, is beyond a reasonable approach and is not likely to yield to a satisfactory solution until the similar, but simpler, problem of pressure stressing with shear stress, rz, present can be performed.

Any attempt at a rigorous statement of the problem will require an iterative method of solution since this is true of the elastic body. The shear stress, rz, cannot be ignored in a small highly stressed area (see ref. 3). The plastic flow criterion used might be either the maximum shear stress or von Mises. The maximum shear stress criterion loses its simplicity if the shear stress, rz, is added and as the direction of maximum shear stress depends upon the stress system (usually $\theta\theta > zz > rr$ but $zz > \theta\theta > rr$ is possible, see ref. 3) it is more satisfactory to have one approach using the von Mises criterion. A rigorous statement of the problem includes the variation of the plastic modulus in both the radial and the axial direction $\left\{\text{from } \frac{\partial^2 w}{\partial r \partial z} = \frac{\partial^2 w}{\partial z \partial r} \text{ and } r\frac{\partial}{\partial r}\left\{\frac{u}{r}\right\} = \frac{\partial u}{\partial r} - \frac{u}{r}\right\}$ and this inevitably creates a huge amount of extra computation even if the total strain theory is used. No satisfactory approximations were discovered and the general case had to be abandoned.

Some idea of the severity of plastic strains can be obtained from solutions for discs and long cylinders and attention was therefore directed at these two problems.

A method of solving centrifugal and thermal stresses in discs of variable thickness was proposed by Brooking et al. (ref. 9). This uses total strain theory and the flow criterion is von Mises. Numerical solution is by an iterative process. Brooking's approach could be used for simple plane stress but little advantage is gained by assuming constant thickness since the use of

von Mises criterion prevents simple integration. Nor does Brooking attempt any solutions for thermal stresses alone and in the solutions given the thermal effects are obscured by the greater centrifugal effects. The simple plane stress problem can be solved much more simply and more quickly using the appropriate maximum shear stress criterion. Such a solution was therefore developed.

Bland (ref. 10) considers the plastic strains produced by both pressure and temperature loading in the case of a long cylinder. The flow criterion is the maximum shear stress, $\frac{\theta\theta - rr}{2}$, but this assumption is not valid in a plastic zone at the bore formed by steady state temperature conditions only. As the first plastic zone formed by a steady state temperature distribution is at the bore, this invalidates Bland's analysis for thermal stresses alone.

The problems of pressure stresses and temperature stresses in axially-symmetrical cylinders are allied problems in most respects. Many solutions of the pressure problem have been proposed. In almost all cases a single plastic zone (in the bore) is assumed, and the maximum shear stress $\frac{\theta\theta - rr}{2}$ is used; total strain theories are adopted and various methods of including work-hardening are proposed. Some of these solutions might be adaptable for an outer plastic zone resulting from a transient temperature distribution due to external heating, but the general case really requires the use of the von Mises criterion. MacGregor, Coffin and Fisher (ref. 11) proposed an iterative solution of the pressure problem using the von Mises flow criterion, the total strain theory and including the possibility of a work-hardening stress-strain curve. This solution has been freely consulted in the derivation of the long cylinder theory presented later, although the actual iterative method used by MacGregor et al. is not given in their paper and is unknown.

3:1

Development of Disc and Long Cylinder Theories

The basic conditions to be satisfied for elastic and plastic analyses are

(a) axial stress is zero for a disc

(b) the axial displacement, w, is constant with radius for a long cylinder

and in both cases, compatability of strains requires

$r.\frac{d}{dr}\left\{\frac{u}{r}\right\} = \frac{du}{dr} - \frac{u}{r}$ or $r\frac{d}{dr}\{e_\theta\} + r\frac{d}{dr}(\alpha T) = e_r - e_\theta$ and with the shear stress (rz) zero, equilibrium of stresses requires $r\frac{drr}{dr} + rr - \theta\theta = 0$. Also the radial stress is zero on the boundaries. Once a plastic zone has formed a further requirement is the continuity of stresses and strains at the elastic/plastic interface.

The positions and order of appearance of plastic zones depends upon the type of temperature distribution and the extent of the effect of temperature upon the yield stress of the material. For most materials and with steady state conditions the first plastic zone appears at the bore and spreads outwards. This provides little or no stress relief for the rest of the body and if the temperature gradients are increased another plastic zone is eventually formed at the outer surface and spreads inwards. For transient conditions, the first plastic zone will usually be in the area of maximum temperature gradients. For rapid transient conditions only one zone is likely. For slow transient conditions one or two zones may form, depending upon circumstances.

The flow criterion chosen depended upon mathematical convenience.

In the disc solution, the maximum shear stress in a plastic zone adjacent to the bore is $\frac{\theta\theta}{2}$ and for an outer plastic zone is $\frac{rr - \theta\theta}{2}$. Here the use of this criterion enables simple integration to be performed and a closed form solution results,

although a small amount of iteration is used to find the radii of the elastic/plastic interfaces.

In the case of the long cylinder with open and free ends the intermediate principal stress may be either zz or $\theta\theta$ depending upon the position of the plastic zone. Bland (ref. 10) takes the maximum shear stress to be $\frac{\theta\theta - rr}{2}$ and, following the analysis, examines the applicability of this assumption for several ratios of temperature and pressure intensities for the closed end condition. From his work it is apparent that zz is greater than $\theta\theta$ for an inner plastic zone due to temperature gradients only, this deduction being equally applicable to open ends, since no end load is involved. The use of $\frac{zz - rr}{2}$ in the maximum shear stress criterion precludes simple integration and in the resultant iterative process has very little advantage over the von Mises criterion. The von Mises criterion was, therefore, adopted and used in both plastic zones.

Hence, for discs, inner plastic zone $\theta\theta = 2S_i$

outer plastic zone $rr - \theta\theta = 2S_o$

where S_i and S_o are constants and for the long cylinder, both zones

$$(rr - \theta\theta)^2 + (\theta\theta - zz)^2 + (zz - rr)^2 = 2k^2$$

where k may be a constant or a variable.

The stress-strain curve is assumed to be non-work-hardening for the disc problem, resulting in a method of solution which gives quick numerical answers with a minimum amount of iteration. The solution for long cylinders does allow for work-hardening, but such a large amount of computation is required to obtain each numerical solution, even without work-hardening, that no attempt has been made to obtain a numerical solution with work-hardening. No mathematical difficulty appears to be involved - just a very large amount of computation.

The effect of temperature on the stress-strain curve is partially allowed for in the disc solution by distinguishing between the maximum shear stresses in each zone (i.e. S_i and S_o),

and the most appropriate values can be used.

Assuming that the tensile stress-strain curves obtained at several temperatures reasonably represent the behaviour of a material under a complex stress system, it is shown that this can easily be included in the long cylinder theory (again at the cost of more computation). The method of including this effect allows either work-hardening or non-work-hardening to be assumed, and in the latter case k can be varied with temperature within a plastic zone or simply be the most appropriate constant in each zone.

The total strain theory is used for both problems, and it is assumed that strains are small enough to neglect their squares, giving the same strain-displacement relationships as in elasticity theory. Thus dimension changes are not significant.

Following the analyses numerical solutions were derived for a radius ratio of $\frac{r_o}{r_i} = 2.25$ with several steady state temperature distributions. These solutions suggest that the ratios of the plastic components of strain are constant for successively severe steady state temperature distributions, for inner and outer plastic zones and for discs and long cylinders. Strains at the bore and at the outer surface are plotted for discs on graph no. 3.2 and for long cylinders on graphs nos. 3.5 and 3.6. These plots show that the plastic components of strain are all linear with increasing mean temperature gradient, although the strain ratios for the plastic components of strain are not the same as the strain ratios for the wholly elastic body. A similar plot is obtained for points inside the plastic zones, once the material at the point becomes plastic. The stress ratios are also constant at all points in the plastic zones. Hence, within computational accuracy for the radius ratio $\frac{r_o}{r_i} = 2.25$, the stress and strain ratios are constant in the plastic zones and for these conditions the incremental and total strain theories

coincide (see Hill, ref. 12 p. 46). This suggests that little error is incurred in the use of the total strain theory.

Temperature Distribution

The analyses are suitable for steady state and moderately transient temperature conditions. Very rapid temperature changes (amounting to shock) will probably be accompanied by a stress wave which is not included in the present analyses.

In the long cylinder theory the temperature distribution is fed into the solution using the term $r\frac{dT}{dr}$. As this solution requires an iterative process and the term $r\frac{dT}{dr}$ must be known at the selected points of computation, it is of little significance whether this term is constant (as for steady state) or a known variable perhaps taken from a separate calculation of temperatures (as for transient state).

The disc theory is first developed for the general temperature distribution and includes temperature in the forms T, $r\frac{dT}{dr}$ and $\int rTdr$ (the lower limit of the integral is arbitrary and can conveniently be the bore radius, as for the wholly elastic analyses). For steady state conditions no serious difficulty arises and a semi-iterative solution results. For transient conditions a fully iterative method may be necessary, but a satisfactory semi-iterative solution may be derived by appoximating the temperature distribution to a simple equation and, for external heating, $E\alpha T = J + Mr^{Y}$ is suggested and the resultant expression derived.

Creep and Stress Relaxation are not included in the analyses. The stress changes due to creep in the disc are considered by Brooking, Brown and Atkins (ref. 9) and in an otherwise elastic cylinder by Poritsky and Fend (ref. 25) and also by Attia, Fitzgeorge and Pope (ref. 21), the latter being supported by experimental evidence.

Temperature Effects on Material Constants E and α are not specifically included in the analyses.

As the variation in E and α is small a reasonable allowance

can be made in most iterative methods by taking the most appropriate values of E and α at each point (or ring) used in the computation. This can be done in the relaxation method for elastic stresses and also in the plastic zone(s) in the long cylinder solution presented here. Nevertheless, the method of solution of the elastic zone in the cylinder would need some modification if this allowance was to extend throughout the cylinder.

Hilton (ref. 22) considered the specific problem of the effect of the variation of E and α with temperature upon thermal stresses in an elastic body and showed that the stresses were decreased and strains increased.

The Analysis of the Elastic Zones is precisely the same as that for a wholly elastic body, and can be found in some elementary text books (see, for example, Wang, ref. 23). The following expressions for stresses are obtained :-

for long cylinders, $\frac{dw}{dz}$ = constant

$$rr = A + \frac{B}{r^2} - \frac{E\alpha}{1-\sigma}\cdot\frac{1}{r^2}\int rTdr$$

$$\theta\theta = A - \frac{B}{r^2} + \frac{E\alpha}{1-\sigma}\left\{\frac{1}{r^2}\int rTdr - \overline{T}\right\}$$

$$zz = D - \frac{E\alpha T}{1-\sigma} \quad \text{where} \quad D = E\frac{dw}{dz} + 2\sigma A$$

for discs,

$$rr = A + \frac{B}{r^2} - \frac{E\alpha}{r^2}\int rTdr$$

$$\theta\theta = A - \frac{B}{r^2} + \frac{E\alpha}{r^2}\int rTdr - E\alpha T$$

The lower limit in the integral can be chosen arbitrarily, since the integration constant can be included in B.

In a wholly elastic body, the constants A and B are found by using rr = 0 at the boundaries r_o and r_i, and D from the end condition for the cylinder, for open and free ends the end load

is zero, giving $\int_{r_i}^{r_o} r\ zz\ dr = 0$

When one or two plastic zones are present, the stress and strain continuity at the interface requires that rr, $\theta\theta$ and zz shall have the same values resulting from the elastic and the plastic zones. Thus by comparing the elastic zone and the plastic zone expressions for stresses at one interface the appropriate values of A, B and D are obtained and the other interface or boundary (if elastic) must agree. This check ensures the correct position(s) of the interface(s); in the long cylinder theory the computation must be corrected and repeated until the check agrees; in the disc theory, the expressions for A and B are compared to give one or two equations for the position(s) of the interface(s).

For the steady state temperature distribution, $T = F + H \ln r$, and $\int r\ T\ dr = \frac{r^2}{2}\left\{T - \frac{H}{2}\right\}$ + constant. The expressions for stresses $\theta\theta$ and rr then take the form :-

for long cylinders

$$rr = A_1 + \frac{B}{r^2} - \frac{E\alpha T}{2(1-\sigma)}$$

$$\theta\theta = A_1 - \frac{B}{r^2} - \frac{E\alpha(T+H)}{2(1-\sigma)}$$

$$zz = D - \frac{E\alpha T}{1-\sigma} \quad \text{where } D = E\frac{dw}{dz} + 2\sigma A_1 - \frac{\sigma E\alpha H}{2(1-\sigma)}$$

for discs

$$rr = A_1 + \frac{B}{r^2} - \frac{E\alpha T}{2} \qquad \theta\theta = A_1 - \frac{B}{r^2} - \frac{E\alpha(T+H)}{2}$$

3:2 The Thermal Stresses in an Overstrained Long Cylinder

a) Flow Condition

It is assumed that there is a unique relationship between the effective stress and the effective strain, where these are given by the following formulae,

$$\text{Effective stress} = k = \frac{\sqrt{2}}{2}\left\{(rr - \theta\theta)^2+(\theta\theta - zz)^2+(zz - rr)^2\right\}^{1/2} \quad (1)$$

$$\text{Effective strain} = \varepsilon = \frac{\sqrt{2}}{3}\left\{(e_r-e_\theta)^2+(e_\theta -e_z)^2+(e_z-e_r)^2\right\}^{1/2} \quad (2)$$

The form of this relationship will be discussed in detail later.

b) Strains

The connection between the stresses, strains and displacements is as follows,

$$E\frac{du}{dr} = rr-\sigma(\theta\theta + zz) + \beta\left\{rr - \cdot5(\theta\theta + zz)\right\} + E\alpha T \quad (3)$$

$$E\frac{u}{r} = \theta\theta-\sigma(zz + rr) + \beta\left\{\theta\theta - \cdot5(zz + rr)\right\} + E\alpha T \quad (4)$$

$$E\frac{dw}{dz} = zz-\sigma(rr + \theta\theta) + \beta\left\{zz - \cdot5(rr + \theta\theta)\right\} + E\alpha T \quad (5)$$

Where β is a function of radius and can usually only be obtained during the progress of the solution of the stress field.

These equations can be written in the form

$$E\frac{du}{dr} = \omega_1.rr - \omega_2(\theta\theta + zz) + E\alpha T \quad (6)$$

$$E\frac{u}{r} = \omega_1.\theta\theta - \omega_2(zz + rr) + E\alpha T \quad (7)$$

$$E\frac{dw}{dz} = \omega_1.zz - \omega_2(rr + \theta\theta) + E\alpha T \quad (8)$$

$$\text{Where } \omega_1 = 1 + \beta \text{ and } \omega_2 = \sigma + \cdot5\beta \quad (9)$$

c) Stress Equilibrium

requires

$$r\frac{drr}{dr} + rr - \theta\theta = 0 \quad (10)$$

$$\text{Putting } x = \log\frac{r}{R} \text{ where R is some convenient radius such as a} \quad (11)$$

boundary radius or any other desired constant radius chosen for computational convenience.

This gives $\frac{d}{dx} = r\frac{d}{dr}$ and writing $\frac{drr}{dx}$ in the form $\dot{rr}$ (10) becomes

$$\dot{rr} + rr - \theta\theta = 0 \quad (12)$$

d) Strain Compatability

$$\text{requires } \frac{d}{dr}\left\{\frac{u}{r}\right\} = \frac{1}{r}\frac{du}{dr} - \frac{u}{r^2} \text{ or } r\frac{d}{dr}\left\{\frac{u}{r}\right\} = \frac{du}{dr} - \frac{u}{r} = \frac{d}{dx}\left\{\frac{u}{r}\right\} \quad (13)$$

$$\text{or } \dot{e}_\theta + \alpha\dot{T} = e_r - e_\theta \quad (14)$$

Substituting from equations 6, 7 and 8 for $\dot{e}_\theta$, e_r and e_θ

$$a_\theta\dot{\beta} + w_1\dot{\theta\theta} - w_2\dot{r}r - w_2\dot{z}z + (w_1 + w_2)(\theta\theta - rr) + E\alpha\dot{T} = 0 \quad (15)$$

and using $\dot{r}r = \theta\theta - rr$ this becomes

$$a_\theta\dot{\beta} + w_1\dot{\theta\theta} + w_1\dot{r}r - w_2\dot{z}z + E\alpha\dot{T} = 0 \quad (16)$$

where $a_\theta = \theta\theta - .5(zz+rr)$

$a_r = rr - .5(\theta\theta+zz)$

$a_z = zz - .5(rr+\theta\theta)$

e) Long Cylinder Conditions

require $\frac{dw}{dz}$ to be constant with radius, this leads to

$$\frac{d}{dx}\left\{\frac{dw}{dz}\right\} = 0 \quad (17)$$

Using equation (8), (17) becomes

$$w_1\dot{z}z - w_2(\dot{\theta\theta} + \dot{r}r) + zz\dot{\beta} - .5(\theta\theta + rr)\dot{\beta} + E\alpha\dot{T} = 0$$

or

$$a_z\dot{\beta} - w_2\dot{\theta\theta} - w_2\dot{r}r + w_1\dot{z}z + E\alpha\dot{T} = 0 \quad (18)$$

f) Flow Condition: connection between ε and k

$$\text{From (2)} \qquad \frac{9}{2}\varepsilon^2 = (e_r - e_\theta)^2 + (e_\theta - e_z)^2 + (e_z - e_r)^2 \quad (19)$$

Differentiate with respect to x

$$9\varepsilon\dot{\varepsilon} = 2(e_r - e_\theta)(\dot{e}_r - \dot{e}_\theta) + 2(e_\theta - e_z)(\dot{e}_\theta - \dot{e}_z) + 2(e_z - e_r)(\dot{e}_z - \dot{e}_r) \quad (20)$$

$$= 4\left\{\left\{(e_r - .5(e_\theta + e_z)\right\}\dot{e}_r + \left\{e_\theta - .5(e_z + e_r)\right\}\dot{e}_\theta + \left\{e_z - .5(e_r + e_\theta)\right\}\dot{e}_z\right\} \quad (21)$$

Using equations (6), (7), and (8)

$$E\left\{e_r - .5(e_\theta + e_z)\right\} = w_1 rr - w_2(zz + \theta\theta) - .5\left\{w_1(\theta\theta + zz) - w_2(2rr + \theta\theta + zz)\right\}$$

$$= a_r(w_1 + w_2)$$

and similar expressions for the other terms in (21), whence (21) becomes

$$9\varepsilon\dot{\varepsilon} = \frac{4}{E}\left\{\left\{w_1 + w_2\right\}\left\{a_r\dot{e}_r + a_\theta\dot{e}_\theta + a_z\dot{e}_z\right\}\right\} \quad (22)$$

Now from (1) $2k^2 = (rr-\theta\theta)^2+(\theta\theta-zz)^2+(zz-rr)^2$ (23)

Differentiated with respect to x this can be written

$$k\dot{k} = a_r\dot{r}r + a_\theta\dot{\theta}\theta + a_z\dot{z}z \tag{24}$$

The expression for $\varepsilon\dot{\varepsilon}$ can be reduced to stresses only using

$$Ee_r = u_1 rr - u_2(\theta\theta + zz)$$

$$E\dot{e}_r = u_1\dot{r}r - u_2(\dot{\theta}\theta + \dot{z}z) + rr\,\dot{u}_1 - (\theta\theta + zz)\,\dot{u}_2$$

$$= u_1\dot{r}r - u_2(\dot{\theta}\theta + \dot{z}z) + a_r\dot{\beta}$$

whence

$$E(u_1+u_2)a_r\dot{e}_r = a_r\{(u_1+u_2)u_1\dot{r}r - (u_1+u_2)u_2(\dot{\theta}\theta+\dot{z}z) + (u_1+u_2)a_r\dot{\beta}\}$$

and with similar expressions for the remaining terms (22) becomes

$$\{u_1+u_2\}u_1\{a_r\dot{r}r+a_\theta\dot{\theta}\theta+a_z\dot{z}z\} - \{u_1+u_2\}u_2\{a_r(\dot{\theta}\theta+\dot{z}z)+a_\theta(\dot{z}z+\dot{r}r)$$

$$+a_z(\dot{r}r+\dot{\theta}\theta)\} + \dot{\beta}(u_1+u_2)\{a_r^2+a_\theta^2+a_z^2\} = \frac{9\varepsilon\dot{\varepsilon}E^2}{4}$$

and using $a_r+a_\theta+a_z = 0$ this reduces to

$$\{u_1+u_2\}\{a_r^2+a_\theta^2+a_z^2\}\dot{\beta} + \{u_1+u_2\}^2\{a_r\dot{r}r+a_\theta\dot{\theta}\theta+a_z\dot{z}z\} = \frac{9}{4}E^2\varepsilon\dot{\varepsilon} \tag{25}$$

Some connection must now be sought between (24) and (25). This connection comes from the effective stress-effective strain-temperature curves for the particular material. It has not, so far, been found possible to include temperature effects on work hardening stress-strain curves without first assuming an idealized stress-strain curve for each temperature and fitting a fixed type of equation to each such curve, thereby obtaining a set of equations which most nearly state the relationship between k, ε and T in the most interesting region for each particular problem.

The equation adopted may take a number of forms, but of the forms investigated the following appears to be the most convenient for computational use, besides giving quite reasonable accuracy.

$$E\varepsilon = k_1 + \left\{\frac{k - k_1}{q}\right\}^\eta$$ where η is a fixed number for the curves considered and k_1 and q are chosen to represent the true curve as closely as possible and are, obviously, temperature dependent. k_1 represents the idealized yield stress. As the temperature

distribution for a particular problem will be known $\dot{k}_1$ and $\dot{q}$ will also be known across the radius.

Differentiate (26) with respect to x

$$E\dot{\varepsilon} = \dot{k}_1 + \frac{\eta\{k-k_1\}^{\eta-1}}{q}\{\dot{k}-\dot{k}_1\} - \frac{\{k-k_1\}^{\eta}}{q^2}\dot{q}$$

$$E\dot{\varepsilon} = \left\{\frac{\eta\{k-k_1\}^{\eta-1}}{q}\right\}\dot{k} - \left\{\frac{\eta\{k-k_1\}^{\eta-1}}{q} - 1\right\}\dot{k}_1 - \left\{\frac{\{k-k_1\}^{\eta}}{q^2}\right\}\dot{q} \qquad (27)$$

Now for each equation representing one temperature only, q and k_1 are constant and therefore

$$\frac{dk}{d\varepsilon} = \frac{qE}{\eta\{k-k_1\}^{\eta-1}} = g \qquad (28)$$

where g is a symbol for the gradient $\frac{dk}{d\varepsilon}$ on a constant temperature curve.

(27) can now be written

$$E\dot{\varepsilon} = \frac{E}{g}\dot{k} - \left\{\frac{E}{g} - 1\right\}\dot{k}_1 - \left\{\frac{E\{k-k_1\}}{qg\eta}\right\}\dot{q}$$

$$g\dot{\varepsilon} = \dot{k} - \left\{1-\frac{g}{E}\right\}\dot{k}_1 - \left\{\frac{k-k_1}{q\eta}\right\}\dot{q} \qquad (29)$$

it should be noted that if $\eta = 2$

$$g = \frac{qE}{2\{k-k_1\}}$$ and (29) reduces to

$$g\dot{\varepsilon} = \dot{k} - \left\{1-\frac{g}{E}\right\}\dot{k}_1 - \left\{\frac{E}{4g}\right\}\dot{q} \qquad (30)$$

which is the most convenient relationship between $\dot{k}$ and $\dot{\varepsilon}$, for computation, that has so far been found.

Writing

$$\frac{\tau}{k} = \left\{1 - \frac{g}{E}\right\}\dot{k}_1 + \left\{\frac{k-k_1}{q\eta}\right\}\dot{q} \qquad (31)$$

or

$$\frac{\tau}{k} = \left\{1 - \frac{g}{E}\right\}\dot{k}_1 + \left\{\frac{E}{4g}\right\}\dot{q} \qquad \text{for } \eta = 2$$

equations (29) and (30) can now be written

$$g\dot{\varepsilon} = \dot{k} - \frac{\tau}{k} \qquad (32)$$

where $\frac{\tau}{k}$ allows for temperature effects on the stress-strain curves and is given by (31) and g is the gradient $\frac{dk}{d\varepsilon}$ on the constant temperature idealized stress-strain curve and is given in (28)

In view of the probable lack of knowledge of the exact state

of the material and the corresponding k-ε-T curves it is considered that $\eta = 2$ should give sufficient accuracy although other values may be preferred for some materials. Nothing more complicated than a power type equation of the form of (26) seems worthwhile unless a strictly mathematical solution is the sole aim.

Substituting for ε from (25) and k from (24) in (32)

$$g\dot{\varepsilon} = \frac{4g}{9E^2\varepsilon}\left\{\left(w_1+w_2\right)\left(a_r^2+a_\theta^2+a_z^2\right)\dot{\beta}+\left(w_1+w_2\right)^2\left(a_r\dot{r}r+a_\theta\dot{\theta}\theta+a_z\dot{z}z\right)\right\}$$

$$= \dot{k} - \frac{\tau}{k} = \frac{1}{k}\left\{a_r\dot{r}r + a_\theta\dot{\theta}\theta + a_z\dot{z}z\right\} - \frac{\tau}{k}$$

Putting

$$h = \frac{gk}{E^2\varepsilon} \tag{33}$$

$$y_1 = \frac{4h}{9}\left(w_1+w_2\right)\left(a_r^2 + a_\theta^2 + a_z^2\right) \tag{34}$$

$$y_2 = \frac{4h}{9}\left(w_1+w_2\right)^2 - 1 \tag{35}$$

gives

$$y_1\dot{\beta} + y_2\left(a_r\dot{r}r+a_\theta\dot{\theta}\theta+a_z\dot{z}z\right) + \tau = 0 \tag{36}$$

The analysis has given four simultaneous first order differential equations, (12), (16), (18) and (36). These are gathered together in the next section.

g) The Simultaneous Equations

$$\dot{r}\dot{r} = \dot{\theta}\dot{\theta} - rr \tag{12}$$

$$a_\theta \dot{\beta} + u_1 \dot{\theta}\dot{\theta} + u_1 \dot{r}\dot{r} - u_2 \dot{z}\dot{z} + E\alpha\dot{T} = 0 \tag{16}$$

$$a_z \dot{\beta} - u_2 \dot{\theta}\dot{\theta} - u_2 \dot{r}\dot{r} + u_1 \dot{z}\dot{z} + E\alpha\dot{T} = 0 \tag{18}$$

$$y_1 \dot{\beta} + y_2 a_\theta \dot{\theta}\dot{\theta} + y_2 a_r \dot{r}\dot{r} + y_2 a_z \dot{z}\dot{z} + \tau = 0 \tag{36}$$

These equations can be rearranged to give $\dot{\theta}\dot{\theta}$, $\dot{z}\dot{z}$, and $\dot{\beta}$

Putting

$$\text{Den} = \left\{u_1^2 - u_2^2\right\} y_1 - \left\{\left\{a_\theta^2 + a_z^2\right\} u_1 + 2a_\theta a_z u_2\right\} y_2 \tag{37}$$

then

$$\dot{\theta}\dot{\theta} = \left\{\left\{\frac{\left\{u_1 - u_2\right\} a_z^2 + a_r a_\theta u_1\right\} y_2 + \left\{u_2^2 - u_1^2\right\} y_1}{(\text{Den})}\right\} \dot{r}\dot{r} + \left\{\frac{u_2 a_z + u_1 a_\theta}{(\text{Den})}\right\} \tau - \left\{\frac{\left\{u_1 + u_2\right\} y_1 + \left\{a_z a_\theta - a_z^2\right\} y_2}{(\text{Den})}\right\} E\alpha\dot{T} \tag{38}$$

$$\dot{z}\dot{z} = \left\{\frac{\left\{a_r - a_\theta\right\}\left\{a_z u_1 + a_\theta u_2\right\} y_2}{(\text{Den})}\right\} \dot{r}\dot{r} + \left\{\frac{u_1 a_z + u_2 a_\theta}{(\text{Den})}\right\} \tau - \left\{\frac{\left\{u_1 + u_2\right\} y_1 + \left\{a_\theta a_z - a_\theta^2\right\} y_2}{(\text{Den})}\right\} E\alpha\dot{T} \tag{39}$$

$$\dot{r}\dot{r} = \dot{\theta}\dot{\theta} - rr \tag{12}$$

$$\dot{\beta} = \left\{\frac{\left\{a_\theta - a_r\right\}\left\{u_1^2 - u_2^2\right\} y_2}{(\text{Den})}\right\} \dot{r}\dot{r} - \left\{\frac{\left\{u_1 + u_2\right\} a_r y_2}{(\text{Den})}\right\} E\alpha\dot{T} - \left\{\frac{u_1^2 - u_2^2}{(\text{Den})}\right\} \tau \tag{40}$$

h) Method of Solution

No general solution has been found to these equations and they must be solved by standard numerical methods for each individual problem. A number of numerical methods are available, the simplest is perhaps Taylors Series in which

$$\phi_1 = \phi_0 + \delta x\left\{\frac{d\phi}{dx}\right\}_0 + \text{higher powers.}$$

The higher powers of rr, ~~θθ~~, zz and β are even more complicated than the first powers but can be obtained by differentiating equations (37) to (40) and may prove necessary if better accuracy is desired. The expressions for $\dot{r}r$, ~~$\dot{\theta}\theta$~~, $\dot{z}z$ and $\dot{\beta}$ contain only the stresses and β as unknowns therefore it is possible to progress from one point to the next across a radius once a solution has been started.

Starting a solution involves guessing ~~θθ~~ and zz on the boundary, chosen as the starting point since rr = 0 on an axial boundary, estimating $\frac{dw}{dz}$ for the particular case and calculating β from (5). Trial and error is then needed to correct the values of ~~θθ~~ and zz until the first two points of the solution satisfy (37) to (40), (8) and the stress-strain curve, using whatever numerical method is chosen. Experience so far suggests that ~~θθ~~ and zz are equal, or nearly equal, on an axial boundary, which is a great help. Having established the first two points the solution can proceed across the radius by the chosen numerical method, until the interface is reached, where β = 0.

Each plastic zone is dealt with individually and the elastic and plastic zones must then be tied together. This involves calculating the values of A, B and D in the elastic equations (Section 3 : 1) from the stresses at the two interfaces (or one interface and an elastic boundary) obtained from the plastic solutions. The equations (37) to (40) reduce and integrate to the elastic equations when the plastic strain components are zero and so the stress values at each interface are mutually consistent.

However, at this point different values of A, B and D will almost certainly result from the two interfaces (or one interface and an elastic boundary). To correct this, the relative values of ~~θθ~~ and zz on one or both boundaries must be changed (slight changes can move the position of the interface by a relatively large amount, the solution is quite sensitive to incorrect values of ~~θθ~~ and zz on the boundary) and the computation repeated. Proceeding in the manner described a solution is eventually obtained which satisfies (37) to (40) in the plastic zone(s) and in which the elastic and plastic zones are compatable.

When a full solution for the elastic and plastic zones has been obtained the end load $= \int_i^o r.zz.dr$ must be calculated and if this is not zero then a re-assessment of $\frac{dw}{dz}$ must be made and another solution must be performed, and so on until a solution is obtained in which the end load is zero.

The method outlined is long and tedious and can be simplified somewhat by assuming an idealized stress-strain curve with $g = 0$. This is discussed in the next few sections.

i) Idealized Stress-Strain Curve, No Work Hardening

The most useful assumption that can be made in the solution of the set of equations (37) to (40) is that the material of the cylinder exhibits no work hardening. This results in the effective stress being known throughout the plastic zone and $\dot{z}z \doteq \dot{\theta}\theta \doteq k$ on all axial boundaries which reduces the trial and error normally needed to find the value of zz and $\theta\theta$ satisfying the boundary conditions. With a no work hardening material the only variation in k is that due to temperature and this is known before the solution is started. Also, as q = 0, g = 0 whence h = 0, $y_1 = 0$ and $y_2 = -1$ from (33), (34) and (35). Putting these values into equations (37) to (40) and $\tau = k\dot{k}$ from (31) gives

$$\text{Den} = \left\{a_\theta^2 + a_z^2\right\} w_1 + 2a_\theta a_z w_2 \tag{41}$$

$$\dot{\theta}\theta = \left\{\frac{\left\{(w_2 - w_1)a_z^2 - a_r a_\theta w_1\right\}}{(\text{Den})}\right\}\dot{r}r + \left\{\frac{\left\{(a_z a_\theta - a_z^2)\right\}}{(\text{Den})}\right\}E\alpha\dot{T} + \left\{\frac{w_2 a_z + w_1 a_\theta}{(\text{Den})}\right\}k\dot{k} \tag{42}$$

$$\dot{z}z = \left\{\frac{\left\{(a_\theta - a_r)\{a_z w_1 + a_\theta w_2\}\right\}}{(\text{Den})}\right\}\dot{r}r + \left\{\frac{\left\{(a_z a_\theta - a_\theta^2)\right\}}{(\text{Den})}\right\}E\alpha\dot{T} + \left\{\frac{w_1 a_z + w_2 a_\theta}{(\text{Den})}\right\}k\dot{k} \tag{43}$$

$$\dot{r}r = \dot{\theta}\theta - rr \tag{44}$$

$$\dot{\beta} = \left\{\frac{\left\{(w_1^2 - w_2^2)\{a_r - a_\theta\}\right\}}{(\text{Den})}\right\}\dot{r}r + \left\{\frac{\left\{(w_1 + w_2)a_r\right\}}{(\text{Den})}\right\}E\alpha\dot{T} - \left\{\frac{w_1^2 - w_2^2}{(\text{Den})}\right\}k\dot{k} \tag{45}$$

The method of solution is the same as previously outlined except that the trial and error needed to establish the relationship between the first two points and the stress-strain curve has been eliminated.

The Derivation of the Effective Stress-Effective Strain Curve from the Tensile Stress Strain Curve

The effective stress-effective strain curve is obtained from the tensile stress-strain curve as follows:-

During a tensile test, $rr = \theta\theta = 0$ and from (6), (7) and (8)

$$Ee_r = -\omega_2 zz \tag{1a}$$

$$Ee_\theta = -\omega_2 zz \tag{1b}$$

$$Ee_z = \omega_1 zz \tag{1c}$$

and effective stress $= k = \frac{\sqrt{2}}{2}\left\{zz^2 + zz^2\right\}^{\frac{1}{2}} = zz$ (1d)

Inserting (1a), (1b) and (1c) into the expression for effective strain in equation (2) gives $E\varepsilon = \frac{2}{3}\left\{\omega_1 + \omega_2\right\}zz$ (1e)

Plastic Region of Curve Ee_z and zz are known at each point on the tensile stress-strain curve therefore ω_1 is known from (1c)

$$\omega_1 = \frac{Ee_z}{zz} = 1 + \beta \tag{1f}$$

$$\beta = \frac{Ee_z}{zz} - 1 \tag{1g}$$

$$\omega_2 = \sigma + \frac{\beta}{2} = \frac{Ee_z}{2zz} + \sigma - 0.5$$

$$\omega_1 + \omega_2 = \frac{3Ee_z}{2zz} + \sigma - 0.5 \tag{1h}$$

and putting this into (1e) $\varepsilon = e_z - \frac{2}{3}\left\{0.5 - \sigma\right\}\frac{zz}{E}$ (1i)

giving $\frac{d\varepsilon}{d\sigma} = \frac{de_z}{dzz} - \frac{2}{3E}\left\{0.5 - \sigma\right\}$ (1j)

Elastic Region of Curve In the elastic region of the tensile stress-strain curve $rr = \theta\theta = 0$, $e_r = e_\theta = -\sigma e_z$ and $\beta = 0$ whence (1e) reduces to $\varepsilon = \frac{2}{3}\left\{1+\sigma\right\}\frac{zz}{E}$ (1k)

Hence the effective stress-effective strain curve has a slope of $\frac{3E}{2(1+\sigma)}$ in the elastic region. The complete effective stress-effective strain curve is constructed from the tensile stress-strain curve using (1d), (1i) and (1k).

3:3 The Thermal Stresses in an Overstrained Disc (i.e. Plane Stress)

STRESSES

Stress Equilibrium Equation

$$r\frac{\partial rr}{\partial r} + rr = \theta\theta \tag{1}$$

Inner Plastic Zone

The maximum shear stress is $\frac{\theta\theta}{2}$

$$\text{therefore } \theta\theta = 2S_i \tag{2}$$

(2) in (1)

$$\frac{\partial}{\partial r}(r.rr) = 2S_i$$

$$r.rr = 2\,S_i\,r + \text{const.}$$

(a) for a hollow disc $rr = 0$ at $r = r_i$

therefore $-2S_i r_i$ is the value of the constant and rr becomes

$$rr = 2S_i\left\{1 - \frac{r_i}{r}\right\} \tag{3}$$

(b) for a solid disc equation (1) can only be satisfied by $rr = \theta\theta = 2S_i$ throughout the zone.

Outer Plastic Zone

The maximum shear stress is $\frac{rr - \theta\theta}{2}$

$$\text{therefore } rr - \theta\theta = 2S_o \tag{4}$$

(4) in (1)

$$\frac{\partial rr}{\partial r} = -\frac{2S_o}{r}$$

$$rr = -2S_o \ln r + \text{constant}$$

and at outer surface $rr = 0$ at r_o therefore constant becomes $2S_o \ln r_o$ and

$$rr = 2S_o \ln\frac{r_o}{r} \tag{5}$$

$$\text{and} \quad \theta\theta = -2S_o\left\{1 - \ln\frac{r_o}{r}\right\} \tag{6}$$

Elastic Zone

The solution of the thermal stress equations under conditions

of plane stress gives rr and $\theta\theta$ in the following form

$$rr = A + \frac{B}{r^2} - \frac{1}{r^2}\int E \alpha r T \, dr \tag{7}$$

$$\theta\theta = A - \frac{B}{r^2} - E\alpha T + \frac{1}{r^2}\int E \alpha r T \, dr \tag{8}$$

Stress Continuity at Inner Interface

(a) Hollow disc. If rr and $\theta\theta$ are to be continuous across the inner interface, r = n, then using (7) = (3) and (8) = (2)

$$A + \frac{B}{n^2} - \frac{1}{n^2}\int^{n} E \alpha r T \, dr = 2S_i\left(1 - \frac{r_i}{n}\right) \tag{9}$$

$$A - \frac{B}{n^2} - E\alpha T_n + \frac{1}{n^2}\int^{n} E \alpha r T \, dr = 2S_i \tag{10}$$

$$\text{whence} \quad A = S_i\left(2 - \frac{r_i}{n}\right) + \frac{E\alpha T_n}{2} \tag{11}$$

$$\text{and} \quad B = \int^{n} E \alpha r T \, dr - \frac{n^2 E\alpha T_n}{2} - S_i r_i n \tag{12}$$

(b) Similarly, with rr = $\theta\theta$ = $2S_b$ at r = n for a solid disc

$$A = 2S_i + \frac{E\alpha T_n}{2} \tag{11a}$$

$$B = \int^{n} E \alpha r T \, dr - \frac{n^2}{2} E\alpha T_n \tag{12a}$$

An inner plastic zone in a solid disc is very unlikely except for peculiar temperature distributions and is not pursued further.

Stress Continuity at Outer Interface

If rr and $\theta\theta$ are to be continuous across the outer interface, r = N, then using (7) = (5) and (8) = (6)

$$A + \frac{B}{N^2} - \frac{1}{N^2}\int^{N} E \alpha r T \, dr = 2S_o \ln\frac{r_o}{N} \tag{13}$$

$$A - \frac{B}{N^2} - E\alpha T_N + \frac{1}{N^2}\int^{N} E \alpha r T \, dr = -2S_o\left(1 - \ln\frac{r_o}{N}\right) \tag{14}$$

whence $A = \frac{E\alpha T_N}{2} - S_o \left\{1 - 2\ln \frac{r_o}{N}\right\}$ (15)

$$B = N^2 S_o - \frac{N^2 E\alpha T_N}{2} + \int^N E\ \alpha\ r\ T\ dr \quad (16)$$

Outer Zone Wholly Elastic

If there is no outer plastic zone then (7) applies at $r = r_o$ and

$$rr = A + \frac{B}{r_o^2} - \frac{1}{r_o^2}\int^{r_o} E\ \alpha\ r\ T\ dr = 0 \quad (17)$$

Inner Zone Wholly Elastic

(a) Hollow Disc. If there is no inner plastic zone then (7) applies at $r = r_i$ and

$$rr = A + \frac{B}{r_i^2} - \frac{1}{r_i^2}\int^{r_i} E\ \alpha\ r\ T\ dr = 0 \quad (18)$$

(b) Solid Disc. At r = 0, stresses ~~θθ~~ and rr are equal and must be finite, therefore B = 0 and the value of $\frac{1}{r^2}\int E\ \alpha\ r\ T\ dr$ at the centre must be $\frac{E\alpha Tc}{2}$ where Tc is the temperature at the centre of the disc.

The Position(s) of the Elastic/Plastic Interface(s)

A preliminary elastic solution using the elastic equations (7) and (8) with boundary conditions (17) and (18) will indicate the likely position(s) of a plastic zone for a given temperature distribution.

Inner and Outer Plastic Zones

For two plastic zones the stress continuity conditions (11) and (12) with (15) and (16) must apply and as A and B are single valued from (11) and (15)

$$A = S_i\left\{2 - \frac{r_i}{n}\right\} + \frac{E\alpha T_n}{2} = \frac{E\alpha T_N}{2} - S_o\left\{1 - 2\ln\frac{r_o}{N}\right\} \qquad (19)$$

and from (12) and (16)

$$B = \int^{n} E\alpha r T dr - \frac{n^2 E\alpha T_n}{2} - S_i r_i n = N^2 S_o - \frac{N^2 E\alpha T_N}{2} + \int^{N} E\alpha r T dr \qquad (20)$$

(19) and (20) are two simultaneous equations which can be solved for n and N. So far a direct method of solving (19) and (20) has not been found and a numerical trial-and-error approach has been adopted.

Inner Plastic Zone Only

For an inner plastic zone only, the stress continuity conditions at r = n are used with the boundary condition (17), i.e. (11) and (12) in (17)

$$S_i\left\{2-\frac{r_i}{n}\right\} + \frac{E\alpha T_n}{2} + \frac{1}{r_o^2}\int^{n} E\alpha r T dr - \frac{n^2}{r_o^2}\,\frac{E\alpha T_n}{2} - S_i\frac{r_i n}{r_o^2} - \frac{1}{r_o^2}\int^{r_o} E\alpha r T dr = 0$$

or

$$\frac{E\alpha T_n}{2}\left\{1 - \frac{n^2}{r_o^2}\right\} - \frac{1}{r_o^2}\int_{n}^{r_o} E\alpha r T dr + S_i\left\{2 - \frac{r_i}{n}\left\{1 + \frac{n^2}{r_o^2}\right\}\right\} = 0 \qquad (21)$$

and this can be solved for n, again using numerical trial and error.

Outer Plastic Zone Only

(a) Hollow Disc. For an outer plastic zone only, the stress continuity conditions at r = N are used with the boundary condition (18) i.e. (15) and (16) in (18) leading to

$$\frac{E\alpha T_N}{2}\left\{1-\frac{N^2}{r_i^2}\right\}+\frac{1}{r_i^2}\int_{r_i}^{N} E\alpha rTdr-S_o\left\{1-2\ln\frac{r_o}{N}-\frac{N^2}{r_i^2}\right\}=0 \qquad (22)$$

and this can be solved for N, again by numerical trial and error.

(b) Solid Disc. The stress continuity conditions (15) and (16) at r = N are used with B = 0 leading to

$$0 = N^2S_o-\frac{N^2E\alpha T_N}{2}+\int_{}^{N} E\alpha rTdr \qquad (16a)$$

from which the value of N can be calculated, following which A can be calculated from (15).

Strains

Stress - Strain - Displacement Relationships

$$E\frac{u}{r} = Ee_\theta+E\alpha T = \bar{\theta\theta} - \sigma rr + \beta\left\{\bar{\theta\theta} - \cdot 5\bar{rr}\right\}+ E\alpha T \qquad (23)$$

$$E\frac{du}{dr} = Ee_r+E\alpha T = \bar{rr} - \sigma\bar{\theta\theta} + \beta\left\{\bar{rr} - \cdot 5\bar{\theta\theta}\right\}+ E\alpha T \qquad (24)$$

$$E\frac{dw}{dz} = Ee_z+E\alpha T = -\sigma(rr+\bar{\theta\theta}) -\cdot 5\beta(rr+\bar{\theta\theta})+ E\alpha T \qquad (25)$$

where β is a proportionality factor, varying with radius, and zero if there is no plastic strain.

Strain Compatability Equation

$$Er\frac{d}{dr}\left\{\frac{u}{r}\right\} = E\frac{du}{dr} - E\frac{u}{r} = (rr-\bar{\theta\theta})(1 + \sigma + \frac{3}{2}\beta) \qquad (26)$$

using $\frac{u}{r}$ and $\frac{du}{dr}$ from above.

Inner Plastic Zone

From (2) $\theta\theta = 2S_i$ and from (3) $rr = 2S_i\left\{1 - \frac{r_i}{r}\right\}$

therefore $rr - \theta\theta = -2S_i\frac{r_i}{r}$

$$E\frac{u}{r} = E\alpha T + 2S_i\left\{\bar{1-\sigma} + \sigma\frac{\bar{r_i}}{\bar{r}}\right\} + S_i\beta\left\{\bar{1} + \frac{\bar{r_i}}{\bar{r}}\right\} \qquad (27)$$

$$\text{therefore } E\alpha r\frac{dT}{dr} - 2\sigma S_i\frac{r_i}{r} + \left\{1+\frac{r_i}{r}\right\}S_i r\frac{d\beta}{dr} - S_i\beta\frac{r_i}{r} = -2S_i\frac{r_i}{r}\left\{\bar{1+\sigma+\frac{3}{2}\beta}\right\}$$

$$\text{giving } \frac{d\beta}{dr} + \frac{2r_i}{r(r_i+r)}\beta + \frac{2r_i}{r(r_i+r)} + \frac{E\alpha}{S_i(r_i+r)}\left\{r\frac{dT}{dr}\right\} = 0 \qquad (28)$$

This is a first order linear equation which can be solved for a known temperature distribution.

Outer Plastic Zone

From (4) $rr - \theta\theta = 2S_o$ and using (5) and (6)

$$E\frac{u}{r} = -2S_o\left\{1-(1-\sigma)\ln\frac{r_o}{r}\right\} - S_o\left\{2-\ln\frac{r_o}{r}\right\}\beta + E\alpha T \qquad (29)$$

$$\text{therefore } -2S_o\left\{1-\sigma\right\} - S_o\left\{2-\ln\frac{r_o}{r}\right\}r\frac{d\beta}{dr} - S_o\beta + E\alpha r\frac{dT}{dr} - 2S_o(1+\sigma+\tfrac{3}{2}\beta) = 0$$

$$\text{therefore } -4S_o - S_o\left\{2-\ln\frac{r_o}{r}\right\}r\frac{d\beta}{dr} - 4S_o\beta + E\alpha r\frac{dT}{dr} = 0$$

$$\text{therefore } \left\{2-\ln\frac{r_o}{r}\right\}r\frac{d\beta}{dr} + 4\beta + 4 - \frac{E\alpha r}{S_o}\frac{dT}{dr} = 0 \qquad (30)$$

This also is a first order linear equation which can be solved for a known temperature distribution.

Steady State Temperature Distribution with Radial Heat Flow Only

The temperature equation for this condition is $T = F + H \ln r$ (31)

and

$$\left.\begin{aligned}\int rT\,dr &= \frac{r^2}{2}\left\{\bar{F} + H\ln r - \frac{\bar{H}}{2}\right\} + \text{constant}\\ &= \frac{r^2}{2}\left\{\bar{T} - \frac{\bar{H}}{2}\right\} + \text{constant}\end{aligned}\right\} \qquad (32)$$

Substituting (31) and (32) into equations for position of interfaces gives equations which are quickly solved by simple trial and error.

Inner and Outer Plastic Zones

from (19)

$$4S_i r_i n + E\alpha H n^2 = N^2\left\{E\alpha H - 4S_o\right\} \tag{33}$$

from (20)

$$2S_i\left\{2 - \frac{r_i}{n}\right\} + E\alpha H \ln\frac{n}{N} + 2S_o\left\{1 - 2\ln\frac{r_o}{N}\right\} = 0 \tag{34}$$

Inner Plastic Zone Only

from (21)

$$\frac{E\alpha H}{4S_i}\left\{1 + \ln\frac{n^2}{r_o^2} - \frac{n^2}{r_o^2}\right\} - \frac{r_i}{r_o}\cdot\frac{r_o}{n}\left\{1 + \frac{n^2}{r_o^2}\right\} + 2 = 0 \tag{35}$$

choosing a value of $\frac{n}{r_o}$ and substituting in this will give the appropriate value of $\frac{E\alpha H}{S_i}$

Outer Plastic Zone Only

from (22)

$$\frac{E\alpha H}{4S_o}\left\{1 + \ln\left\{\frac{N}{r_i}\right\}^2 - \frac{N^2}{r_i^2}\right\} + \frac{N^2}{r_i^2} + 2\ln\frac{r_o}{r_i}\frac{r_i}{N} - 1 = 0 \tag{36}$$

and choosing a value of $\frac{N}{r_i}$ and substituting in this will give the appropriate value of $\frac{E\alpha H}{S_o}$ It should be noted that it is very unlikely that this temperature distribution will give an outer plastic zone only.

Value of β in Inner Plastic Zone

With this temperature distribution $r\frac{dT}{dr} = H$ whence (28) becomes

$$\frac{d\beta}{dr} + \frac{2r_i}{r(r_i+r)}\beta + \frac{2r_i}{r(r_i+r)} + \frac{E\alpha H}{S_i(r_i+r)} = 0 \tag{37}$$

and using the integrating factor $\left\{\frac{r}{r_i+r}\right\}^2$ this integrates to give

$$\left\{\frac{r}{r_i+r}\right\}^2\cdot\beta = \frac{r_i^2+2rr_i}{(r_i+r)^2} - \frac{E\alpha H}{S_i}\left\{\ln(r_i+r) + \frac{3r_i^2+4rr_i}{2(r_i+r)^2}\right\} + \text{constant} \tag{38}$$

The constant can be found by putting $\beta = 0$ at $r = n$

$$\text{Constant} = -\frac{r_i^2+2nr_i}{(r_i+n)^2} + \frac{E\alpha H}{S_i}\left\{\ln(r_i+n) + \frac{3r_i^2+4nr_i}{2(r_i+r)^2}\right\}$$

$$\left\{\frac{r}{r_i+r}\right\}^2\beta = -\frac{r_i^2+2nr_i}{(r_i+n)^2}+\frac{r_i^2+2rr_i}{(r_i+r)^2}+\frac{E\alpha H}{S_i}\left\{\ln\frac{r_i+n}{r_i+r}+\frac{3r_i^2+4nr_i}{2(r_i+n)^2} - \frac{3r_i^2+4rr_i}{2(r_i+r)^2}\right\}$$

and putting $a = 1+\frac{r}{r_i}$ and $b = 1+\frac{n}{r_i}$ this becomes

$$\left\{\frac{a-1}{a}\right\}^2\beta = -\frac{2b-1}{b^2} + \frac{2a-1}{a^2} + \frac{E\alpha H}{S_i}\left\{\ln\frac{b}{a} + \frac{4b-1}{2b^2} - \frac{4a-1}{2a^2}\right\} \qquad (39)$$

Value of β in outer plastic zone

Putting $r\frac{dT}{dr} = H$ in (30) and rearranging

$$\left\{2 + \ln\frac{r}{r_o}\right\} r\frac{d\beta}{dr} + 4\beta + 4 - \frac{E\alpha H}{S_o} = 0 \qquad (40)$$

and making the substitution $x = \ln\frac{r}{r_o}$ and separating variables this integrates to

$$\beta = \left\{\frac{\text{const.}}{2+x}\right\}^4 - 1 + \frac{E\alpha H}{4S_o}$$

and at $r = N$ $\beta = 0$ and $x = x_N$ from which

$$(\text{const.})^4 = \left\{2+x_N\right\}^4\left\{1 - \frac{E\alpha H}{4S_o}\right\}$$

and putting $c = \frac{r}{r_o}$ and $d = \frac{N}{r_o}$

$$\beta = \left\{\frac{E\alpha H}{4S_o} - 1\right\}\left\{1 - \left\{\frac{2+\ln d}{2+\ln c}\right\}^4\right\} \qquad (41)$$

Transient Temperature Distribution

In the case of a known transient temperature distribution the appropriate equations can be solved by graphical integrations of the temperature terms. Alternatively, the temperature distribution can be expressed as a power function of radius. In most cases the maximum shear strain will be of paramount interest and it is essential that the function representing the temperature distribution can be fed into the appropriate differential equations giving the plastic modulus, β, and the resultant equations solved for β. It is advantageous to keep this power function in simple form.

Some transient temperature distributions for turbine rotors have been calculated at Imperial College, for the Admiralty. During the middle period of the warming-up of a rotor, say after ten minutes, when the temperature at the bore is just beginning to rise, the maximum temperature gradients and probably the worst strain conditions are obtained. At the worst strain conditions an outer plastic zone only is anticipated. The temperature distributions at this time can be approximated by the simple equation

$$T = J + Mr^{\gamma} \tag{42}$$

where J, M and γ are constants obtained by fitting this equation to the known temperature curve.

Whence $$\int rTdr = \frac{Jr^2}{2} + \frac{Mr^{\gamma+2}}{\gamma+2} + \text{constant} \tag{43}$$

Outer Plastic Zone Only

Substituting (42) and (43) into equations for position of interface at N gives

$$\left\{\frac{J+MN^{\gamma}}{2}\right\}\left\{1 - \frac{N^2}{r_i^2}\right\} + \frac{1}{r_i^2}\left\{\frac{J}{2}(N^2-r_i^2) + \frac{M}{\gamma+2}\left\{N^{\gamma+2} - r_i^{\gamma+2}\right\}\right\}$$

$$- \frac{S_o}{E\alpha}\left\{1 - 2\ln\frac{r_o}{N} - \frac{N^2}{r_i^2}\right\} = 0 \tag{44}$$

and this can be solved for N by numerical trial and error.

Value of β in Outer Plastic Zone

Substituting $\frac{dT}{dr}$ from (42) in equation (30) and rearranging

$$\frac{d\beta}{dr} + \frac{4\beta}{r(2+\ln\frac{r}{r_o})} + \frac{4}{r(2+\ln\frac{r}{r_o})} - \frac{E\alpha\gamma M r^{\gamma-1}}{S_o(2+\ln\frac{r}{r_o})} = 0 \qquad (45)$$

and using an integrating factor $\left\{2 + \ln\frac{r}{r_o}\right\}^4$ this integrates to give

$$\left\{2+\ln\frac{r}{r_o}\right\}^4 \beta = -\left\{2+\ln\frac{r}{r_o}\right\}^4 + \text{constant}$$

$$+ \frac{E\alpha M r^{\gamma}}{S_o}\left\{\left\{2+\ln\frac{r}{r_o}\right\}^3 - \frac{3}{\gamma}\left\{2+\ln\frac{r}{r_o}\right\}^2 + \frac{6}{\gamma^2}\left\{2+\ln\frac{r}{r_o}\right\} - \frac{6}{\gamma^3}\right\}$$

and putting $\beta = 0$ at $r = N$ gives

$$\text{constant} = \left\{2+\ln\frac{N}{r_o}\right\}^4 - \frac{E\alpha M N^{\gamma}}{S_o}\left\{\left\{2+\ln\frac{N}{r_o}\right\}^3 - \frac{3}{\gamma}\left\{2+\ln\frac{N}{r_o}\right\}^2 + \frac{6}{\gamma^2}\left\{2+\ln\frac{N}{r_o}\right\} - \frac{6}{\gamma^3}\right\}$$

writing $m = 2+\ln\frac{r}{r_o}$ and $m_N = 2+\ln\frac{N}{r_o}$

$$\beta = -1 + \left\{\frac{m_N}{m}\right\}^4 + \frac{E\alpha M r^{\gamma}}{S_o}\left\{\frac{1}{m} - \frac{3}{\gamma m^2} + \frac{6}{\gamma^2 m^3} - \frac{6}{\gamma^3 m^4}\right\}$$

$$- \frac{E\alpha M N^{\gamma}}{S_o m^4}\left\{m_N^3 - \frac{3m_N^2}{\gamma} + \frac{6m_N}{\gamma^2} - \frac{6}{\gamma^3}\right\} \qquad (46)$$

Method of Solution

The radius of each interface, n and/or N, is first obtained, after which the stresses are calculated, then β and finally the strains. The precise equations used depend upon the type of temperature distribution, whether the disc is hollow or solid and the number of plastic zones present.

Thus n and/or N is calculated from the appropriate equations as follows

if $T = F + H \ln r$, equations (33) and (34), (35) or (36)

if $T = J + Mr^{\gamma}$, equation (44)

and for a known graphical temperature distribution, equations (19) and (20), (21), (22) or (16a).

For stresses in the plastic zone the appropriate equations are (2) to (6) and in the elastic zone equations (7) and (8), the temperature integrals being given by equations (32) or (43) or being obtained graphically. Also in the elastic stress expressions the constants A and B must satisfy the stress continuity at the interface(s) and are obtained from the appropriate equations (11) and (12), (11a) and (12a) or (15) and (16).

β is now calculated from the appropriate equations as follows

for $T = F + H \ln r$, equation (39) or (41)

for $T = J + Mr^{\gamma}$, equation (46)

and if the temperature distribution is only known graphically then equations (28) and (30) must be solved either by writing the temperature distribution as a suitable equation and integrating or by starting with $\beta = 0$ at n or N and proceeding into the plastic zone by finite difference methods.

Finally the strains for all cases are given by equations (23), (24) and (25).

3: 4 Computations

The stresses and strains in a long cylinder with free ends and also in a disc, in both cases for a radius ratio $\frac{r_o}{r_i} = 2{\cdot}25$, have been computed for several mean temperature gradients for steady state conditions. The results are given in graphs nos. 3·1 to 3·13.

The radius ratio $\frac{r_o}{r_i} = 2{\cdot}25$ was chosen as being fairly representative of the radius ratios of the specimens tested.

In the presentation of these computations, the stresses are given as a ratio of the appropriate flow criterion, e.g. $\frac{\sigma\theta}{k}$ or $\frac{\sigma\theta}{2S}$ etc., the strains are given in the form $\frac{Ee_\theta}{k}$ or $\frac{Ee_\theta}{2S}$ etc., and the mean temperature gradient in the form $\frac{E\alpha(T_o - T_i)}{k}$ or $\frac{E\alpha(T_o - T_i)}{2S}$. This enables the results to be used with any chosen value of k or S, but only, of course, for the radius ratio $\frac{r_o}{r_i} = 2{\cdot}25$. It is assumed that $k_i = k_o$ and $S_i = S_o$.

The movement of the interfaces is traced on graphs 3·1 and 3·4.

The surface strains, e_θ, e_z and e_r are plotted, against temperature gradient, for long cylinders on graphs 3·5 and 3·6 and for discs on graph 3·2.

3: 5 A Discussion of Computational Results

for steady state conditions and a radius ratio $\frac{r_o}{r_i} = 2{\cdot}25$ with $k_i = k_o$ and $S_i = S_o$.

It was known from elastic theory that the bore is more highly stressed than the outer surface, and the first plastic zone does start at the bore. By taking higher temperature gradients it is shown that the size of this plastic zone increases with temperature and provides surprisingly little (perhaps up to 5 per cent.) stress relief for the rest of the body. Another plastic zone

soon begins at the outer surface and spreads inwards with increasing temperature gradient, at a rather higher rate than the spread of the inner zone. The rate of spread of both zones decreases with increasing temperature gradient leaving a concentric ring or tube of elastic material through which the stresses and strains change signs. The bodies will never, of course, be wholly plastic (except in the fictitious case of an infinite temperature gradient) due to the push-pull nature of this type of loading.

The stress distributions for the long cylinder show that zz > $\theta\theta$ > rr for most of the inner plastic zone and rr > zz > $\theta\theta$ for most of the outer plastic zone. There is some evidence that $\theta\theta$ and zz cross over near the boundaries in both zones but, equally, this may be due to small errors still remaining in the solutions. In a wholly elastic cylinder it can be shown that zz = $\theta\theta$ + rr. This is very nearly true for the plastic zones investigated. No way of using this fact with this analysis has been discovered and there is some doubt about the validity of such an assumption for the general case.

The strains in the plastic zones all exhibit similar behaviour. The strains increase linearly with increasing mean temperature gradient until the element itself yields. The strains then continue linearly, but with a different rate of increase, as the mean temperature gradient is increased. This change in the gradient $\frac{\text{strain}}{T_o - T_i}$ is abrupt and, prior to this change, the effect of plastic straining at a point remote from the element under consideration is hardly discernable. This is rather surprising - it is quite reasonable to expect much more interaction between the two plastic zones and the intervening elastic zone.

As in the wholly elastic bodies, the largest strains are to be found in the bore. Unfortunately, the strains e_θ and e_z on both boundaries show only a small change in the gradient

$\frac{e_\theta}{T_o - T_i}$ and $\frac{e_z}{T_o - T_i}$ following yield. Presumably, this gradient change will be even less in a work-hardening material, and the detection of a plastic zone emanating from an axial surface, by the normal techniques of measuring surface strains, will not be easy and, indeed, in many cases may not be possible.

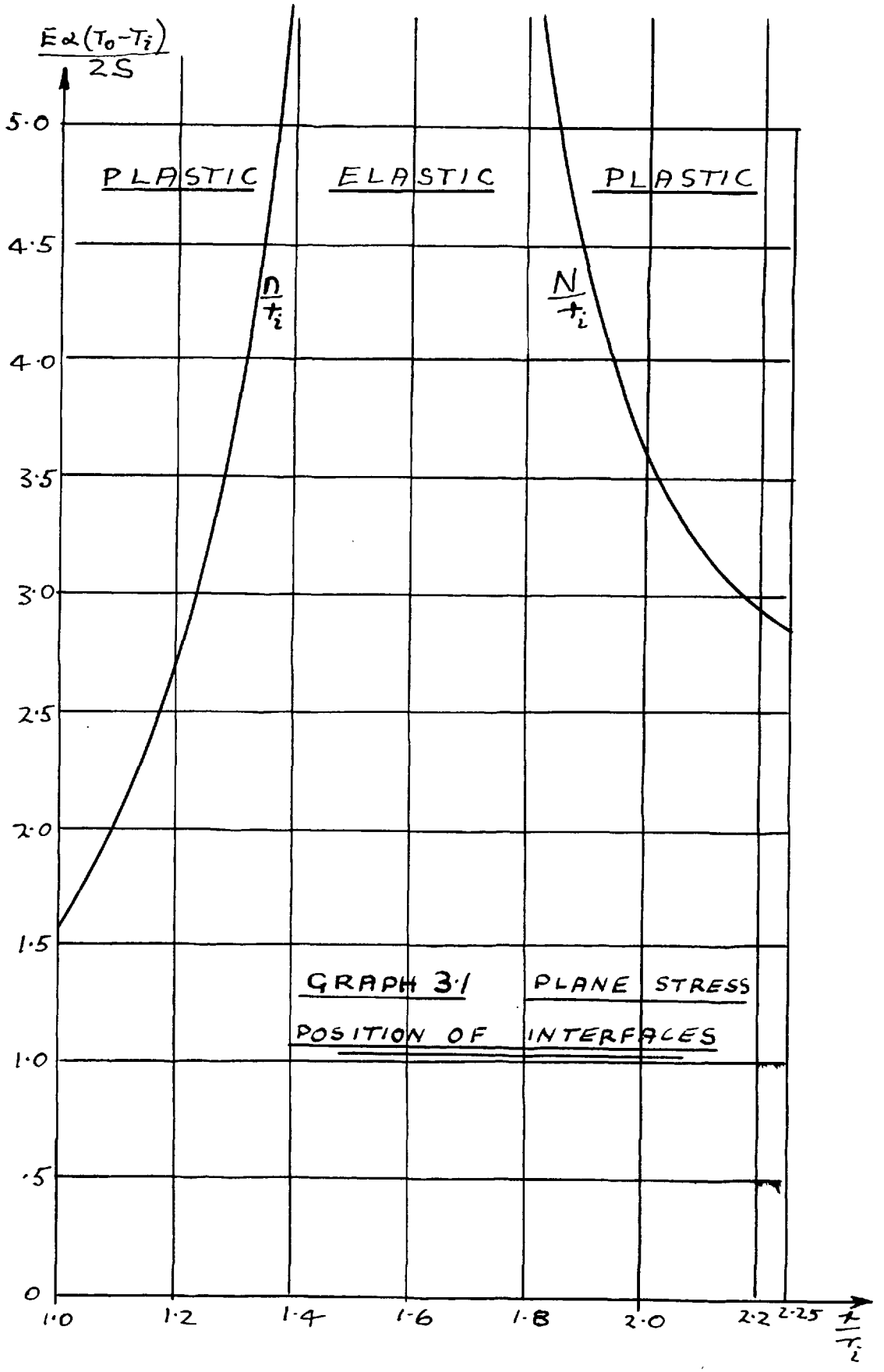
The only large strain which can be seen to be significantly affected by plastic straining is the radial strain e_r in the cylinder, especially in the inner plastic zone. At the bore boundary, $\frac{e_r}{T_o - T_i}$ suffers a gradient change in the ratio 1·0:2·6. The change in this gradient, $\frac{e_r}{T_o - T_i}\left\{= \frac{e_z}{T_o - T_i}\right\}$ in the bore of the disc is in the ratio 1·0:2·0 but here the strain is relatively small.

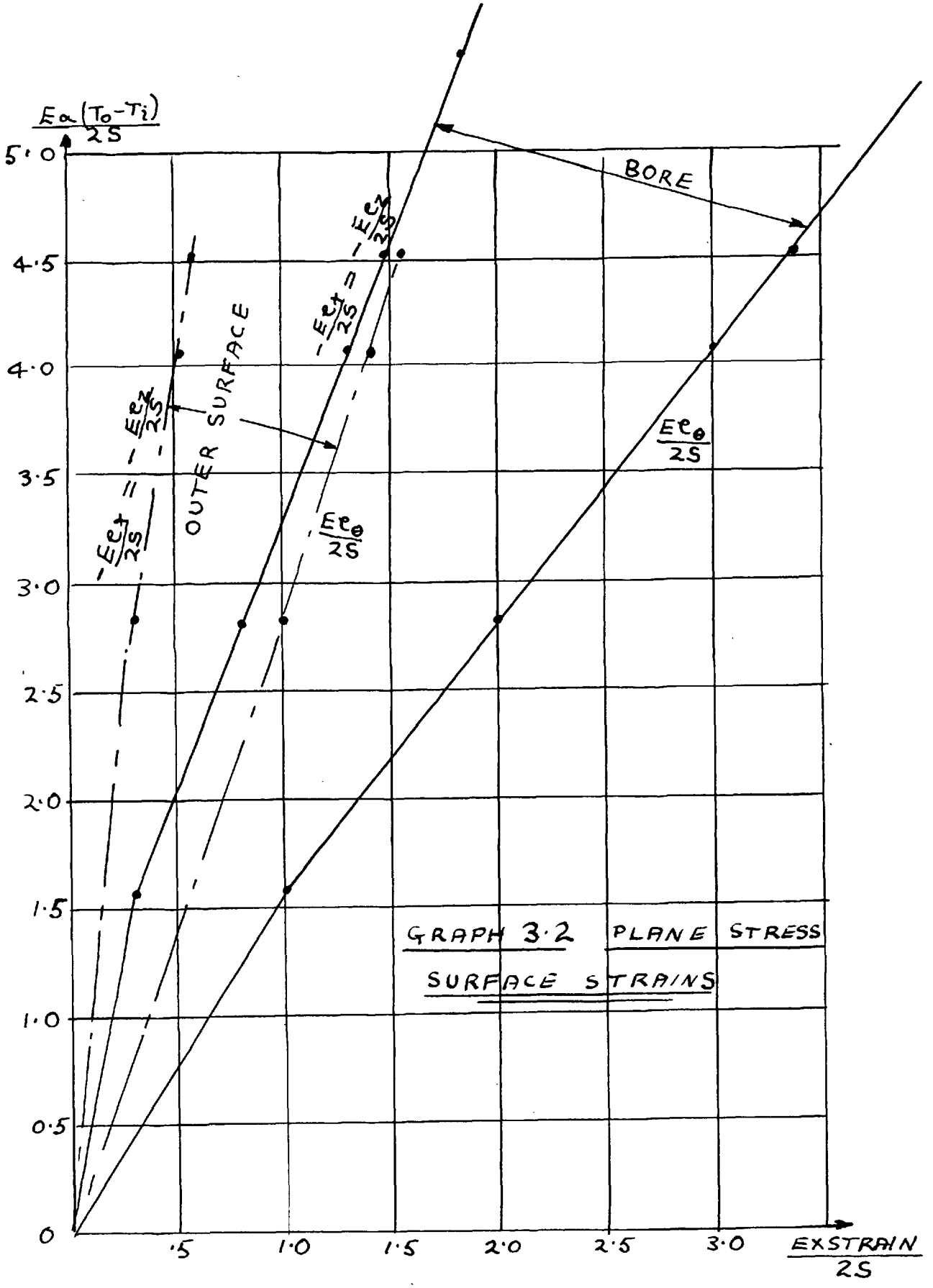
The computations were stopped when the bodies were over 60 per cent. plastic and at this stage the mean temperature gradient, in both cases, was some 3·4 times higher than that at which the inner plastic zone started. At this point the highest maximum shear strain in the disc (at the bore) is given by $Ee = 5{\cdot}8 \times 2S$ with $E\alpha\,(T_o - T_i) = 5{\cdot}5 \times 2S$. Assuming, as an example, that $\frac{2S}{E} = \frac{10}{12{,}000}$ and $\alpha = {\cdot}0000125$ this gives a maximum shear strain of about ·48 per cent. for a mean temperature gradient of 370°C (yield at about 110°C). This is equivalent to a proof strain of about ·25 per cent. on the non-work-hardening tensile stress strain curve. In the case of the cylinder, the highest effective strain (at the bore) is given by $E\varepsilon = 4{\cdot}5\ k$ with $E\alpha\,(T_o - T_i) = 3{\cdot}6.k.$ If it is assumed that $\frac{k}{E} = \frac{10}{12{,}000}$ and $\alpha = {\cdot}0000125$ this gives an effective strain of about ·375 per cent. for a mean temperature gradient of 240°C (yield at about 70°C) which is equivalent to proof strain of about ·3 per cent. on the non-work-hardening tensile stress-strain curve. These plastic strains are not, in themselves, serious and (in view of the apparent linear increase of strain with temperature) suggest that, for the conditions and dimensions specified, single loading up to any reasonable mean

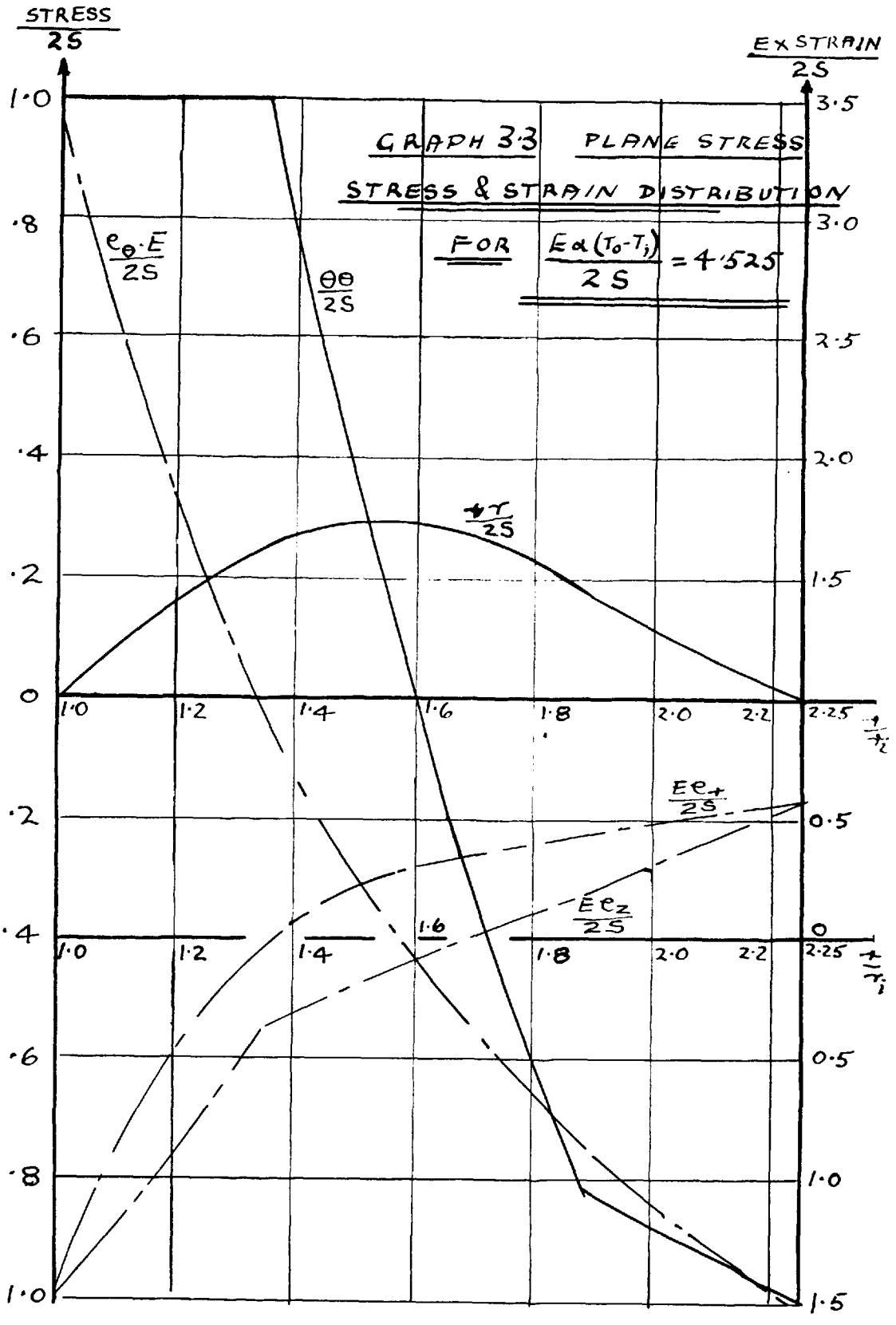
temperature gradient is quite acceptable from the safety angle. Slow cyclic loading (with temperature distribution approximating to $T = F + H \ln r$) amounting to a fatigue problem, may repay study although Prager (ref. 24) has demonstrated that shakedown will occur in elastic, plastic media subjected to cycles of load and/or temperature.

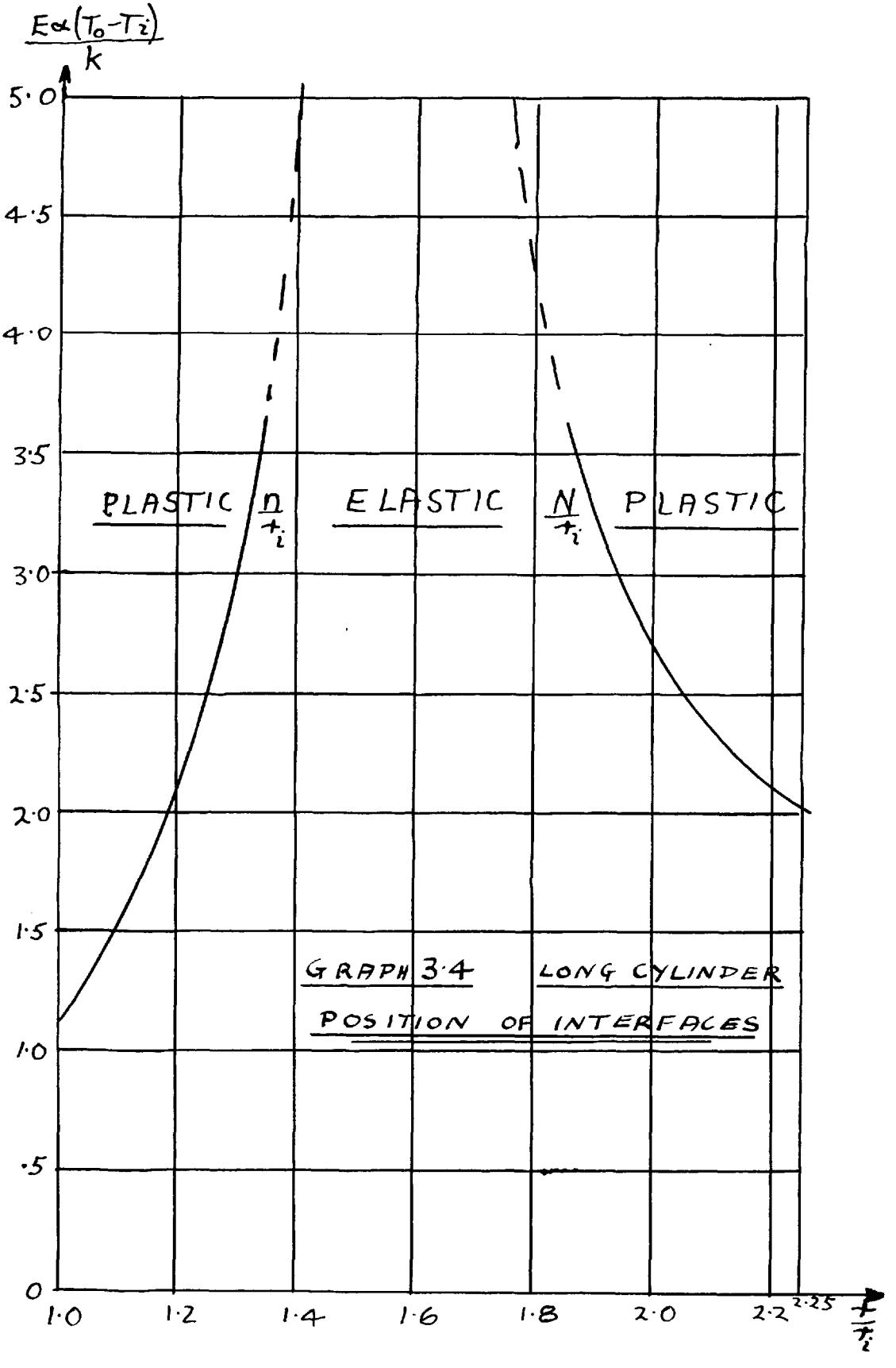
Comment has already been made upon the linear behaviour of all the plastic strains with increasing mean temperature gradient and as the stresses remain sensibly constant once the element has yielded it may prove that the total strain theory is in good agreement with the incremental strain theory. Considerably more computing is necessary for various radius ratios $\frac{r_o}{r_i}$ and temperature distributions before the statement above can be taken as representative of thermal stresses in axially symmetrical bodies. The disc problem could probably be tackled using the incremental strain theory and a comparison made[i]. The object here was to devise the means of assessing the degree of seriousness of thermal stresses beyond the elastic limit and the total strain theory is certainly sufficiently accurate for this.

Footnote[i]. Hill (ref. 12 P.125) states that the predictions of the total and incremental strain theories in the autofrettage of tubes with both plain strain and closed end conditions are in close agreement. He suggests, "that the reason for the close agreement . . . . . is to be found in the circumstance that the stress vector is restricted to a small segment of the yield circle". This will always be true of the disc solution given here, the stress distribution being independent of strain theory.


$\frac{E\alpha(T_0-T_i)}{2S}$
5·0
4·5
4·0
3·5
3·0
2·5
2·0
1·5
1·0
·5
0
PLASTIC
ELASTIC
PLASTIC
$\frac{n}{t_i}$
$\frac{N}{t_i}$
GRAPH 3·1
PLANE STRESS
POSITION OF INTERFACES
1·0
1·2
1·4
1·6
1·8
2·0
2·2
2·25
$\frac{x}{t_i}$

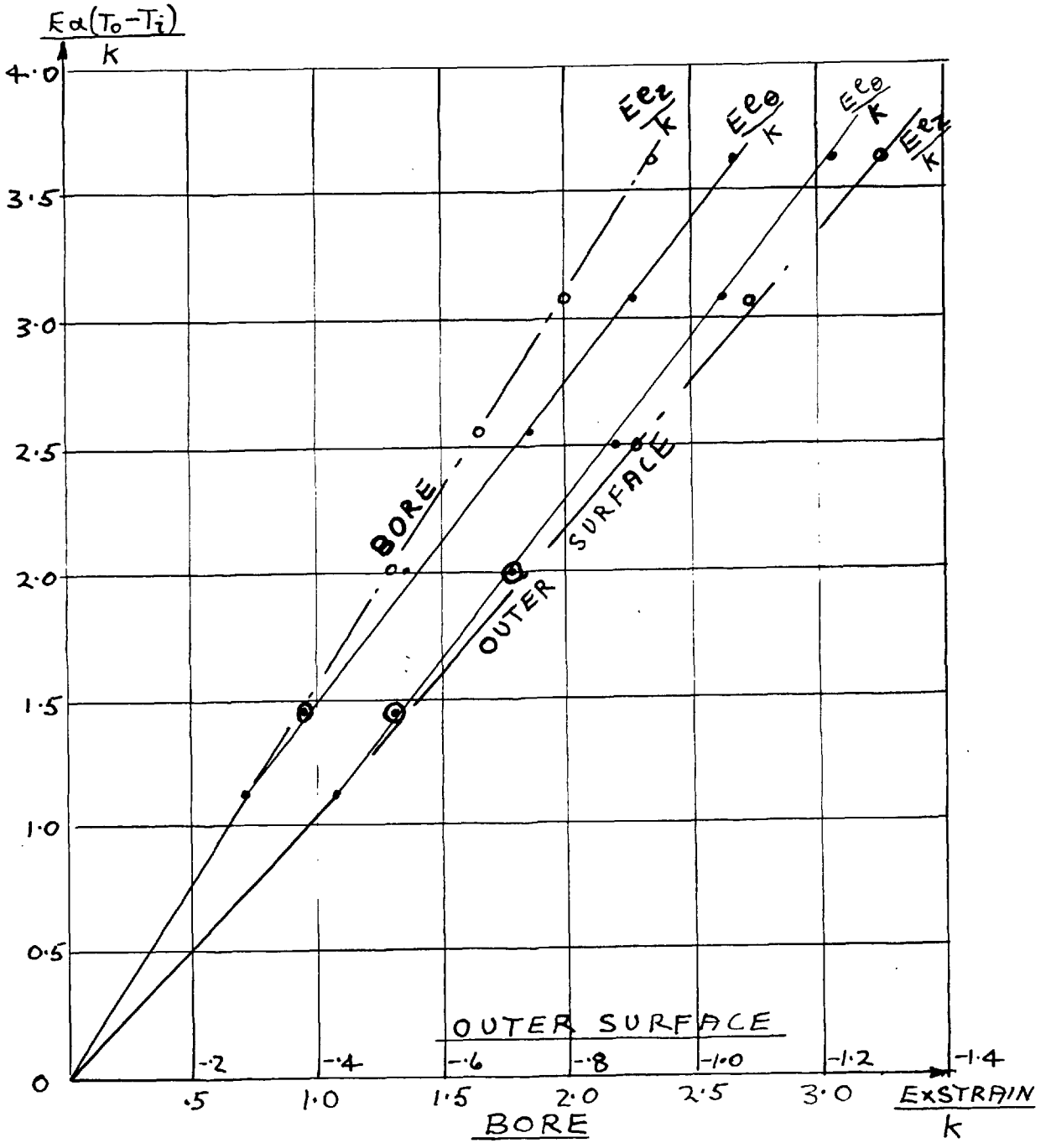

$\frac{E\alpha(T_o-T_i)}{2S}$
5·0
4·5
4·0
3·5
3·0
2·5
2·0
1·5
1·0
0·5
0
·5
1·0
1·5
2·0
2·5
3·0
$\frac{EEx}{2S}$
BORE
$-\frac{EEz}{2S}$
$-\frac{EEx}{2S}$
OUTER SURFACE
$-\frac{EEz}{2S}$
$-\frac{EEx}{2S}$
$\frac{EE_\theta}{2S}$
$\frac{EE_\theta}{2S}$
GRAPH 3·2 PLANE STRESS
SURFACE STRAINS

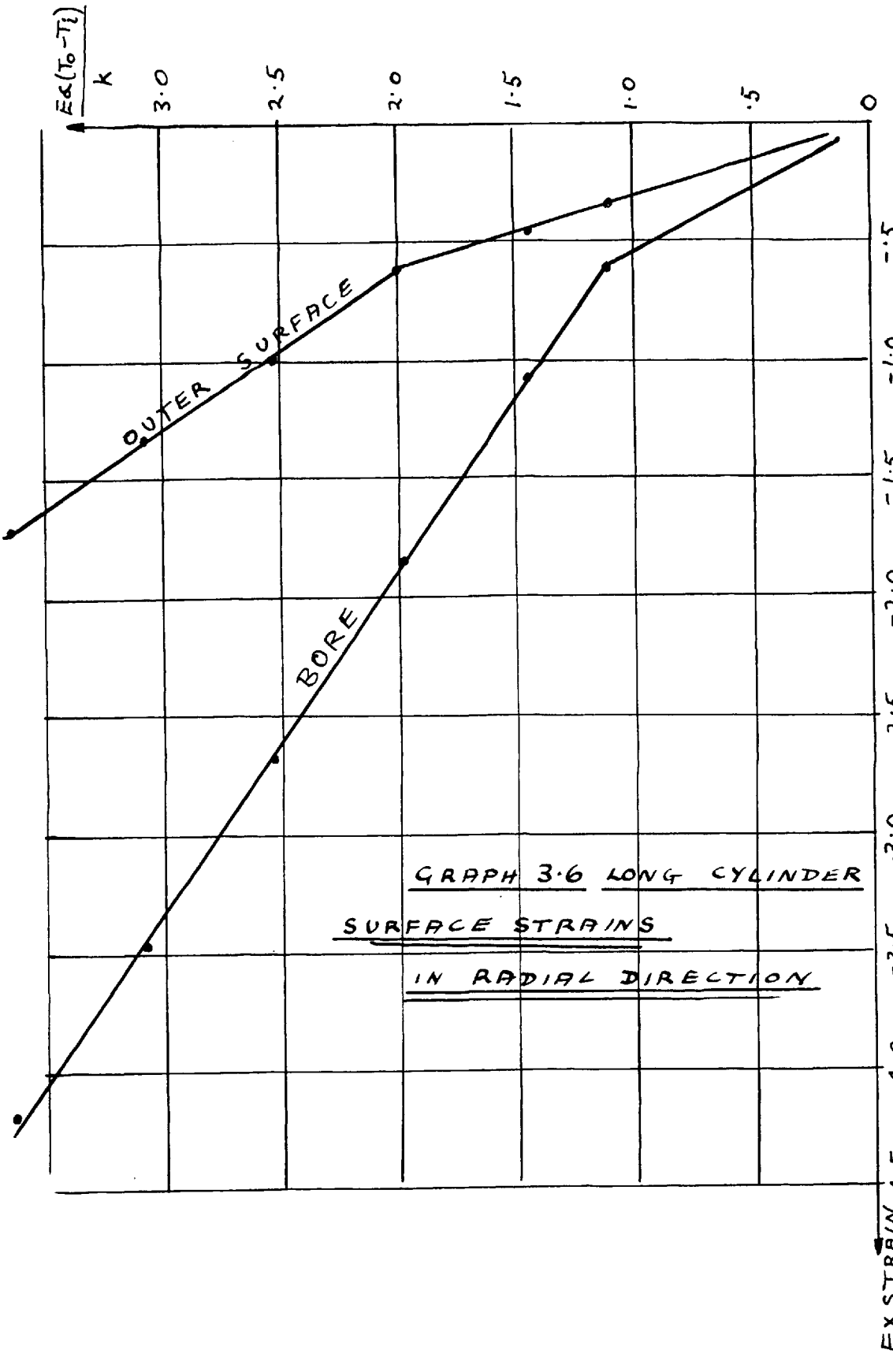

STRESS / 2S
EX STRAIN / 2S
GRAPH 3·3 PLANE STRESS
STRESS & STRAIN DISTRIBUTION
FOR Eα(T₀-Tᵢ)/2S = 4·525
eθ·E/2S
θθ/2S
+r/2S
Eez/2S
Eez+/2S
1·0
·8
·6
·4
·2
0
3·5
3·0
2·5
2·0
1·5
0·5
1·2
1·4
1·6
1·8
2·0
2·2
2·25
T/Tᵢ


$\frac{E\alpha(T_o - T_i)}{k}$
5·0
4·5
4·0
3·5
3·0
2·5
2·0
1·5
1·0
·5
0
PLASTIC $\frac{n}{r_i}$
ELASTIC
$\frac{N}{r_i}$ PLASTIC
GRAPH 3·4 LONG CYLINDER
POSITION OF INTERFACES
1·0
1·2
1·4
1·6
1·8
2·0
2·2
2·25
$\frac{r}{r_i}$

GRAPH 3·5 LONG CYLINDER

SURFACE STRAINS IN AXIAL & HOOP DIRECTIONS





GRAPH 3·6 LONG CYLINDER

SURFACE STRAINS

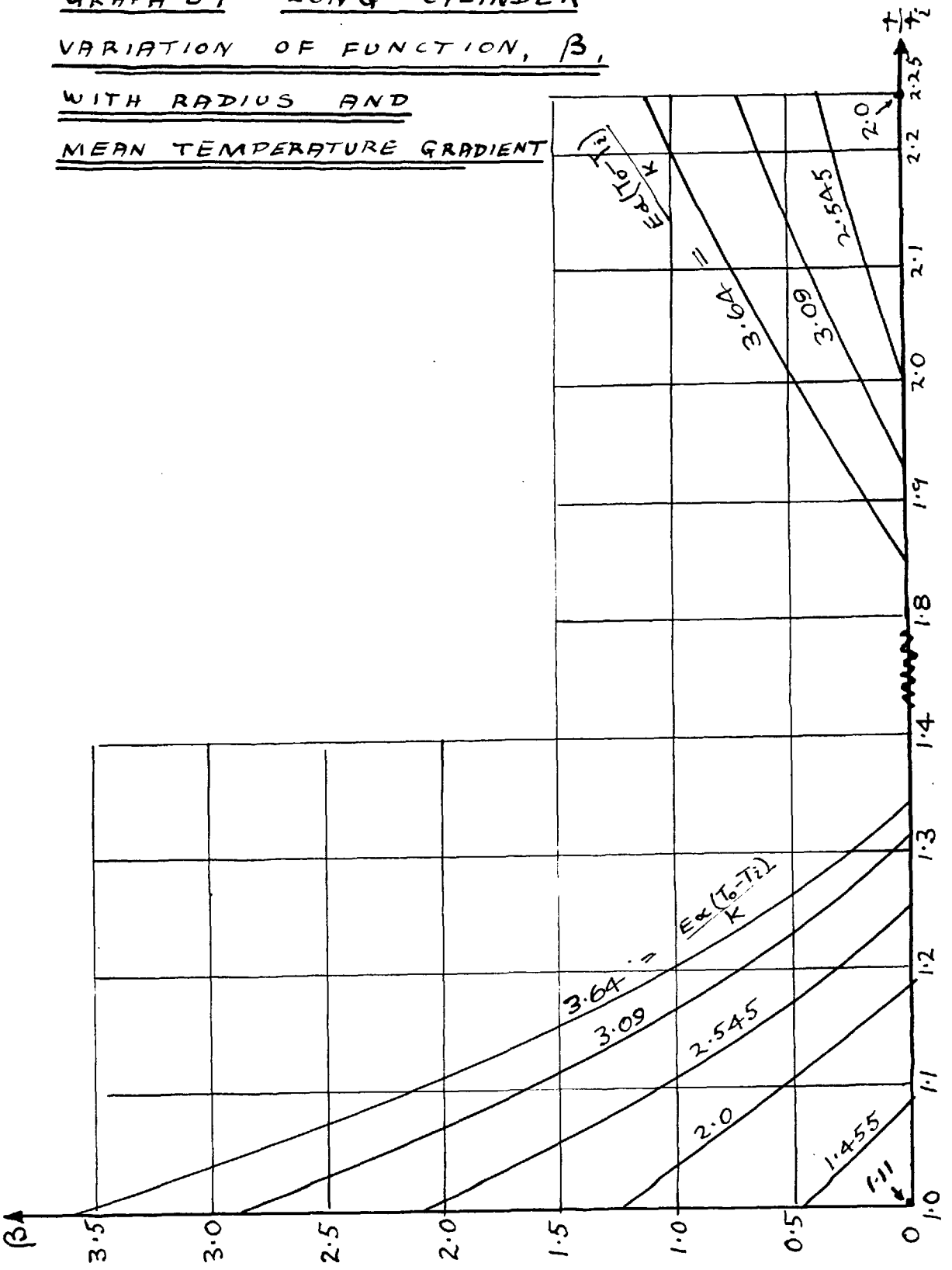
IN RADIAL DIRECTION

GRAPH 3·7 LONG CYLINDER

VARIATION OF FUNCTION, β,

WITH RADIUS AND

MEAN TEMPERATURE GRADIENT

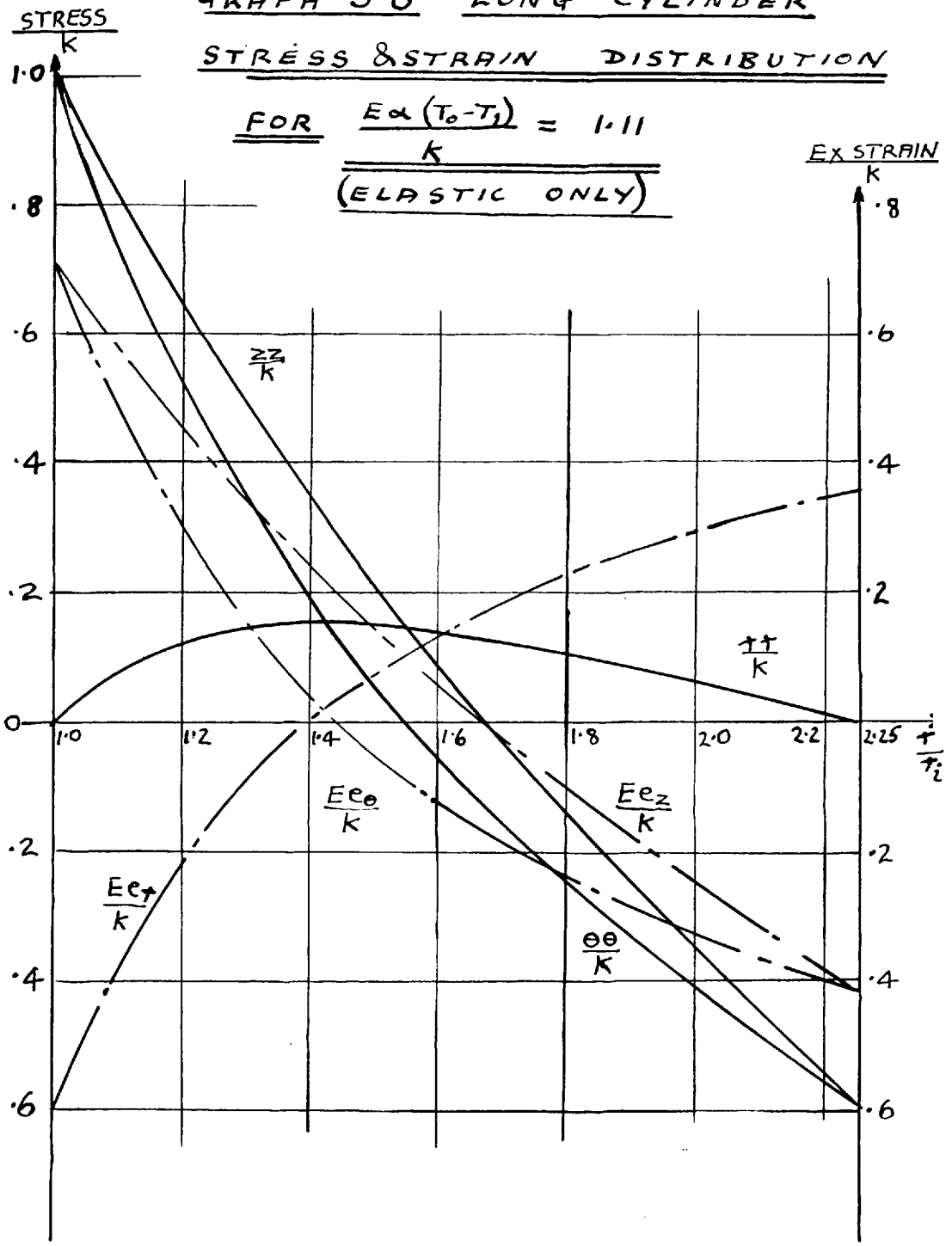


GRAPH 3·8 LONG CYLINDER

STRESS & STRAIN DISTRIBUTION

FOR $\frac{E\alpha(T_o - T_i)}{k} = 1.11$

(ELASTIC ONLY)

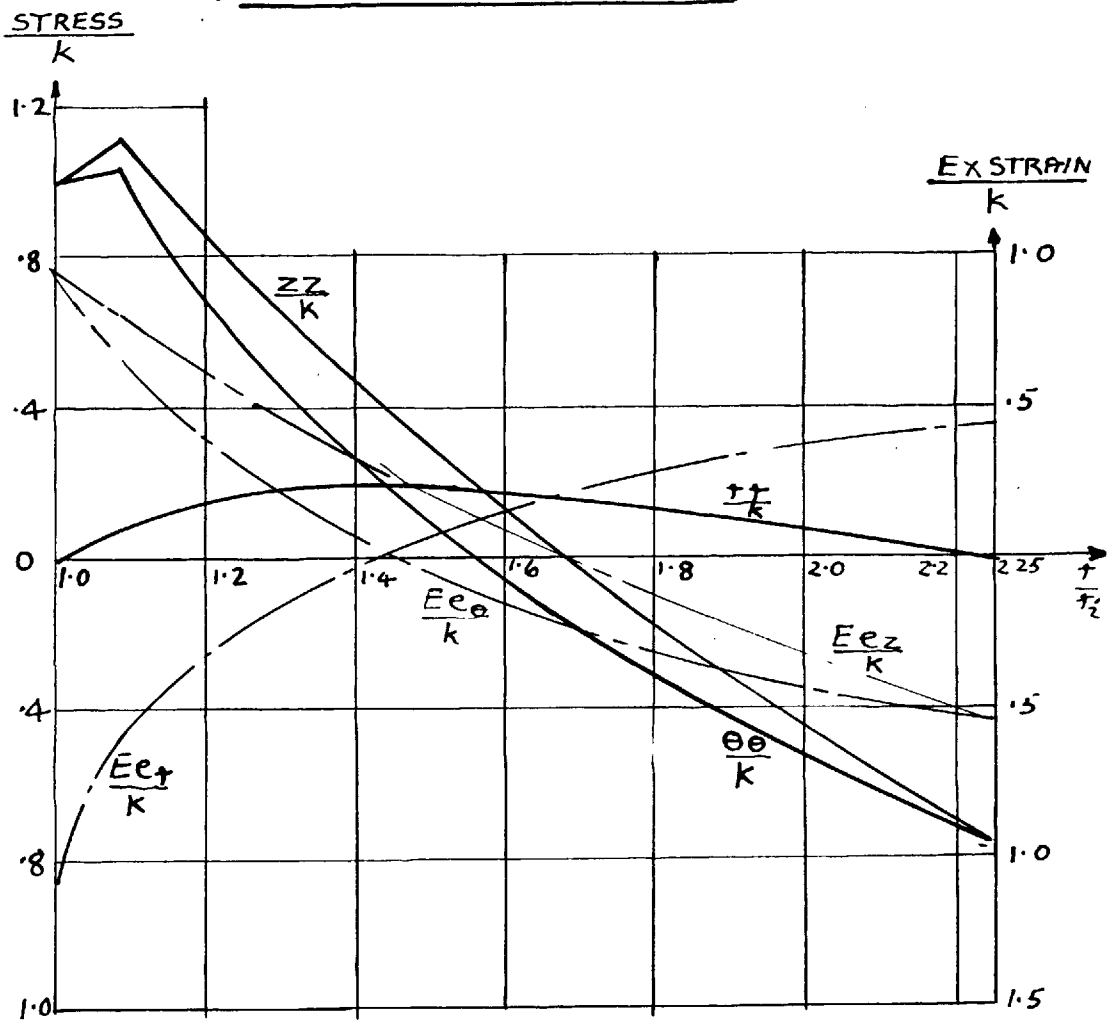


GRAPH 39 LONG CYLINDER

STRESS & STRAIN DISTRIBUTION

FOR $\frac{E\alpha(T_o - T_i)}{k} = 1.455$

(ONE PLASTIC ZONE)

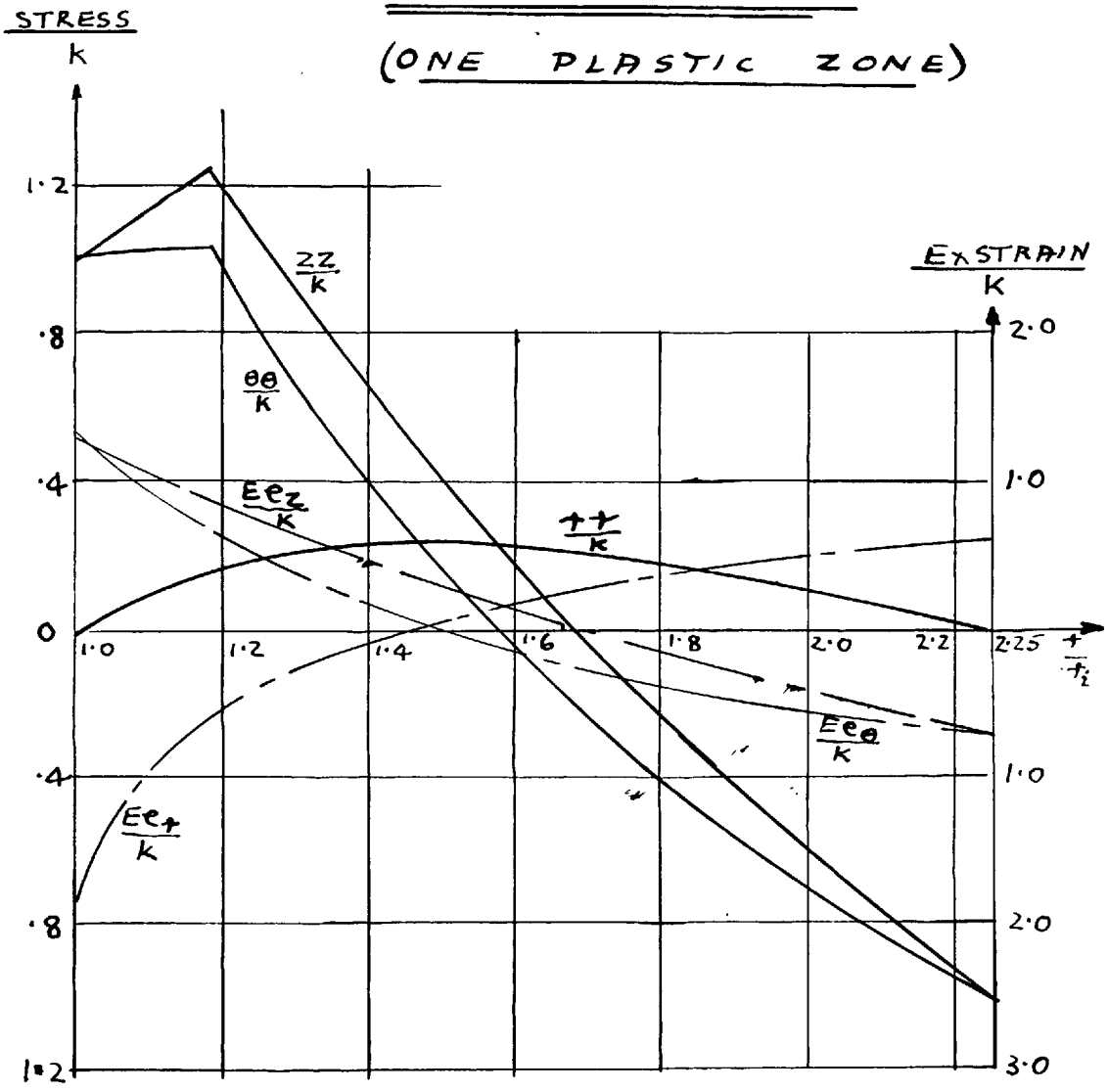


GRAPH 3·10 LONG CYLINDER

STRESS & STRAIN DISTRIBUTION

FOR $\frac{E\alpha(T_o - T_i)}{k} = 2.00$

(ONE PLASTIC ZONE)

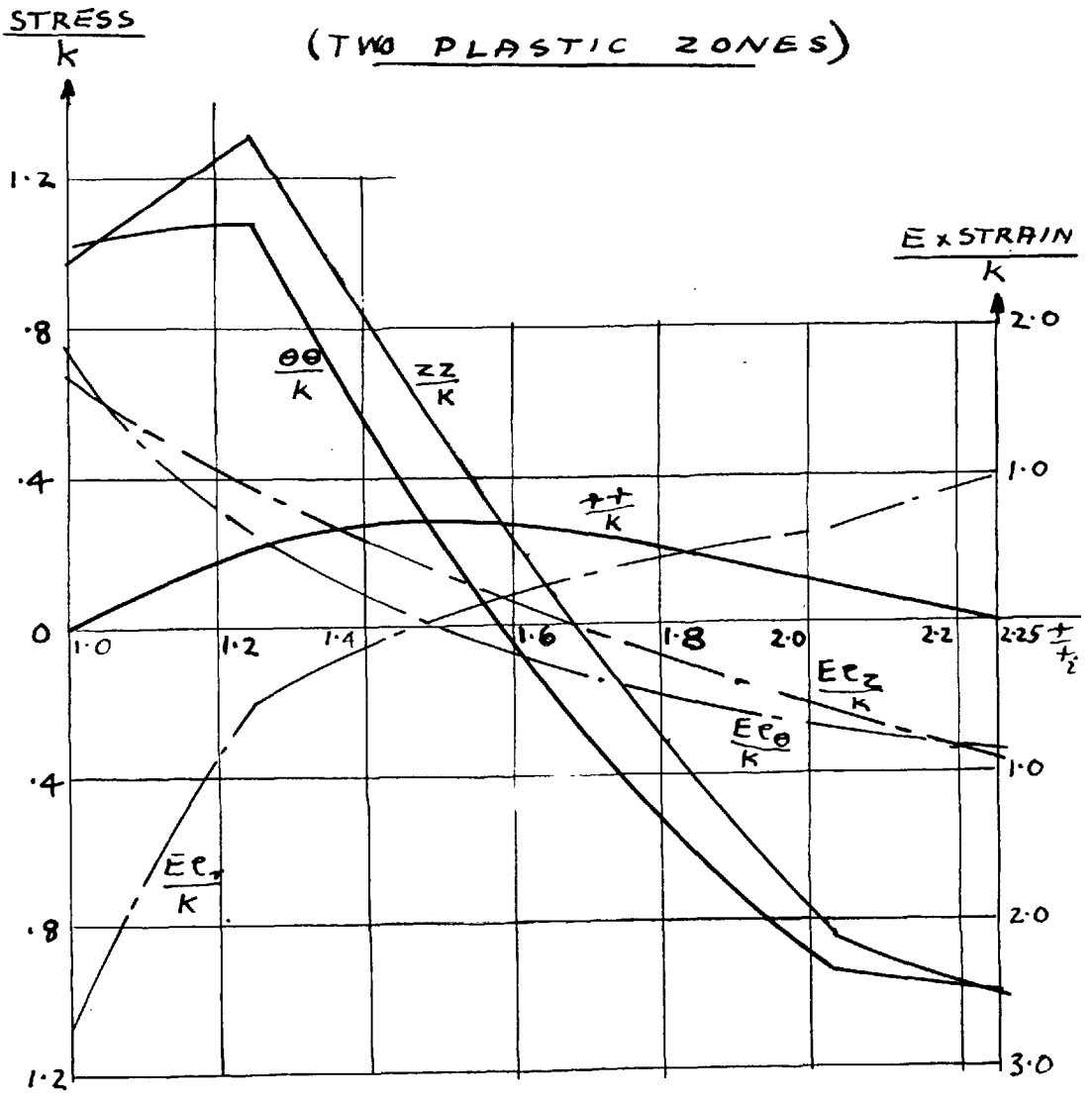


GRAPH 3·11 LONG CYLINDER

STRESS & STRAIN DISTRIBUTION

FOR $\frac{E\alpha(T_0 - T_2)}{k} = 2.545$

(TWO PLASTIC ZONES)

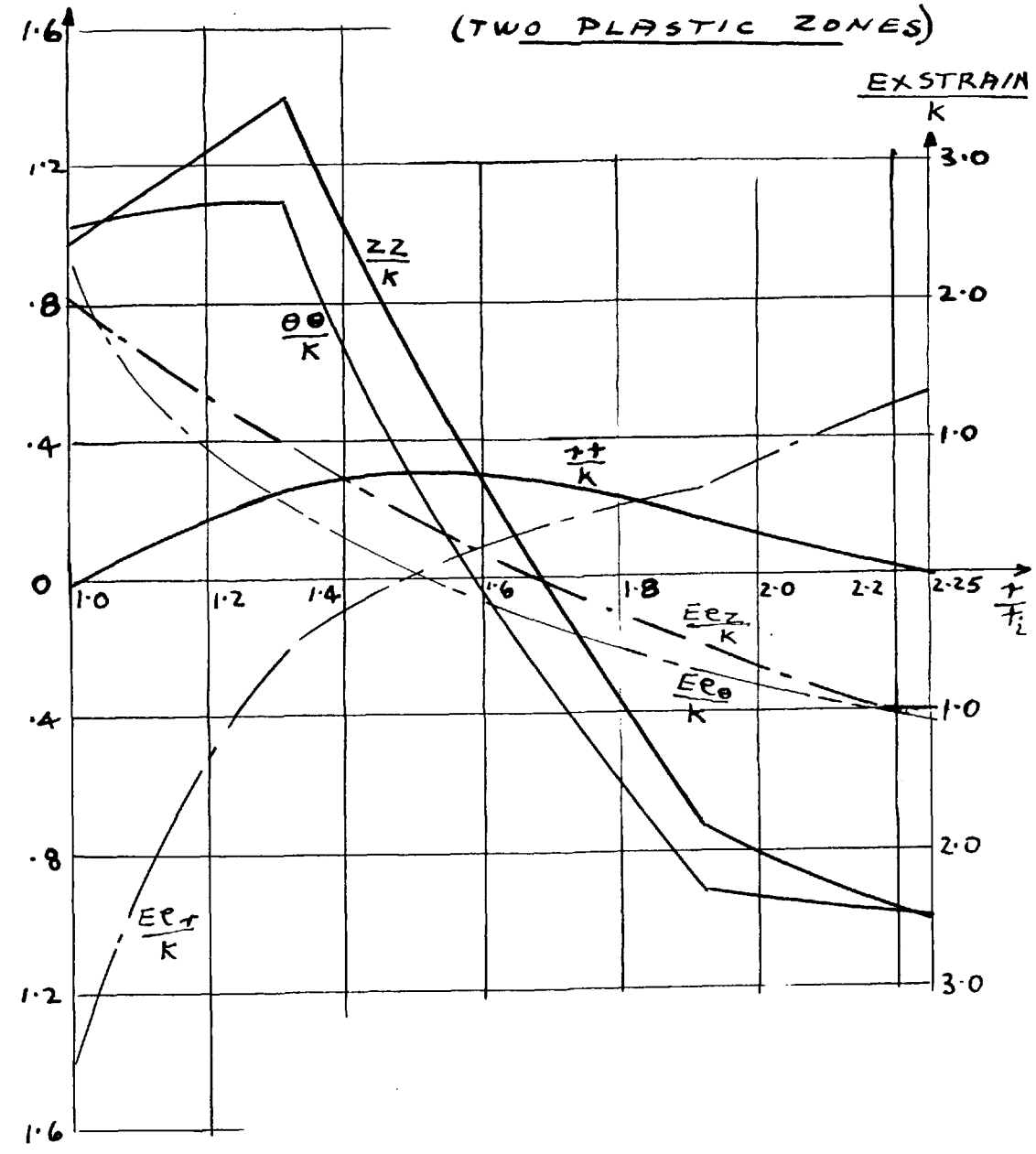


GRAPH 3·12 LONG CYLINDER

STRESS & STRAIN DISTRIBUTION

FOR $\frac{E\alpha(T_o - T_i)}{k} = 3·09$

(TWO PLASTIC ZONES)

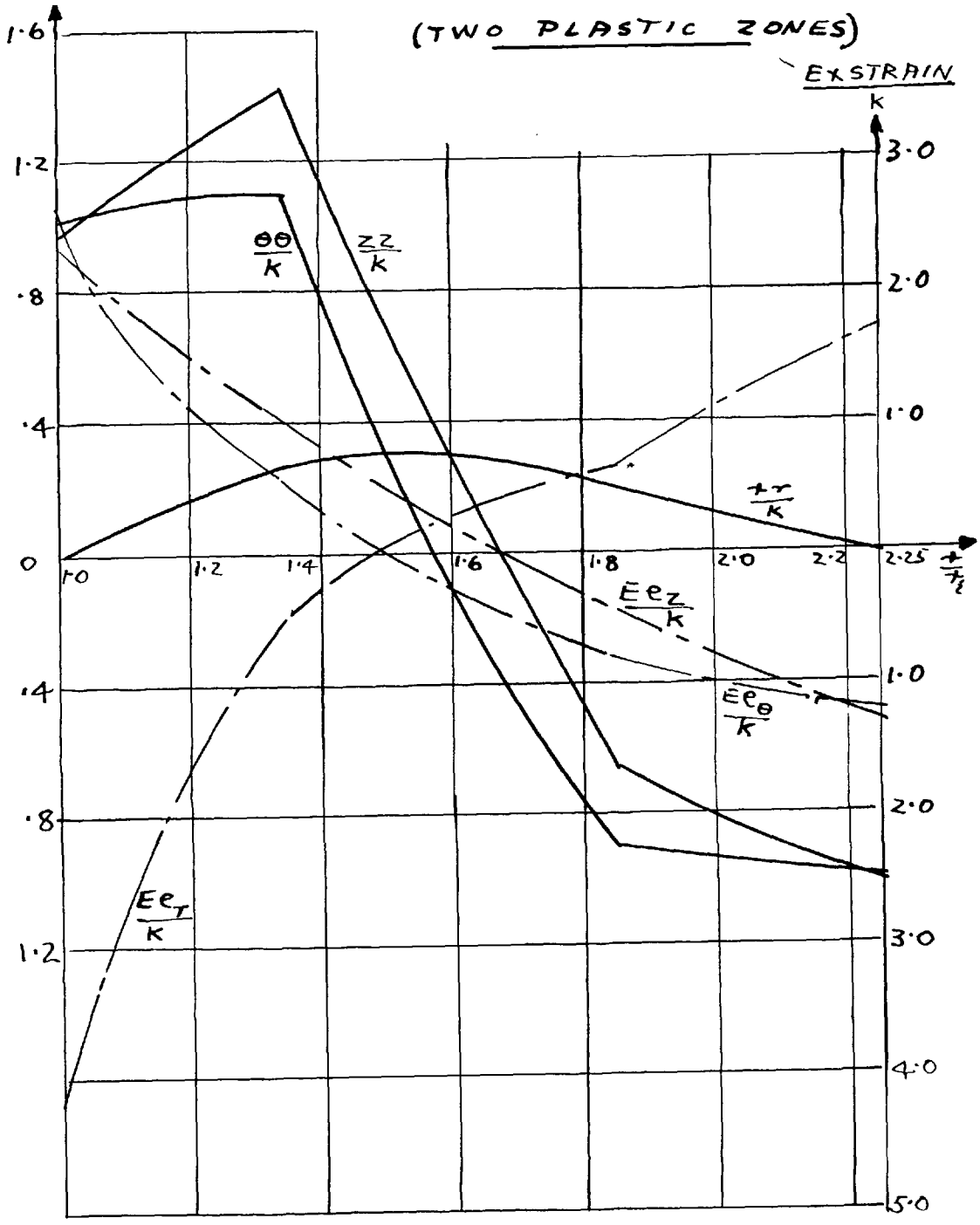


GRAPH 3·13 LONG CYLINDER

STRESS & STRAIN DISTRIBUTION

FOR $\frac{E\alpha(T_o - T_i)}{k} = 3.64$

(TWO PLASTIC ZONES)



4. THE EXPERIMENTAL DETERMINATION OF THERMAL STRAINS IN AXIALLY SYMMETRICAL SPECIMENS

4:1 The experimental programme was intended to do two things

a) confirm that the elastic computations give results which are in reasonable agreement with conditions prevailing in a practical case, such as a turbine rotor,

b) form part of a preliminary investigation into the behaviour of an axially-symmetrical body which is subjected to a temperature distribution more severe than that which theoretically causes the onset of plastic yielding.

However, overriding these requirements was the question of whether or not strains caused by differential thermal expansions can be measured with reasonable accuracy and repeatability. No experimental results of this nature could be found in the literature although creep in a hollow cylinder subjected to thermal gradients was investigated by Attia, Fitzgeorge and Pope (ref. 21) by the method of machining the specimen and examining the effect of the release of residual stresses.

General Consideration

At the time of writing the only practical way of measuring strains in a solid body which may ultimately contain a plastic zone is by strain gauges. Their use in dynamic stressing, even at high temperatures, is well established but the measurement of static strains, at temperature, over long periods is extremely difficult due to the effects of creep in the adhesive, inaccurate temperature compensation etc. This meant locating the strain gauges in the coolest part of the test specimen.

The question of transient versus steady state temperature distribution raises two practical problems against the transient condition, (a) the transient temperature distribution would be difficult to repeat, (b) more important, the maximum stress condition would occur at the hottest part of the rotor. Added to this is the greater control of all conditions for static state temperature distributions.

Another consideration is the similarity that can be obtained between one steady state temperature distribution and another more severe case; with care temperature gradients can all be increased by a common factor. This enables a graph of mean temperature gradient, $T_o - T_i$, versus strain, to be drawn and it was assumed that the presence of a plastic zone would manifest itself by this graph deviating from a straight line for increasingly severe mean temperature gradients. This cannot be done with the same certainty with the transient state.

As a result of the points outlined above, it was decided that the steady state condition was better for a first attempt at this problem, between each set of readings increasing the mean temperature gradient and allowing conditions to settle before taking further temperature and strain readings. With steady state temperature distribution the most severe stresses in a hollow cylinder occur in the bore, irrespective of whether the heat flow is outward radially or inward radially. Hence, as putting strain gauges in the bore and applying heat to the outer surface will record the maximum strains whilst keeping the strain gauges as cool as possible, this configuration was adopted.

The experimental rig took the form of a hollow specimen heated on the outer surface by electric heaters, cooled in the bore by a through flow of water with strain gauges in the bore and thermocouples strategically placed to cover the specimen surface as well as possible.

Difficulties

With this system three serious difficulties were encountered :

(a) waterproofing strain gauges and leads

(b) attaining an axially symmetrical temperature distribution

(c) ensuring adequate temperature compensation for the strain gauges.

The drift of strain gauge readings due to such factors as creep in the adhesive at temperature, proved to be much less serious at temperatures up to 70°C than was feared. The waterproofing

of strain gauges was also successfully achieved leaving (b) and (c) as the main obstacles.

Strain Gauge Temperature Compensation

Sticking strain gauges on a surface through which heat is passing prevents any possibility of that heat flow being uniform over the whole surface. Worse still, if heat is allowed to flow through the gauge the element will adopt an unknown temperature and compensation becomes impossible. In the case of a paper covered element, coated both sides with adhesive and two or three coats of waterproofing resin, heat flow will be negligible - but the metal under the gauge will adopt a slightly higher temperature than the surrounding free surface. The effect of this on strains is unknown but will undoubtedly be small if the strain gauge area is kept small. With a limited number of thermocouples it is impractical to record small undulations in the temperature profile and hence temperature compensation of the strain gauges can best be achieved by adopting a similar system to that created by the active gauge. The compensating gauge was stuck onto a shaped piece of metal and pressed against the specimen bore as near as possible to the active gauge. Each gauge pair was also calibrated by heating the specimen to a uniform temperature and recording the out-of-balance "strain".

Strain gauges with much improved temperature characteristics have recently been introduced and any future work in this field should be more accurate - and easier.

Accuracy of Axial Symmetry

It was realised at the outset that absolute axial symmetry was improbable with simple contact heaters and water as the cooling medium. In the event, thermocouples at three circumferential positions, 120° apart, recorded, at the worst, a circumferential variation of about 10 per cent. of the mean radial temperature gradient and most cases were appreciably better than this. This was with extreme care and it is the author's opinion

that improvement in this respect will only be achieved by adding the complication (but greater control) of heaters with variable heat output in the circumferential direction and variable underwater sprays in the bore. This system would help to combat capricious heat transfer and/or contact resistances at the specimen surfaces, but will require considerable development if control is to be effective and cost reasonable.

The accuracy of axial symmetry in the bore is reduced if the strain gauges are left as "islands". On the other hand, painting the bore to provide a complete hoop of heat insulation entails using very few strain gauges or allowing the bore temperature to rise and thereby increasing the problems of temperature compensation, creep in the adhesive, etc. The loss of accuracy in axial symmetry was regarded as the lesser of two evils and the strain gauges were left as "islands". In all tests with maximum heat flow, the bore temperature exceeded 50°C despite the fact that over 90 per cent. of the bore surface was free of gauges etc., which is considered to justify, at this stage, the "island" policy.

Thermal Stresses by Photo-elastic Techniques

The experimental investigation reported here was long, arduous and required considerable patience. Furthermore, the accuracy of the strains obtained can only be guessed at the moment. Resistance strain gauge techniques are certainly not sufficiently advanced, as yet, for reliable scale model testing of steam turbine rotors (for example) with their relatively slow strain changes. Also, strain gauges on the surface are undesirable impedimenta restricting the free flow of heat through the surface.

A photo-elastic method would have many advantages over the strain gauge approach, but much development of a suitable material and technique is still required. Hopeful signs in this direction are reported by Tramposch and Gerard (ref. 19) who produced two-dimensional transient thermal stresses in bars of photo-elastic materials by the sudden application of dry ice. The

results of these tests are encouraging, but a three-dimensional approach has not yet been reported.

An interesting analogy to thermal stresses was proposed by Clark and Hess (ref. 20). After pointing out that the same differential equation governs the conduction of heat in a homogeneous solid as governs the diffusion of gases and vapours, under certain restrictions, in organic solids, they analogise the two problems. As "the adsorption of water vapour by certain organic photoelastic materials causes swelling to occur, then small water-vapour concentration differences should cause swelling which, inside a restricted range, is linearly proportional to the quantity of water adsorbed, just as thermal expansion is proportional to the temperature". A comparison of theoretical and experimental results for a strip with heated edges is given to support their analogy. Perhaps most important is their claim to have cut specimens after "loading" and that this did not produce a disturbance of the stress pattern. This being so, it is possible that this stressing by the diffusion analogy might eventually lead to a very useful three dimensional technique. As Jennings (ref. 18) has shown that the photoelastic technique can be extended to include a plastic zone, this is probably the most promising experimental line for thermal stresses in the immediate future, especially if a photoelastic material can be found which exhibits plastic flow within the prescribed limits of the diffusion analogy.

4:2 Detailed Description of Experimental Apparatus

Test specimens

Three specimens were tested, two of the same simple shape, designated A and B, and one of more complicated shape, designated C (see diagram)*. The specimens were manufactured from an austenitic steel, F.C.B./T, by the suppliers, Firth-Brown Ltd. F.C.B./T has a rather high thermal expansion coefficient and a rather low thermal conductivity. This combination gives a high thermal stress for a low heat flow enabling the heaters to operate on lower power than with many steels. Another factor in favour of this material is its low limit of proportionality (about 7·0 in/in^2 at room temperature), which allows a study of plastic strains without the necessity of very large temperature gradients.

The two shapes were chosen in order to give computed solutions in a reasonable time. The experimental computing (trying new stress functions, etc.) was all performed on the simpler shape involving axial and radial boundaries only. The larger specimen has an irregular bore since this emphasises any computational difficulties with a small radius, whereas with a large radius the axial symmetry aspect of the problem is less important. A computed solution for each specimen is given in Appendix 2·7 and the temperature distributions of the experimental tests were, as near as could be achieved, proportional to the temperature distributions used in these computations.

Heat Supply

The heat supply was by electric contact heaters working from the 230V mains. In order to maintain steady conditions whilst strain temperature readings were taken, a Cambridge temperature controller was used to control the heater circuit, working from a thermocouple on the outer surface of the specimen under the heater. Phillips auto-transformers regulated the voltage applied to the heaters since the temperature controllers work on a cycle such that the power can only be switched on or off at intervals of

*(see page 122)

10 seconds and this would enable quite serious up and/or down temperature cycles if the applied voltage was vastly different from the ideal voltage to hold a steady temperature. As the on/off contacts inside the temperature controller will only take 2 amps. and a maximum of 8 amps. was desired at the heaters the controller was wired to operate a mercury relay through which passed the power to the heaters. An ammeter was also in the circuit in order to give some assessment of the operation of the heater.

The Heaters

The heaters were of the wrap around contact type, being wrapped around the specimen and the free ends bolted together. Initially, these were supplied by Hedin Ltd. but their design did not give even heat output throughout the length of the heater (i.e. all around the circumference of the specimen) and the construction had to be modified somewhat. In the final design the heaters consisted of six 400 watt (at 230V) helical elements separated by knuckle type ceramic insulators. After every six insulators a steel strip was inserted to ensure that the resistance of each increment of each element was the same and of equal value throughout the length of the heater. By this means the heat output per unit length of heater was constant around the circumference of the specimen. The elements terminated at $\frac{1}{16}$ in. mild steel plates. These plates were stuck to the end insulator and also given a coating of insulation using a paste compounded of Araldite 15 and flowers of sulphur, and cured at 200°C. The power supply was taken to these two M.S. plates. The knuckle type insulators were backed by a strip of sheet asbestos $\frac{1}{16}$ in. thick and 3 in. wide throughout the length of the heater and the whole held in place by a stainless steel strap the ends of which were bent outwards and were drilled for two $\frac{1}{4}$ in. bolts.

Cooling Water

a) Supply. The cooling water supply was piped from a mains

tap using rubber hose pipe and discharged into the vertical bore of the specimen.

A $\frac{1}{4}$ in. rubber sheet, of the same inner and outer diameters as the upper surface of the specimen, was placed on this surface to reduce heat loss.

An 8 in. diameter can, 2 in. deep and with a hole in the bottom (of the same diameter as the specimen bore) acted as a reservoir above the specimen. This can had a $\frac{1}{4}$ in. rim projecting downwards at a slightly larger diameter than the specimen bore and stood on the afore mentioned rubber sheet. A water-tight seal between can, rubber sheet and specimen (near bore) was made using Araldite 820 RH.

The discharge into the specimen bore was via 3, $\frac{5}{16}$ in. diameter copper pipes, the open ends of which were arranged to give the water a high velocity swirl as it passed through the specimen. The reservoir, mentioned above, was necessary to reduce this centrifugal effect on the free water surface.

The specimen stood on a rubber insertion pad (backed with sponge rubber) and this formed a water-tight seal around the bottom of the bore. A pipe from the middle of this pad passed the cooling water to a centrifugal pump which pumped the water to an adjacent sink. It was impossible to adjust the pump speed and rate of water inlet such that the water level in the specimen could be maintained steady because of fluctuations of the mains pressure. The possibility of sealing the specimen and passing the water through under mains pressure (50 lb/in^2 gauge) was considered but rejected because of the difficulty of bringing thermocouple and strain gauge wires through the seal and also because of the possible need to renew strain gauges and thermcouples in the event of failure. The electric motor driving the centrifugal pump was A.C. series wound and by putting an adjustable resistance in the electricity supply the speed of the motor (and hence the rate of water flow) could be adjusted. A device was therefore constructed which increased the resistance in the motor circuit if the water level fell and decreased the resistance if the water level rose.

b) Water level regulator. This was built around a pivotted arm made of ebonite and shaped to hold a seven contact mercury switch supplied by Engel and Gibbs Ltd. Into one end of this arm a length of $\frac{3}{16}$ in. screwed brass rod was fixed and to this rod a small carburettor float was fastened using two nuts and a legth of $\frac{1}{16}$ in. brass rod soldered to the float. To the other end of the lever was fastened a copper contact and another length of screwed rod to hold an adjustable counter-balance. The arm was supported by a pair of steel cup and cone bearings held by the base, and could rotate by about $\pm 5^{\circ}$ from the horizontal. Further movement was prevented by two copper contacts on an ebonite block also fixed to the base and in such a position that one of these contacts touched the copper contact on the end of the arm at each extremity of its movement. The contacts, which also acted as stops, were connected to an electric bell which thus gave warning if the water level rose or fell beyond a certain amount. As the float was raised the mercury flowed to cover successive contacts in the switch and with the float at its highest point all the contacts were surrounded by mercury. A resistance was built into the base of the device and connected in the motor circuit. Tappings were taken from parts of this resistance to the mercury switch contacts and raising the float thus caused an electric short across successive parts of this resistance. The resistance in the motor circuit was therefore dependent upon the position of the float which was in the water surface. An adjustable resistance, also in the base of the instrument, was connected in parallel with the whole of the aforementioned tapped resistor and enabled the sensitivity of the instrument to be adjusted. The power supply to the motor was from a small Phillips auto-transformer and by adjusting this and the sensitivity of the water level regulator the water level could be held steady to a total rise and fall of $\frac{1}{16}$ in. when the water flow was 3 gallons/minute.

Temperature Measurement

a) Instruments. All temperatures were measured using

chromel-constantan thermocouples. Twenty-four direct reading temperature indicators were supplied by the Foster Instrument Co. Ltd., nineteen had a range of 0 - 150°C and the remaining five were 0 - 200°C. The 0 - 150°C instruments required separate cold junctions.

These instruments were purchased with a view to recording twenty-four temperatures instantaneously by photography, using a modified Air Force camera. The temperature ranges on the instruments can be changed quickly and cheaply by changing a calibration coil. The temperature recording equipment should, therefore, be suitable for higher temperatures than those used so far, with transient conditions if required. In the investigation reported here, steady state conditions existed whilst readings were being taken and so the temperatures were recorded manually.

b) Cold Junctions The cold junctions were in metal pockets in two separate 4 in. vacuum flasks, 13 junctions in one flask and 14 in the other. Each flask was fixed into a wooden box, the lid of which supported the metal pockets and also a pocket for a thermometer. Each box was fitted with terminal strips to facilitate connecting up, the leads from the input terminals to the junctions being of the appropriate thermocouple wires, and those from the junctions to the output terminals being of copper wire. The box with fourteen junctions was fitted with six special silver contact two-throw, two-way switches and five of these were connected with two pairs of copper leads to the output terminals. This enabled two thermocouples to be read on one instrument. The remaining switch was used in conjunction with a temperature compensated instrument but otherwise in a similar manner. Thus thirty thermocouples could be read and the connections were arranged such that seven couples could be read on the 0 to 200°C instruments and twenty-three on the 0 - 150°C instruments.

c) Thermocouple Circuits The optimum operating position for the instruments was lying flat on a horizontal surface and

they were grouped in this position. The instruments were connected to the cold junction (where appropriate) using copper flex. Terminal strips were mounted on a panel near the operating position of the specimen and these terminals were connected to the input terminals of the cold junction boxes by 3 ft. of the appropriate compensating cable. The three circuits not passing through the junction boxes were connected in similar manner, the compensating cable being connected to the copper flex using terminal strip. The appropriate designation of each circuit was engraved on the terminal strips on the panel and an engraved plastic plate fixed to each instrument. Each instrument was calibrated for the circuit resistance of a thermocouple and 3 ft. of compensating cable by the makers, and checked after installation.

d) Fixing thermocouples to specimen

i. Outer surface Three axial grooves, $\frac{3}{32}$ in. x $\frac{3}{32}$ in. were cut along the outer surface of the specimen, equi-spaced around the circumference. These were necessary to enable the heaters to fit in contact with the specimen all around the circumference and allow thermocouple leads to be passed to the desired stations. These thermocouples therefore give the temperature about $\frac{1}{16}$ in. inside this surface. This results in the temperature recorded being below the outer surface temperature by perhaps 2 per cent. of the mean temperature gradient.

The thermocouple junction was formed by silver solder, the thermocouple terminating in a small sphere which was peened into the slot.

ii. Inside surface and upper radial surface Devices for pressing plates holding temperature compensating strain gauges and thermocouples were developed for the bore and also the upper radial surface and are described later in the strain gauge section.

iii. Lower radial surface The rubber pad upon which the specimen stood reduced the heat flow from the lower radial surface to negligible proportions and therefore allowed a very simple system to be used. Thermocouples were passed through the pad

from underneath, and glued into position to leave the junction very slightly proud of the rubber surface. The specimen was then very carefully positioned on the pad and the electrical contact between thermocouple and specimen checked by using an Avometer.

Note In the case of the larger specimens when thermocouples could be more usefully employed in the bore and on the outer surface, no temperatures were recorded on radial faces. Both radial faces were covered with a $\frac{1}{4}$ in. thick rubber sheet which would make the heat flow in the axial direction very small compared with the radial heat flow and, therefore, during the relaxation of temperatures, $\frac{\partial T}{\partial z} = 0$ could be assumed on radial faces.

Strain Measurement

Strain Gauge Bridge Strain measurements were taken using a Tinsley Strain Gauge bridge in conjunction with a Tinsley 25-way Apex Unit and Selector Switch thus giving a maximum of 25 channels for strain measurement.

Strain Gauges The strain gauges used were manufactured by British Thermostat and carried their designation SE/A/6. The element in these gauges is made of Eureka and is 6 mm long and 4 mm. across and has a nominal resistance of 200 ohms. At the time these gauges were purchased no computation of the strains in either specimen was available and the only guide was the solution given by Hoyle (ref. 3) which showed that rapid strain changes in axial and radial directions are possible with the thermal stress system. A small gauge element was therfore chosen but it transpired that for these specimens a larger (and more robust) element could have been used.

These gauges, unfortunately, proved to have a disproportionately large paper covering (perhaps intended to increase the mechanical strength of the gauge) of 1·5 in x ·375 in. This would prevent heat flow over an unnecessarily large area and the gauges were pared to about 0·75 in. x ·3 in.

So far as could be ascertained from strain gauge manufacturers the temperature characteristics of these gauges were not significantly different from the best of other makes available at the time of purchase.

Strain Gauge Adhesive The adhesive used for all strain gauges was Araldite Strain Gauge Cement. This cement was also used to anchor the gauge leads where they were soldered to the gauge. This adhesive can be cured at room temperature (24 hours) or for a shorter time at higher temperatures and requires no evaporation process during curing. This is a definite advantage since the gauges can be held in place using an adhesive tape (such as Sellotape) during the curing time. The gauges were pressed lightly against the specimen bore during curing by inflating a rubber inner tube in the bore.

The adhesive was initially cured at room temperature but before any straining tests were performed the specimen was heated several times to a uniform temperature of about 70°C to check temperature compensation, adhesion and general stability. This ensured that the curing process was complete and also served to put the gauge through a number of strain cycles.

Waterproofing Araldite Strain Gauge Cement provides little or no barrier to water and a gauge thus mounted without any protection becomes inoperative in seconds after submersion. Several attempts to waterproof strain gauges are reported (ref. 14 and bibliography) but all rely on ease of accessibility with no restriction on the area covered by the waterproofing.

Coating the strain gauge and leads with a suitable paint or resin is the most practical way of waterproofing. For this task the paint must be completely waterproof and have good adhesion to metal to prevent water seeping between the specimen and the paint. One substance which combines these two qualities is Araldite 820RH.[i]

i. Concurrent with this work, research was being performed at Imperial College upon the protection of springs against corrosion fatigue and Araldite 820RH was one of the more successful substances tested (ref. 17).

This is a resin which is mixed with a hardener and can be applied with a brush. At room temperature the drying time is about six hours but curing is not complete for six days; this delay can be cut by heating, at 60°C curing time is only one hour.

After the active gauges were stuck in position in the bore, any surplus adhesive around the gauges was carefully scraped away to reduce the area occupied by each gauge to a minimum. The connections to the gauges were then made using plastic coated wire and these leads were anchored to the end of the gauge using Araldite Strain Gauge Cement. The whole gauge and exposed leads were given a minimum of four coats of Araldite 820RH, the resin being allowed to overlap the edge of each gauge by upwards of 0·1 in. all round. Experience of this method of waterproofing suggests that one or two coats of Araldite 820RH would be extremely effective in easily accessible positions; but in more inaccesible positions, where painting and adequate inspection is difficult, it was found that two coats were an unreliable covering whereas four coats seldom gave trouble.

Temperature Compensation

General According to Jones (ref. 13) eureka strain gauge elements have a much lower temperature coefficient of resistivity than other commercial strain gauge materials. Jones also suggests that the temperature characteristic of a gauge can be affected by manufacture and it is advisable to compensate a gauge by another manufactured in the same batch from the same reel of wire. This precaution was, therefore, observed. The seriousness of the problem can be judged by the fact that a strain gauge stuck on F.C.B./T and subsequently heated to a uniform temperature gives a reading equivalent to about - ·0023 per cent. strain/°C difference between active and compensating gauges. This is a rough average figure, several gauges taken as a random sample varied by ± 5 per cent. To counteract this variation a calibration was obtained for each strain gauge pair after installation. As a calibration was necessary the opportunity

was taken to mount all compensating gauges on copper, which has a very similar expansion coefficient to F.C.B./T and is easier to use.

In the case of specimen C all the strain gauges mounted on the non-axial part of the bore and several confirmatory gauges on the axial part of the bore were not compensated. The "dummy" gauges were gauges on specimen B, which was maintained at constant temperature. A calibration was obtained for these gauges and although some estimation of temperature was required, this calibration system worked very satisfactorily. On the non-axial part of the bore gauges were paired, two gauges at right angles to each other fixed as close together as was feasible. Thus the difference between the strain readings for each pair of gauges should be reliable even if the calibration system was not acceptable.

Mounting Compensating Gauges and Thermocouples for Bore Locations* Each compensating gauge was stuck onto a copper pad, .75 in. x .375 in. x .125 in., the free surface of which was filed to the corresponding bore radius. Before sticking the gauge in place a small hole was drilled into one end face of this pad and a thermocouple soft soldered into this hole. After the gauge was stuck in place, a piece of $\frac{1}{16}$ in. rubber sheet was stuck into the gauge followed by a piece of $\frac{3}{16}$ in. Tufnol, the rubber being the same size as the copper pad, the Tufnol backing being of the same width but $\frac{1}{8}$ in. longer and the adhesive Araldite 820RH. The Tufnol backing was arranged so that the $\frac{1}{8}$ in. surplus length was adjacent to the nickel leads from the gauge element. Two holes were drilled through this free end of the backing and a legth of plastic coated connecting wire was passed through each hole, the hole diameter being such as to grip the plastic coating of the wire. The nickel gauge leads were soldered to the ends of these connecting wires.

The thermocouple was at the opposite end of the pad to the gauge leads and was fastened to the Tufnol backing by a piece of

* (see diag. 4.2 p. 123)

brass wire wrapped round the edges. All exposed parts, except the curved surface of the copper pad, were then given several coats of Araldite 820RH which was also used to firmly glue the gauge connecting wires to the Tufnol.

This arrangement allowed the strain gauge connecting wires to be handled without fear of damage to the strain gauge or waterproofing. The rubber sheet, sandwiched between the strain gauge and the backing, allowed the arrangement to be mounted on a device for pressing the copper pad against the bore thereby giving an even pressure on the strain gauge but not allowing the backing to impose any restraint upon the expansion of the copper pad.

For mounting the arrangement, a hole, in a position corresponding to the centre of the copper pad, was drilled and tapped 5 B.A. in the backing.

Device for locating Compensating Gauges and Thermocouples in the Bore A device was made to hold the compensating gauge and thermocouple pads, which both located the pads and pressed them against the bore with a force of about 10 lbs. each. The compensating gauges were to occupy positions between the active gauges, i.e. on stations 120° apart. This meant that the compensating gauge pads could be fixed in their appropriate positions on three vertical brass bars which could then be pressed outwards against the bore by a toggle action actuated by a screwed rod passing down the centre of the bore. The pads were fixed to the brass bars by 5 B.A. countersunk screws which passed through clearance holes in the bars and were screwed into the Tufnol backing using a locknut to position the pad at the appropriate radius. To take up any misalignment and ensure that the curved surface of the pad was in complete contact with the bore the 5 B.A. screws also passed through a flat strip of spring steel which pressed upon the lock nuts and pushed the pads outwards. This spring was tensioned by screws passing through the bars between the pad positions.

Two of these devices were constructed, one for each specimen

shape. The device for the larger specimens allowed for two different bore radii but no attempt was made to apply compensating gauge pads to the non-axial part of the bore.

Compensating Gauges and Thermocouples for Upper Radial Surface * Strain gauges were applied to the upper radial surface of the two simple specimens and the compensating gauges were again mounted upon copper pads. On this surface, heat flow is radial only and a mean temperature gradient of about 50°C/in. was obtained. Assuming the strain gauge element faithfully adopts the temperature of the specimen surface, the temperature variation within the element may be about 15°C. An exact copy of this temperature distribution in the compensating gauge is impractical and a mean temperature was aimed for by shaping the underside of the copper pads to form an arc of the required radius and about ·05 in. wide.

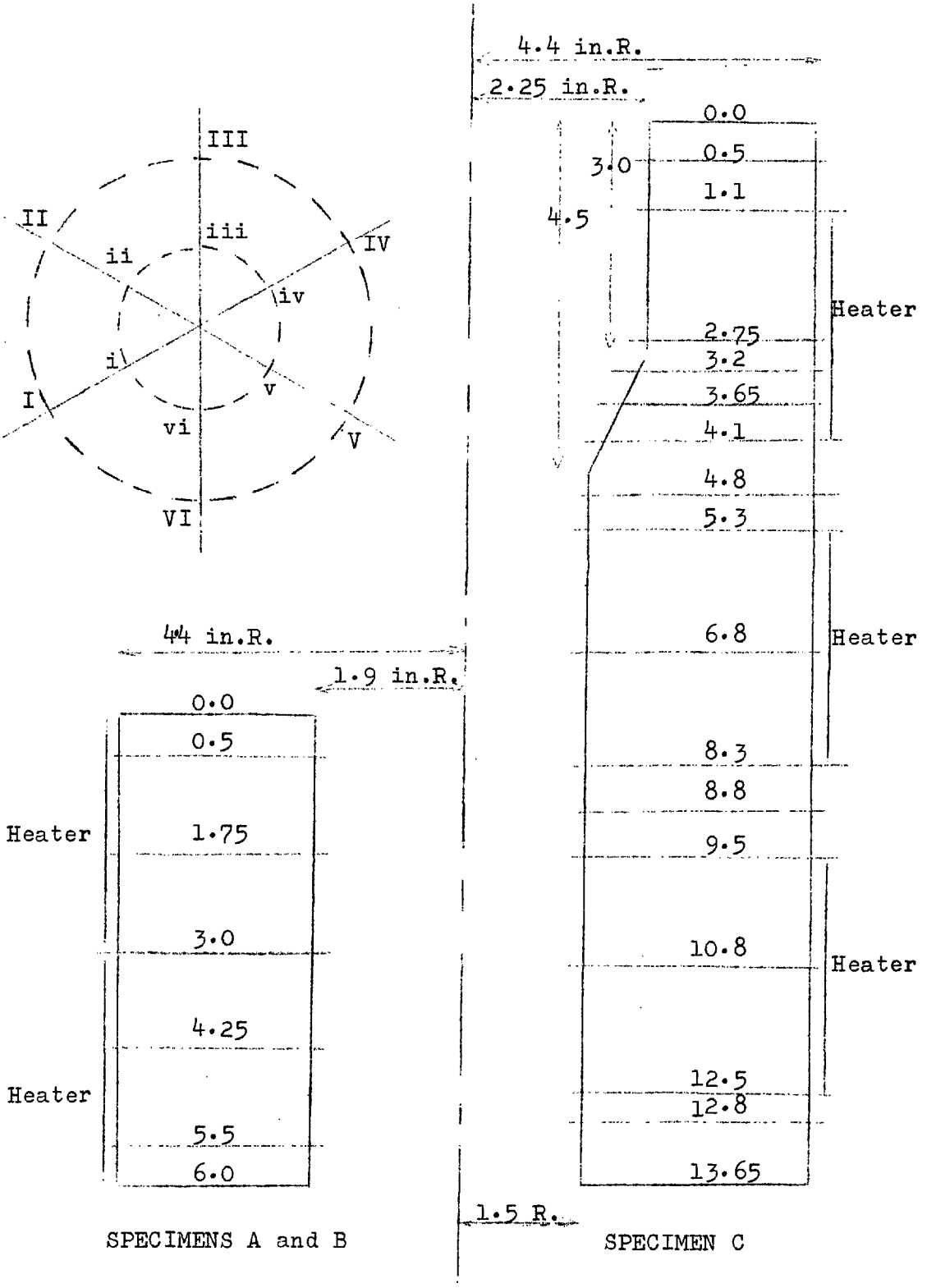
At the radius chosen, two active gauges were used, one radial and one circumferential, and both the compensation gauges were mounted on one copper pad and can therefore be taken to be at the same temperature. As both active gauge elements experience similar temperature variations and both compensating gauges are at the same temperature, the difference between the strain readings recorded should be reasonably acceptable even if the individual temperature compensation is not highly reliable.

A thermocouple was soldered to the copper pad before the compensating gauges were stuck in place. As a precautionary measure the compensating and active gauges were waterproofed.

Locating Compensating Gauges on Upper Radial Surface * Each copper pad took the form of a very open vee with one gauge on each leg. A frame was made from $\frac{3}{16}$ in. Tufnol sheet. The copper pads were a good sliding fit in the shaped holes and were each pressed downwards by two flat springs, screwed to the frame, so as to press the pads about the middle of each arm: the frame was carefully located and fixed to the specimen by two screws (previously stuck to the specimen) and nuts.

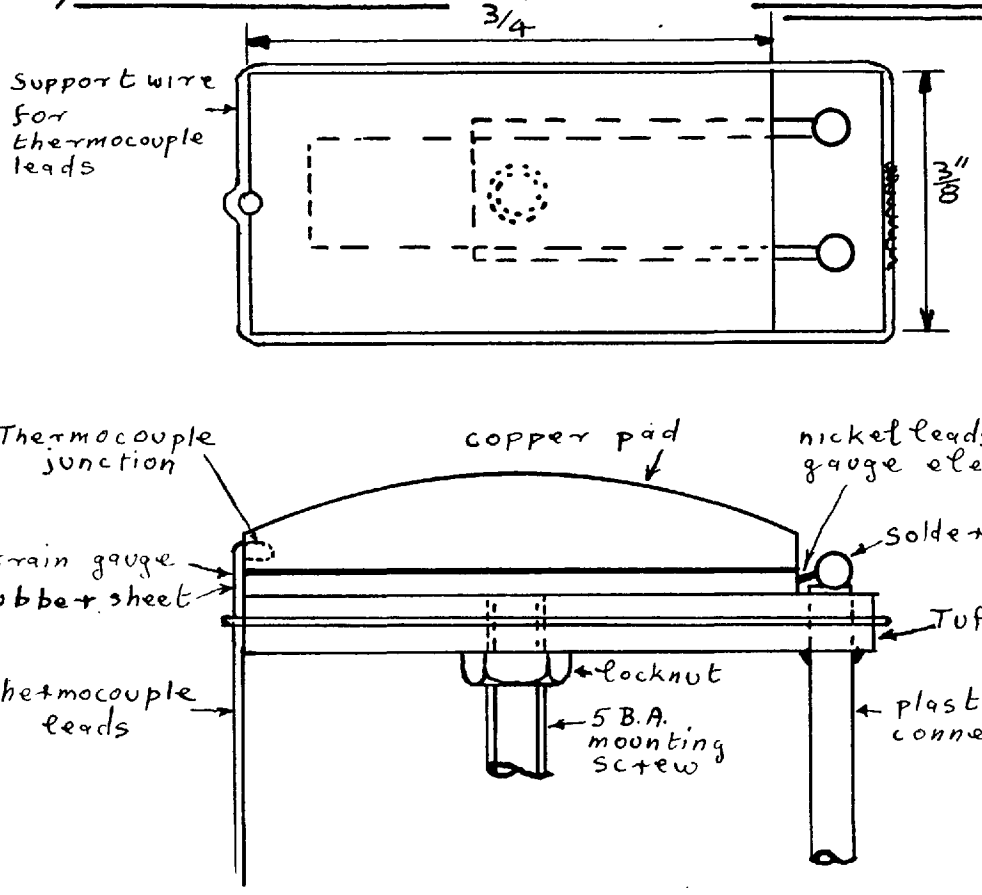
* (See diag. 4.2 p. 123)

Diagram 4.1 Specimens A, B and C, indicating dimensions, and axial and circumferential station positions.

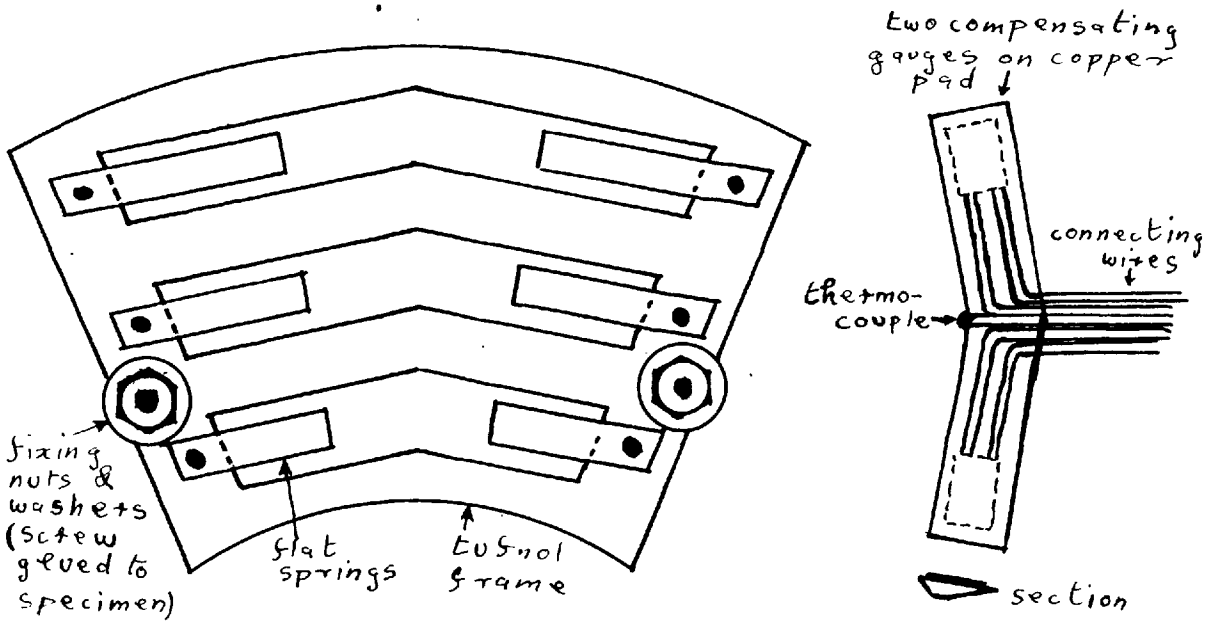


DIAG. 4·2 Mounting temperature compensating gauge

a) For bore locations and thermocouples



b) For upper radial surface



Locating device

4:3 Subsidiary Checks and Tests

Strain Gauge Sensitivity

The strain gauges were bought in bulk and the strain gauge sensitivity quoted by the manufacturers was 2·10. To check this a random sample of eight gauges was taken and tested on the usual four point bending rig. The bar used was of mild steel, 1·0 in. wide and 0·2495 in. deep. Four gauges were mounted on the upper surface and four gauges in corresponding stations on the under surface, an upper gauge being compensated by the corresponding lower gauge. The gauges were stuck with Araldite Strain Gauge Cement cured at 60°C. Two gauges were covered with Araldite 820RH and two were not. The four strain gauge pairs were connected to apex resistors 10, 11, 12 and 13, gauges 11 and 12 being coated with Araldite 820RH.

After putting the gauges through a few strain cycles the test was performed in the usual way, readings of maximum deflection and strain being recorded, the gauge sensitivity scale on the bridge being set at 2·00. The beam was strained to a final reading of 0·5 per cent. (maximum available with this bridge) and so each gauge was strained to 0·25 per cent. which is about the maximum strain (including expansion) obtained in the straining tests.

The maximum deflection is plotted against strain reading in Graph 4.1. The correlation between readings was good, 12 and 13 were coincident and gave the highest strain readings and 10 gave the lowest strain readings with 11 in between 10 and 13. From this graph it can be seen that the strain gauge sensitivity is constant up to at least 0·25 per cent. strain and the mean gradient $\frac{\text{max. deflection}}{\text{strain reading}}$ is 49·0

Simple bending theory gives

$$\text{strain} = \frac{4 \times \text{max. deflection} \times \text{beam thickness}}{L^2}$$

where L is distance between the two inner supports and was 10 ins. with this rig.

The distance between the upper and lower strain gauge

elements is ·2495 + ·01 = ·26 ins. (the strain gauge is about ·01 in. thick with the element apparently in the centre) and the strains will, therefore, correspond to a beam of ·26 in. thickness. From simple theory

$$\frac{\text{max. deflection}}{\text{strain reading}} = \frac{100}{8 \times \cdot 26} = 48.1$$

and the true strain gauge sensitivity = $\frac{49.0}{48.1} \times 2.0 = 2.04$

A value of 2·10 was used for all tests and the measured strains are, therefore, 2·9 per cent. low.

Temperature Effect on Strain Gauge Sensitivity

The effect of temperature on the strain gauge sensitivity is known to be small. Figures given by Jones (ref. 13) suggest a drop of about 1 per cent. for a temperature rise of 50°C for a Baldwin-Southwark cupro-nickel strain gauge and a Rotol publication (ref. 16) suggests no change up to 200°C. Even a 1 per cent. change is well within reasonable error for a first attempt at this problem and so the strain sensitivity was assumed constant for all tests.

Creep in Adhesive at Temperature

The term creep is here used to denote the phenomena causing the drift of the strain reading when the strain gauge is held at a constant temperature and all other controllable factors are held constant. Jones (ref. 13) reports that for an acetate the creep rate is initially fairly rapid but decreases with time so that after about four hours at temperature the total creep strain remains constant. For a temperature of about 70°C, Jones gives the creep after four hours as about ·01 per cent. Little information is given on the method of obtaining these creep results and such relevant factors as rate of heating, number of times previously heated to this temperature etc., are omitted. Nevertheless these are the only known creep tests reported.

With both active and compensating gauges at temperature, creep may occur in either or both gauges and, consequently, it is the

out-of-balance creep which will be significant. With the specimen at constant and uniform temperature the zero drift was recorded for several hours. Most gauge pairs gave a small zero drift in the negative direction but a few went positive. The results of several tests at each of the temperatures given can be summarised as follows: the zero drift over four hours was within the ranges $\pm$ .002 per cent. at 40°C, $\pm$ .005 at 55°C and +.001 to -.008 at 70°C. Few gauges were operated as high as 55°C.

In the test described, both strain gauges were strained by differential expansions only and could not confirm the possibility of the high initial strain rate reported by Jones. The most satisfactory method of assessing the out-of-balance creep under operating conditions is to compare the strains recorded early in an elastic straining sequence with the strains for the same temperature gradient after the specimen has suffered maximum straining and is being cooled down. This type of test was performed on Specimens B and C. The specimen was "loaded" by increasing temperature gradients between readings and then "unloaded" by decreasing temperature gradients between readings. There is, therefore, an individual assessment of creep for each gauge pair on specimens B and C, the loading and unloading graphs should, of course, coincide for elastic tests and the displacement of these two graphs will indicate the well-being of each gauge pair. However, it is by no means easy to distinguish between a small plastic strain and a small amount of creep although it is probable that for large strains creep will manifest itself as a reduction in the rate of increasing strain whereas for plastic straining an increase in the rate of increasing strain might be expected. This argument is based upon the fact that the active gauge being more highly strained is more likely to slip.

Using this criterion the "elastic" straining sequences indicate that a total creep of under .005 per cent. strain from beginning to end of a test sequence was usual although a few gauges did exceed this.

The residual "strains" following elastic test sequences and

also those following simple heating and cooling of the specimen were, with very few exceptions, within the range ± .01 per cent. strain and a significant proportion were outside the range ± .005 per cent. strain. There was no evidence of repeatability. All residual strains will, of course, include zero drift over the time required for cooling the specimen. Thus no residual inside the range ± .01 per cent. strain can be considered as definite evidence of plastic straining, and few residual strains in this range are recorded on the graphs of experimental results.

Waterproofing Checks

Test 1 The effectiveness of the waterproofing of each gauge was checked by leaving the specimen bore full of water for about twenty-four hours i.e. double the time taken for each test cycle. The resistance between each strain gauge and the specimen was then checked using the strain measuring bridge; one arm of the bridge was left open, one connection for the other arm went to the specimen and one connection to each strain gauge in turn. Hence if water reached a strain gauge element or leads an unbalanced current flowed in one arm of the bridge and a galvanometer deflection was recorded, a deflection of about 3·5 cms. per megohm with this bridge. If any readings were obtained the specimen was drained and after a few minutes these gauges were again checked. If the reading persisted this almost certainly meant that water had been absorbed by the adhesive and the gauge was scrapped and either replaced or ignored according to the importance of the station. On the occasions when the reading disappeared waterproofing was rendered effective simply by putting one or two more coats of Araldite 820 RH over the soldered joints and exposed leads.

Test 2 Following this check and after the specimen was prepared for straining tests all gauges were balanced whilst dry and any zero change noted immediately after filling the bore with water and again after some hours. Most gauges showed a small

zero change but for no gauge reported was this outside the range ± .002 per cent. before the initial straining sequence.

Between straining sequences the resistance between the specimen and the busbars was checked using the procedure outlined in test 1. Test 2 was also performed for $\frac{1}{2}$ to $\frac{3}{4}$ hour before each straining sequence.

During service a few gauges developed reactions to these tests. For all the gauges reported only three developed unsatisfactory (i.e. less than 20 megohms) earth resistances. These were* A, 4·25, iii, z ($\frac{1}{4}$ megohm following initial straining sequence) B, 6·0, I, 3·9, r and B, 6·0, I, 3·9, θ. The reading for specimen A disappeared when the specimen was dry (probably exposed leads) and during the attempt to re-waterproof this gauge several gauge leads were, unfortunately, disturbed. There is, consequently, only one straining sequence for specimen A and as the repeatability etc. of strain readings for specimen B was established and found to confirm specimen A results, this specimen was not re-equipped for further straining.

Following the initial straining sequence on specimen B, gauges at 5·5, v, z:0·5,iii, z and 4·25, iii, z showed zero changes on filling the specimen with water, 4·25, iii, z proved to be very time dependant even when dry and subsequently failed. The zero changes for 5·5, v, z and 0·5, iii, z were in the order of +·006 and -·008 respectively after three hours under water following the final straining sequence. Continuous efforts to remove this effect were not successful and as the cause was not known these two gauges must be considered with some reserve.

All gauges not mentioned, on all three specimens, had resistances to earth of at least 20 megohms and suffered zero changes inside the range ± .002 per cent. "strain" several hours after filling the specimen with water.

* See list of symbols for explanation of system used to refer to strain gauge and thermocouple stations.

Temperature Compensation Calibration

When the specimen was nominally ready for straining tests (i.e. heaters, thermocouples and strain gauges connected up) but before straining tests were performed, the effectiveness of the temperature compensation within each gauge pair was checked. The check consisted of balancing the gauges, heating the specimen to a uniform temperature and recording the "strain" readings. The specimen was allowed to cool to the initial temperature simply by leaving it for twenty-four hours, or more, with no power to the heaters. The residual "strains" were then recorded.

By changing and/or rearranging active and compensating gauges the "strain" at a uniform temperature could be arranged to be not greater than - .02 per cent. for a 50°C rise in strain gauge temperature, and many gauge pairs were better than this.

To ascertain the general repeatability of this type of test the strain gauges on specimens B and C were extensively tested. In some of the checks "strain" readings were obtained at two or three temperatures before the specimen was allowed to cool. In other tests the temperature was maintained constant over a few hours and readings taken periodically. The first type of test might be expected to reveal any serious lack of linearity of this out-of-balance temperature compensation "strain" with increasing temperature. The second type of test should reveal any out-of-balance creep and indicate the general stability of the gauge pair.

In general, the figures obtained in these tests were relatively small, moderately repeatable and linear with temperature, suggesting that it is not unreasonable to assess a suitable calibration figure for each gauge pair from the "strains" obtained at a uniform temperature. These calibrations, based upon the temperature reached by the gauge pair, were applied to all experimental strains reported.

GRAPH 4.1 STRAIN GAUGE SENSITIVITY

4:4 Straining Tests

Power was supplied to the strain gauge circuits and whilst the strain gauges stabilised the thermocouple readings were checked and set at the specimen temperature. When the strain gauge circuits were judged stable, the gauges were balanced. The specimen was filled with water and the balancing of the strain gauges checked to ensure that the presence of the water had a negligible effect. The flow of the cooling water was then started, power supplied to the heaters and the temperature controllers set to the required temperatures.

Power to the heaters was usually arranged during all warming up periods such that the outer surface temperature rose by about 1°C per minute. This slow rate should prevent any serious plastic zone being created by the steeper temperature gradients formed near the outer surface during transient heating.

As the outer temperatures approached the required values, 2 or 3 of the larger strains and 2 or 3 of the thermocouple readings were kept under observation until it became apparent that the outer temperatures, the bore temperatures and the bore strains had been sensibly constant for upwards of fifteen minutes, i.e. steady state conditions could be assumed. Strains were recorded first, followed by temperatures, after which the strains were quickly repeated as a safeguard and to ensure that the steady state assumption was not premature.

The settings on the temperature recorders and the voltages on the heaters were also recorded for use when the test was repeated later.

The temperature controllers were then set on the next temperature required, the heater voltages adjusted as necessary and the procedure described in these last two paragraphs repeated. A set of readings was obtained in this way for a number of outer surface temperatures up to a maximum of 200°C, the limit on the temperature recording instruments.

During a test cycle of this sort the rate of flow of

cooling water was usually maintained constant in order that, as far as possible, the differences between one set of strains and the next set of strains should not be a function of the cooling system. Thus with a fixed cooling system, the bore temperatures change as the outer temperatures change, but the bore temperature change follows a pattern and there is, therefore, a close similarity between successive temperature distributions.

Following the test cycle the specimen was allowed to cool to its initial temperature and the residual strain readings recorded.

Before the initial test sequence, a number of preliminary straining tests (not reported) up to a maximum mean temperature gradient of 55°C were performed, in order to establish repeatability.

Test Results

Due to the unfortunate accident to specimen A only one test sequence is given for this specimen, the results are, however, well supported by specimen B. With all specimens it was found that a change in the rate of flow of cooling water could affect the strain readings for a few gauges, in general a moderate (2 galls./min.) flow giving the largest strains. The initial straining sequences were therefore performed with a moderate water flow; in the subsequent tests on specimen B different rates of water flow were used but not varied throughout a straining sequence. The variation from axial symmetry was also modified in some tests. All tests on specimen C used a moderate water flow and the effect of the water flow checked by straining the specimen and then varying the water flow.

An axial temperature gradient in specimens A and B could not be avoided and a straining sequence (30-36) was performed on specimen B in which power was supplied to the lower heater only, thereby creating larger axial gradients and intensifying the effects of the axial gradients.

Interpretation of Test Results

At each important station the average temperature over an axial distance of $\pm$ 1.0 in., using all three circumferential positions, was calculated. The mean temperature gradient, $T_o - T_i$ was calculated from these average temperatures. The tests on specimen B suggest that the presence of axial temperature gradients has a very small effect on bore strains and the distance $\pm$ 1.0 in. should, therefore, give adequate indication of the significant temperature gradient.

The strain readings were corrected for out-of-balance temperature compensation using the temperature at the station and the calibration for each gauge pair.

The mean temperature gradients and the corrected strains are shown in graphical form in the Appendix at the end of this report.

In the case of specimen C, the mean temperature gradients at 2.75, 6.8 and 10.8 increase linearly relative to each other and gauges between these stations were therefore related to the nearest of these three mean temperature gradients.

4:5 Assessment of Test Results

Repeatability

A review of the whole of the experimental programme confirms that thermal strains can be estimated by strain gague techniques. The repeatability of readings is reasonable, in general any elastic reading could be repeated within $\pm$ 10 per cent. and many cases were much better than this. There is little doubt that repeatability could have been improved with greater control over the axial symmetry of the specimen, especially in the bore. Any connection between variations in the gradient $\frac{\delta e}{\delta T}$ and the degree or direction of the lack of axial symmetry is very obscure and no practical way of reliably correcting the resultant out-of-balance temperature compensation is possible with only three circumferential temperature stations in the bore.

In this work, the strain gauges are very severely tested and many had to be replaced during preliminary straining tests in order to have a reasonable number of gauges on each specimen during the main tests. Several gauges showed signs of withstanding one or two straining sequences and then weakening, especially at large strains.

Accuracy

Due to the nature of the problem an assessment of the accuracy of the test results is particularly difficult. Strains are known to vary rapidly in the radial direction near the axial surface. The surface strains are also extremely sensitive to heat flow through the surface. This was demonstrable with all specimens:- starting with a fairly high mean temperature gradient at steady state conditions, power to the heaters and the flow of cooling water were both switched off, creating slow transient conditions as the temperature of the specimen moved towards uniformity, with a very small amount of heat passing to the still water in the bore. The temperature gradient at the bore surface will then drop to a small value. A most significant discovery was the fact that the larger strains in the bore dropped to perhaps a third of

their former value in two or three minutes, whilst the mean temperature gradient did not drop by anywhere near this proportion. This clearly emphasises the sensitivity of a bore surface strain to the radial temperature gradient at that surface. Now the temperature gradient immediately beneath a strain gauge must be very low, with heat flow being diverted to the free surface surrounding the strain gauge. The precise effect of this on the strain pattern in the neighbourhood of the gauge is unknown, and although undoubtedly a secondary effect, whether this is 5 per cent. or 10 per cent. or more of the measured strain is purely conjecture at this stage. Nevertheless, this is the most likely explanation of the small strain changes found to accompany a change in the rate of cooling water flow which could not be accounted for in any other way. This unknown was, of course, anticipated and the area occupied by each gauge was kept as small as possible.

Absolute axial symmetry could not be expected with the fairly simple heating and cooling systems adopted. In most cases the recorded variations are only two or three degrees C but variations up to 10 per cent. of the mean temperature gradient were reached. The effect on strains of such a small circumferential temperature variations seems, from the results, to be negligible but a mathematical analysis would best show this (the apparatus could not do so satisfactorily, without modification to give more circumferential temperatures, etc.).

The mean temperature gradients may be 2 or 3 per cent. low due to the position of the outer thermocouples and additionally may differ from the true mean temperature gradient by up to $\pm$ 5 per cent. in the worst cases of circumferential temperature variation. As little heat will flow through the surface under the copper pads holding the bore thermocouples the pads may adopt a slightly higher temperature than the free surface. A reasonable estimation (assuming circumferential variation not worse than that recorded) is that the mean temperature gradients should be within 5 per cent. and probably low rather than high.

Errors due to poor temperature compensation of strain gauges

in the bore are reasonably predictable. The temperature profile immediately under the copper pad holding the compensating gauge should approximate to that under the active gauge, and superimposed upon this is the circumferential temperature variation. The difference in temperature between active and compensating gauges should seldom exceed 5°C and most cases give reasonable evidence of being better than this. Poor temperature compensation might, therefore, result in error of ± .01 per cent. strain for almost all gauges and up to, perhaps, ± .02 per cent. strain in the worst cases. This is common to all gauges, but for the larger strains measured represents an error of ± 5 per cent. up to ± 10 per cent. This is probably also true for gauges on non-axial surfaces.

Creep in the adhesive has been assessed at around .005 per cent. strain. Also the gauge factor set on the instrument being 2.9 per cent. high the measured strains are 2.9 per cent. low, due to this alone.

From the above discussion it is apparent that the overall error in the test results is largely a matter of opinion; a reasonable estimate is probably ± 10 per cent. for most large strains with the reservation that some results could well be much better than this. For smaller strains, the same errors will be proportionately larger and for these the test results should give a general estimate within, say, ± .02 per cent. strain and again some cases could be much better than this.

4:6 A Discussion of the Results of the Initial Straining Sequences

4:6:1 Specimens A and B Sequences 10A to 18A and 16B to 25B

There is no simple evidence of plastic strains for specimens A and B. Using the manufacturers' stress-strain curves for this material and the test results the limit of proportionality would be reached at a mean temperature gradient of about 33°C at the station 3 in. and in the bore.

During the first straining sequences both A,3·0,θ and B,3·0,θ exhibit a small sudden decrease (at 110°C and 130°C respectively) and then apparently continue at a slightly smaller gradient (the same gradient in both cases but there is no reason to suppose this is particularly relevant). The change in B,3·0,θ is known to coincide with an increase in water flow when an attempt was made to increase the range of the test sequence and subsequent tests showed that a high water flow did result in slightly lower strains than at a moderate flow. Also, the gradient of the first straining tests lies within the range of gradients subsequently obtained for elastic tests.

The gradient for B,3·0,θ-z is linear throughout and was subsequently reproduced.

During the first straining sequences both A,3·0,z and B,3·0,z are small, follow a non-linear path and have a relatively large residual. However, subsequent behaviour of B,3·0,z is similar, although perhaps not quite so severe. The behaviour of B,5·5,θ follows a similar pattern and also subsequently repeats itself with sufficient accuracy to nullify evidence of plastic strains. This behaviour of A,3·0,z and B,3·0,z and B,5·5,θ is discussed later.

It is just possible that A,0·5,θ and A,5·5,θ both suffer a slight gradient change but in both cases a constant gradient could be inferred with a few points showing scatter within the range ± .005 per cent. strain. This is not sufficient evidence of plastic straining considering the gauges were situated in areas of

rapid stress changes.

Gauges situated on radial faces are, of course, difficult to compensate due to the radial temperature gradients and a fair degree of scatter might be expected.

The gauges at A,0,3·9,r and A,0,3·9,θ both failed at a mean temperature gradient of about 70°C. This is amply demonstrated by the fact that neither specimen suffered sufficient permanent deformation for this to be detected by external and internal micrometers.

In the case of B,0,2·4,θ and B,0,3·15,θ the readings show some tendency to gradient changes but again a constant gradient can be drawn with scatter not exceeding $\pm$ ·005 per cent. strain. This is also true of B,0,3·9,r and B,0,3·9,θ up to a mean temperature gradient of about 100°C but as the operating temperature of the gauges was then in excess of 130°C, creep in the adhesive becomes very probable and the unaided evidence of these two gauges is not acceptable. In subsequent "elastic" tests the results are linear beyond this point, but this might be explained by assuming that further curing of the adhesive took place at the higher temperatures during the initial straining test. However, reasonable doubt exists especially as the gradient changes do occur at, or about, the limit of proportionality (using test results and manufacturers' figures). Nevertheless, creep in the adhesive is most likely since the residual strain at r = 4.4 in. would exceed that at r=3·9 and should have been detected by the micrometer if this residual is genuine.

4:6:2 Specimen C Sequence 8C to 18C

During the initial straining sequence 8C to 18C seven gauges exhibited some behaviour which could not be repeated in the subsequent "elastic" test sequences. These are the θ gauges at 3.65, 4.1, 6.8 and 10.8 and the z gauge at 10.8. Of these, the gauges at 3.65, 4.1 and 10.8 appear satisfactory both in the initial straining sequence and in their subsequent repeatability. This is not entirely true of the θ gauges at 6.8, the behaviour of which is difficult to explain, especially as the two gauges are

partly in agreement during the initial straining sequence and wholly consistent and repeatable afterwards.

Taking the strain readings of all gauges at their face value, the onset of plastic straining manifests itself by an abrupt change of gradient $\frac{\delta e}{\delta T}$ to a gradient which could not, subsequently, be repeated. The relevant gauges and a summary of the results are given in the following table:

	Elastic Gradient $\frac{\delta e}{100^{\circ}C}$		Plastic Gradient $\frac{\delta e}{100^{\circ}C}$	Apparent Yield		Residual Strain
	Initial Straining	Subsequent Straining		$T^{\circ}C$	e	
3·65,θ	+·120	+·124	+·200	50	+·060	+036
3·65,θ-z	+·055	+·060	+·130	45	+025	+036
4·1,θ	+·107	+096	+·148	47	+·050	+025
4·1,θ-z	+·084	+083	+·164	48	+·040	+039
6·8,θ,i	+·110	+·085	+·126	60	+066	+019
6·8,θ,v	+·076 ?	+·086	+·124	72	+054	+006
10·8,θ,i	+·127	+·122	+·180	63	+078	+020
10·8,θ,v	+·128	+·125	+·164	52	+068	+008
10·8,iii,z	+·065	+068	+·044	55	+039	-006

The first four readings are from two gauges, 3·65,θ and 4·1,θ, initially "compensated" by constant temperature gauges as were 3·65,z and 4·1,z, thereby allowing the two interpretations. 3·65,z is of constant gradient and 4·1,z is small and of almost constant value and so the gradient changes in θ-z graphs come solely from the two θ gauges.

The first four graphs follow a similar pattern - loading up an elastic gradient which was subsequently repeated, yield at a mean temperature gradient of 45 to 50°C after which loading continued along a higher gradient which could not subsequently be repeated. Unloading is down a gradient consistent with the elastic gradient but does not lead directly to the residual strain but is consistent with some plastic straining towards the end of unloading. The residual strains are also fairly large and did not

repeat. In subsequent straining tests 3·65,θ and 3·65,θ-z both show a slight tendency to a gradient change with a consistent displacement of the unloading line but having small negative residual strains. This effect is small and could be considered in the range of scatter, although further plastic straining cannot be ruled out. 4·1,θ and 4·1,θ-z subsequently show no sign of gradient change although θ apparently unloads down a slightly displaced path and both gauges have small negative residual strains. The evidence of plastic straining given by these two gauges is completely acceptable as their behaviour throughout cannot be faulted. Even temporary failure or slip of the gauges is ruled out; gauge failure would result in a decrease in gradient.

6·8,i,θ exhibits a very slight gradient change whilst loading but a constant gradient could just as well be inferred, the degree of scatter being practically unaffected. Unloading appears to be by the same gradient, displaced positive by about +·01 per cent. This gradient could not be attained within 15 per cent. subsequently and as the elastic loading and the unloading were by the same unrepeatable gradient the results from this gauge are not entirely satisfactory and must be treated with some reserve. The drop in gradient following the first test sequence (from about +·11 to +·085) is too large to be due to out-of-balance temperature compensation.

Preliminary straining tests before the initial test sequence (8C to 18C) established that at small mean temperature gradients 6·8,θ,i was appreciably larger than 6·8,θ,v. During the initial test sequence this proved to be true but after a shaky start 6·8,θ,v adopted the same gradient as 6·8,θ,i for most of the loading. Again this gradient was subsequently unrepeatable. Unloading again apparently follows a similar path to loading, but up to +·01 per cent. displaced.

In subsequent straining tests 6·8,i,θ and 6·8,v,θ agree with each other to a fair degree of accuracy, having an average gradient of about ·085. The gauges both show perceptible

gradient changes, but these changes are too small to be significant.

Throughout the initial test sequence the gradient of 6·8,v,z was +·07 but for subsequent tests this dropped to about +·055 to +·060. Thus all three gauges at 6·80 indicate beyond doubt that this part of the specimen was more highly strained during the initial straining test than during the subsequent tests. As the residual strains are all comparatively small and the hoop strains follow a somewhat nebulous path during unloading, the most plausible explanation is that the gauges exhibited some creep or slip at the higher strains, including the early part of the unloading. Such evidence of plastic straining as can be deduced is not spectacular and the degree of slip or creep involved is only of the order of ·01 or ·02 per cent. over a period of several hours. The subsequent behaviour of these two gauges also suggests that a small amount of slip or creep was present.

Three gauges at 10·8 exhibit signs of plastic straining, loading being elastic up to 52°C to 63°C after which a different gradient is assumed; unloading is down the original gradient to a residual strain consistent with plastic straining. This effect could not subsequently be repeated, although the elastic gradient could be repeated with sufficient accuracy.

4:6:3 Comparison of Test Results and Stress-Strain curves for F.C.B./T.

Specimens A and B

Using the test results and the manufacturers' stress-strain curves (which they vouch for) all specimens should have passed yield at a mean temperature gradient of under 60°C. Specimens A and B should have a plastic zone in the middle and specimen C at 6·8, 10·8 and on the oblique boundary. The test results show that plastic strains on axial boundaries are either small, in some cases too small to be detected by the methods described here - or contribute to the total strain in such a manner that the total strain is linear with increasing mean temperature gradient.

Accepting the manufacturers' stress-strain curves and using the test results it is possible to deduce the radial strain and the

degree of plastic straining according to the total strain theory, and allowing for work-hardening. As the shear stress rz is zero on axial boundaries, considerable simplification is achieved by using the maximum shear stress as the flow criterion. At the stations being considered e_θ is larger than e_z, therefore the maximum shear stress is $\frac{\theta\theta - rr}{2} = \frac{\theta\theta}{2}$ since rr is zero and the maximum shear strain is $e_\theta - e_r$. The maximum shear stress plotted against maximum shear strain is given in graph no. 4.2. Therefore, in the relationship

$$E\left\{e_\theta - e_r\right\} = f\left\{\frac{\theta\theta}{2}\right\} \qquad (1)$$

the function is known and for any value of $e_\theta - e_r$ there is a unique value of $\theta\theta$ from the maximum shear stress versus maximum shear strain curve.

In the nomenclature of chapter 3 using rr = 0

$$E\, e_\theta = u_1\, \theta\theta - u_2 zz \qquad (2)$$

$$E\, e_z = u_1 zz - u_2 \theta\theta$$

$$E\, e_r = -u_2(\theta\theta + zz)$$

whence

$$E\left\{e_\theta - e_r\right\} = \left\{u_1 + u_2\right\}\theta\theta \qquad (3)$$

and $$E\left\{\bar{u_1 e_\theta} + \bar{u_2 e_z}\right\} = \left\{u_1^2 - u_2^2\right\}\theta\theta \qquad (4)$$

$$E\left\{\bar{u_1 e_z} + \bar{u_2 e_\theta}\right\} = \left\{u_1^2 - u_2^2\right\} zz \qquad (5)$$

Choosing a value of e_θ and e_z from the test results this set of equations can be solved for β etc. by an iterative process, as follows. Estimate $e_\theta - e_r$ and obtain $\theta\theta$ from the maximum shear stress versus maximum shear strain curve using equation (1). β can now be obtained from equation (3) using $u_1 = 1+\beta$ and $u_2 = \sigma + \frac{\beta}{2}$ whence $\beta = \frac{2}{3}\left\{u_1 + u_2 - (1+\sigma)\right\}$. This can now be checked for compatability using equation (4). The whole process is repeated until a guessed value of $e_\theta - e_r$ is compatable with the test results. zz can then be obtained from equation (5).

The following computations were performed for specimen B at station 3.0 in. which is the most highly strained axial surface.

No allowance is made for temperature effects on the stress-strain curve since this is small.

Mean Temperature Gradient	Strains per cent. e_θ	e_z	$e_\theta - e_r$	e_r	β	$\theta\theta$	zz
70	·108	034	·185	-·077	·330	13·5	8·1
90	·138	043	·24	-·102	·520	15·1	9·3
110	·169	052	·31	-·141	·786	16·4	10·1
130	·200	061	·38	-·18	1·066	17·2	10·7

N.B. e_z from e_θ - e_z readings.

The strains e_θ, e_z and e_r can be broken down into plastic and elastic components using β, $\theta\theta$ and zz.

Mean Temperature Gradient	e_θ Elastic	e_θ Plastic	e_z Elastic	e_z Plastic	e_r Elastic	e_r Plastic
70	+084	+024	+031	+003	-·050	-·027
90	+·094	+·042	+·036	+·007	-·055	-·048
110	+·101	+·068	+·040	+·012	-·061	-·080
130	+·106	+·096	+·042	+·017	-·065	-·114

The values of e_r, β, $\theta\theta$ and zz are plotted on graph no. 4·3 and the positions deduced on the maximum shear stress versus maximum shear strain curve are marked on graph no. 4·2.

These deductions would seem to suggest the possibility of a serious plastic zone in specimen A and B, despite the apparent anomaly of the test results giving no acceptable evidence of such a zone. Furthermore, yield would have occured at a mean temperature gradient of 33°C and the specimens were taken above 130°C i.e. at least four times the gradient which should have caused yield. The long cylinder and the disc theories suggest that the radial strain is the most affected by the presence of a plastic zone. It is interesting to see that these deductions agree with this but even so the total radial strain is not here drastically different from what might be expected elastically.

The linearity of the strains e_θ and e_z with increasing temperature gradient would, of course, be repeated as the temperature gradient is reduced thereby leaving no significant residual strain. If the unloading were wholly elastic there would be a residual hoop stress of - 14·2 tn/in.^{2}, (i.e. a maximum shear stress of - 7·1 tn/in.^{2}) and so there may well be some plastic reduction of the initial plastic strains. It is certain, however, that more of the unloading is elastic than was the loading, with the consequence that there will be positive plastic residual strains which are in elastic compression in such a manner that the apparent strain is zero. The radial strain will probably have a genuine residual strain since these deductions suggest that unloading is not linear with increasing temperature gradient. This is not detected on the radial surface of specimens A and B due to the bending of the specimen (see elastic computation) which gives the inner part on the radial face a very low stress intensity.

Specimen C

The same method was used to deduce the position on the maximum shear stress versus maximum shear strain curve for specimen C at 6·8 and 10·8 (2·75 only just about reached the yield stress). Taking the measured strains at their face value, the following deductions were computed.

Station	Mean Temperature Gradient	Strains per cent. $e_{\theta,i}$,	e_z	$e_\theta - e_r$	e_r	β	$\theta\theta$	zz
6·8	134	·159	·092	·320	-·161	·813	16·6	13·1
10·8	96	·140	·057	·260	-·120	·586	15·6	10·5

At the two stations where the θ gauge shows large plastic strains, i.e. 3·65 and 4·2, the surface is neither axial nor radial. The principal planes are then θ, s and p where s and p are the directions around the boundary and perpendicular to it. From the elastic test results it can be seen that the maximum shear strain is $e_\theta - e_p$, and the maximum shear stress is again $\frac{\theta\theta}{2}$. Thus by substituting p for r and s for z the approach outlined for axial

boundaries can be used on this boundary to deduce e_p etc.

There is some doubt about the strain e_s at 4.2 and so the computations are performed for 3.65 only.

Mean Temperature Gradient	Strains per cent. e_θ	e_s	$e_\theta - e_p$	e_p	β	$\theta\theta$	ss
40	.048	.024	.079	-013	-	7.9	5.5
60	.080	.036	.140	-060	.177	11.7	7.8
80	.120	.048	.215	-095	.427	14.5	9.6
110	.179	.067	.340	-.161	.900	16.8	11.3

Breaking down e_θ, e_s and e_p into their respective elastic and plastic components using β, $\theta\theta$ and ss.

Mean Temperature Gradient	e_θ		e_s		e_p	
	Elastic	Plastic	Elastic	Plastic	Elastic	Plastic
40	+.048	-	+.024	-	-031	-
60	+.071	+.010	+033	+003	-046	-014
80	+.0885	+.0315	+040	+008	-055	-039
110	+.102	+077	+047	+020	-0645	-0965

The elastic and plastic components of the strains e_θ and e_p are indicated on Graph 4.4.

These computations again suggest that the strain normal to the boundary is the most affected by the presence of a plastic zone. Further, even when a plastic zone can be detected by strain measurements on the surface, the plastic components of strain may be very much higher than the surface strains suggest.

4:6:4 Comparison of Test Results and Long Cylinder Solutions given in Chapter 3

The strain curves at those stations showing signs of plastic straining confirm, by their general behaviour, the predictions made in the theoretical studies of plastic straining in long cylinders and discs (chapter 3). On specimen C good confirmation was obtained for the following:

a) at the onset of plastic straining in the bore the gradient $\frac{e_\theta}{T_o - T_i}$ changes abruptly to a higher value and

then continues constant at the higher value as the mean temperature gradient increases.

b) the axial strain appears to continue almost unaffected by plastic straining.

Absolute numerical comparisons cannot be made as the radius ratio $\frac{r_o}{r_i}$ used in the computations $\left\{\frac{r_o}{r_i} = 2{\cdot}25\right\}$ was chosen as an average for all specimens. Nevertheless, helpful comparisons can be made as an elastic solution for a long cylinder with a radius ratio $\frac{r_o}{r_i} = 3{\cdot}0$ predicts strains in the bore only 5 per cent. higher than those for a radius ratio of 2·25 for the same mean temperature gradient. Theoretical predictions for $\frac{r_o}{r_i} = 2{\cdot}25$ suggests that the gradient $\frac{e_\theta}{T_o - T_i}$ increases following yield, to 1·3 times the wholly elastic gradient. The following ratios were obtained experimentally:-

Station	3·65	4·1	6·8	10·8
ratio $\frac{\text{gradient after yield}}{\text{gradient before yield}}$	1·65	1·4	1·55	1·6
$\frac{r_o}{r_i}$	2·38	2·75	2·93	2·93

These ratios are rather higher than the theoretical prediction.

Another way of comparing the long cylinder theoretical analysis (obviously more applicable here than the disc) with the experimental results is to compare the surface strains e_θ, e_z and e_r plotted on graphs 3·5 and 3·6 with the experimental and deduced results for a specific mean temperature gradient. Taking the stations 6·8 and 10·8 on specimen C as being most suitable for this and reproducing, in part, the strains deduced in the last section, the comparison is as follows:-

Station	$T_o - T_i$		e_θ	e_z	e_r	Maximum shear strain $e_\theta - e_r$
6.8	134	Exp.[1]	·159	·092	-·161	·320
		Theor.[1]	·148	·134	-·208	·356
10.8	96	Exp.[1]	·140	·057	-·120	·260
		Theor.[1]	·105	·114	-·133	·238

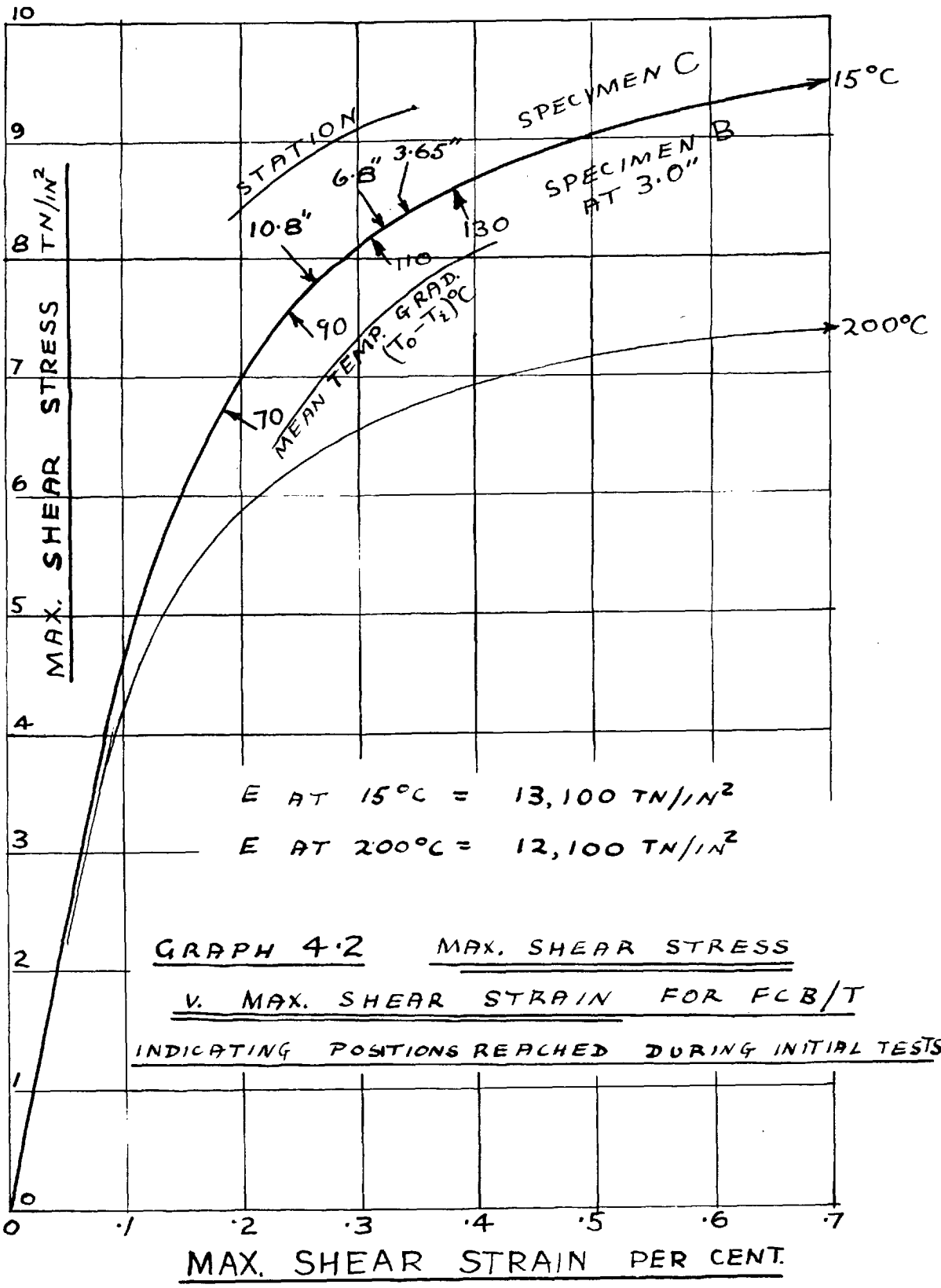
The long cylinder elastic solution (graph 3·8) predicts the hoop strains obtained experimentally within about ten per cent. but over-estimates the experimental axial strains by around fifty per cent. The maximum shear strains from this elastic long cylinder solution over-estimates the experimental maximum shear strain at 6·8 by about 20 per cent. and underestimates that at 10·8 by about 5 per cent.

Under these circumstances the above comparisons are quite good, and although the orientation of the strains is different, this is obviously due to the long cylinder condition, $\frac{\partial w}{\partial r} = 0$, not being applicable to these stations. Most important, the maximum shear strains which here indicate the severity of plastic straining, are within $\pm$ 10 per cent. i.e. of similar order as the wholly elastic comparison. Even at the station 3·65 (on the oblique boundary) where the radial temperature distribution is not nearly logarithmic the theoretical maximum shear strain, $e_\theta - e_r$, compares with the deduced experimental $e_\theta - e_p$, within 15 per cent. which is again of similar order to the wholly elastic comparison. In the cases of specimen A and specimen B, the long cylinder elastic/plastic solution under-estimates the maximum shear strains deduced for the station 3 ins. from the test results by about 10 per cent., which is again of similar order to the wholly elastic comparison.

N.B. At the stations considered above, the long cylinder conditions are more nearly satisfied than the disc conditions and the disc solutions seldom compare with the experimental results within 30 to 50 per cent.

Thus, at all stations considered, the degree of error in estimating the maximum shear strain from the long cylinder solutions (elastic, followed by elastic/plastic) is fairly consistent, or so comparison with the deductions from the experimental results appears to indicate. This is despite the fact that the orientation of strains at these stations is different from the orientation of strains in a long cylinder. It is suggested, therefore, that the elastic/plastic long cylinder (or, if more appropriate, disc) solution incorporating the desired

temperature distribution, can be used to give a useful indication of the likely severity of plastic straining at a particular section of a body. Also a comparison between an elastic long cylinder solution for the particular section and a more rigorous solution (probably based on the relaxation methods described in Chapter 2) for the whole body will indicate the likely error in using the elastic/plastic approximate solution.



GRAPH 4·2 MAX. SHEAR STRESS V. MAX. SHEAR STRAIN FOR FCB/T INDICATING POSITIONS REACHED DURING INITIAL TESTS

GRAPH 4·3 SPECIMEN B DEDUCTIONS FROM TEST RESULTS AT STATION 3·0"

GRAPH 4·4 SPECIMEN C DEDUCTIONS FROM TEST RESULTS AT STATION 3·65"

4:7 Comparison between Test Results and Computed Solutions for the Elastic Specimens

The value of $E\alpha$ (0·225 tn/in^2) was taken as constant during the computations. For the maximum mean temperature gradient obtained, the value of $E\alpha$ probably varies from about ·21 tn/in^2 at the bore (E = 13,100 tn/in^2) up to about ·225 tn/in^2 at the outer surface, taking the manufacturers' figures. The computed results for the bore have been scaled to suit the bore values of E and α and marked on the graphs thus, T. The influence of $E\alpha$ increasing with radius will be to increase these marked values and so the marked values on the graphs are minimum values and the true value is expected to be higher by, perhaps, 5 per cent.

4:7:1 Specimens A and B

The computed solution (p. 53 and 54) assumes a constant temperature along the outer surface and a constant temperature along the bore. The test results indicated an axial temperature gradient in the bore, the temperature dropping through the length of the specimen by about five per cent. of the mean temperature gradient. To ascertain the effect of this axial temperature gradient a much larger axial gradient was imposed in test sequence 30B to 36B. This showed that the axial temperature gradient has negligible effect on bore strains except near the ends of the specimen. Direct comparison between computed and test results is therefore possible for almost all stations.

The following strains give reasonable confirmation of the computed solution.

A, 3·0, θ — test results 5 to 10 per cent. high

B, 3·0, θ — within range - 5 per cent. to + 15 per cent. This gauge was particularly sensitive to the rate of flow of cooling water but nevertheless gave good repeatability

B, 3·0, θ - z — earlier sequences (up to 46B) are up to 10 per cent. high. In the two sequences from 47B to 61B, the early gradient is some 15 per cent. low, followed by

a sharp decrease in gradient with unloading down a gradient 5 per cent. lower than the computed value to the residuals of -·028 and -·018. This is not likely to be plastic straining and, although these two sequences had poorer axial symmetry, the most plausible explanation is that one gauge had begun to fail.

B, 3·0, z
A, 3·0, z
give confirmation of small strain at this station. Graphs slightly curved but within possible experimental error.

A, 4·25, θ up to 20 per cent. high, early gradient may be under 10 per cent. high.

B, 4·25, θ up to 20 per cent. high, with perhaps a small tendency to creep at higher strains.

B, 0, 3·9, θ
B, 0, 3·9, r
both gauges are about ·02 higher than computed value at $T_o - T_i = 100^{\circ}C$. With both compensating gauges on one pad this is consistent with pad being low in temperature. θ - r strains are within ± 5 per cent. of computed value.

B, 0, 3·15, θ within ± 10 per cent. but radial gauge failed leaving no cross check on temperature compensation.

B, 0, 2·4, θ
B, 0, 2·4, r
Strains are very small and errors comparatively large but give fair confirmation of smallness of strains.

Of the remaining gauges, B, 0·5, z; A, 4·25, z; B, 4·25, z; B, 5·5, z and B, 6·0, 3·9 θ had unsatisfactory reactions to the waterproofing checks and are, therefore, not acceptable. The behaviour of all these gauges is peculiar and in all cases the "strains" become appreciably more negative than expected. B,0·5,z; B, 5·5, z and B, 6·0, 3·9, θ show a degree of repeatability which emphasises the fact that, with so many possible variables, repeatability alone does not guarantee the reliability of a strain gauge reading.

Gauges A, 0, 3·9, θ; A, 0, 3·9, r both failed during test and their readings prior to failure do not agree with the same gauge stations on specimen B, nor with the computed solution.

Finally, the strain gauge readings at B, 5·5, θ exhibit a decreasing gradient, $\frac{\delta e}{\delta T}$, with increasing temperature gradient, and are less than half the computed value. This is not due to poor temperature compensation since the temperature of the pad holding the compensating gauge is comparable with the temperature at the same spot during the test on specimen A, and A, 5·5, θ is much larger and almost linear. There is no evidence that B, 5·5, θ failed, but this station is in an area where stress changes over the surface are rapid and are sensitive to temperature distribution. This is indicated by the test sequence 30B - 36B (where a large axial temperature gradient was deliberately introduced) in which the curved strain path is very much more pronounced than in other tests. This may also explain the apparent gradient change in both A, 0·5, θ and A, 5·5, θ and the difference between these two strain readings.

The overall comparison between computed and experimental values can certainly be considered as confirmation of the computation. Most of the large strains compare within ± 10 per cent. and the small strains are confirmed as small although the experimental accuracy for small strains is not very good. The comparison is such that it would not be reasonable to attempt to gauge the accuracy of the computation since the main differences between computed and experimental results are of the order of the estimated possible experimental errors.

4:7:2 Specimen C

The temperature variation around the specimen boundary compares reasonably in all tests with a surface temperature variation obtained by suitably scaling the temperatures used in the computed solution (p. 55 and 56). The experimental temperature variations were smoother than those assumed for the computation, giving discrepancies near the ends of the heaters and between heaters, such that the assumed temperature is rather higher than the experimental. These discrepancies did not exceed 10 per cent. of the mean temperature gradient, and were a localised effect in areas of no great interest. Their influence upon strains in the

areas under consideration will be small but will tend, if anything, to show higher computed strains than measured strains.

The overall comparison between computed and experimental values suggests that hoop strains are in fair agreement but strains along the boundary (s or z) are over estimated in the computed solution. The most serious differences are around the boundary discontinuity at the larger bore radius i.e. 3 inches from the top of the specimen. The computed solution anticipates the presence of a stress concentration (large values of e_s and e_z) not reflected in the experimental results. The precise reason for this difference is obscure; most of the strain gauges on specimen C gave good repeatable results and the computation has, in effect, been performed twice - independently as the X and η functions were used originally - and the two solutions do not differ significantly. It is impossible to say definitely whether the computations over-estimate, or the test results under-estimate, the strains along the boundary. At the bore surface, both axial and hoop strains are varying rapidly in the radial direction (fifty per cent. in under 0.25 in.) and this variation may be affected by the change of heat flow created by the presence of a strain gauge, but why hoop strains would apparently be less affected than axial strains is not clear. With regard to the presence or otherwise of a stress concentration at the station, 3 in., it is possible that, with the assumption of an abrupt boundary discontinuity, a very small stress concentration is present which is magnified by the short-comings (finite mesh lengths etc.) of the finite difference method. The mesh lengths in the area were reduced to about $\frac{1}{4}$ in. because of the rapid changes in functions, and the main stress concentration is confined to the two mesh points adjacent to the boundary discontinuity. A specimen containing prominent boundary discontinuities is obviously not the best shape for just simple comparison between computational and experimental results (a curved boundary would have been better for this) and for this reason the comparison is particularly interesting.

Consider first the strains on and adjacent to the area of changing bore radius, i.e. stations 2·75 to 4·1 and containing the spurious stress concentration at station 3·0. All the gauges in this area gave consistent repeatable results and the strains corresponding to a mean temperature gradient of 120°C at station 2·75 are compared in the following table with the strains from the computed solution (p. 55 and 56).

Station	Experimental or Computational	e_θ	e_s or e_z	$e_\theta - e_s$ or $e_\theta - e_z$
1·95	Comp.	·093	·080	+·013
2·48	Comp.	·093	·124	-·031
2·75	Exp.	·062	·066	-·004
2·95	Comp.	·087	·212	-·125
3·2	Exp.	·06	·06	0
3·4	Comp.	·104	·221	-·117
3·65	Exp.	·144	·074	+·070
3·87	Comp.	·122	·105	+·015
4·1	Exp.	·120	·024	+·096
4·1	Comp.	·14	·045	+·095

The hoop strains, e_θ, compare not too badly although the test results indicate a rapid rise between stations 3·2 and 3·65 whereas the computation shows a similar rise but slower and smoother (which is what might be expected with the finite difference approach). The comparison is within ·03 per cent. strain i.e. about twenty per cent. on the larger strains.

The strains along the boundary, e_z or e_s, do not compare in the region of the spurious stress concentration at station 3·0. Two axial strain gauges were used at station 2·75 and both gave strains of about one third of the computed strain. Similarly, 3·2, e_s is about a quarter of the computed value. Moving along the boundary the comparison of $e_\theta - e_s$ improves and only 1·1 in. away from the spurious stress concentration at station 4·1, the comparison is very good, $e_\theta - e_s$ being within $\pm$ ·003 per cent.

strain. Nevertheless, the value of e_s from the test results, although small, may still be in the order of half the computed value.

On the axial boundary the hoop strains are in good agreement viz:-

6·8, i, θ 6·8, v, θ	within ± 10 per cent. Some evidence of slight gauge creep at higher strains in some sequences. Slight gradient change in subsequent straining sequences but not sufficiently pronounced to be considered significant.
10·8, i, θ 10·8, v, θ	test results up to 15 per cent. high.
12·8, θ	test results within range zero to ·015 per cent. strain low. Good indicative results within possible experimental error.

The axial strain gauges gave good repeatable strains but for both 6·8, z and 10·8, z the test results were only about 60 per cent. of the computed results. It is very unlikely that these computed strains are affected by the spurious stress concentration.

Computationally boundary discontinuities are far more difficult to deal with than smooth, curved boundaries. The shape of specimen C was chosen partly with a probable stress concentration in mind, and also as being reasonably representative of the type of problem encountered in such discontinuities as are present in the complex shape of a rotor. The comparison between the test and the computational results suggests that the computation may have over-emphasised the presence of a small stress concentration coupled with a tendency to over-estimate axial strains at the bore surface by up to, perhaps, 50 per cent. of the computed strain. These effects are expected to be dependent upon mesh length and it would be a useful exercise to take an area containing a rapidly changing stress pattern and perform several computations using progressively smaller mesh lengths. Until such an investigation has been performed small stress concentrations anticipated by computations using reasonable mesh lengths should be taken as indicative rather than absolute.

5. CONCLUSIONS

The analysis of stresses and strains in axially symmetrical elastic bodies using stress function techniques, results in a biharmonic equation which must be satisfied throughout the body in conjunction with certain additional conditions to satisfy stress equilibrium on the boundaries. The problem is thus reduced to finding the most satisfactory mathematical method of solving a biharmonic equation with two boundary conditions specifying relationships between mixed derivatives of the function concerned.

The only satisfactory way of dealing with such a difficult equation when representing irregular shapes such as steam turbine rotors is by the use of the relaxation techniques devised by Southwell. Southwell and several other workers reported that the relaxation of a single function was very difficult and slow and a method of using two inter-related functions was devised. At the outset of this report Hoyle had demonstrated that the two function method of solution could be used to solve the thermal stresses in an irregular solid but had found that the two functions used were not entirely satisfactory.

Further consideration was given to the solution of the biharmonic equation by relaxing a single stress function. This met with very limited success, convergence being extremely slow. The problems encountered in stating boundary conditions in finite difference form for curved boundaries are serious The development of a satisfactory method of solving the biharmonic equation for thermal stresses using only one stress function is unlikely, even with the aid of modern computing devices.

In this report two new stress functions X and γ are presented, each of which can be relaxed satisfactorily, γ being particularly easy. Convergence is satisfactory when both functions are completely relaxed alternately, which should make it possible to perform the relaxation on an electrical resistance network.

It is shown that an expression for the gradient of each function normal to the boundary is obtained when the boundary stress conditions are written in terms of these functions. A new approach is developed to non-axial and non-radial boundaries when the gradient of the function normal to the boundary is known. This approach gives one algebraic finite-difference equation for each function representing all boundary shapes and is apparently the first attempt to rationalise boundaries in this way. The method outlined is more accurate than earlier methods and also gives finite difference equations which are easy to relax. Moreover, ease of relaxation and high accuracy are directly connected, the equations giving the most accurate representation of the function field being the easiest to relax.

It is also shown that any combination of centrifugal, pressure and thermal components of stress can be brought into the stress functions X and γ and the boundary equations with very little extra complication, although numerical solutions, so far, have not included pressure and centrifugal effects.

The problem of stressing an over-strained body with an irregular boundary has been examined. A rigorous solution, even using relaxation techniques, seems very remote. However, by making suitable simplifying assumptions it is shown that a solution can be obtained for a disc and also for a long cylinder. The analysis for discs results in a semi-iterative method of solution and numerical solutions can be obtained quickly and simply. In the case of long cylinders an iterative method of solution is necessary and one numerical solution may take weeks of hand computation. Both analyses use the total strain theory but there is some evidence that this will be in reasonable agreement with the incremental strain theory.

Several numerical solutions for steady state conditions in a disc and a long cylinder, with radius ratios $\frac{r_o}{r_i} = 2{\cdot}25$, are given,

the bodies being taken over 60 per cent. plastic. All plastic strains were found to be linear with increasing mean temperature gradient, yield manifesting itself only by a change in the gradient $\frac{\text{strain}}{T_o - T_i}$. The change in this gradient for e_θ and e_z on the surface of the bodies is small for a non-work-hardening material but the change in gradient for e_r is much more pronounced, especially in the case of a long cylinder.

The computations so far performed have demonstrated that, for some temperature distributions, two plastic zones may form in one body, one zone being compressive and the other tensile. The inter-action between these two zones is very small, indeed the stress relief obtained by the rest of the body following the formation of a plastic zone is slight. This is probably due to the axial and hoop strains in the plastic zone(s) increasing at a similar rate to that for a wholly elastic body as the temperature gradient is increased.

The measurement of surface strains produced by temperature gradients within a body is extremely difficult. However, using steady state conditions and heating the outside surface of a hollow cylinder whilst cooling the bore, the maximum strains are produced at the coolest part of the cylinder. By confining strain gauges to the coolest part of the specimen it was found that reasonable evidence of the behaviour of these surface strains could be obtained.

Computed solutions for the elastic specimens were obtained and compared with the strains measured during elastic straining of the specimens. In all tests performed the computed solutions estimated hoop strains on the bore surface within $\pm$ 20 per cent. (often better than this) of the measured strains. As the hoop strains are usually the largest and most important this is very satisfactory. The comparison of the axial strains, computed and experimental, suggests that the computed solution over-estimated

the axial strains on the bore surface by up to 50 per cent. Also there is strong evidence that the computed solution for one specimen over-emphasised the possible presence of a small stress concentration at the boundary discontinuity.

Although, in this part, the comparisons between test and elastic computational results are a little disappointing they serve to emphasise the necessity to view computed solutions intelligently and within the limits of the finite difference method. In areas where only one or two adjacent mesh points show high stress levels these stresses should be considered only indicative of a likely stress concentration and for more definite information the mesh length must be considerably reduced. Elsewhere the computed stresses can be considered an adequate guide, with the proviso that there may be a tendency to over-estimate the axial strains.

Evidence of plastic straining was not spectacular, despite imposing temperature gradients over three times more severe than that expected to cause yield. Only one specimen gave results suggesting the formation of a plastic zone in the bore. This was in good indicative agreement with the solutions for the over-strained long cylinder in as much as the specimen hardly satisfied the long cylinder condition $\frac{\partial w}{\partial r} = 0$. Yield did manifest itself by a change in the gradient $\frac{e_\theta}{T_o - T_i}$ and at about the mean temperature gradient deduced from the elastic experimental results and the stress-strain curve for the material. After yield the gradient remained constant during "loading", and "unloading" was, in the main, consistent with the original elastic gradient. This was true on axial and non-axial surfaces in the bore of the specimen. The strains along the boundary, e_s or e_z, were almost unaffected by the apparent presence of plastic straining in the hoop direction.

For all specimens it is deduced that the radial strain is the most affected by the presence of plastic straining, again in agree-

ment with the overstrained long cylinder solutions, and that the short cylinder specimens must have contained a plastic zone although showing no outward indication of this. An odd type of plastic straining results, in which elastic and plastic components of e_θ and e_z contribute to the total strain in such a manner that the total strains are linear and have the same rate of increase with increasing temperature gradients after yield as before. As unloading will have more elastic and less plastic straining than loading final residual strains in each direction will result, which are in elastic compression (in this case) back to zero. Thus it would be true to speak of residual stresses in these two directions although there would certainly be a residual strain also in the radial direction. This can only be a hypothesis but it is by no means inconsistent with the predictions of the overstrained long cylinder or disc solutions.

It is suggested that, by intelligent use of the overstrained long cylinder and/or disc solutions performed for the appropriate radius ratio $\frac{r_o}{r_i}$ and temperature distribution, the likely severity of plastic straining in most irregular bodies can be estimated. Predictions from an elastic long cylinder solution were compared with the elastic tests results and it is shown that, by assuming that this degree of comparison is maintained after yield, the estimate of the severity of plastic straining given by the overstrained long cylinder solution would not have been in error by more than a few per cent., and this includes the non-axial part of the bore.

Future experimental work on the plastic straining caused by temperature gradients must take into account the greater changes in the strain normal to the surface and for this strain gauge techniques are too limited.

REFERENCES

1. Southwell, R.V.
   Proc. Royal Society A 180 1942 367 - 396
2. Allen, D.N. de G., Fox L., Southwell R.V.
   Phil. Trans. Royal Society C, 1 1943 99 - 135
   Proc. Royal Society A 239 1945 501 - 537
3. Hoyle, R.D.
   Proc. I Mech. E., 169 1955 pp. 553 - 562
   also Ph.D. Thesis, London, 1952
4. Southwell,R.V. 1956 Relaxation Methods in Theoretical Physics, II. Oxford University Press
5. Allen D.N. de G., Relaxation Methods,1954
6. de Vries J.P. and Oerth R.A. "Thermal Stresses in Bodies of Revolution" July 1958 U.S.A.E.C. Research and Development Report W A P D - 201 Contract AT-11-1-GEN-14
7. Fox, L.
   Phil. Trans. Royal Society A 242 1949-50, pp. 345-378
8. Parkus, H.
   Journal Applied Mechs. Dec. 1953 20 No. 4
9. R.L. Brooking, J. Brown and Miss B.R. Atkins
   "A direct, easily computable method for the evaluation of centrifugal and thermal stresses in discs, and stress changes due to plastic flow and creep". N.G.T.E. Report No. R.122 July, 1952
10. D.R. Bland
    Journal of the Mechanics and Physics of Solids
    4 1955-56 pp. 209-229
11. C.W. McGregor, L.F. Coffin and J.C. Fisher
    Journal Franklin Institute 245 1948 p. 135
12. R. Hill "The Mathematical Theory of Plasticity"
    Oxford Clarendon Press, 1950.
13. Jones, E. "Some Physical Characteristics of the wire-resistance Strain Gauge".
    Measurement of Stress and Strain in Solids,
    Inst. of Physics, 1948.

14. Perry, C.C. and Lissner, H.R. The Strain Gage Primer
McGraw-Hill Book, Inc. 1955
This book has a good bibliography.

15. Dobie, W.B. and Isaacs, P.C.G. Electric Resistance Strain Gauges E.U.P. Ltd. 1948

16. The Principles of Stress Measurement by means of Resistance Strain Gauges Rotol Ltd., Gloucester

17. Hobson, J.A. M.Sc. Thesis, London, 1959.

18. Jennings, C. Ph.D. Thesis, London, 1958.

19. Tramposch, H. and Gerard, G.,
Journal Applied Mechs. 25 No. 4 Dec. 1958 pp. 525-8.

20. Clark, S.K. and Hess, R.L.
Journal Applied Mechs. 25 No. 4, Dec. 1958 pp. 627

21. Attia, Y.G., Fitzgeorge, P. and Pope, J.A.
Journal of the Mechanics and Physics of Solids
2 1954 pp. 238-258.

22. Hilton, H.H.
Journal Applied Mechanics 19 No. 3 pp. 350-54

23. Wang, C.T. "Applied Elasticity".
McGraw-Hill Publishing Co. Ltd. 1953

24. Prager, W. "Shakedown in elastic, plastic media subjected to cycles of load and temperature".
Symposium sulla plasticita nella scienza delle construzioni. Varenna September 1956.

25. Poritsky, H. and Fend, F.A.
Journal Applied Mechanics 25 No. 4 Dec. 1958
pp. 589-97.

GRAPH NO 4·5
A & B, 0, 3·9, 9
ALL STRAINING SEQUENCES

MEAN TEMPERATURE GRADIENT $(T_0 - T_i)$ °C.

140
120
100
80
60
40
20

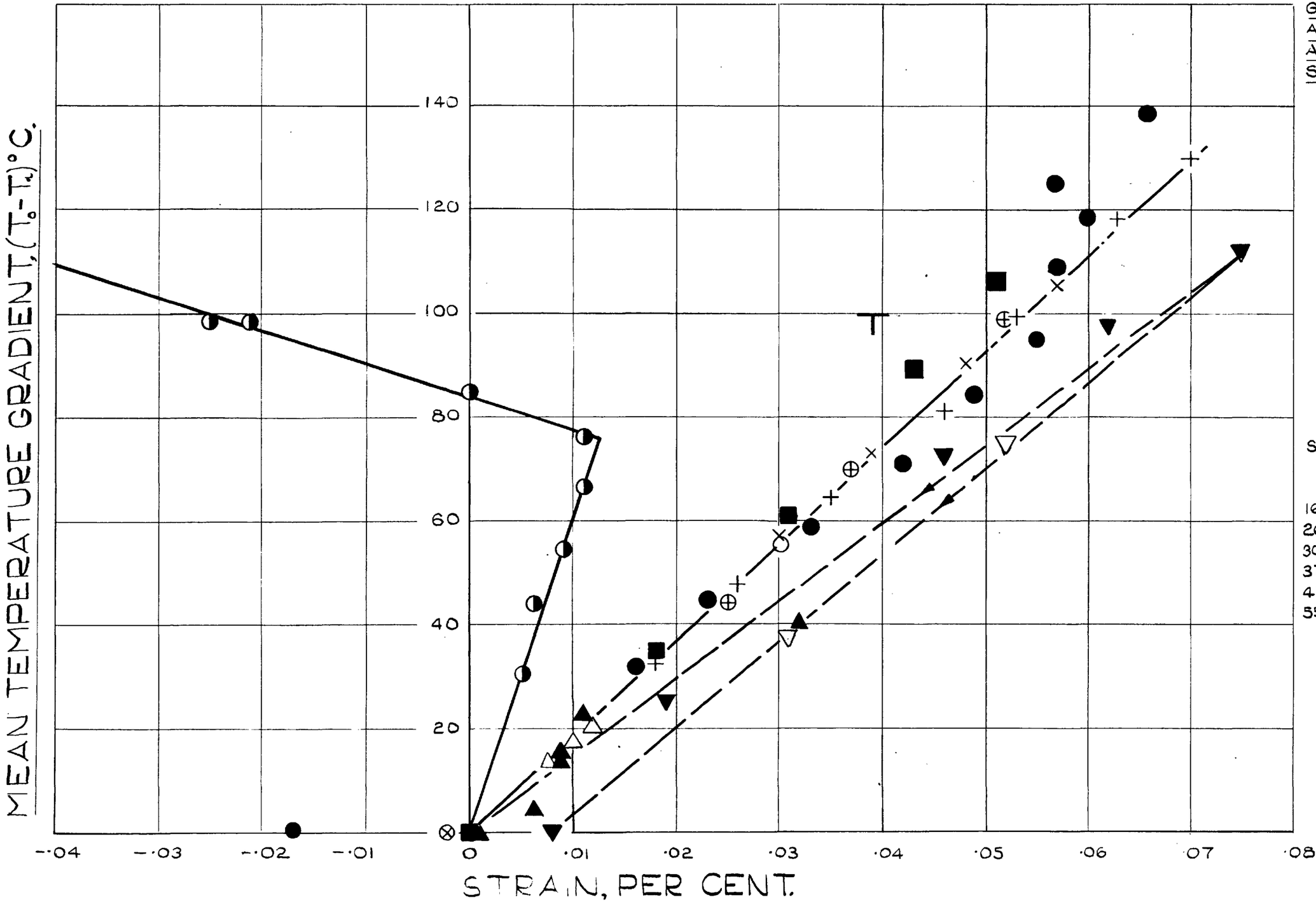
SPECIMEN A
" B

	UP	DOWN
16–25	●	○
26–29	■	□
30–36	▲	△
37–46	+	⊕
47–54	×	⊗
55–61	▽	▽

−·13 −·12 −·11 −·10 −·09 −·08 −·07 −·06 −·05 −·04 −·03 −·02 −·01 0

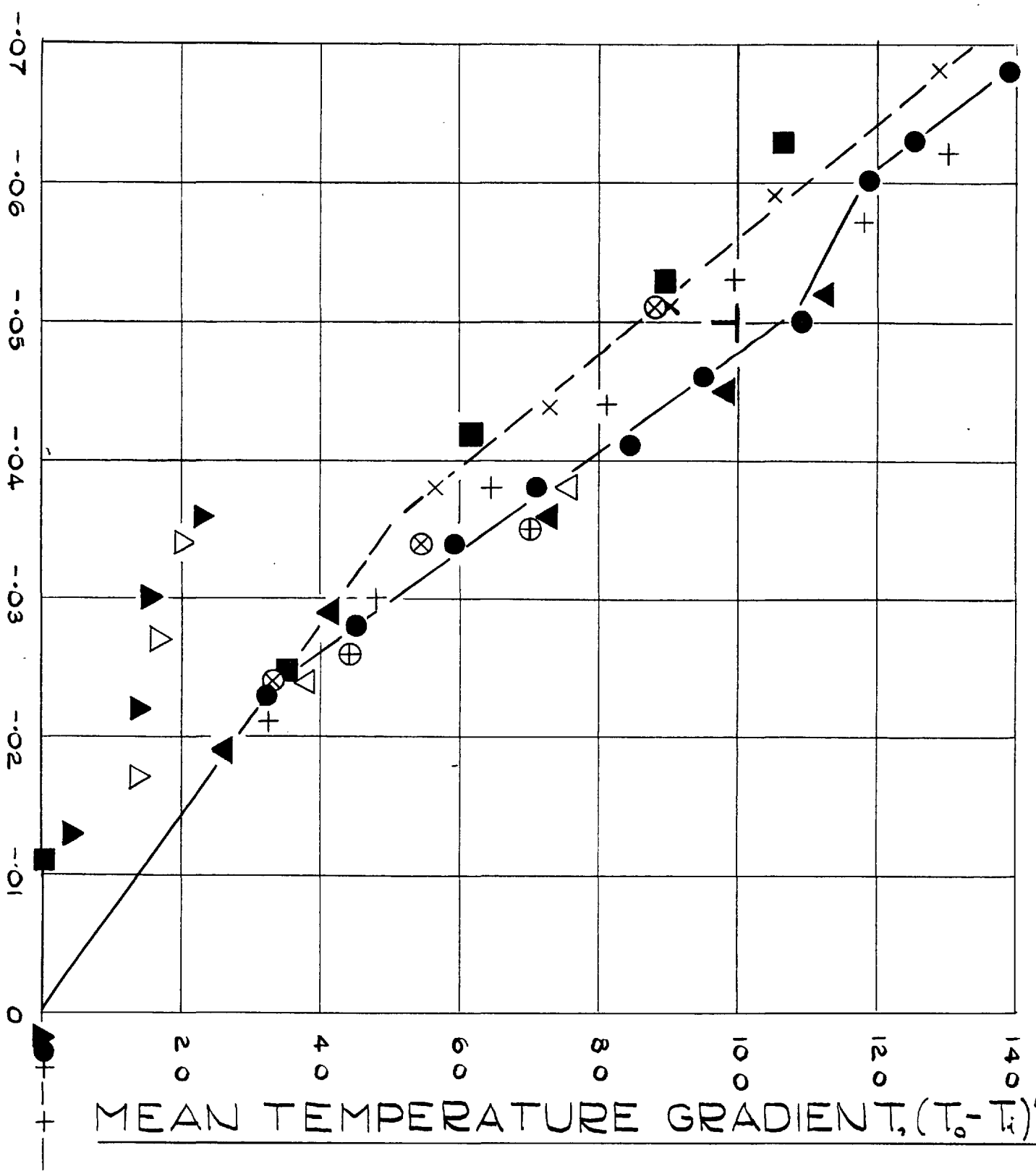
STRAIN, PER CENT.

GRAPH NO 4·6
A & B, O, 3·9 +
ALL STRAINING
SEQUENCES



SPECIMEN A ◑
" B

	UP	DOWN
16–25	●	○
26–29	■	□
30–36	▲	△
37–46	+	⊕
47–54	×	⊗
55–61	▼	▽



GRAPH NO 4·7
B, O, 3·15, ⊕
ALL STRAINING SEQUENCES

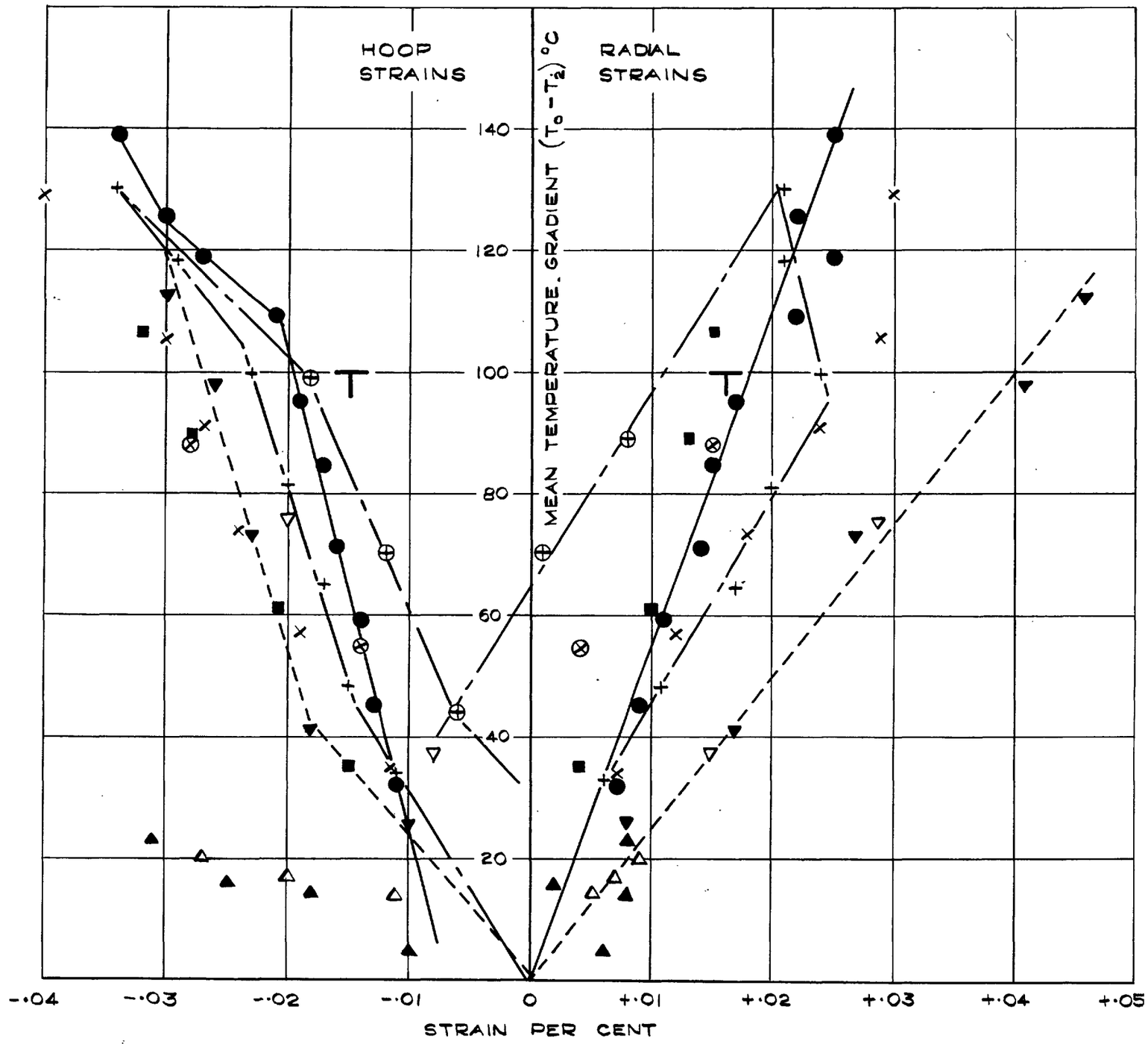
	UP	DOWN
16–25	●	○
26–29	■	□
30–36	◀	◁
37–46	×	⊗
47–54	+	⊕
55–61	▶	▷

GRAPH No. 4·8

B, 0, 2·4 †

B, 0, 2·4 θ

ALL STRAINING SEQUENCES



	UP	DOWN
16 – 25	●	——
26 – 29	■	
30 – 36	▲	△
37 – 46	+	⊕
47 – 54	×	⊗
55 – 61	▼	▽

GRAPH NO 49
B, 0·5, Z
ALL STRAINING SEQUENCES

MEAN TEMPERATURE GRADIENT $T_1(T_0-T_4)$°C.

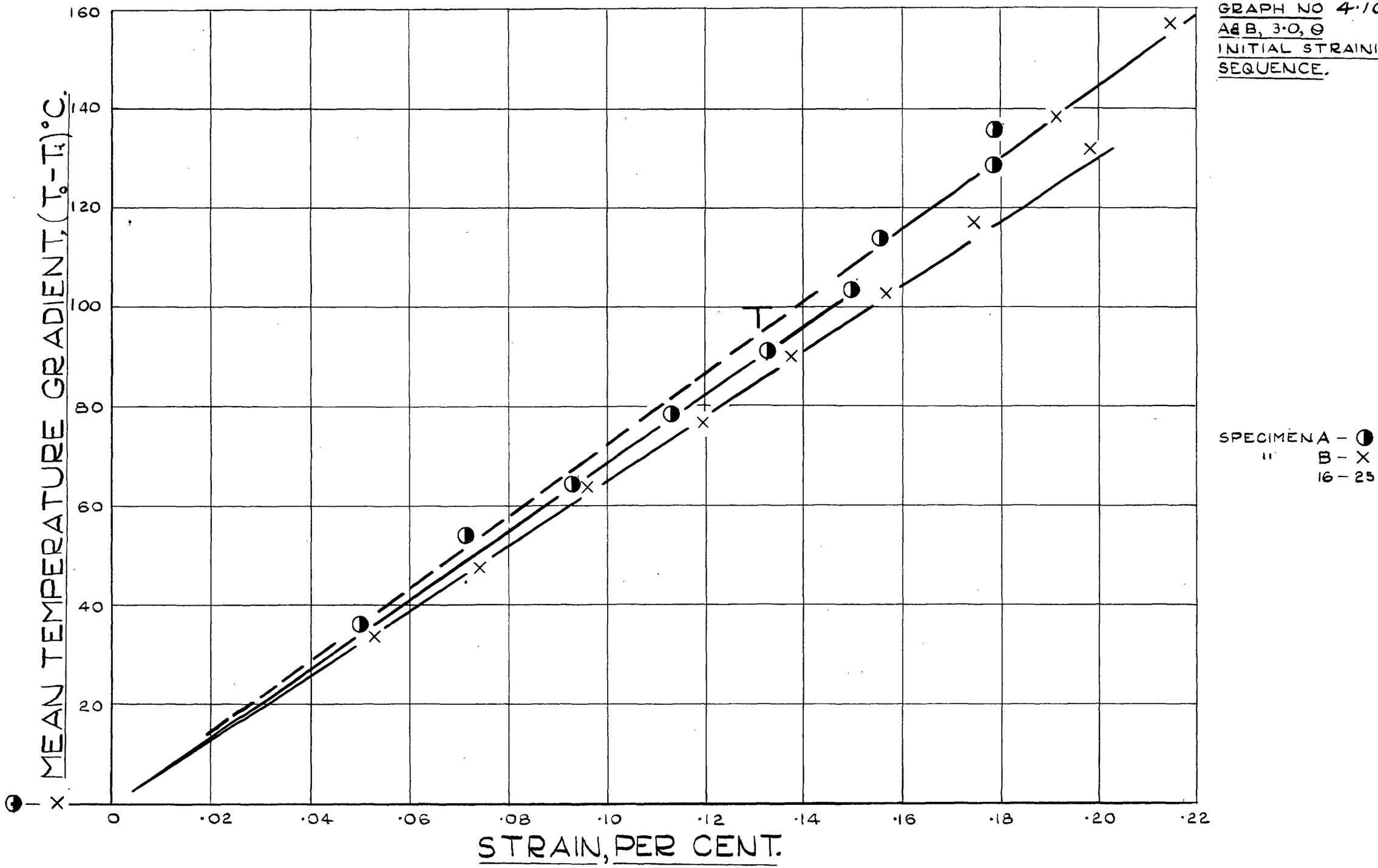
140
120
100
80
60
40
20

−·08 −·07 −·06 −·05 −·04 −·03 −·02 −·01 0 +·01 +·02

STRAIN, PER CENT.

	UP	DOWN
16 – 25	●	○
26 – 29	■	□
30 – 36	▲	△
37 – 46	+	⊕
47 – 54	×	⊗
55 – 61	▼	▽

GRAPH NO 4·10
A & B, 3·0, Θ
INITIAL STRAINING
SEQUENCE.



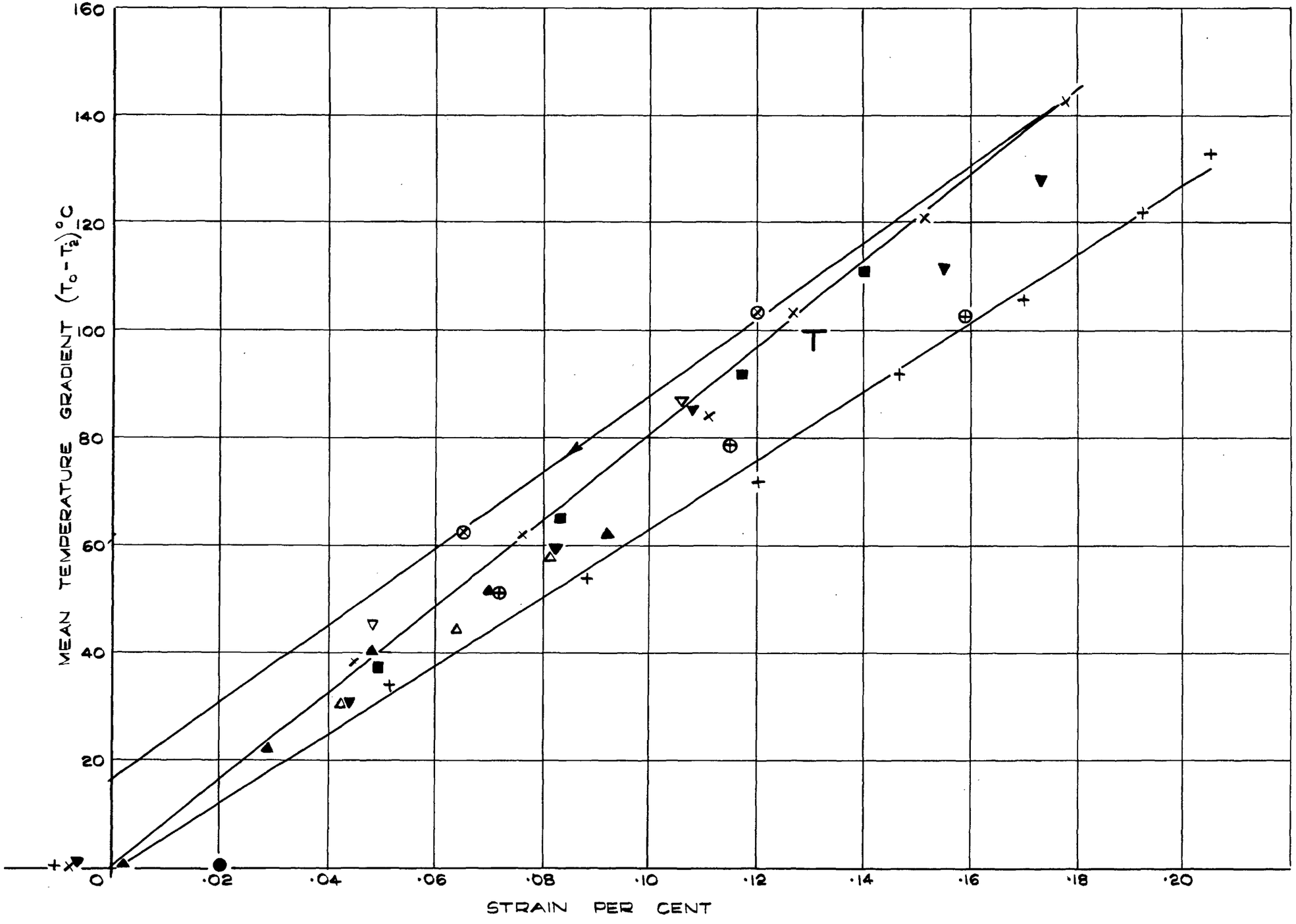
SPECIMEN A – ◑
" B – X
16 – 25

GRAPH No. 4·11

B, 3·0, 0

SUBSEQUENT

STRAINING SEQUENCES



			UP	DOWN
26	to	29	■	□
30	–	36	▲	△
37	–	46	+	⊕
47	–	54	×	⊗
55	–	61	▼	▽

GRAPH NO 4·12
B, 3·0, θ-Z
ALL STRAINING
SEQUENCES

MEAN TEMPERATURE GRADIENT, $(T_o - T_i)$ °C.

140
120
100
80
60
40
·20

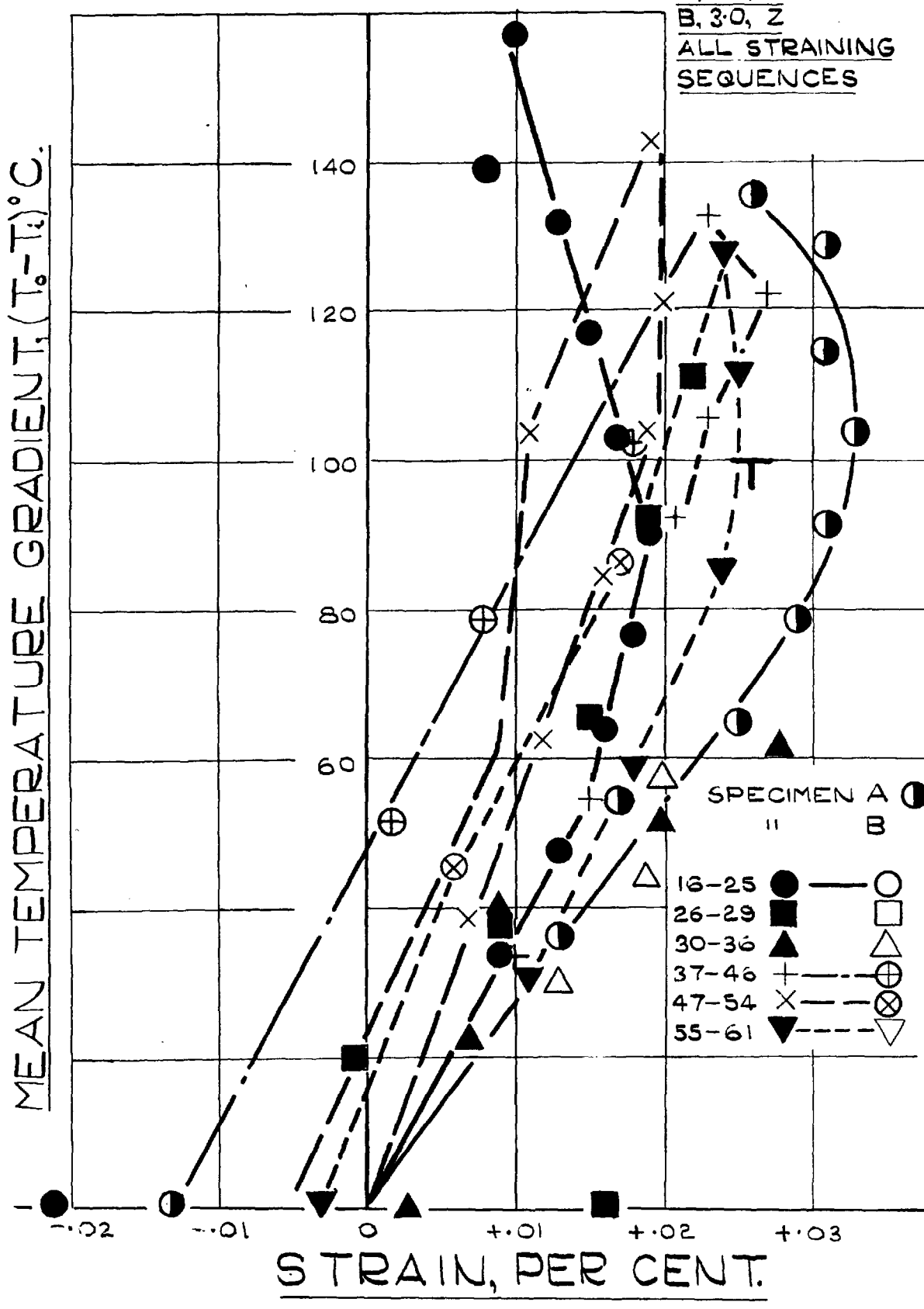
0 ·02 ·04 ·06 ·08 ·10 ·12 ·14 ·16 ·18

STRAIN, PER CENT.

	UP	DOWN
16–25	●	○
26–29	□	■
30–36	▲	△
37–46	+	⊕
47–54	×	⊗
55–61	▼	▽

GRAPH NO 4·13

A, 3·0, Z
B, 3·0, Z
ALL STRAINING SEQUENCES



GRAPH No. 4·14

A, 1·75, θ

A, 4·25, θ

A, 4·25, Z

B, 4,25, θ

INITIAL STRAINING SEQUENCES

MEAN TEMPERATURE GRADIENT, $(T_0 - T_1)$°C.

160
140
120
100
80
60
40
20

A, 4·25, Z
(POOR WATERPROOFING CHARACTERISTICS)

T (A, 4·25, Z)

T

-·04 -·02 0 ·02 ·04 ·06 ·08 ·10 ·12 ·14 ·16 ·18 ·20

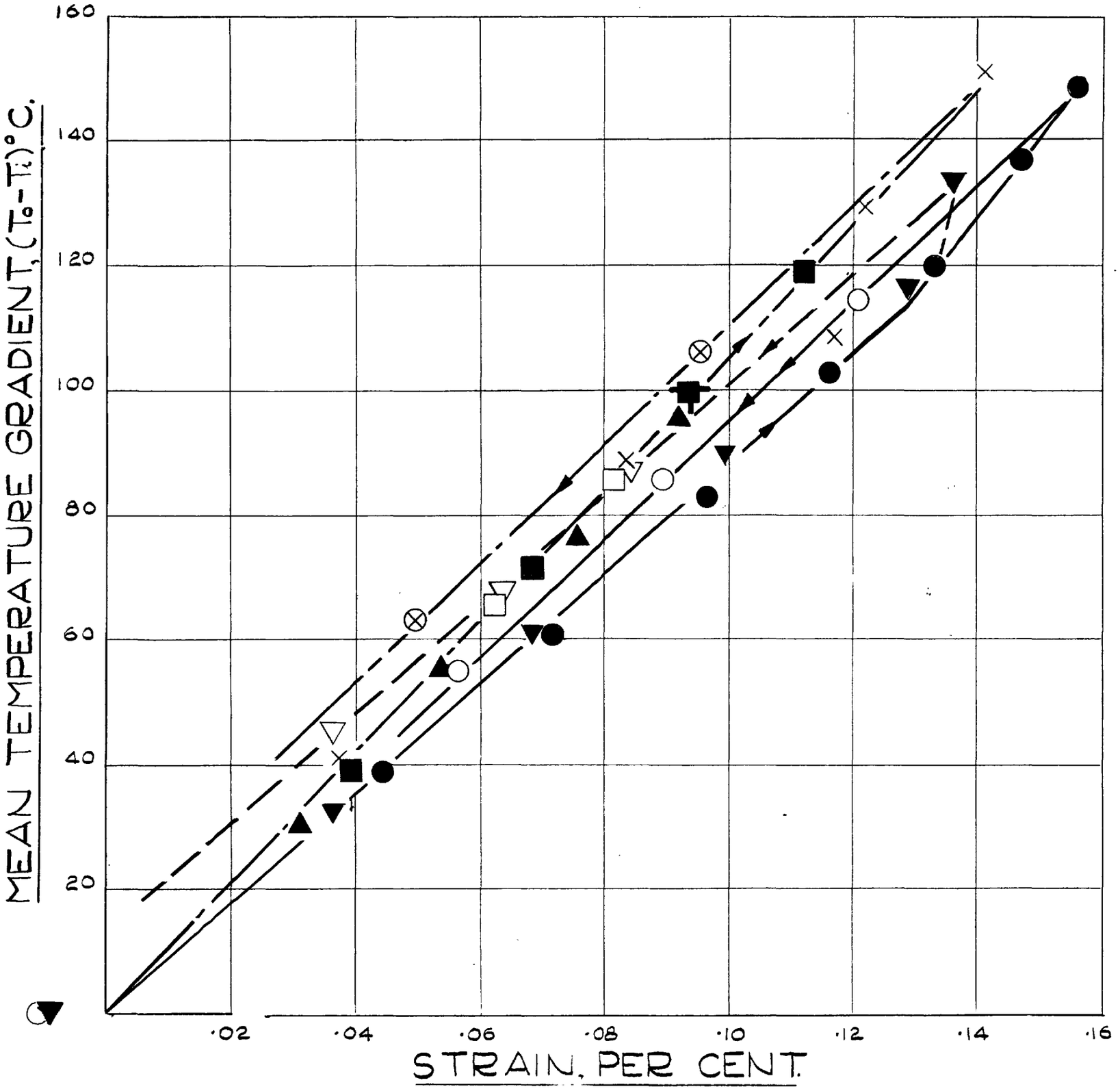
STRAIN, PER CENT.

● 4·25 A

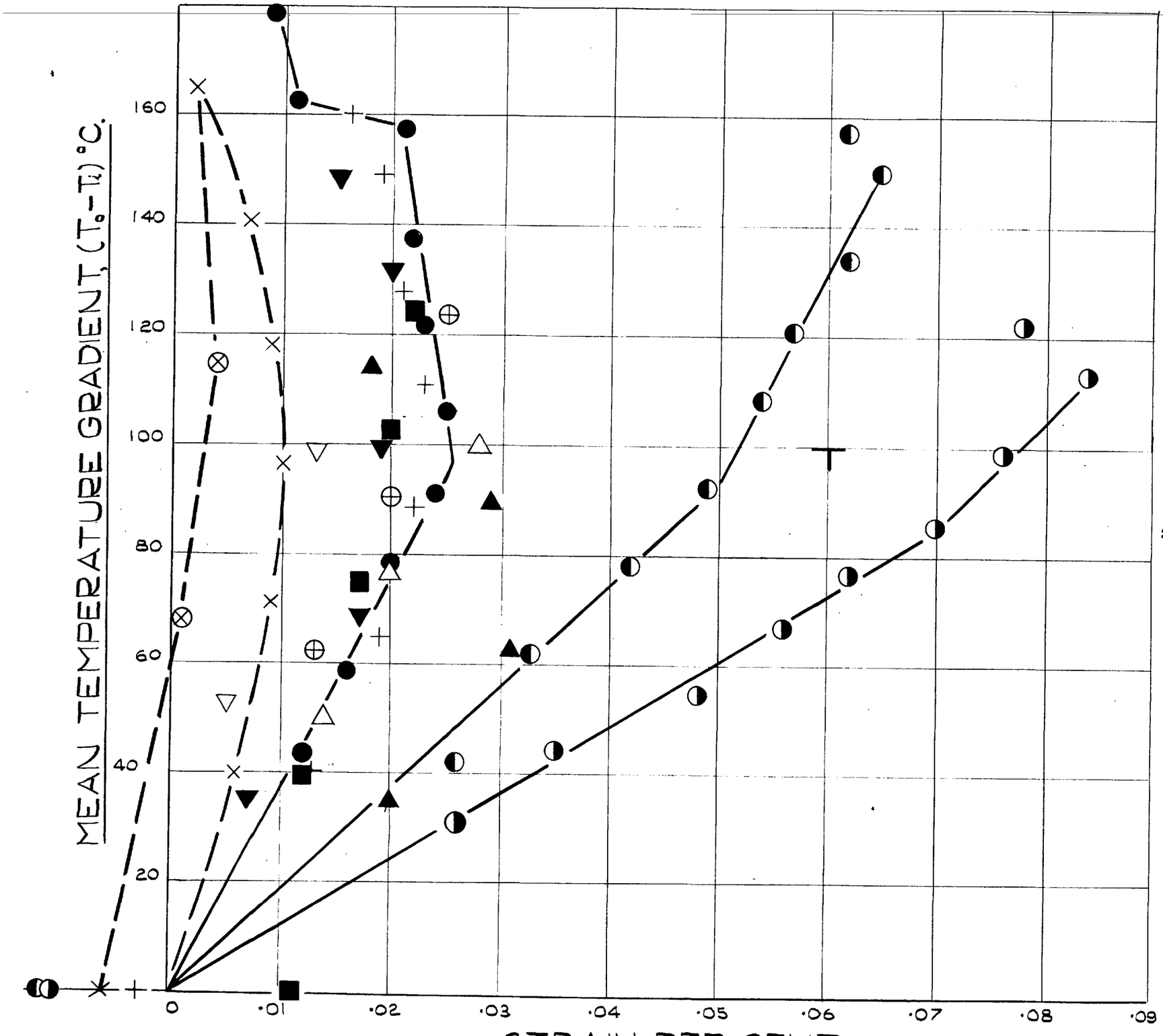
■ 1·75 A

+ 4·25 B

GRAPH NO 4·15
B, 4·25, θ
SUBSEQUENT STRAINING SEQUENCES



GRAPH NO. 4·16
A, 0·5, θ
A, 5·5, θ
B, 5·5 θ
ALL STRAINING SEQUENCES.



SPECIMEN A, ·5 ◑
" ", 5·5 ◑

SPECIMEN B	UP	DOWN
16-25	●	○
26-29	■	□
30-36	▲	△
37-46	+	⊕
47-54	×	⊗
55-61	▼	▽

GRAPH NO. 4·17
B, 5·5, Z.
ALL STRAINING SEQUENCES.

POOR WATERPROOFING CHARACTERISTICS

MEAN TEMPERATURE GRADIENT, $(T_o - T_i)$ °C.

100
140
120
100
80
60
40
20

UP
16-25 ●
26-29 ■
30-36 ▲
37-46 +
47-54 ×
55-61 ▼

DOWN
○ □ △ ⊕ ⊗ ◁ ▽

-·09 -·08 -·07 -·06 -·05 -·04 -·03 -·02 -·01 0

STRAIN, PER CENT.

GRAPH NO 4·18
B, 6·0, 3·9, 9
SUBSEQUENT STRAINING SEQUENCES

(POOR WATERPROOFING CHARACTERISTICS.)

MEAN TEMPERATURE GRADIENT, $(T_0 - T_1)$°C.

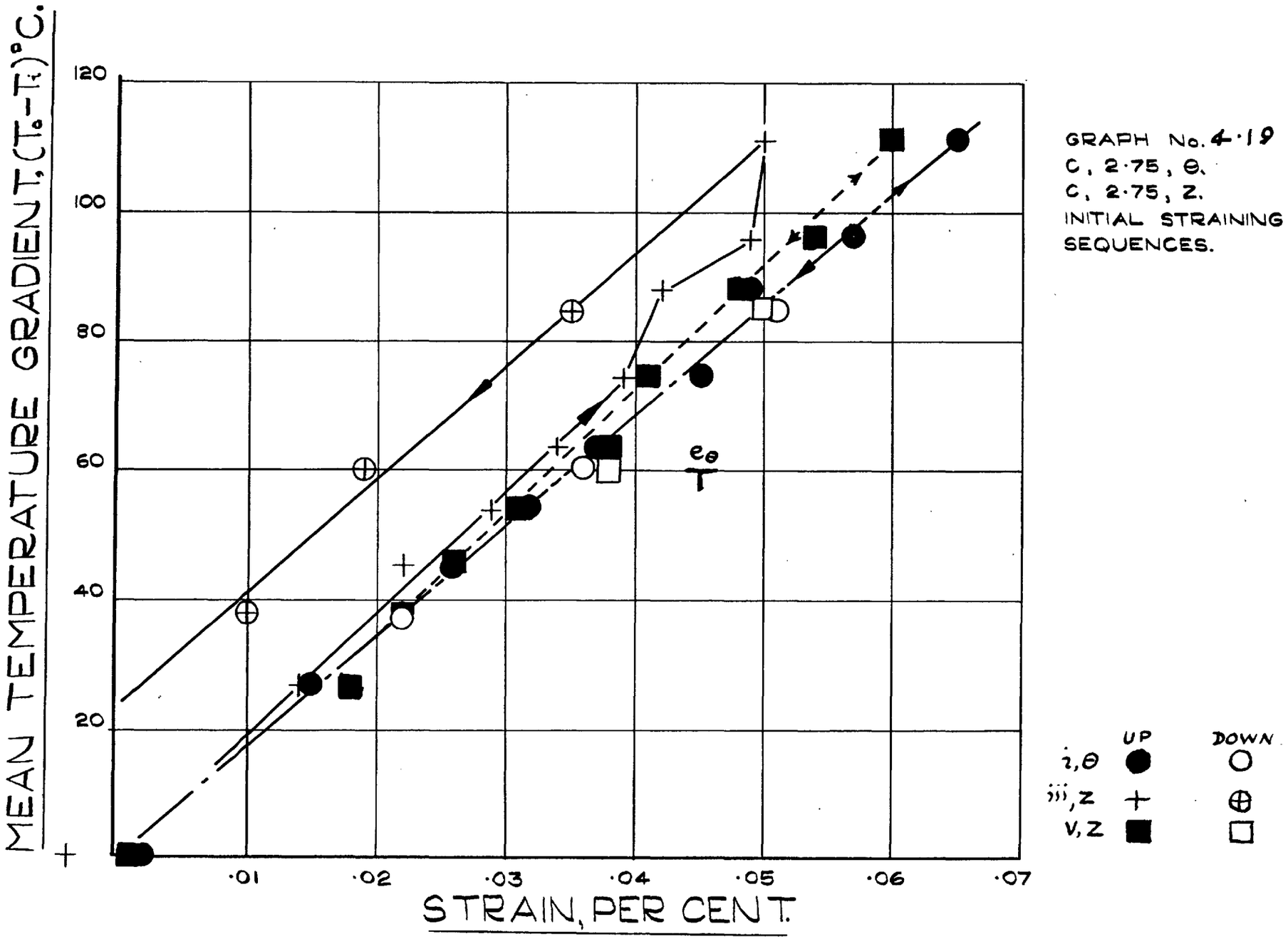
140
120
100
80
60
40
20

UP
26-29 ■
30-36 ▲
37-46 +
47-54 ×
55-61 ▼

DOWN
□
△
⊕
⊗
▽

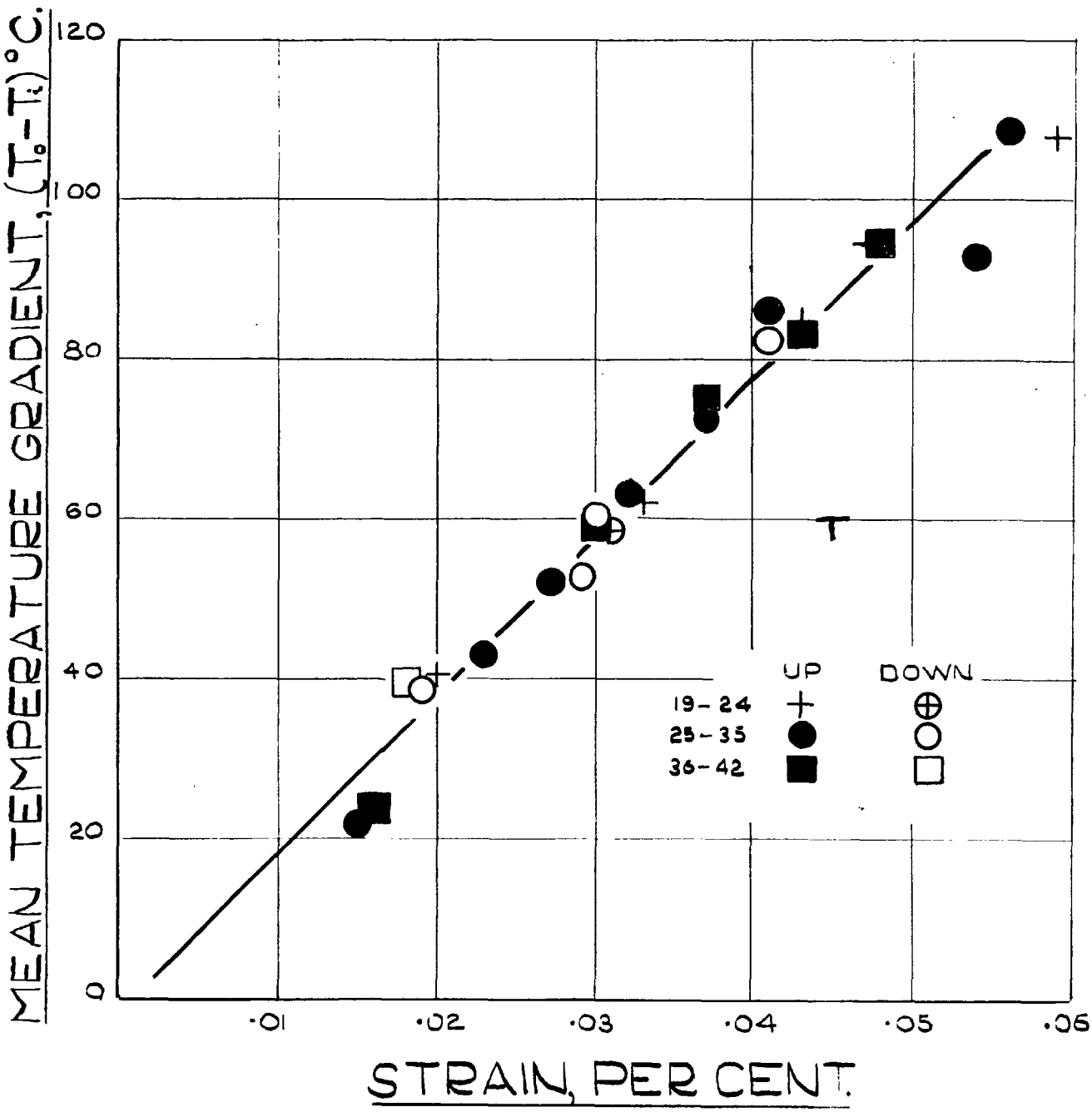
−·11 −·10 −·09 −·08 −·07 −·06 −·05 −·04 −·03 −·02 −·01 0

STRAIN, PER CENT.

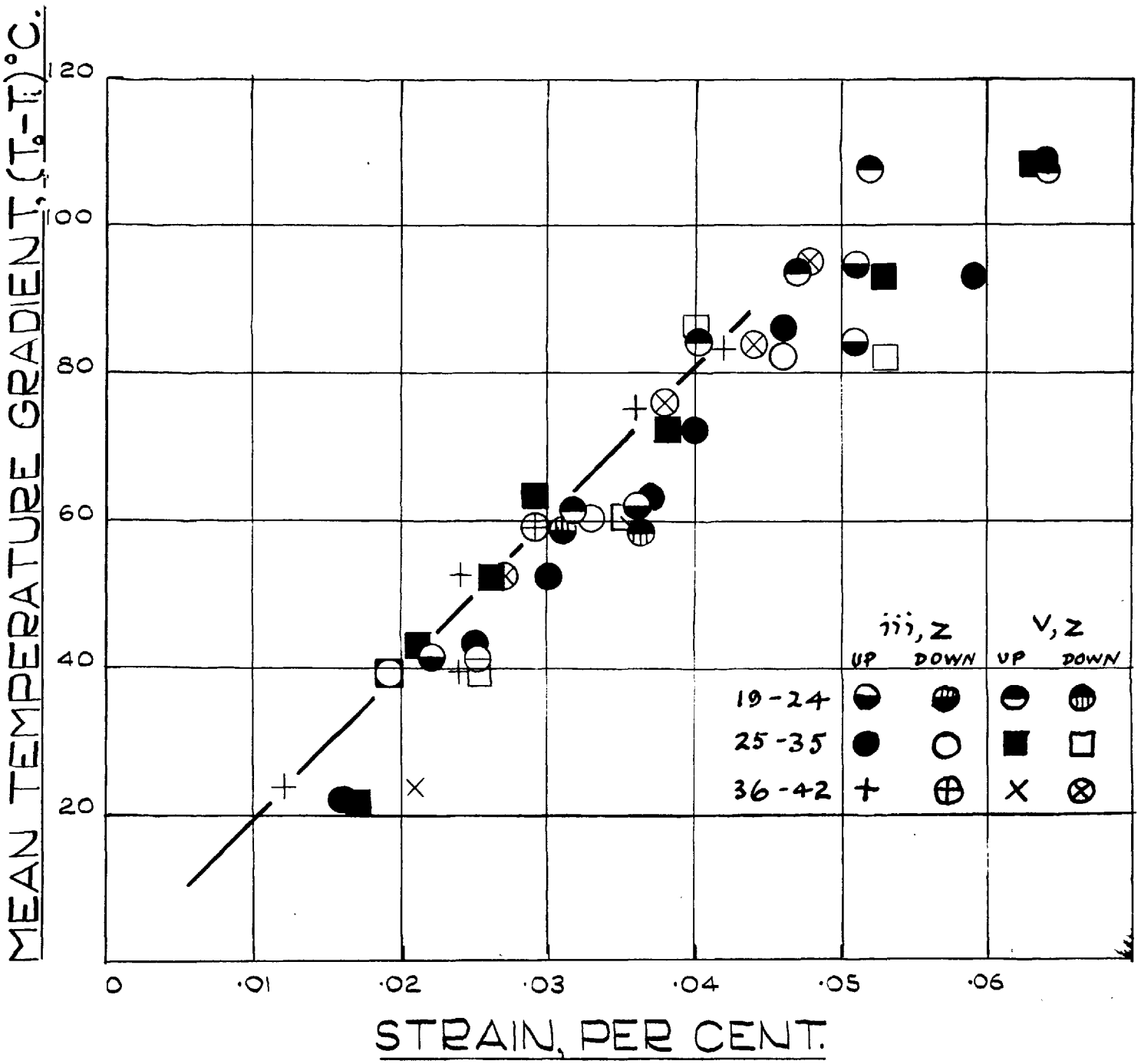


GRAPH No. 4·19
C, 2·75, θ.
C, 2·75, Z.
INITIAL STRAINING SEQUENCES.

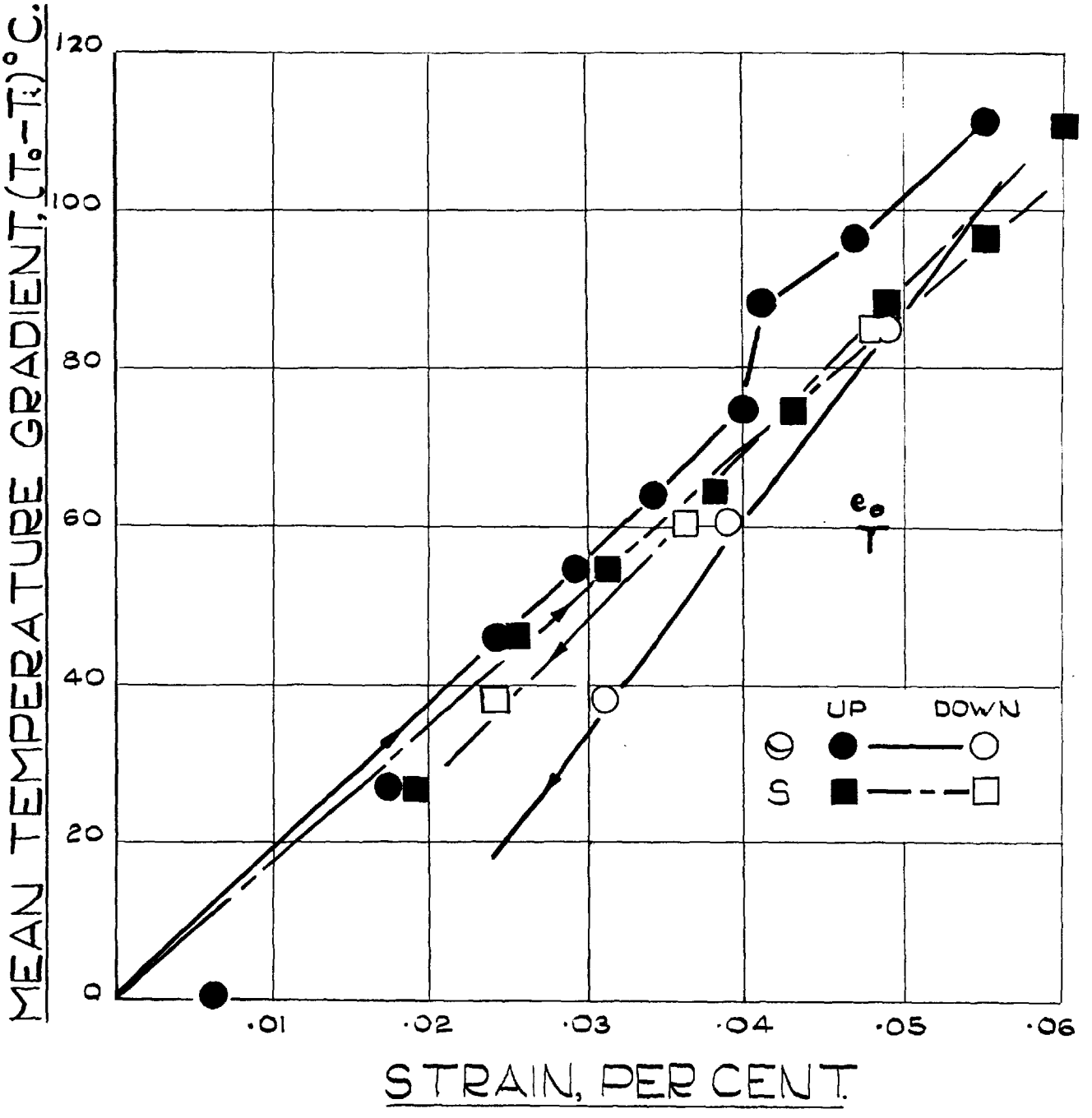
GRAPH NO 4·20
C, 2·75, θ
SUBSEQUENT STRAINING SEQUENCES



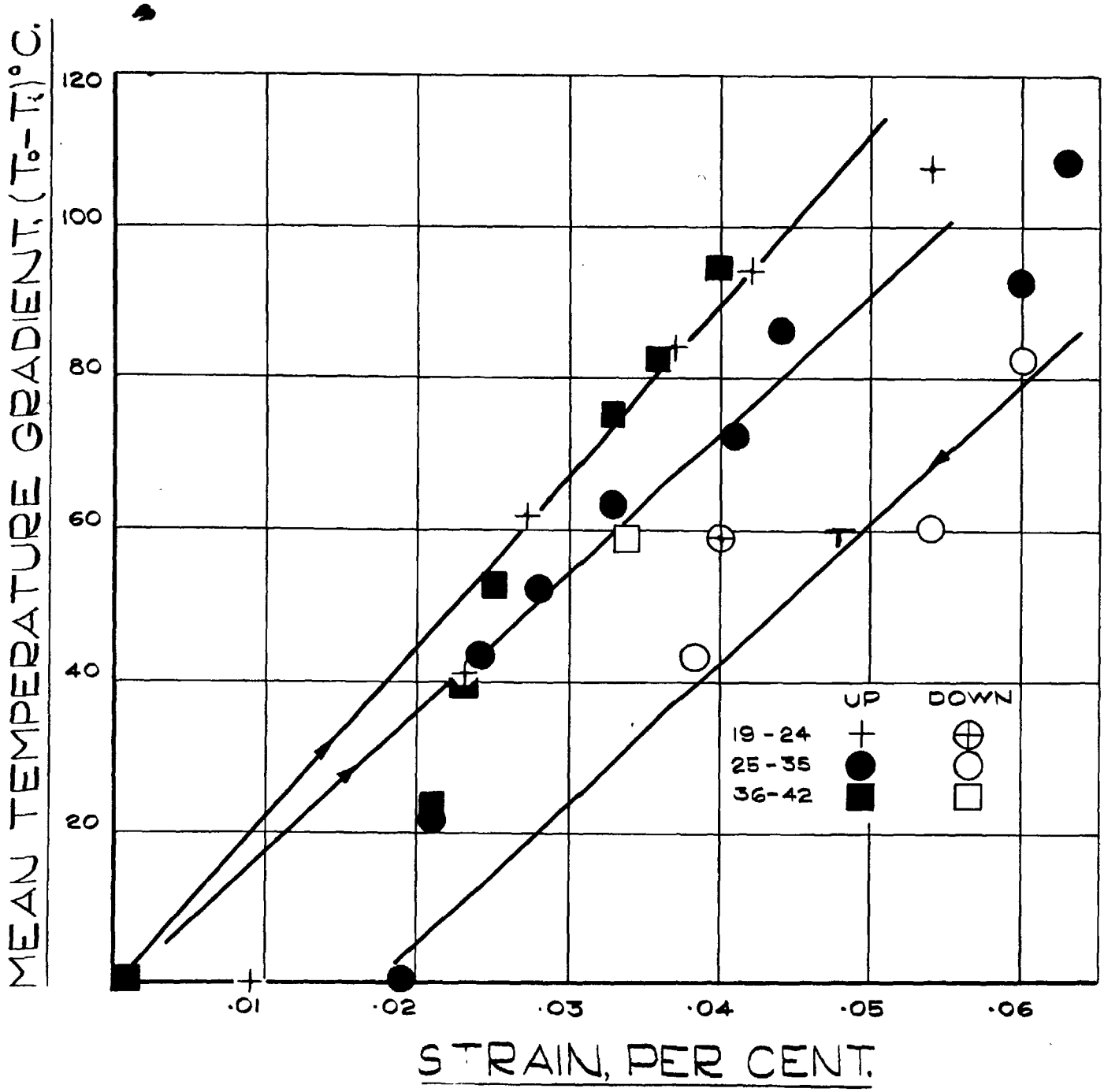
GRAPH NO 4·21
C, 2·75, Z
SUBSEQUENT STRAINING SEQUENCES



GRAPH NO 4·22
C, 3·2, Θ
C, 3·2, S
INITIAL STRAINING
SEQUENCE.



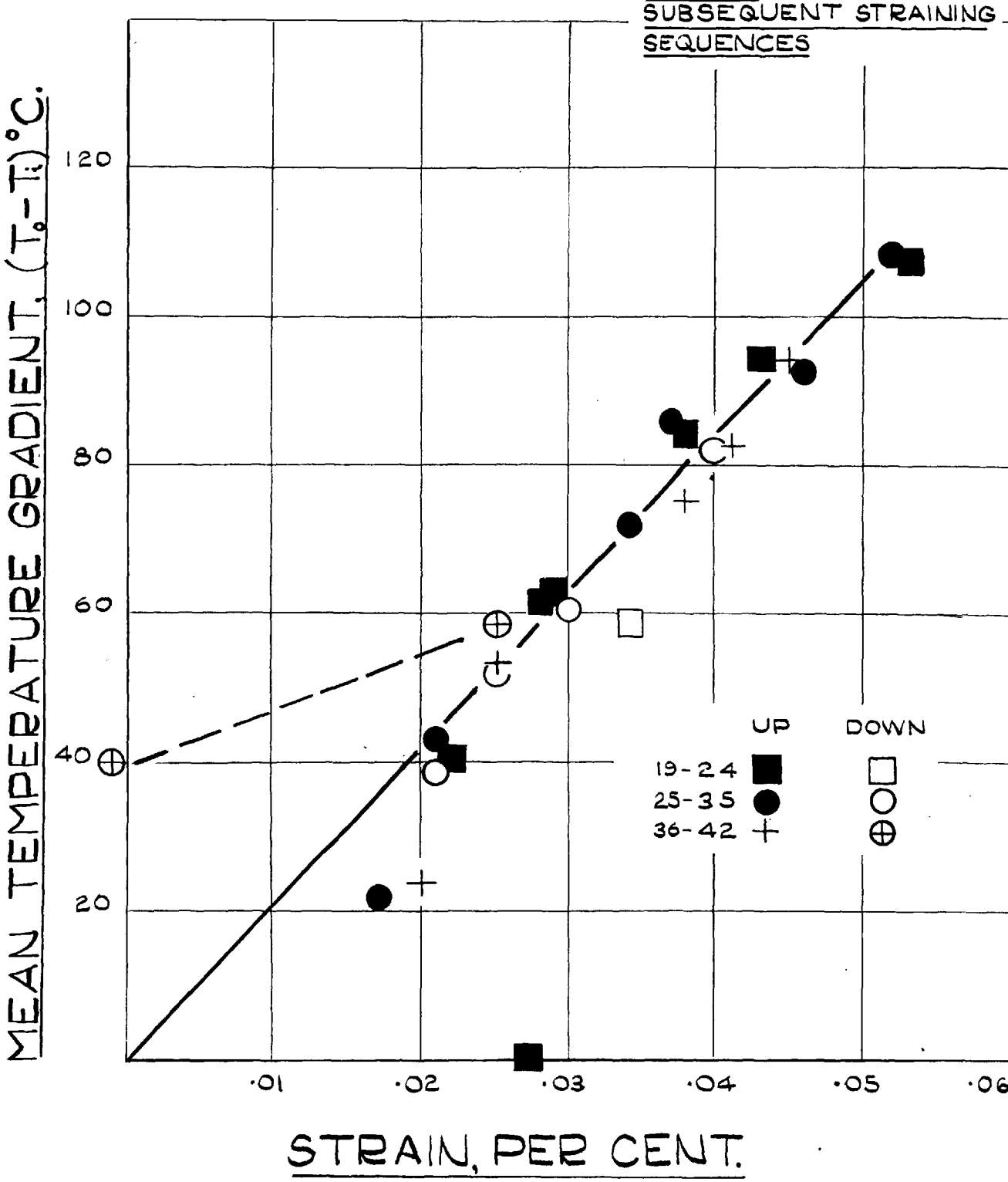
GRAPH No. 4·23
C, 3·2, 9.
SUBSEQUENT STRAINING SEQUENCES.



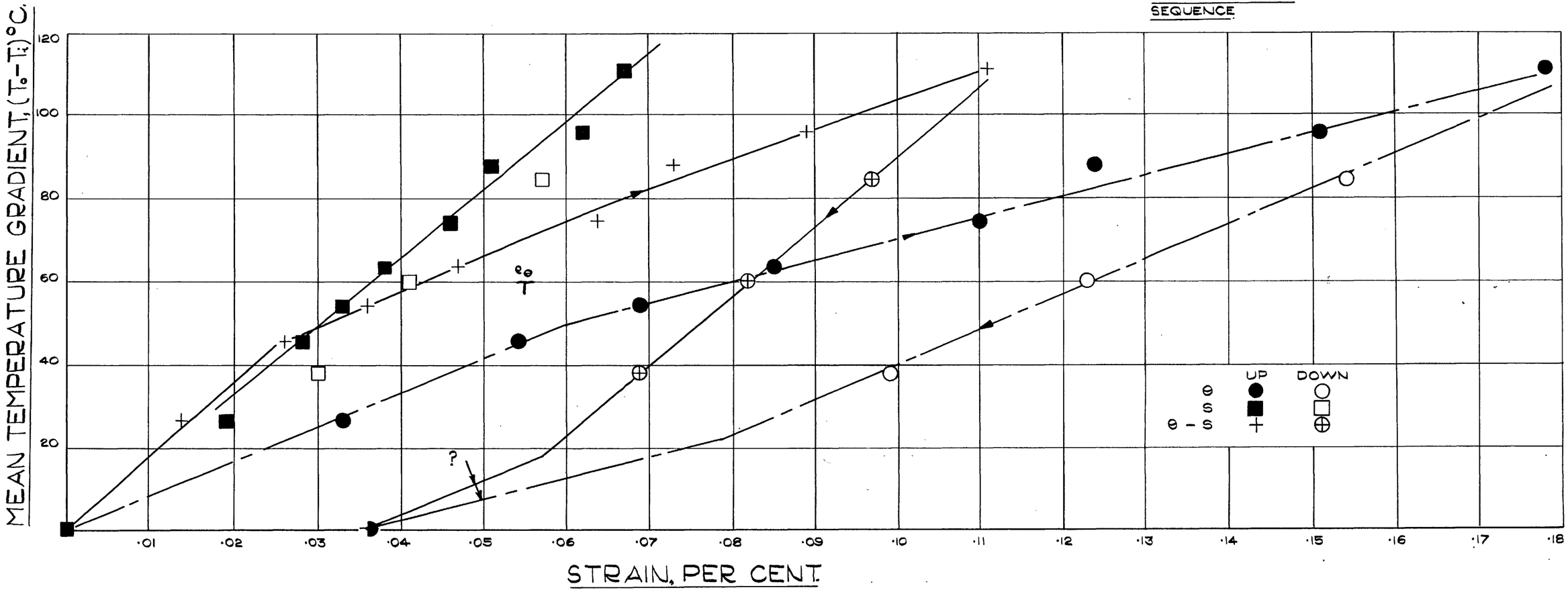
GRAPH NO 4·24

C, 3·2, S

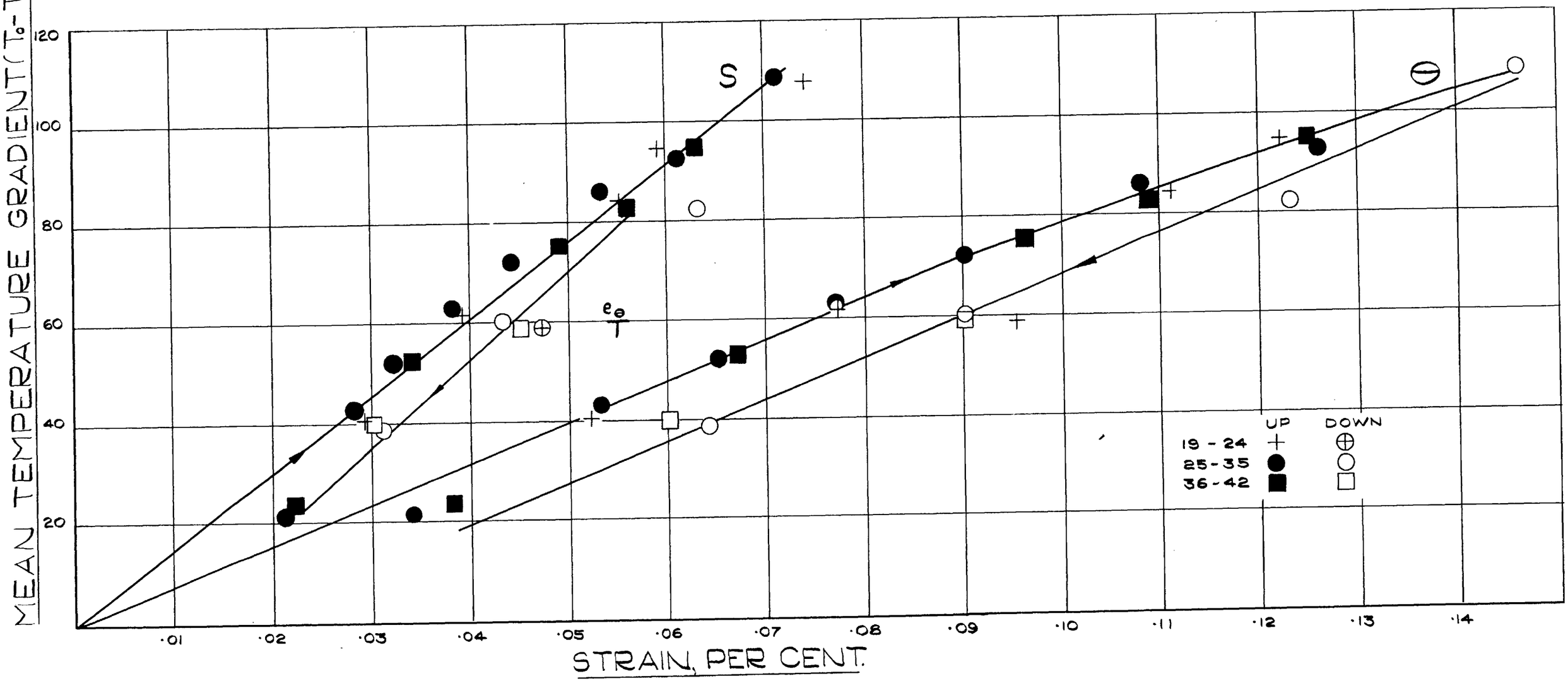
SUBSEQUENT STRAINING SEQUENCES



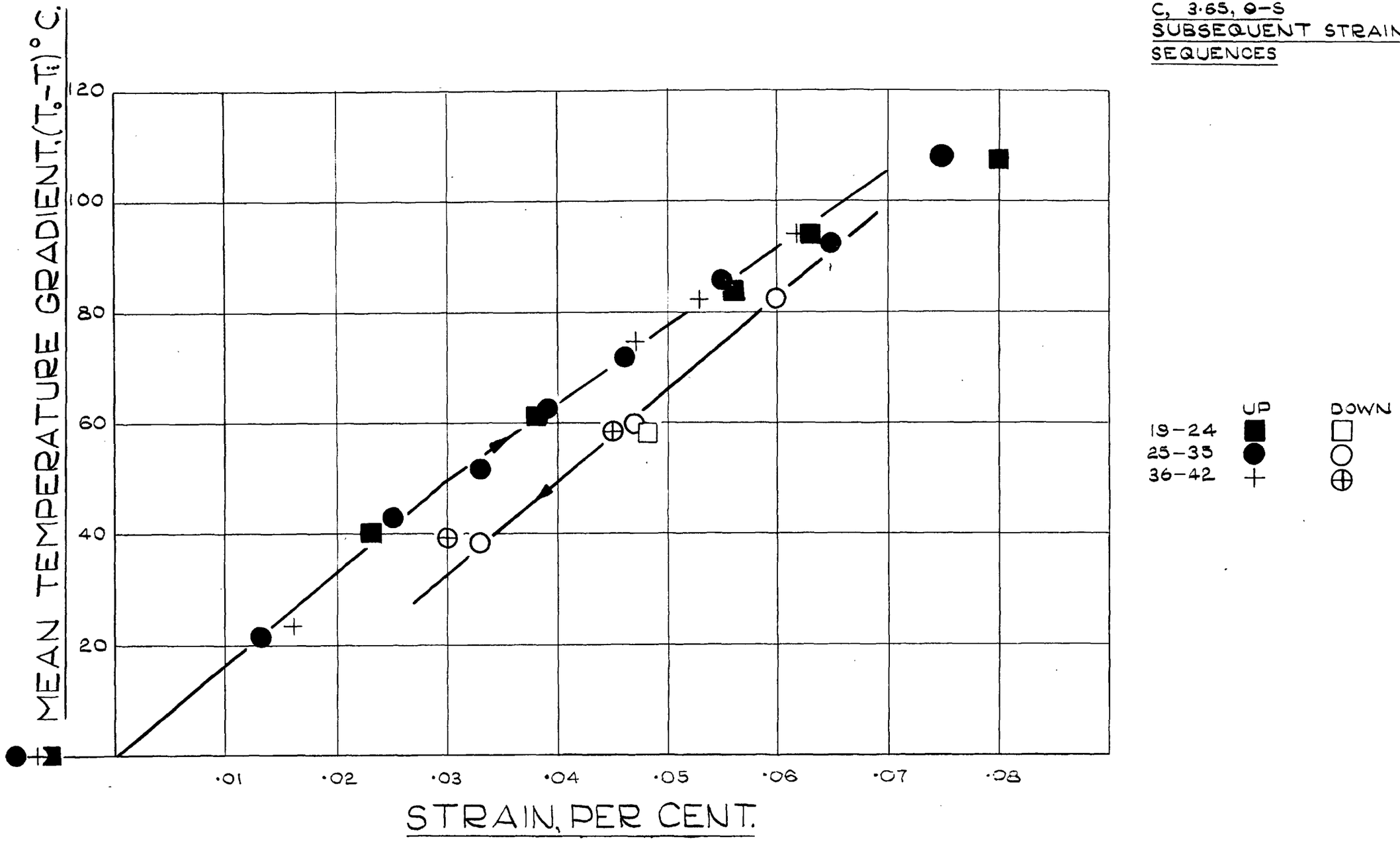
GRAPH No. 4·25
C, 3·65, Θ
C, 3·65, S
C, 3·65 Θ-S,
INITIAL STRAINING
SEQUENCE



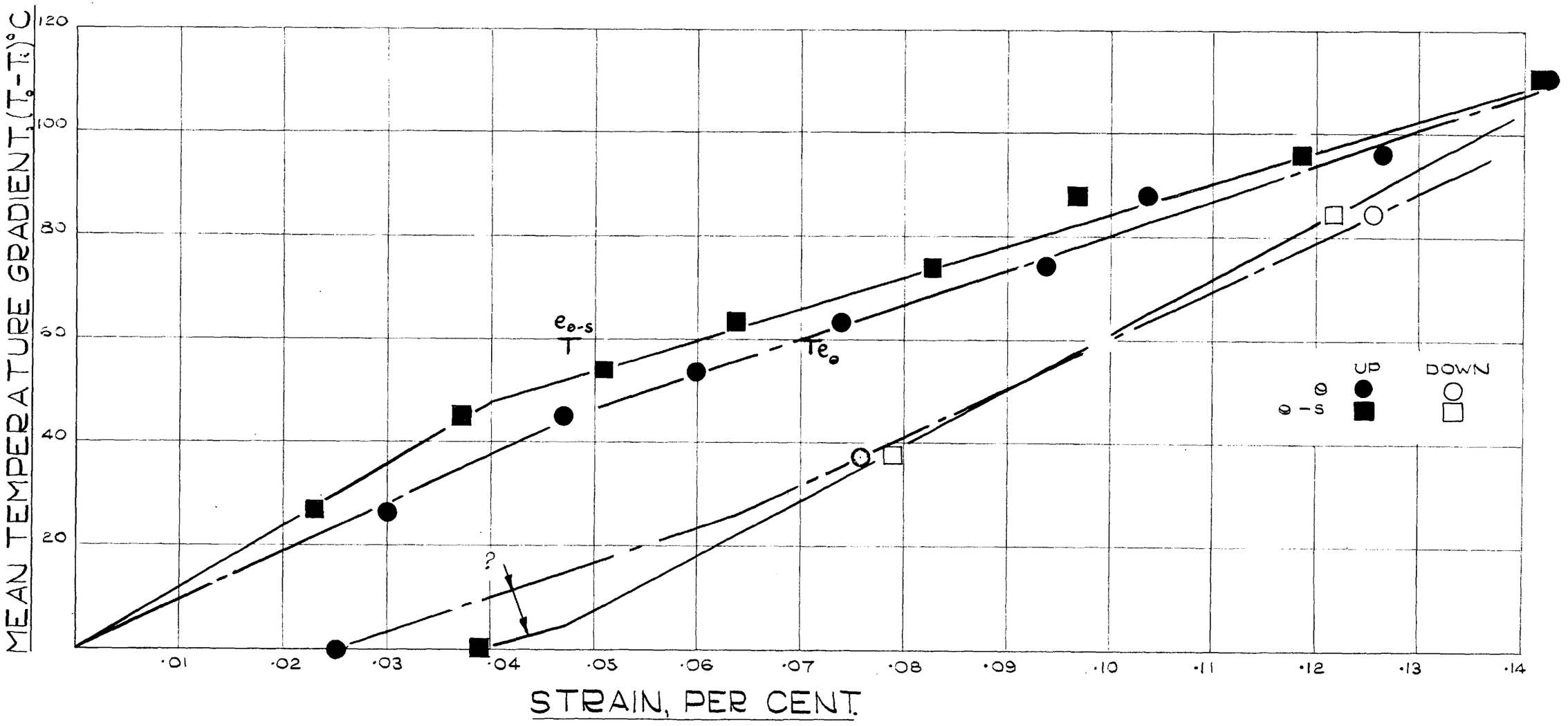
GRAPH No. 4·26
C, 3·65, Θ
C, 3·65, S
SUBSEQUENT STRAINING SEQUENCES



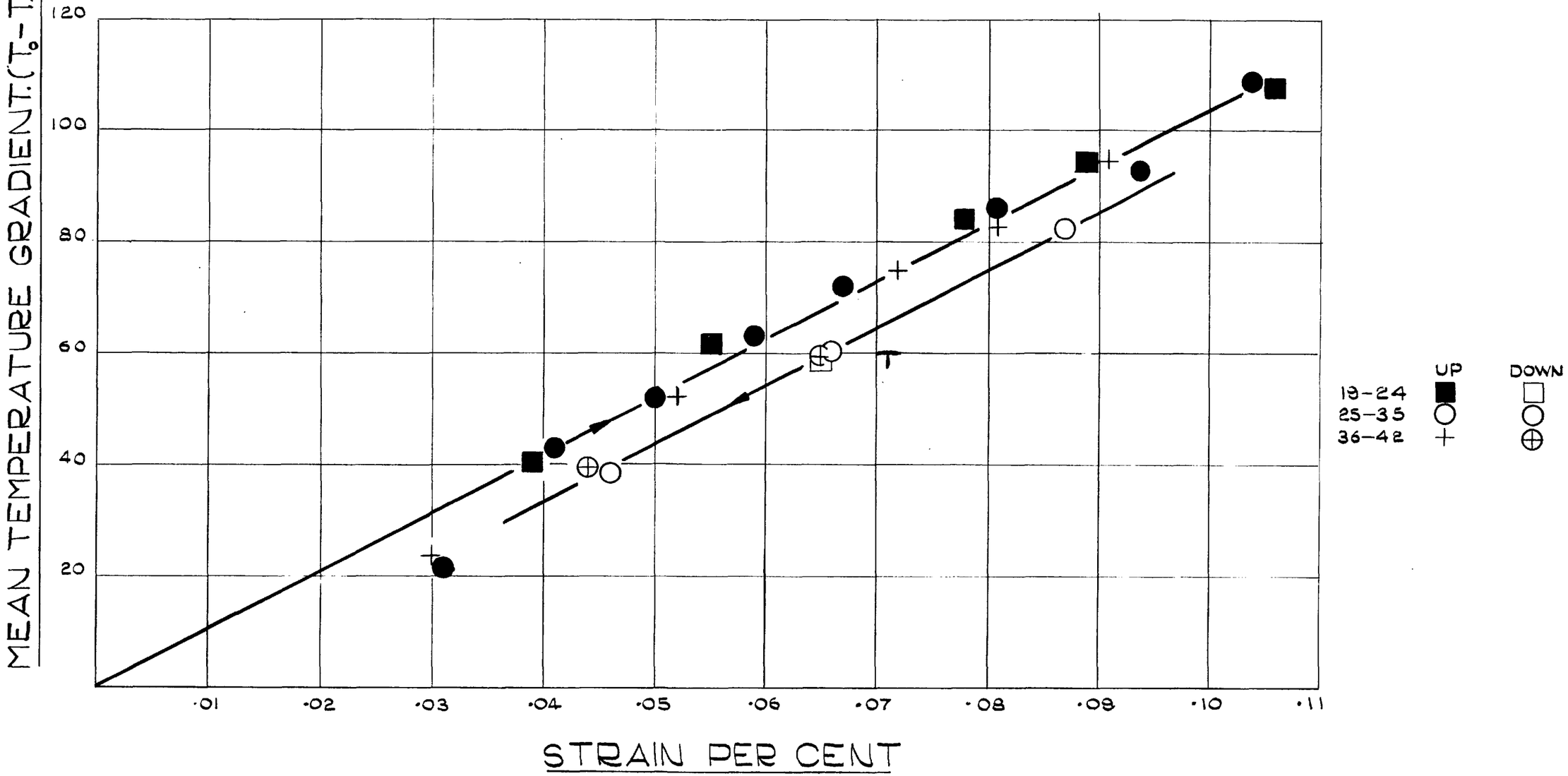
GRAPH NO 4·27
C, 3·65, O–S
SUBSEQUENT STRAINING SEQUENCES



GRAPH NO 4·28
C, 4·1, θ
C, 4·1 θ-S
INITIAL STRAINING
SEQUENCE



GRAPH NO 4·29
C, 4·1, θ
SUBSEQUENT
STRAINING SEQUENCES



GRAPH NO 4·30
C, 4·1, 8-S
SUBSEQUENT STRAINING SEQUENCES

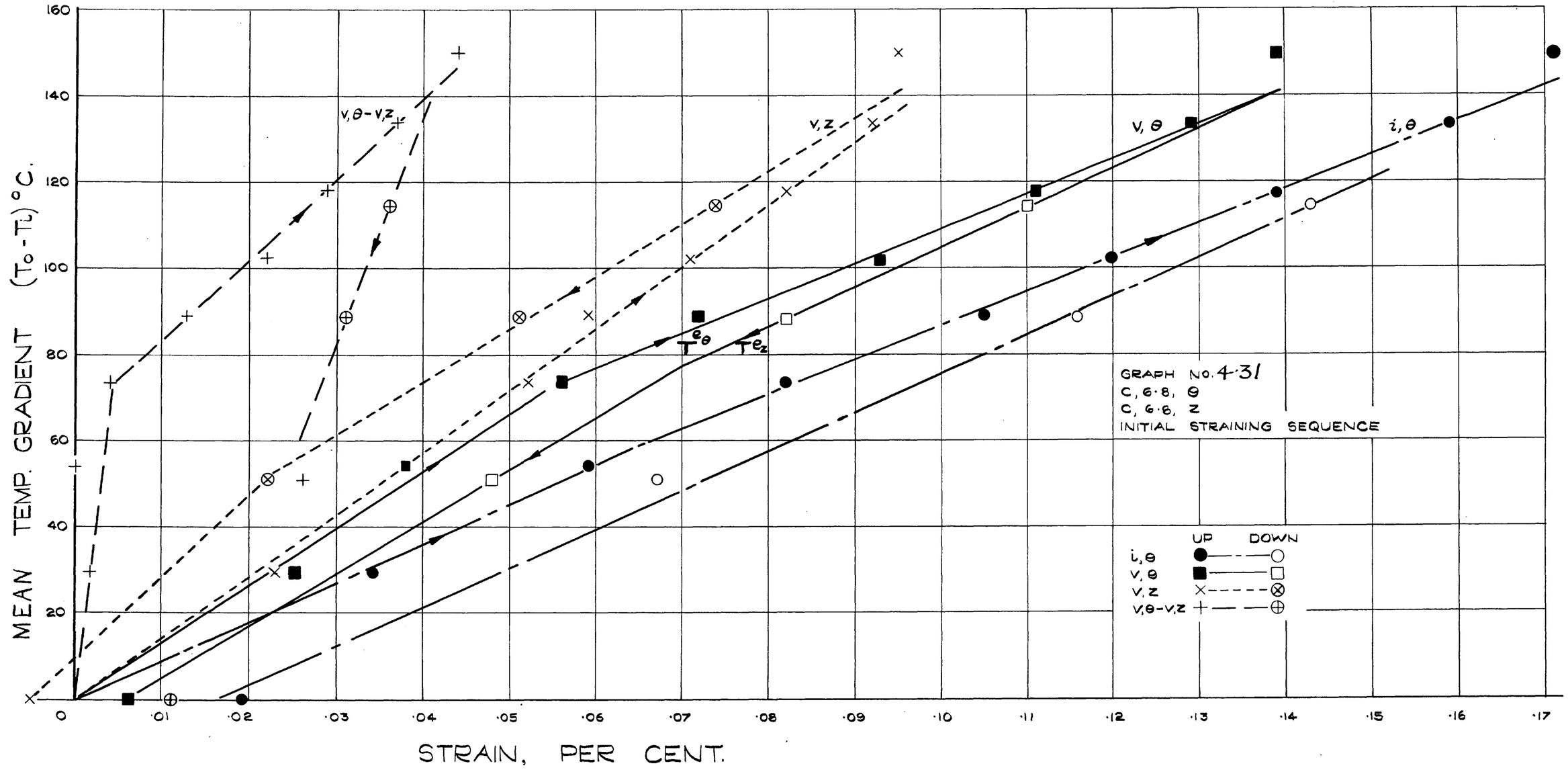
MEAN TEMPERATURE GRADIENT, $(T_0 - T_i)$ °C.

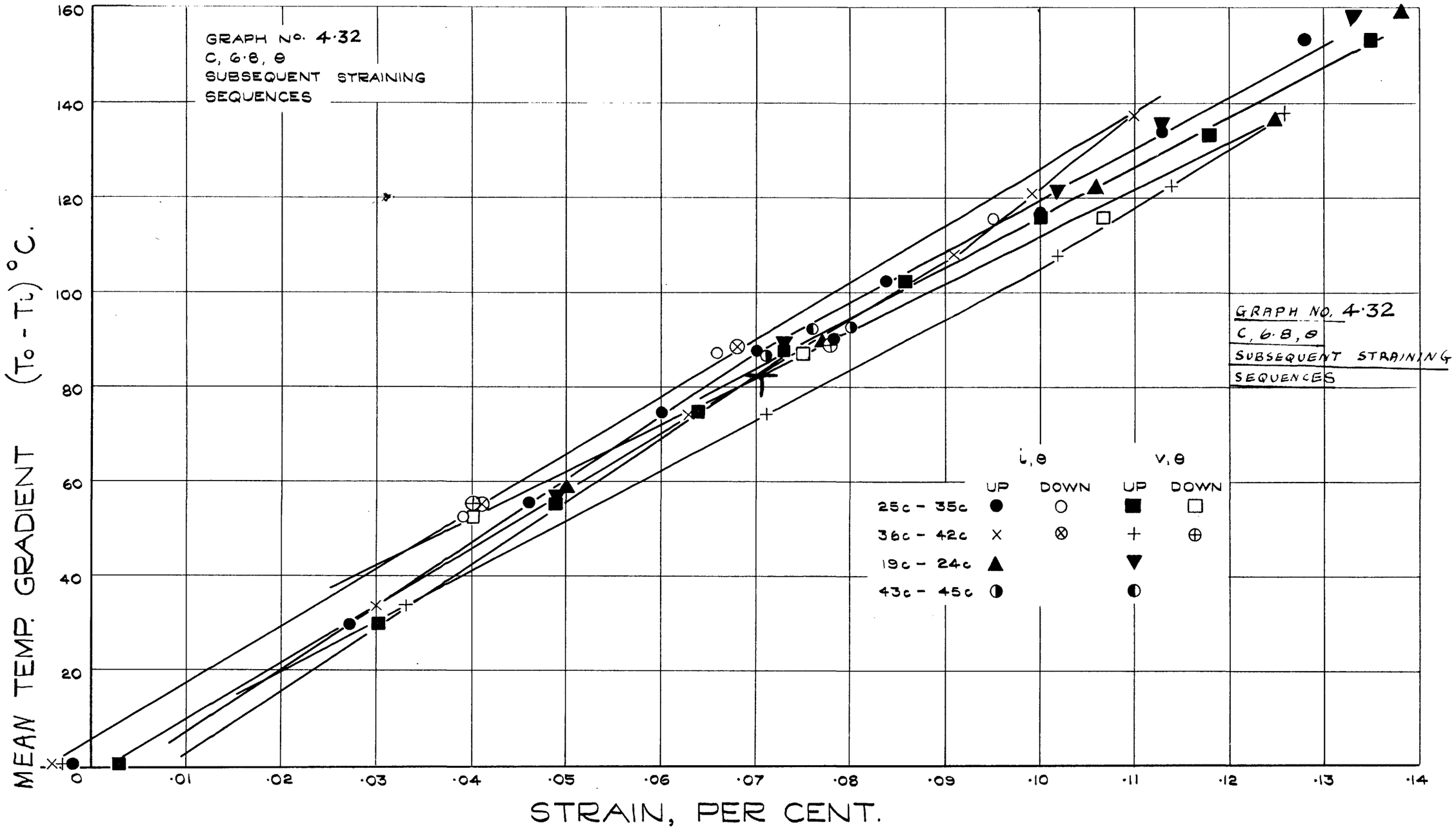
120
100
80
60
40
20

·01 ·02 ·03 ·04 ·05 ·06 ·07 ·08 ·09 ·10

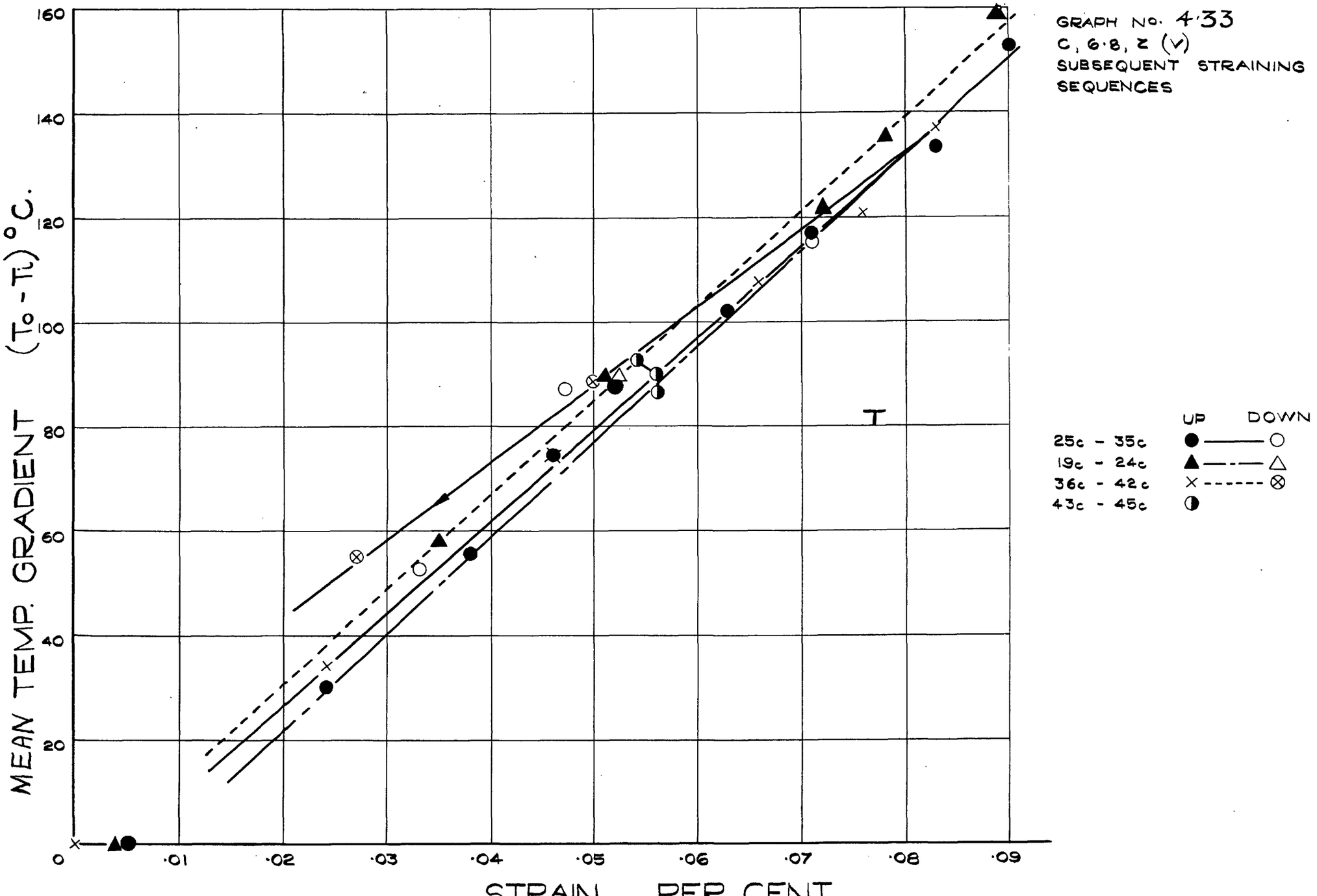
STRAIN, PER CENT.

	UP	DOWN
19-24	■	□
25-35	●	○
36-42	+	⊕


MEAN TEMP. GRADIENT (T₀-T₁) °C.
STRAIN, PER CENT.
160
140
120
100
80
60
40
20
0
·01
·02
·03
·04
·05
·06
·07
·08
·09
·10
·11
·12
·13
·14
·15
·16
·17
V,θ-V,z
V,z
V, θ
i,θ
T_{e_θ}
T_{e_z}
GRAPH No. 4·31
C, 6·8, θ
C, 6·8, z
INITIAL STRAINING SEQUENCE
UP
DOWN
i,θ
V,θ
V,z
V,θ-V,z


GRAPH No. 4·32
C, 6·8, θ
SUBSEQUENT STRAINING
SEQUENCES
MEAN TEMP. GRADIENT (To - Ti) °C.
STRAIN, PER CENT.
160
140
120
100
80
60
40
20
0
·01
·02
·03
·04
·05
·06
·07
·08
·09
·10
·11
·12
·13
·14
i, θ
V, θ
UP
DOWN
UP
DOWN
25c - 35c
36c - 42c
19c - 24c
43c - 45c
GRAPH NO. 4·32
C, 6·8, θ
SUBSEQUENT STRAINING
SEQUENCES

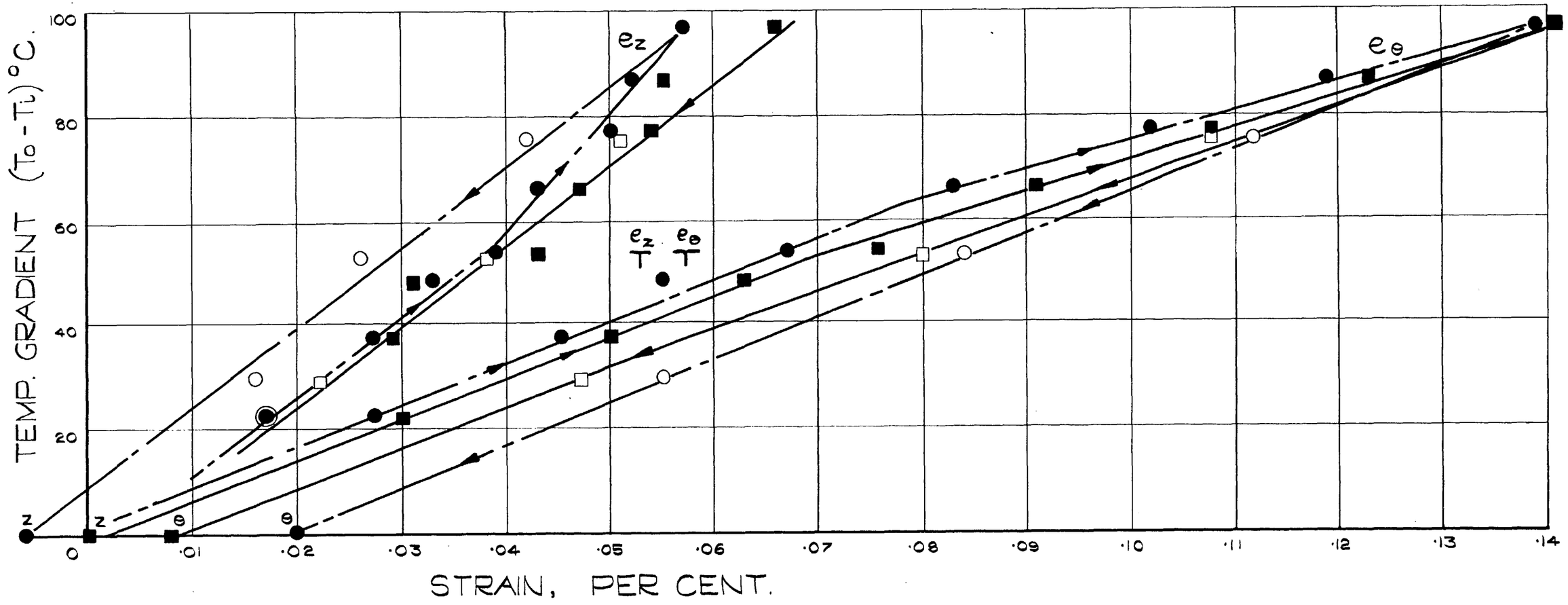
GRAPH No. 4·33
C, 6·8, Z (V)
SUBSEQUENT STRAINING SEQUENCES



GRAPH Nº 4·34
C, 10·8, θ
C, 10·8, Z
INITIAL STRAINING
SEQUENCES

UP DOWN
i,θ ●—·—○
V,θ ■——□
iii,Z ●—·—○
V,Z ■——□

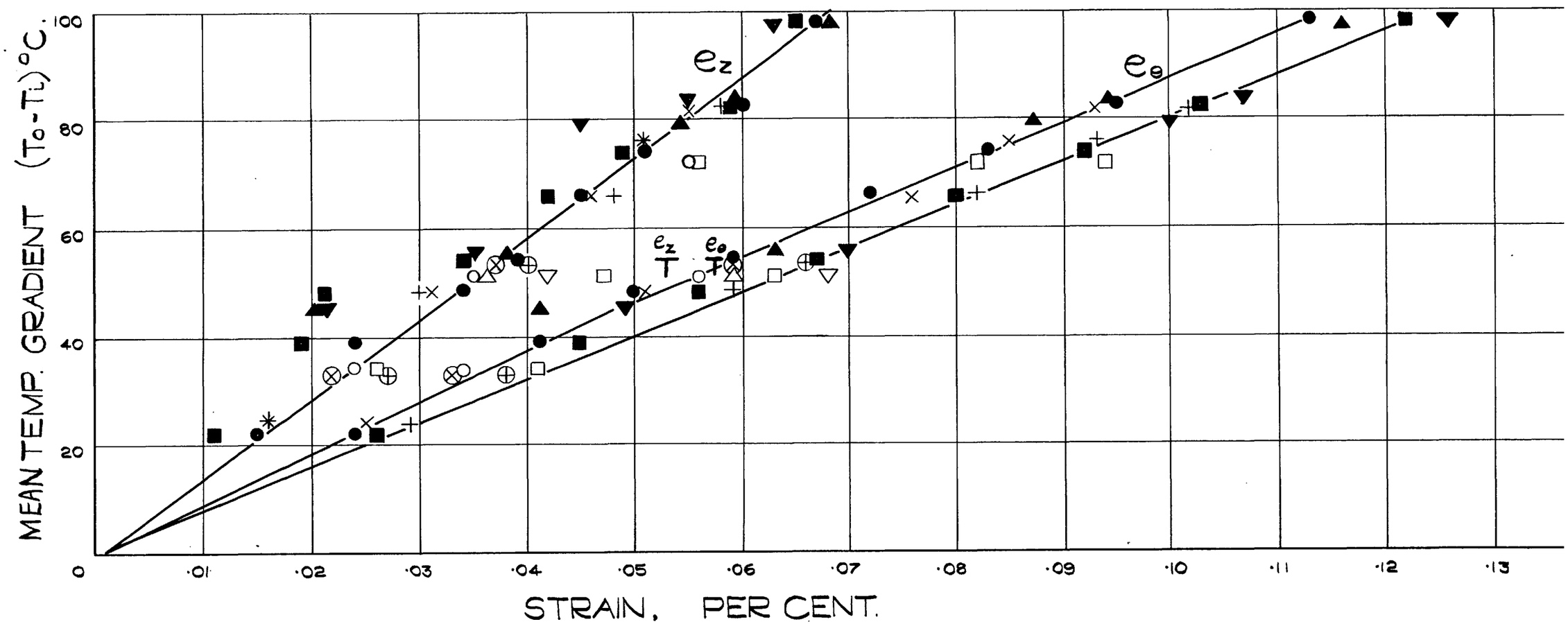
GRAPH No. 4·34
C, 10·8, θ
C, 10·8, Z
INITIAL STRAINING
SEQUENCES



GRAPH No. 4·35
C, 10·8, θ
C, 10·8, z
SUBSEQUENT STRAINING
SEQUENCES

	i,θ & iii,z		vθ & vz	
25c – 35c	●	○	■	□
36c – 42c	×	⊗	+	⊕
19c – 24c	▲	△	▼	▽

GRAPH No. 4·35
C, 10·8, θ
C, 10·8, z
SUBSEQUENT STRAINING
SEQUENCES



GRAPH No. 4·36
C, 12·8, 9
ALL STRAINING
SEQUENCES

	UP	DOWN
8 – 18	●	○
19 – 24	■	□
25 – 35	×	⊗
36 – 42	+	⊕

